CONJUGATED POLYELECTROLYTES BASED ON POLY(ARYLENE ETHYNYLENE): SYNTHESIS, SOLUTION PHOTOPHYSICS AND APPLICATIONS TO SENSORS AND SOLAR CELLS

By

XIAOYONG ZHAO

A DISSERTATION PRESENTED TO THE GRADUATE SCHOOL
OF THE UNIVERSITY OF FLORIDA IN PARTIAL FULFILLMENT
OF THE REQUIREMENTS FOR THE DEGREE OF
DOCTOR OF PHILOSOPHY

UNIVERSITY OF FLORIDA

2007

To my parents
To my wife
To my daughter

ACKNOWLEDGMENTS

At this point of my academic career, there are many people I want to acknowledge. First, I would like to thank my advisor, Dr. Kirk Schanze. Without his support, advice and encouragement, my work at the University of Florida would not have been possible.

I also want to acknowledge all the former and current members of Schanze group who have helped and contributed to my projects. Specifically, Dr. Mauricio Pinto taught me many tricks of polymer synthesis and characterization, which helped me pass the most difficult "induction period" when I started my training here as an organic chemist. Dr. Hui Jiang has been a wonderful co-worker and is always willing to teach and share his knowledge in photochemistry. Dr. Jeremiah Mwaura trained me how to fabricate solar cells and light emitting diodes. I also want to thank many other people, Dr. Xiaoming Zhao, Dr. Fengqi Guo, Dr. Thomas Cardolaccia, Emine Demir, Dr. Kye-Young Kim, Dr. John Peak, Youngjun Li, Eunkyung Ji, Johnathan Sommer for their willingness to share their success and mistakes in their experiments. I give my thanks to, Kye-Young Kim and Julia Keller for managing the orders for the group, Emine Demir and Yan Liu for organizing the group meetings.

I would like to thank Dr. John Reynolds and Dr. William Dolbier for their great help in my career and my life. And my committee members, Dr. Ronald Castellano, Dr. Elliot Douglas and Dr. Valeria Kleiman are appreciated for their suggestions. I also thank Dr. Stephen Hagen for letting me use the CD spectrometer in his lab, giving me instructions and answering my questions.

Finally, I am grateful to my family for their love and support. I would not be able to come this far without my parent, they have provided me the best conditions they can to let me continue my education. I want to thank my wife for her love and understanding. I also thank her family for taking care of our daughter in the past year.

TABLE OF CONTENTS

LIST OF TABLES

Table page

LIST OF FIGURES

Abstract of Dissertation Presented to the Graduate School
of the University of Florida in Partial Fulfillment of the
Requirements for the Degree of Doctor of Philosophy

CONJUGATED POLYELECTROLYTES BASED ON POLY(ARYLENE ETHYNYLENE): SYNTHESIS, SOLUTION PHOTOPHYSICS AND APPLICATIONS TO SENSORS AND SOLAR CELLS

By

Xiaoyong Zhao

December 2007

Chair: Kirk S. Schanze
Major: Chemistry

In this dissertation, we present the research that was focused on the design, synthesis and photophysical properties of conjugated polyelectrolytes (CPEs) based on poly(arylene ethynylene) (PAE). Applications of these materials for anion sensing and dye-sensitized solar cell (DSCs) were also explored.

First, a *meta*-linked poly(phenylene ethynylene) featuring chiral anionic groups was designed and synthesized. Because of the presence of chiral side chains, the conjugated backbone of this polymer folds preferentially into a left-handed helix in water, as proven by absorption, fluorescence and circular dichroism spectroscopy. Similar to the helix formed by double-strand DNA, the helical conformation of the synthetic polymer interacts with a metallointercalator $[Ru(bpy)_2(dppz)]^{2+}$ and turns on the emission from the complex. Cationic cyanine dyes can also bind to the helical conformation of the polymer in a "groove-binding" manner. A chiral and optically active aggregate of cyanine dyes is formed by transferring the chirality of the polymer template.

Second, we have systematically investigated the photophysical properties of *para*-linked poly(phenylene ethynylene)s (PPEs). These CPEs are shown to undergo a solvent-driven

aggregation in solution. By chemically tuning the polymer structure, the influence of charge density and polymer chain length to the aggregate formation was carefully examined. Further, the fluorescence quenching by metal ions and organic cations (methyl viologen derivatives) was also studied. It was found that aggregate formation and polymer chain length both have a strong effect on the quenching efficiency of these polymers by the quencher molecules. Based on these results, a highly selective and sensitive sensor for pyrophosphate (PPi) was developed.

Third, we have successfully synthesized a series of poly(arylene ethynylene)s with variable absorption and emission properties. The photoluminescence of PAEs with linear ionic groups is strongly quenched in water due to aggregation. By replacing the linear ionic groups with dendritic ionic groups, the aggregation-induced self-quenching is suppressed. PAEs with dendritic ionic groups show high quantum efficiency in water and interesting optical properties when the solution conditions (pH, ionic strength) are varied. The application of PAEs with linear ionic groups in dye-sensitized solar cells was explored and the relationship between the polymer band gap and the cell performance provides valuable information regarding the further improvement of the cells.

CHAPTER 1
INTRODUCTION

Conjugated Polymers

In the past 30 years, a class of fascinating materials (i.e. conjugated polymers) has been developed.[1] The ground-breaking work is the discovery that the conductivity of polyacetylene (PA) was increased 10 million times with chemical doping by I_2 vapor in 1977, which was recognized by the Chemistry Nobel Prize in 2000.[2,3] Hideki Shirakawa of the University of Tsukuba in Japan, Alan MacDiarmid of the University of Pennsylvania at Philadelphia and Alan Heeger of the University of California at Santa Barbra shared the prize for the discovery of conducting polyacetylene. Ever since, the interest of scientists has expanded to a variety of other conjugated polymers (CPs),[4] including polypyrrole (PPy),[5] poly(*para*-phenylene) (PPP),[6] polythiophene (PT),[7] polyanaline (PANI),[8] poly(phenylene vinylene) (PPV),[9] poly(phenylene ethynylene) (PPE)[10] and polyfluorene (PF),[11] as shown in Figure 1-1.

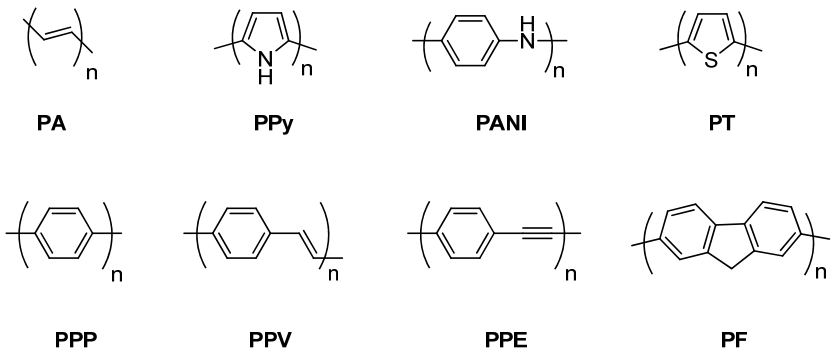

Figure 1-1. Molecular structures of some commonly seen CPs.

One of the most important breakthroughs in the field is the first polymer light-emitting diode (PLED) fabricated with poly(phenylene vinylene).[12] In the past three decades, conjugated polymers have found numerous applications, including light-emitting diodes (LEDs),[9] light-emitting electrochemical cells (LECs),[13] plastic lasers,[14] solar cells,[15] field-effect transistors

(FETs)[16] and chemical and bio-sensors.[17,18] Figure 1-2 highlights the most important developments related to this field.

1972 Metallatic films of polyacetylene were accidently discovered in Japan;

1977 Hideki Shirakawa, Alan G. Macdiarmid and Alan J. Heeger prepared the first conductive polymers, I_2-doped polyacetylene;

1990 The first polymer light emitting diode was prepared by Richard Friend and Andrew Holmes;

1995 The first polymer photovoltaic cell was fabricated in Heeger's lab;

1995 "Molecular wire effect" in CPs was first demonstrated by Swager and co-workers;

1999 The first biological sensor was demonstrated by Whitten and co-workers;

2000 Nobel Prize in Chemistry was awarded to Hideki Shirakawa, Alan G. MacDiarmid and Alan J Heeger;

2003 Displays using CPs were first commercialized by Philips Inc.

Figure 1-2. Historical aspect of CPs.

Poly(Arylene Ethynylene)s

The Pd-Methodology

Compared with other types of conjugated polymers, poly(arylene ethynylene) (PAEs) did not receive much attention until their applications in the area of explosive detection,[19] molecular wire[20] and polarizers for LC displays were discovered in mid-1990s.[21,22]

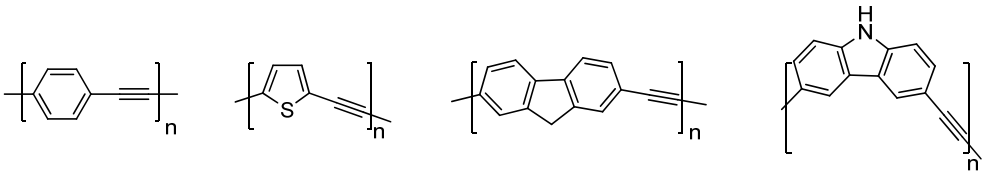

PPE PTE PFE PCE

Figure 1-3. Molecular structures of a few PAEs.

In the past decade, a wide variety of PAEs with different chemical structures have been synthesized and studied,[10] some examples of which are shown in Figure 1-3. Despite their

structural variety, they all share the same backbone feature, i.e. they are conjugated through ethynyl linked aromatic or hetero-aromatic rings.

To date, the most common approach used to prepare poly(arylene ethynylene)s is the Palladium-catalyzed cross-coupling reactions between terminal alkyne and aromatic bromides or iodides in the presence of a catalytic amount of copper (I) iodide, known as Sonogashira coupling or Sonogashira-Hagihara coupling.[23,24] Actually, earlier in the same year of 1975, Heck[25] and Cassar[26] independently reported similar coupling reactions. Heck used phosphate-palladium as the catalyst and triethylamine or piperidine as the base and also the solvent. In Cassar's procedure, sodium methoxide was used as the base and the reaction was performed in DMF. In general, both reactions required high temperature up to 100 °C. In the Sonogashira-Hagihara reaction, the addition of copper (I) iodide as the co-catalyst enables the reaction to be run at a lower temperature or even room temperature. Therefore, it provides a mild method and is more compatible with a wide variety of functional groups and solvents.

The mechanism of Sonogashira coupling has been under considerable dispute for many years and the generally accepted mechanistic pathway involves two independent catalytic cycles, as shown in Figure 1-4. In the Pd-cycle, the active catalyst, 14-electron Pd^0L_2 is generated from the initial pre-catalyst, commonly a palladium (II) complex by reduction with either solvent or substrate. Then, a fast oxidative addition of an aromatic bromide or iodide occurs at the electron deficient Pd center. At this point, the Pd-cycle connects with the copper co-catalyst cycle (Cu-cycle) and a transmetalation from copper acetylide to the Pd-center generates the $R^1Pd(-C\equiv CR^2)L_2$ species. The final coupled alkyne is produced by reductive elimination after *trans/cis* isomerization and the active catalyst is regenerated. In the Cu-cycle, the base (usually

amine) promoted formation of copper acetylide is believed to occur via a π-alkyne-Cu complex based on the fact that the amines are not basic enough to deprotonate the free alkyne.

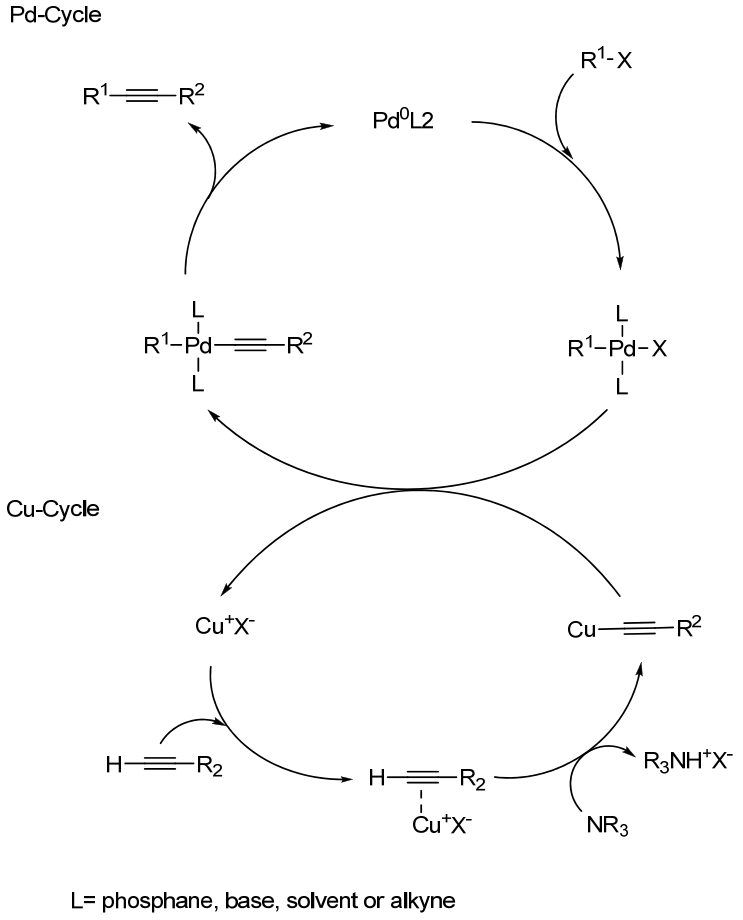

Figure 1-4. Mechanism of Pd (0) and CuI catalyzed Sonogashira reaction.[24]

In most examples of Sonogashira coupling, the commercially available $Pd(PPh_3)_2Cl_2$ is the source of Pd. Since Pd (II) is inactive, it is believed that the copper acetylide formed in the Cu-cycle is involved in the generation of the initial active Pd (0) species. In such a process, $Pd(-C{\equiv}CR^2)_2L_2$ is formed and subsequent reductive elimination affords the Pd^0L_2 and some amounts of diacetylene byproduct. This consumption of alkyne is not a problem in the synthesis of small organic molecules. However, since the polycondensation based on Sonogashira coupling follows a step-growth mechanism, the molecular weight of the polymer is strongly related to the stoichiometry between the monomers.[10] Such an activation step will cause a stoichimetric

imbalance between the two monomers, leading to polymers with reduced molecular weight. To circumvent the problem, several methods have been proposed including the addition of a small excess of the alkyne monomer,[27] and/or using the combination of $Pd(PPh_3)_2Cl_2$ and triphenylphosphine, etc.[10] Most commonly, a Pd (0) complex, such as $Pd(PPh_3)_4$ is employed in a polymerization to reduce the problem and give rise to polymers with satisfactory molecular weights.

In the synthesis of low molecular weight organic molecules, both aromatic bromides and iodides have been used. Since the oxidative addition step in the catalytic cycle is thermodynamically more favorable for aromatic iodides than aromatic bromides, the reactions involving aromatic iodides occur considerably faster and proceed at room temperature. By contrast, when aromatic bromides are used as the reagents, the reactions require higher temperatures and a longer reaction time. Thus, in a typical polymerization, when aromatic iodides are used, the reaction generally produces higher molecular weight polymer with less defects.

Although Sonogashira coupling has been widely used to synthesize a variety of PAEs, there are several shortcomings of this Pd-methodology.[28] First, the addition of copper (I) iodide catalyzes the homocoupling of the terminal alkyne when the copper acetylides are formed *in situ*, which generates the diacetylene by-product and/or diyne defects in the polymer chain. Use of Pd (0) complexes and careful exclusion of air could circumvent the formation of structural defects based on the literature and the author's own experience.[10] Second, the molecular weight of PAEs prepared from polycondensation based on Sonogashira coupling is strongly dependent on the monomer structure. Typically, when dialkoxy- and dialkyldiiodobenzenes were used, polymers with degrees of polymerization (DPs) less than 100 were obtained.[10] In fairly few

examples, polymers with DP around 200 were reported.[10] To date, PAEs with the highest molecular weight using this methodology were obtained by Swager *et al.* when acceptor-substituted monomers were polymerized.[27] Third, since dehalogenation and substitution of iodides by triphenylphosphine can occur in all of the Pd-catalyzed reactions, thus polymerization based on Sonogashira coupling may lead to the formation of polymer chains with poorly defined end groups.[29]

Alkyne Metathesis

An alternative approach to prepare PAEs is the alkyne metathesis reaction, which refers to the exchange of substituents between two alkynes. Alkyne metathesis is commonly catalyzed by molybdenum or tungsten based complexes.[30] The first homogenous catalyst for alkyne metathesis was reported by Mortreux *et al.* in 1974.[31] They found that a mixture of $Mo(CO)_6$ and simple phenol additives could catalyze the metathesis of alkynes. This system has been used widely and is referred as the "Mortreux system". However, the nature of the catalytically reactive species formed *in situ* from the mixture remains unknown. Structurally defined catalysts were later developed by Schrock *et al.*, which involves the usage of tungsten and molybdenum alkylidynes of the type $(RO)_3M{\equiv}C\text{-}CMe_3$, where M is W or Mo and R is Me_3C or aryl groups.[32] These catalysts have been found to be remarkably active, but they are extremely air and moisture sensitive, which poses some difficulties for large-scale synthesis and polymerization.[28,30]

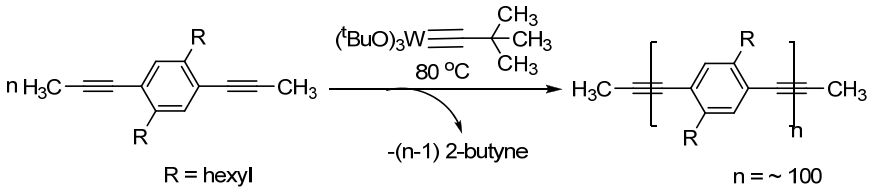

Figure 1-5. Acyclic diyne metathesis (ADIMET) as an alternative approach to prepare PPEs.

The application of the alkyne metathesis to prepare PAEs was first demonstrated by Müllen and co-workers in 1997.[33] Based on this work, the term "acyclic diyne metathesis"

(ADIMET) was termed, as shown in Figure 1-5. Bunz *et al.* successfully prepared poly(Phenylene ethynylene)s (PPEs) with DP of 100 and 1260 using Schrock's molybdenum alkylidyne and "Mortreux system", respectively.[28] In the latter case, when a combination of $Mo(CO)_6$ and 4-chlorophenol was employed, the obtained polymer is the PPE with the highest molecular weight synthesized so far. In another example, a group of alkyne-bridged carbazole polymers was synthesized using the same reaction condition, which demonstrated the "Mortreux system" is not only efficient to prepare hydrocarbon PPEs.[34] Although "Mortreux system" shows the advantages that a commercially available metal complex is used directly and no strict purification of solvent is needed, unfortunately the system requires a high activation temperature and is only compatible with limited functional groups. Recently, Moore and his co-workers developed an *in situ* strategy to prepare trialkoxymolybdenum alkylidyne (Schrock's catalyst)[35,36] from readily available molybdenum complex $Mo[N(t\text{-}Bu)Ar]_3$ (Ar = 3,5-$C_6H_3Me_2$). They found that the resulting alkylidyne is highly active and is compatible with a variety of functional groups. They utilized it to catalyze the polymerization of thiophene-containing monomers, which are not reactive in the presence of any earlier alkyne metathesis catalysts, and successful prepared poly(2,5-thienylene-ethynylene)s with alkyl chains.[37]

Although ADIMET shows its potential to produce PAEs with high molecular weight and well-defined end groups, this methodology also has several major drawbacks. First, a catalytic system thats meet multiple requirements (stability toward moisture and air; low activation temperature and wide compatibilities with most functional groups) is still not available.[38] Second, since alkyne metathesis is an equilibrium process,[30] to get polymers with a high molecular weight, the polymerization has to be conducted under open-driven conditions (high vacuum or continuous air flow) to remove the alkyne byproducts. Thus the polymerization is

required to be carried out in a high boiling solvent, such as 1,2-dichlorobenzene or 1,2,4-trichlorobenzene, which is another factor that impedes the application of alkyne metathesis in the synthesis of PAEs.

Besides Sonogashira coupling and alkyne metathesis, Mori and co-workers reported a copper-free method to prepare PAEs in 2001.[39] In their reactions, trimethylsilyl-protected diacetylene compounds and diiodoarenes were polymerized in THF in the presence of Pd(0) and silver (I) oxide. Recently, Watson reported a transition-metal-free synthesis of PAEs that contain alternating arenes and perfluoroarenes.[40,41] Although these methods have led to the preparation of PAEs with high molecular weights, they have drawbacks of using an stoichiometric amount of Ag_2O or limited applicability to fluorinated substrates, which impedes their general use to prepare PAEs.

Poly(Phenylene Ethynylene)s

The most common type of PAEs is poly(phenylene ethynylene)s, where all of the aromatic groups are benzene rings. Based on the main chain conformation, there are three isomers, namely, *para*-, *meta*- and *ortho*- poly(phenylene ethynylene)s (Figure 1-6). These three isomers display extraordinarily different electronic and physical properties.

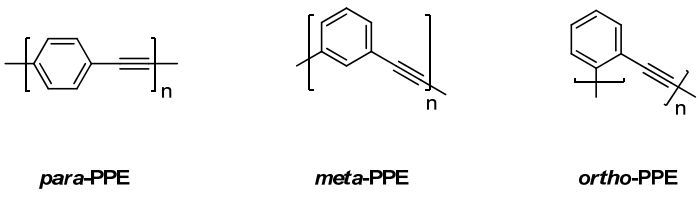

Figure 1-6. Molecular structures of PPEs with different backbone configurations.

Poly(*para*-phenylene ethynylene): Truly a Rigid Rod?

Poly(*para*-phenylene ethynylene)s (*para*-PPEs) are ideally shape persistent structures because the bond angle between the phenyl carbon and sp carbon (triple bond) is 180 °C. Initially because of their rod-like structures, oligo-phenylene ethynylenes (oligo-PEs) and *para*-

PPEs have been synthesized and explored as promising materials for nonlinear optics,[42] liquid-crystal displays[22] and molecular wires to bridge nanoelectrodes.[43] While low-molecular-weight PPEs and oligo-PEs are certainly rigid rods,[44] substantial researches have led to the conclusion that PPEs above certain chain length actually behave as wormlike chains and should not be considered as rigid rods.[45,46]

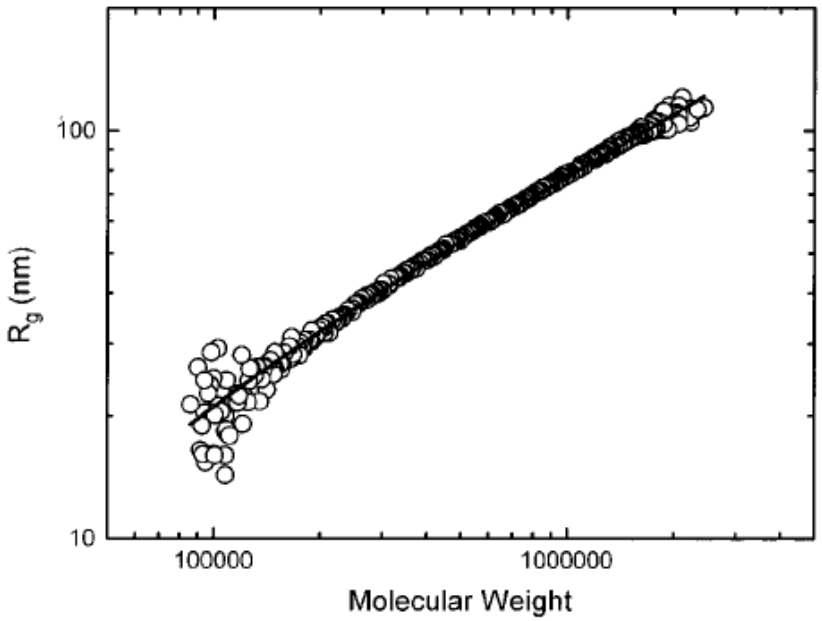

Figure 1-7. Radius of gyration R_g of a PPE sample with a broad molecular weight distribution (PDI = 1.4) in THF solution, plotted as a function of molecular weight (M_w). Figure was taken from Cott *et al*.[45]

Cotts and Swager[45] synthesized a series of PPEs with different molecular weights and investigated the solution properties of PPE chains using a variety of light scattering techniques, coupled with size exclusion chromatography. One of the most important conclusions of their work is that PPEs can be described as coil-like polymers at higher molecular weight (M_n > 50,000 kD). In a diluted polymer solution, the root-mean-square radius of gyration (R_g) is often used to measure the size of a polymer molecule.[47] This term is described being dependent on the molecular weight of the polymer in the form of $R_g \sim M^{\nu}$, in which the exponent ν indicates the rigidity of the polymer chain.[47] For a random-coil polymer, the exponent ν is 0.5; while for rod-

like polymer, ν is 1.0. Figure 1-7 shows the log-log plot of R_g vs M_w for a PPE sample with a broad molecular weight distribution. The results were obtained by size exclusion chromatography coupled with an on-line light scattering detector, which measures the molecular weight simultaneously and instantaneously as the narrow distribution "fractions" of the polymer is separated by the column. The dependence of R_g on the molecular weight shows an exponent near 0.5, indicative of a random coil conformation. Also the plot shown in Figure 1-7 can be fitted with Kratky-Porod worm-like chain model and the persistent length of PPEs is estimated to be around 15 nm, which equals 20 PE repeating units.

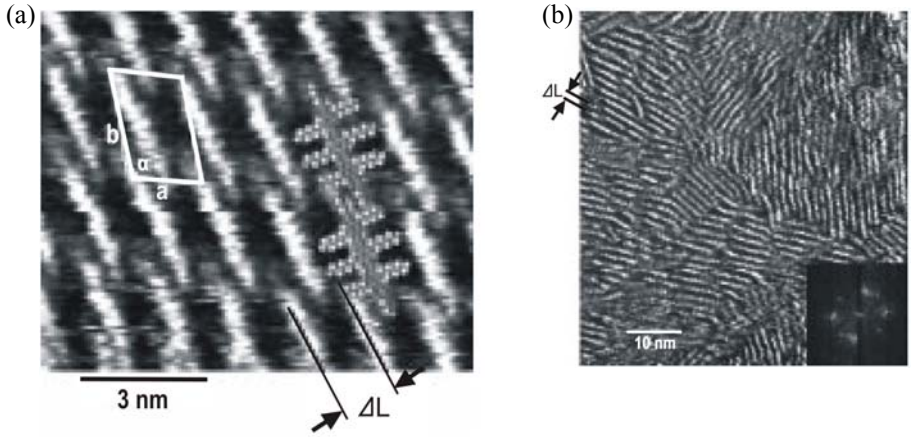

Figure 1-8. STM current images of oligo-PE (a) and PPE (b) at the solid-liquid interface on the graphite substrate. Δ *L* is the distance between the neighbouring backbones. Figure was taken from Samorí *et al*.[48]

In another study carried out by Rabe and Müllen,[48] the self-assembly of PPEs with different molecular weights at the solid/liquid interface was investigated by scanning tunneling microscopy (STM). The rigid rod-like structures of PPE and oligo-PE are directly visualized with molecular resolution, as shown in Figure 1-8. At the interface between an oligo-PE solution and a highly oriented pyrolytic graphite (HOPG) substrate, an epitaxial 2D crystal structure is observed (left). For the polydispersed PPE, a 2D nematic-like molecular order is revealed (right). The stiffness of the oligomer (trimer) and the polymer (DP = 9) is apparent in these images and is believed to play a key role for the molecular packing. In both cases, the

conjugated skeleton and the side groups lie flat on the HOPG substrates. The distance between the backbones is around 1.6 nm. This number is smaller than the distance of 1.9 nm calculated for the case with the side chains (hexyl) extended, indicating a slightly disordered arrangement of side groups between the backbones.

Further studies of the self-assembly on the mica substrate shows that the morphology of the dry samples prepared by evaporation of PPE solutions on the mica surfaces is dependent on the molecular weight of the polymers. For polymers with DPs of 9, 11, 20, 22, ribbons are observed, while for high molecular weight samples (DP = 28, 42), a grainy morphology is obtained. The cut-off molecular weight of the polymers for different morphologies corresponds also to about 20 phenylene ethynylene repeat units, which in another way supports Cotts and Swager's result that PPEs with chain length beyond 20 repeat units behave differently from PPEs with low molecular weight.

***Meta-* /*Ortho*-Linked Phenylene Ethynylenes: Helical Folding**

Compared with *para*-linked poly(phenylene ethynylene)s, *meta*-linked oligo-phenylene ethynylenes (oligo-PEs) and poly(phenylene ethynylene)s received much less attention before their folding properties were discovered by Moore and co-workers in 1997.[49]

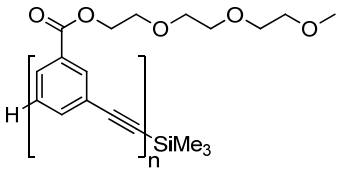

n = 2, 4, 6, 8, 10, 12, 14, 16, 18

Figure 1-9. *Meta*-linked oligo-phenylene ethynylenes studied by Moore group.

In a series of well-designed work, *meta*-linked oligo-PEs with oligo(ethylene glycol) side chains were synthesized (shown in Figure 1-9) and their folding process was carefully studied using ^{1}H NMR, UV absorption, fluorescence spectroscopy and computational modeling.[50]

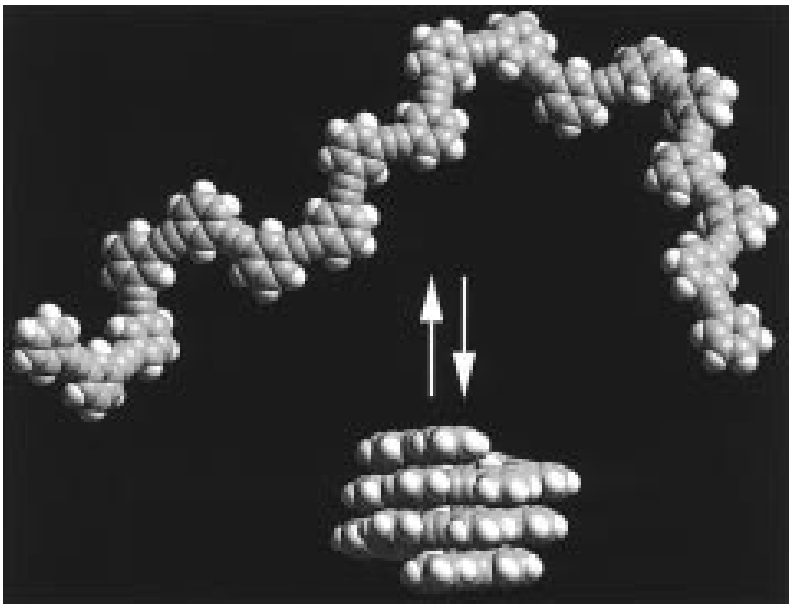

Figure 1-10. A space-filling model showing the folding process for an oligo-PE (n=18). The side chains were omitted for clarity. Figure was taken from Prince *et al*.[50]

As shown in Figure 1-10, these oligo-phenylene ethynylenes are able to fold into a helical structure in a polar solvent, such as acetonitrile. In a typical non-polar solvent, such as chloroform or methylene chloride, the oligomers are well-solvated and exist in an expanded form. When the solvent composition ($CHCl_3/CH_3CN$) is changed, the polar side chains are extended to the environment and the non-polar backbone folds into a helical conformation, which is stabilized by the favorable π-π interaction between the phenyl rings. The ability of such PE systems to fold and unfold is believed to arise from the fact that the free rotation around the ethynylene linkers allows for the switching between the *transoid* and *cisoid* state of the conjugated chains,[50] which is illustrated in Figure 1-11. In the helical conformation, the *cisoid* state is populated. The coil-helix transition is also found to be strongly dependent on the oligo-PEs' chain length and the environment temperature.

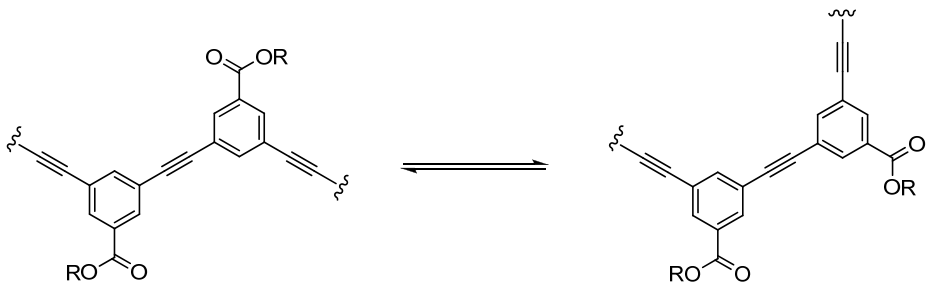

transoid *cisoid*

Figure 1-11. The *transoid*↔*cisoid* interconversion existing in *meta*-linked PEs.

Recently, Tew and co-workes synthesized *ortho*-linked oligo-PEs and demonstrated that these *ortho* isomers with very short sequences can also undergo the folding process. By theoretical modeling[51] and experimental studies using 1D and 2D NMR methods,[52] the helical folding in *ortho*-linked oligo-PEs was confirmed. In a polar solvent such as acetonitrile, a helical conformation with 3 rings per turn is expected, as shown in Figure 1-12.

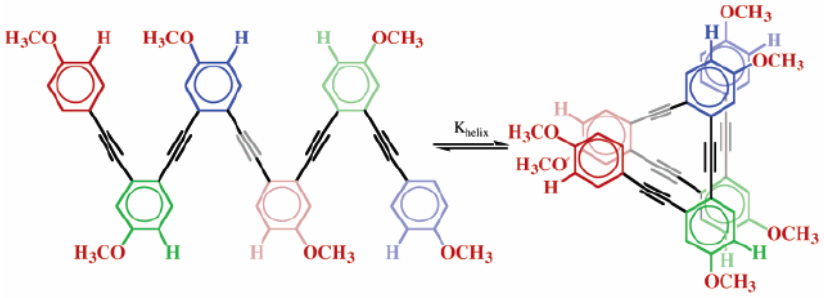

Figure 1-12. Helical folding of *ortho*-linked oligo-phenylene ethynylenes. Figure was taken from Blatchly *et al*.[51]

Conjugated Polyelectrolytes

Conjugated polyelectrolytes (CPEs) are π-conjugated polymers with ionic solubilizing side groups, such as sulfonate ($-SO_3^-$), carboxylate (CO_2^-), phosphate (PO_3^{2-}) and alkyl ammonium (NR_3^+).[53] Some examples of these materials are shown in Figure 1-13. CPEs retain the intrinsic electronic and optical properties of their organic π-conjugated backbones; in addition, their charged side chains integrate water solubility/hydrophilicity to the polymers. Because of this

unique combination, CPEs feature a variety of useful material properties. First, CPEs can be processed into films from water or other polar solvents, such as methanol, which is much more environment-friendly compared with the processing of conjugated polymers from organic solvents. Second, CPEs interact strongly with other ionic species,[18] such as metal ions, anions, polyelectrolytes, proteins and DNA, which provides a useful platform for developments of chemo- and bio-sensors. Third, due to their intrinsic amphiphilicity, CPEs could self-assemble into supramolecular assemblies such as colloids and polyelectrolyte layer-by-layer films, which could provide functional materials with internal molecular order.

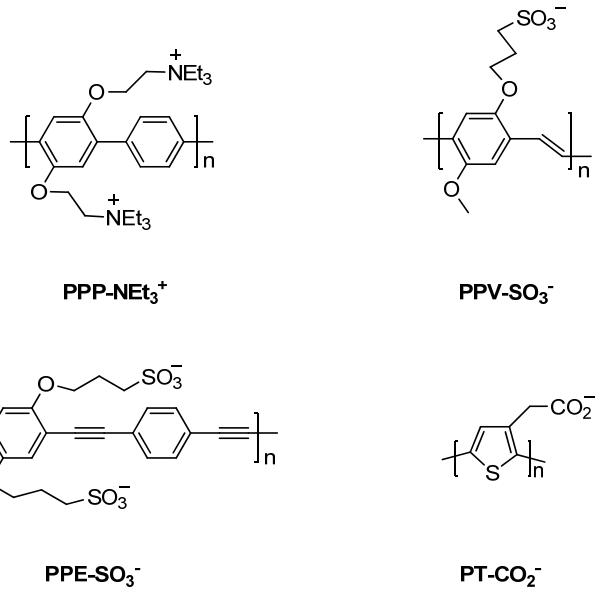

Figure 1-13. Molecular structures of some common CPEs.

Amplified Quenching of Conjugated Polyelectrolytes

Stern-Volmer (SV) Quenching

Much of the excitement regarding the properties and applications of CPEs is associated with the observation of the "amplified quenching effect", *i.e.* very efficient fluorescence quenching at low concentration of the quenching species. Before discussing this phenomenon, we provide a brief overview of fluorescence quenching and standard mechanisms used to explain the effect.

Fluorescence quenching can occur by two limiting mechanisms, dynamic (eq. 1-1) and static (eq. 1-2).[54] In eqs. 1a and 1b, F* is an excited-state fluorophore, Q is a quencher, k_q is the bimolecular quenching rate constant and K_a is the association constant for formation of the ground state complex [F,Q].

$$F^* + Q \xrightarrow{k_q} F + Q \qquad (1\text{-}1)$$

$$F + Q \rightleftharpoons[K_a] [F,Q] \xrightarrow{h\nu} [F^*,Q] \xrightarrow{fast} F + Q \qquad (1\text{-}2)$$

Treatment of fluorescence intensity quenching data according to the Stern-Volmer (SV) equation yields,

$$\frac{I_0}{I} = 1 + K_{SV}[Q] \qquad (1\text{-}3)$$

where I and I_0 are the fluorescence intensity with and without Q, respectively, and K_{SV} is the SV quenching constant. In the limit where quenching is dominated by the dynamic pathway (eq. 1-1), $K_{SV} = k_q\tau^o$, where τ^o is the fluorescence lifetime of F*, whereas in the limit where static quenching dominates, $K_{SV} = K_a$.

There are several ways to distinguish between dynamic and static quenching. First, note that k_q cannot exceed the diffusion rate constant (ca. 10^{10} $M^{-1}s^{-1}$) when quenching is fully dynamic. Since $K_{SV} = k_q\tau^o$, for a fluorophore that has a 1 ns lifetime this places an upper limit on $K_{SV} \approx 10$ M^{-1} for dynamic quenching (i.e., 10^{10} $M^{-1}s^{-1}$ x 10^{-9} s = 10 M^{-1}). Thus, static quenching is likely to be important if the experimentally observed K_{SV} is significantly greater than 10 M^{-1}. Another method for distinguishing when static quenching is important is to compare the ratio of emission lifetimes (τ^o/τ) and emission intensities (I_o/I) vs. quencher concentration. If the

K_{SV} obtained from intensity quenching is greater than that from lifetime quenching, then static quenching is occurring.

When the quenching is dominated by either a purely static or dynamic pathway, the quenching behavior follows eq. 1-2 and consequently SV plots of I_0/I vs. [Q] are linear. However, in many situations (as shown below) the SV plots are curved upward (i.e., superlinear). Superlinear SV plots can arise from a variety of processes, including mixed static and dynamic quenching, variation in the association constant with quencher concentration, and chromophore (or polymer) aggregation.

Molecular Wire Effect

The concept of "amplified fluorescence quenching" in conjugated polymers was first described by Swager and co-workers in 1995.[55,56] Although their work was focused on neutral, organic soluble poly(arylene ethynylene)s, the concept is also very important for the development and applications of conjugated polyelectrolytes.

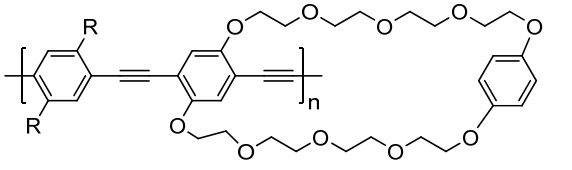

6, 7, 8
R = $CONH(C_8H_{17})_2$

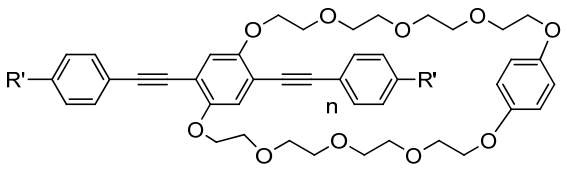

2
R' = $OC_{12}H_{25}$

Figure 1-14. Molecular structures of the CPs studied by Swager's group.

In the work, a series of organic soluble PPEs with a cylcophane receptor on each repeating unit were synthesized using Pd (0)/CuI catalyzed Sonogashira coupling , as shown in Figure 1-14. The polymers have the same chemical structure but different molecular weights; the number-average molecular weights for **6, 7, 8** are 31 kD, 65 kD and 122 kD respectively with a similar polydispersity (PDI = 2.0).

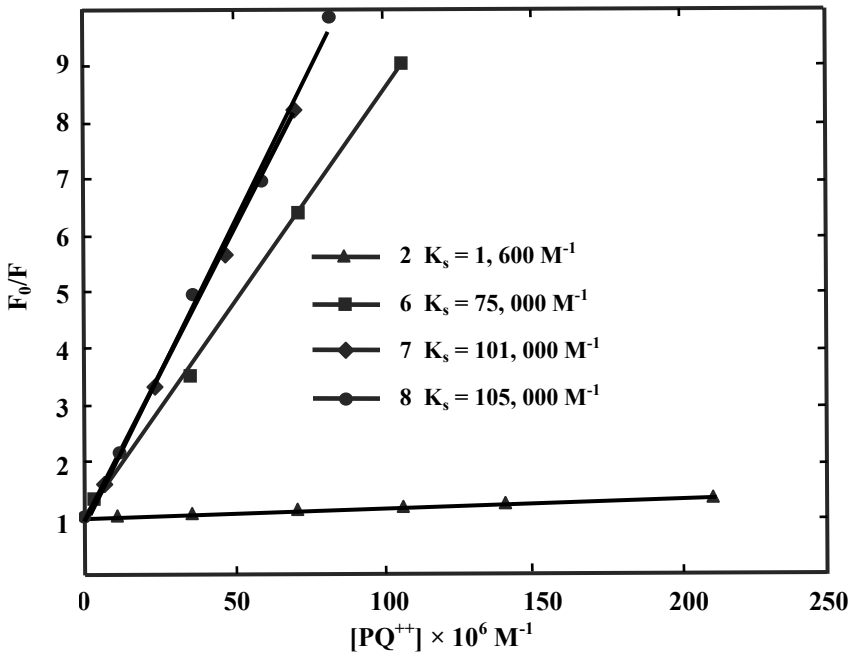

Figure 1-15. Stern-Volmer plots of Swager's polymers **6**, **7**, **8** with MV^{2+}. Figure was taken from Zhou *et al*.[55]

Because N,N'-dimethyl-4,4'-bipyridinum (PQ^{++} or MV^{2+}) could bind to the cyclophane unit, the fluorescence of the polymer is quenched by MV^{2+} via the electron transfer mechanism. As shown in Figure 1-15, linear Stern-Volmer (SV) relationships are observed and K_{sv} values in the order of 10^5 M^{-1} are obtained for all the polymers. By comparing intensity quenching and lifetime quenching, a static quenching mechanism was confirmed in these systems. Compared with the quenching by MV^{2+} of the model compound **2**, polymers **6-8** show greatly enhanced K_{sv} values (66-fold increase relative to **2** at most), which suggests that there is an amplified response

for the polymers. Even more, the amplification factor, defined as the ratio of K_{sv} for the polymer divided by K_{sv} for the model compound, is also shown to be dependent on the chain length of the polymers. When the molecular weight of the polymer is increased from 31 kD (**6**) to 65 kD (**7**), there is an additional 1.4-fold enhancement of K_{sv} value. Although further increase of the molecular weight (**8**, M_n = 122 kD) results in a K_{sv} value close to that of **7**, it still demonstrates that the amplified response is an inherent property of the conjugated polymers.

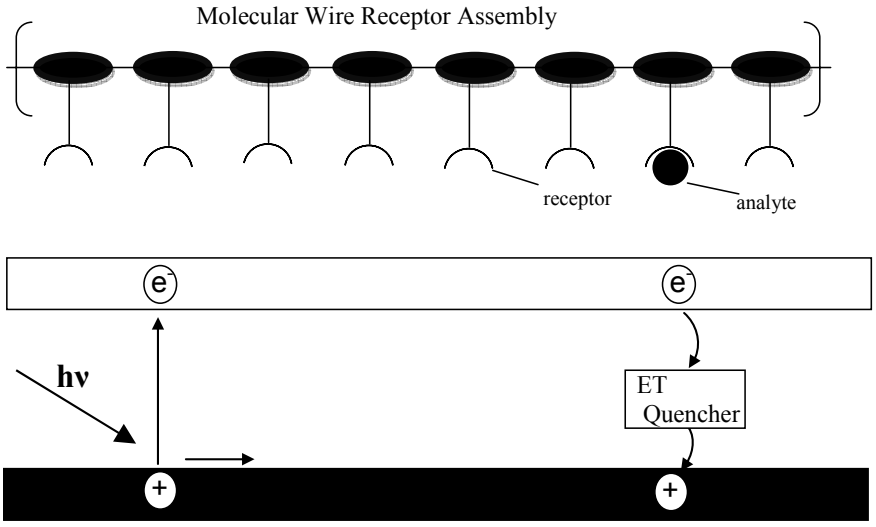

Figure 1-16. Schematic illustration of the "molecular wire effect" expressed by conjugated polymers. Figure was taken from Zhou *et al*.[55]

The amplification of quenching efficiency by the polymer (**6**, **7**, and **8**) compared with the model compound (**2**) is ascribed to the extended electronic communication and transport by the conjugated polymer chain,[56] as shown in Figure 1-16. Upon the absorption of light, an exciton (bound electron-hole) is generated randomly and migrates along the polymer backbone. At the time when the exciton reaches a viologen occupied receptor, it is then quenched. Due to the extremely rapid exciton diffusion in the polymer excited state ("molecular wire effect"), a single MV^{2+} bound to the receptor site can quench many repeat units in the polymer chain. Thus the response of the polymer to the target (here, the viologen molecules) is amplified. Based on the

concept, successful sensors for nitroaromatics have been developed by Swager's group,[19] which led to the commercialization of explosive detectors, Fido® by the ICx Technologies, Inc.

Fluorescence Quenching in Conjugated Polyelectrolytes

The amplified quenching effect in CPEs was first observed by Chen and Whitten in their study of quenching of the fluorescence of PPV-SO_3^- (structure shown in Figure 1-13) by MV^{2+}.[57] This work has stimulated intensive investigations concerning CPE fluorescence quenching with a variety of organic, inorganic analytes and biomolecules.[18,58,59]

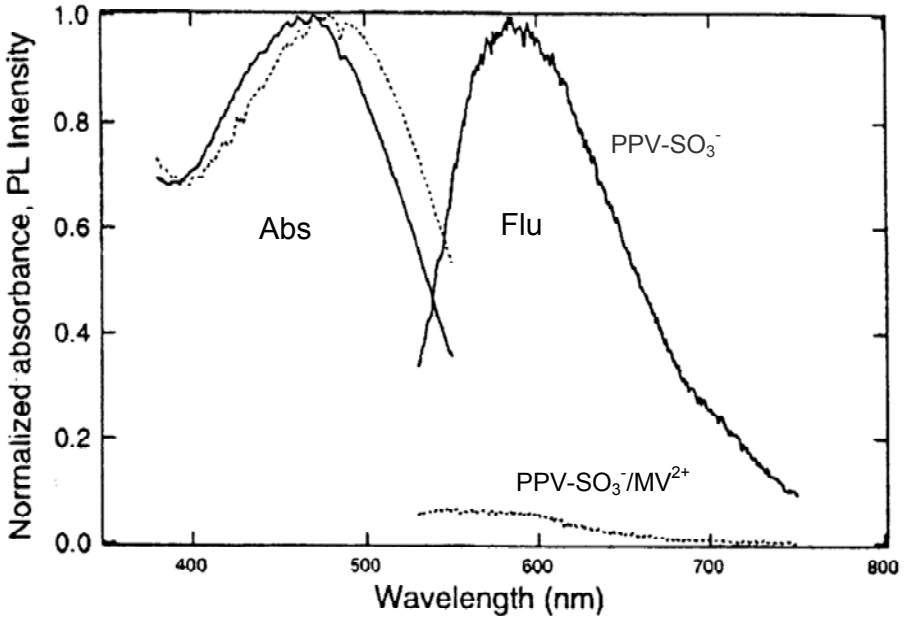

Figure 1-17. Absorption (left) and fluorescence (right) of PPV-SO_3^- in water with and without 100 nM MV^{2+}. Figure was taken From Chen *et al*.[57]

As shown in Figure 1-17, in the initial study of PPV-SO_3^-, the addition of 100 nM of MV^{2+} to a solution of the polymer ($c \approx 10^{-5}$ M in polymer repeat units) results in a very efficient quenching of the polymer's fluorescence and a distinct red-shift in the absorption spectrum. The SV plot for quenching of the PPV-SO_3^- fluorescence by MV^{2+} is linear at very low concentrations of MV^{2+} (0 – 1 μM), with $K_{SV} \approx 2 \times 10^7$ M^{-1}. Compared with the quenching constants of stilbene in sodium lauryl sulfate micelles and in dilute solutions, it is four orders of

magnitude and six orders of magnitude greater, respectively. Such a million-fold amplification of K_{sv} value is attributed to two effects: the ion-pair complex formation between the oppositely charged polymer and quencher and the ultrafast exciton migration along the conjugated polymer chain ("molecular wire effect").[57] The mechanism of fluorescence quenching in CPEs has been intensively studied by many other research groups in the following years. The quenching constant (K_{sv}) is shown to be dependent on various factors, such as the polymer concentration,[60] quencher properties (charge,[61] hydrophobocity[62] and size[63]), solution properties (pH,[64,65] ionic strength[65,66] and buffer[66]), and additives.[67-70]

Aggregation of CPEs

As pointed out earlier, CPEs are inherently amphiphilic materials and their photophysical properties are strongly influenced by the tendency of the materials to self-assemble. In a series of work, Schanze *et al.* have carefully studied the aggregation of PPE-SO_3^- and its effect on fluorescence quenching by small molecules via electron or energy transfer mechanism.[71,72]

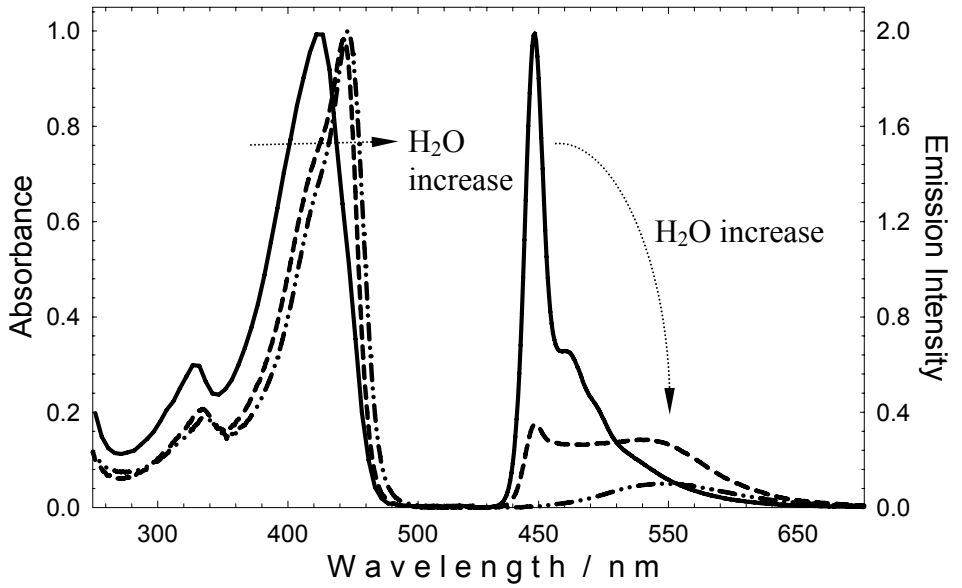

Figure 1-18. Absorption (left) and fluorescence (right) of PPE-SO_3^- in methanol, methanol:water (50:50) and water. Arrows show the direction of change with increasing water content. Figure was taken from Tan *et al*.[71]

As shown in Figure 1-18, as the amount of water in the solvent increases, the absorption and fluorescence of PPE-SO_3^- undergo a red-shift. The most pronounced changes are seen in the fluorescence. In methanol the fluorescence appears as a sharp, narrow band that has a very small Stokes shift relative to the absorption, whereas in water the fluorescence appears as a very broad and red-shifted band. The structured emission seen for PPE-SO_3^- in methanol is very similar to that which has been reported for structurally-related, neutral PPEs in dilute solutions of "good" organic solvents such as $CHCl_3$ or THF, where the polymer chains surely exist in an unaggregated "monomeric" state.[73] Thus, it is concluded that in methanol the PPE-SO_3^- chains are well solvated and the material exists in a monomeric state. Consequently in this solvent the fluorescence is dominated by excitons that are confined to single chains. By contrast, in aqueous solution it is believed that PPE-SO_3^- is strongly aggregated, and the fluorescence emission is dominated by excitons that are trapped in aggregate states arising from interactions between two or more PPE chains in the aggregate. It is important to note that the aggregate emission observed for PPE-SO_3^- in water is very similar to that observed from excimers (excited π-dimers) of small aromatic fluorophores such as naphthalene or pyrene.[74] From this they concluded that a dominant structural feature in the aggregates must be π-π stacking between two or more polymer chains. Most importantly, when the quenching of PPE-$SO_3^-$with MV^{2+} was studied in methanol and water, a larger K_{sv} was observed in water, which indicated that the fluorescence quenching was further amplified in the aggregate.

Bazan and co-workers[75] also studied the solvent-dependent aggregation of cationic water-soluble poly(fluorene) and found that the aggregate structure of the polymer has a strong effect on the efficiency of fluorescence resonance energy transfer from the polymer to the dye-labeled DNA. In another publication,[76] they found that for a copolymer consisting of fluorene and 2,1,3-

benzothiadiazole (BTD) segments, efficient energy transfer from the fluorene units to the lower energy BT sites occurs when the polymer is aggregated by changing the concentration or adding ssDNA.

Applications of Conjugated Polyelectrolytes

Optical Biosensors

One of the most exciting applications of conjugated polyelectrolytes is their biological sensing in aqueous environments for many analytes,[18] including small biomolecules, nucleic acids and various proteins. Because of the signal amplification imparted by conjugated backbone of these polymers, biosensors with extraordinary sensitivity are obtained. Typically the detection limits for CPE-based biosensors are in the nanomolar concentration range[58] and in a few cases, sensors that can detect the target analytes at zeptomole level were also reported.[77] To fabricate these sensors, different formats of conjugated polyelectrolytes have been used, including homogenous aqueous solutions,[78] glass slide supported CPEs[79] and particle supported CPEs.[58] Regardless of the sensing targets and the formats of the fluorescent CPEs, there are three general sensing mechanisms that have been employed to build the sensors, i.e., quenching-unquenching mechanism, chain conformation perturbation mechanism and fluorescence resonance energy transfer mechanism.

Quenching-unquenching mechanism

Sensors that are built using the "quenching-unquenching" strategy take advantage of the superquenching property of CPEs by electron or energy accepting quenchers.[58] By connecting such a quencher to biologically interesting ligands, a fluorescence response is produced when the ligands bind to their specific targets. Chen and Whitten reported the first example of a CPE-based biosensor using this strategy.[57] They covalently linked MV^{2+} via a flexible tether chain to biotin, a small ligand that binds specifically to avidin. Initially such a quencher-tether-ligand

(QTL) system is mixed with a solution of PPV-SO_3^- (structure shown in Figure 1-13). Because of the superquenching effect, the polymer's fluorescence is substantially quenched at very low concentration of the QTL system. The fluorescence is recovered by adding small amounts of avidin, which disrupts the association between the polymer and the QTL system through binding to the biotin unit, as shown in Figure 1-19. Using this strategy, Whitten and co-workers have developed a sensor platform based on CPE-coated polystyrene microspheres for detecting enzymatic activity and DNA hybridization.[58]

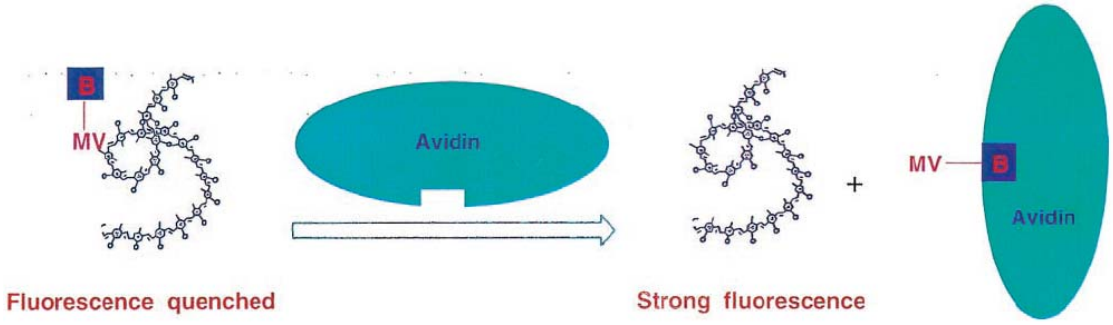

Figure 1-19. Biosenser applications of CPEs by the "quencher-tethered-ligand" (QTL) approach. Figure was taken from Chen *et al*.[57]

Chain conformation perturbation mechanism

CPE-based sensors that rely on signal transduction by the conformational change of the polymer have mainly focused on water-soluble poly(thiophene) derivatives.[59,80]

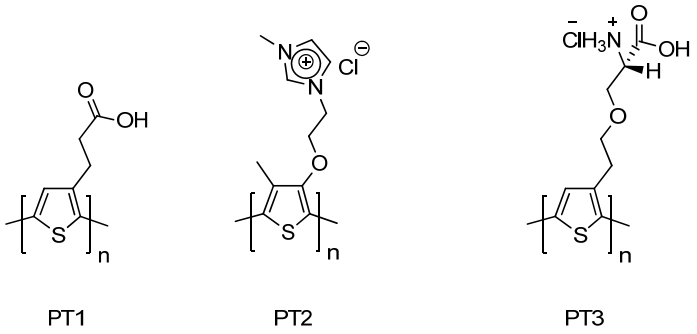

PT1 PT2 PT3

Figure 1-20. Molecular structures of some poly(thiophene) derivatives.

Poly(thiophene)s with pendant carboxylic acid groups (as an example, PT1, Figure 1-20) show interesting ionchromatic sensing in water, which is ascribed to the ion-induced conformation change of polymer backbone.[81] Leclerc pioneered the application of a cationic regioregular poly(thiophene) (PT2, Figure 1-20) in the detection of DNA.[59,82]

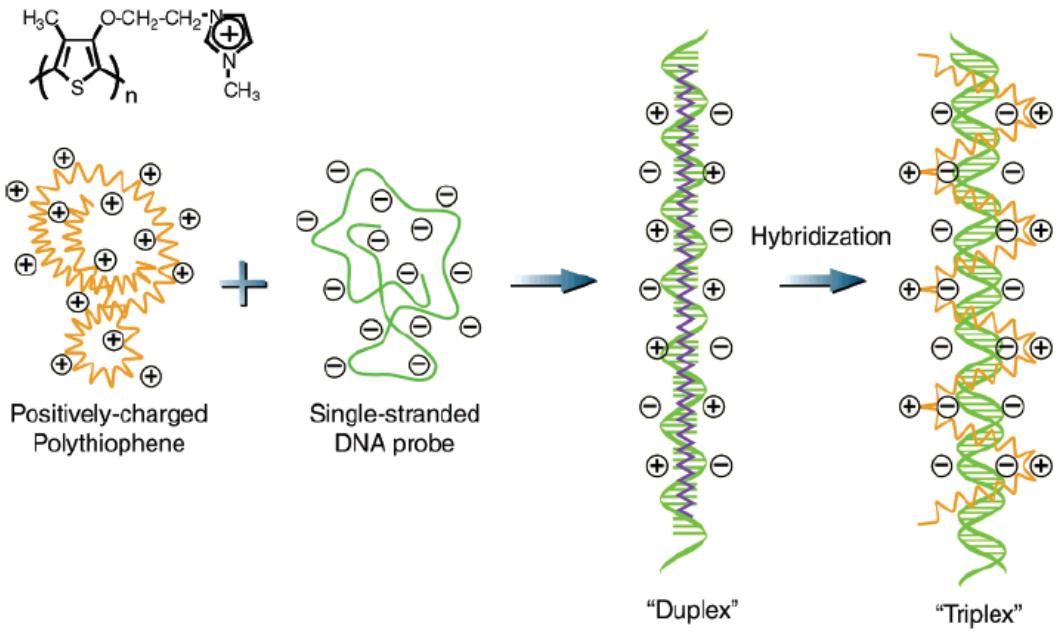

Figure 1-21. Schematic illustration of the formation of polythiophene/ss-DNA duplex and polythiophene/ds-DNA triplex. Figure was taken from Ho *et al*.[59]

As shown in Figure 1-21, before the addition of oligonucleotide, PT1 exists as a random-coil polyelectrolyte; upon the addition of the single-stranded oligonucleotide (ssDNA), an electrostatic complex, called duplex, is formed between PT1 and ssDNA, in which PT1 takes a more planar conformation; a helical conformation of PT1 results when a complementary ssDNA is added to the duplex solution. Corresponding to the conformational change, PT1 shows completely different absorption and fluorescence spectra. By monitoring either the absorption spectra or fluorescence spectra, oligonucleotide hybridization can be detected with a high sensitivity (10^{-14} M) and oligonucleotides with one mismatch can be discriminated from the perfect complementary oligonucleotide. More recently, Nilsson and co-workers synthesized a

new poly(thiophene) with zwitterionic side groups (PT3) and studied its interaction with a wide variety of biomolecules.[83,84]

Fluorescence resonance energy transfer (FRET) mechanism

Another method for DNA detection using CPEs was developed by Bazan, Heeger and co-workers.[78,85] Their method is based on the amplified FRET from a CPE to a signaling chromophore attached to a probe oligonucleotide. Cationic CPEs based on polyfluorene (Figure 1-22) were synthesized and utilized in these sensors. These CPEs exhibit relatively high fluorescence quantum efficiencies in aqueous environment compared to other CPEs, which is very important for increased sensitivity.

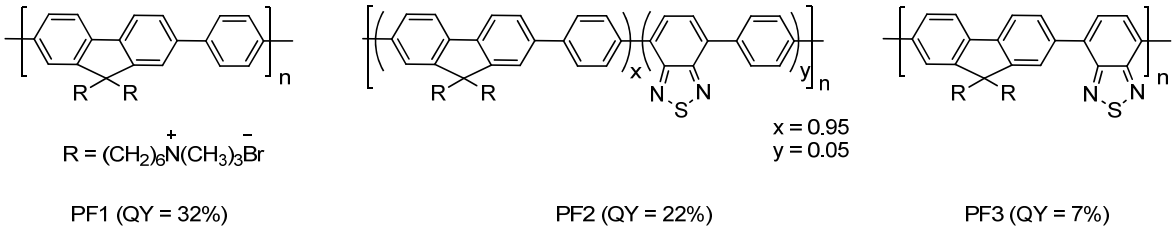

Figure 1-22. Molecular structures of CPEs based on polyfluorene (PF) reported by Bazan and co-workers.[78]

Figure 1-23 is a schematic representation of a sensing system based on the FRET from PF1 to a dye-labeled oligonucleotide probe.[85] In the system, a peptide nucleic acid (PNA) which can hybridize with ssDNA is labeled at 5′-end with fluorescein and used as the probe. Since PNA is neutral, there is no electrostatic interaction between PNA and PF1. Thus the average distance between PNA and PF1 is too large for effective FRET. Upon the addition of complementary ssDNA to the PNA probe, a strong PNA/ss-DNA complex is formed with a net negative charge, which enables the binding of the complex to PF1. The reduced distance between PNA and PF1 allows for the efficient FRET to take place between the polymer and the fluorescein. Thus the enhance emission from fluorescein signals the presence of target ssDNA. For

noncomplementary ssDNA, because the hybridization with PNA does not occur, there is still no electrostatic interaction between PNA and PF1, and the distance between them remains too large for FRET. Following the strategy, a homogenous three-color DNA-sensing array[76] that utilized PF2 was later developed and a solid-state assay was also fabricated using PF3.[79]

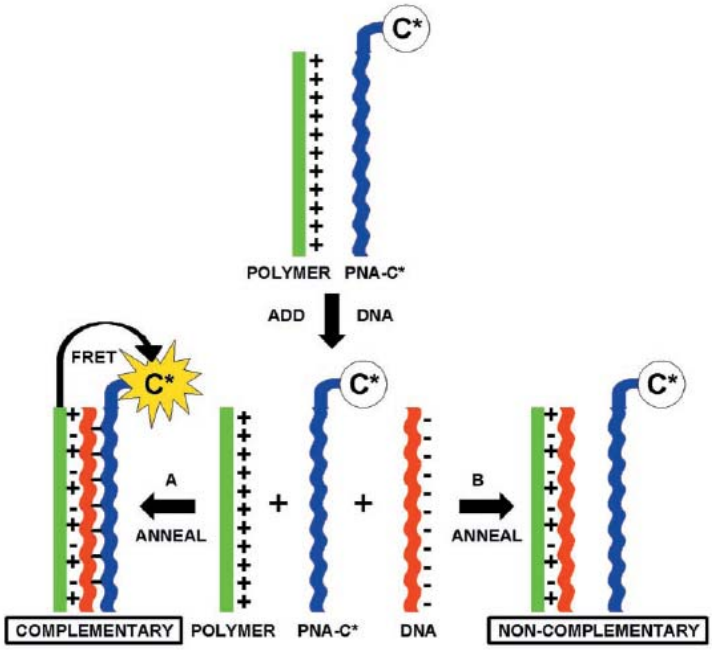

Figure 1-23. Schematic illustration of the PNA/PF1 assay for ss-DNA detection. Figure was taken from Gaylord *et al*.[85]

Dye-sensitized Solar Cells (DSCs)

Nanocrystalline TiO_2-based dye-sensitized solar cells invented by Gräzel in 1991 have attracted much attention and are promising for large-scale technological development.[86] Figure 1-19 shows a schematic representation of the operating principle of such a device.[87] On the top of a thin film of fluorine-doped tin oxide supported by glass or polymer, a mesoporous layer of TiO_2 (typically 5 – 10 μm thick) is placed. A monolayer of sensitizer is attached to the surface of the nanocrystalline film. After photoexcitation, electrons are injected to the conduction band of the semiconductor from the sensitizer's excited state. The sensitizer is

restored to its ground state by electron donation from the mediator, usually a redox couple, such as iodide/triiodide. The reducing species is then regenerated by reduction of the oxidizing species at the electrode. Overall, the cell converts light to electric power without chemical transformation.

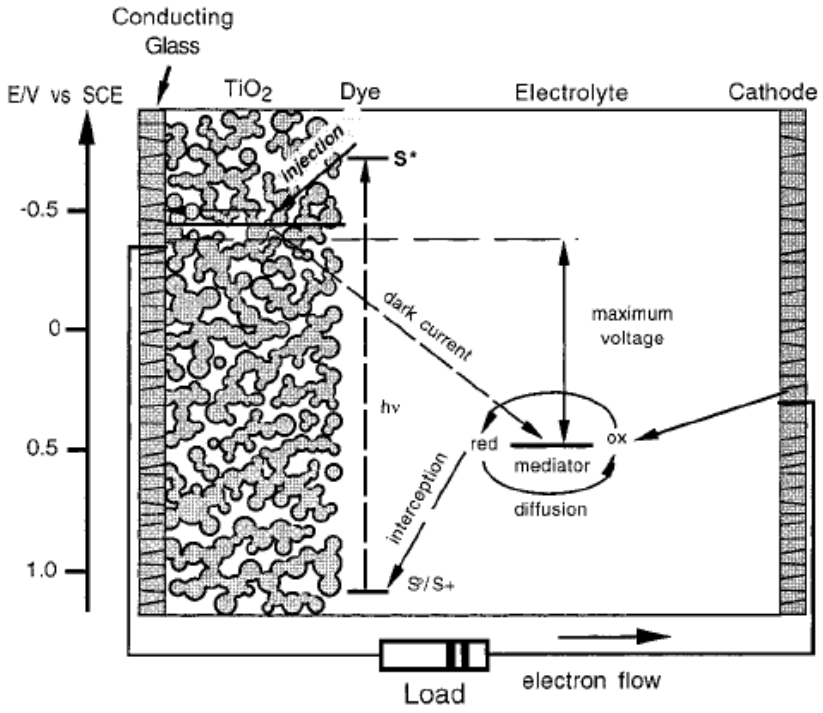

Figure 1-24. Schematic representation of the principle of dye-sensitized solar cells (DSCs) based on nanocrystalline TiO_2. Figure was taken from Hagfeldt.[87]

The highest light conversion efficiency (η) of DSCs till today is 11%, which was obtained using ruthenium (II) complex as the sensitizer.[88] Because of the high cost of transition metal complexes and the long-time availability of noble metal materials, DSCs based on metal-free organic dyes have also been pursued.[89] To date, η values of 6% - 9% using organic dyes, such as coumarin derivatives, indoline, etc. under solar simulator (AM 1.5) have been attained.[89]

Conjugated polymers have been widely used in polymer-based solar cells. Bulk heterojuction solar cells have been prepared from CPs and different electron-accepting materials such as C_{60} derivatives, CdSe and TiO_2 nanparticles.[15,90] However, conjugated polymer-based

DSCs have received much less attention in the past years. Given the tunable band gaps, high molar absorption coefficients and multiple binding sites to the oxide of conjugated polymers, it is possible that CPs could be valuable alternatives for ruthenium complexes in DSCs. Figure 1-25 shows some CPs with carboxylic acid functionalities that have been employed in DSCs without ruthenium complexes. In 2003, Kumar and co-workers[91] reported DSCs that were based on carboxylated polythiophenes (PTAA or H-PURET) with a power conversion efficiency of ~ 1.5%. Using the same polymer, PTAA, Yangida *et al*[92] showed that the power conversion efficiency could be doubled by simply adding an electron-donating ionic liquid to the liquid electrolyte (0.5 M LiI/0.05 M I_2). Recently, a collaborated work from Schanze and Reynold's labs demonstrated the concept of spectral broadening to enhance the performance of polymer based DSCs using CPs.[93] In the work, two CPs (PT-CO_2H and PPE-CO_2H), which absorb at the red and blue regions of the solar spectrum respectively, were mixed and co-adsorbed to the nano-crystalline TiO_2 films. Unoptimized DSCs using these films show a light conversion efficiency of 1.5%, which is among the highest for CP based DSCs.

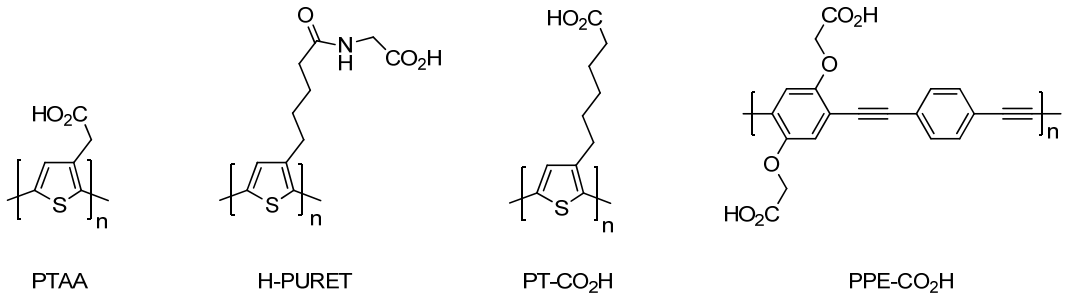

Figure 1-25. Molecular structures of some CPs with carboxylic acid functionalities that were used in DSCs.

Scope of the Present Study

The aims of the present study are to design and synthesize poly(arylene ethynylene)s with different chemical structures, investigate their photophysical properties in solution and develop their applications in the areas of sensors and solar cells.

In Chapter 2, to further confirm that *meta*-linked poly(phenylene ethynylene)s carrying ionic side chains self-assemble into a helical conformation in water, a polymer featuring chiral ionic side groups derived from *L*-alanine was designed and synthesized. The self-assembly behavior of the polymer in solution was studied using absorption, emission and circular dichroism spectroscopy. Due to the strong analogy between our polymer and DNA, interaction of the polymer helix with some metallo- and organic dyes were also studied in the aqueous solution.

In Chapter 3, two poly(phenylene ethynylene)s with different carboxylate substitution patterns were synthesized via the precursor route. The photophysical properties of the new polymers were investigated and compared to each other, as well as to those of the perviously studied PPE-SO_3^-. Moreover, the carboxylate groups on the polymer chain provide receptor sites for metal ions, which lead to the possibility of tuning the polymer fluorescence with metal ions. Interactions of the polymer with different metal ions were studied by absorption and emission spectroscopy in methanol, as well as in (2-hydroxyethyl)-1-piperaziethanesulfonic acid (HEPES) buffer solution. Quenching of the polymer fluorescence with MV^{2+} was studied in methanol in the presence of different amounts of Ca^{2+}. And based on these studies, a highly selective and sensitive sensor for pyrophosphate was developed.

In Chapter 4, to further understand the amplified fluorescence quenching in conjugated polyelectrolyte system, poly(phenylene ethynylene)s with 5 different chain lengths were synthesized. By controlling the loading ratio of monofunctional monomer in the initial mixture of AA and BB type monomers, the molecular weight of the neutral polymer was systematically varied. The water soluble polymers were subsequently obtained by hydrolyzing these organic PPEs containing dodecyl carboxylic esters. The dependence of the basic photophysical

properties, such as molar extinction coefficient, absorption maximum, was studied in methanol and water. Also, the fluorescence quenching with different quenchers was studied in methanol. The relationship between the Stern-Volmer constant and chain length was discussed.

In Chapter 5, poly(arylene ethynylene)s with variable band gaps were synthesized by copolymerizing diiodoarenes and ethynylated heteroarenes. The photophysical properties of the PAE series with carboxylate groups were carefully studied in different solvents. And aggregation was found to have a detrimental effect on the emission of red-emitting polymers. To prevent the aggregation-induced fluorescence quenching, two dendritic ionic side groups were designed. Photophysical properties of these PAEs containing dendritic solubilizing groups were also studied in aqueous solution at various conditions. Also, the application of these PAEs containing carboxylate groups in the conventional Gräzel-type solar cell without ruthenium complexes was explored.

CHAPTER 2
SELF-ASSEMBLY OF *META*-LINKED POLY(PHENYLENE ETHYNYLENE)

Introduction

Soon after the self-assembly properties of *meta*-linked phenylene ethynylene oligomers were revealed,[49,50,94] Tew[95] and our group[96] independently synthesized and studied *meta*-linked poly(phenylene ethynylene)s (PPEs) carrying ionic side groups. In a series of studies,[97-100] Tew and co-workers synthesized a group of *meta*-linked PPEs functionalized with various non-polar alkyl and ammonium ionic side chains (for an example, see Figure 2-1). It was shown that these amphiphilic PPEs could self-assemble into either ordered bilayers or helical conformations in aqueous solution dependent on the substitution patterns. In the meantime, we have synthesized two *meta*-linked PPEs with sulfonate and carbonate side chains, as shown in Figure 2-1. Studies of their optical properties (absorption and fluorescence) in methanol and water suggested that these polymers exist in a random-coil conformation in methanol and fold into a helical conformation in water. It was also shown that common DNA intercalators, such as 9-aminomethylanthracene and $[Ru(bpy)_2(dppz)]^{2+}$, could interact with the helical conformation of these polymers in the same manner as with DNA.[96]

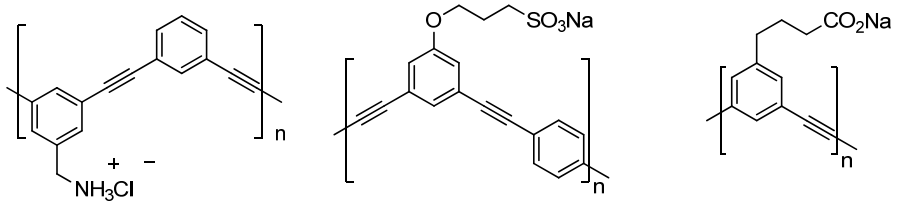

*m*PPE-NH_3^+ *m*PPE-SO_3^- *m*PPE-CO_2^-

Figure 2-1. Structures of *meta*-linked PPE reported in the literature.

One of the most useful techniques to study the chiral structures is circular dichroism (CD) spectroscopy. The appearance of a CD signal requires either an enantiomeric excess of chiral molecules or the existence of a chiral environment. When an achiral oligomer or polymer folds

into a helical structure, a racemic mixture of the right- and left-handed forms (the P and M forms) would be expected. Therefore, no CD signal can be observed. In order to probe the helical structure using CD spectroscopy, chirality induction is required. To produce an enantiomeric excess in the helical conformation of *meta*-linked oligomers, Moore and co-workers used several different strategies, including incorporation of chiral side chains,[101] chiral binaphthylene groups in the oligomer backbone,[102] and host-guest binding of (-)-α-pinene.[103] Arnt and Tew also observed a weak CD signal when they mixed *m*PPE-NH_3^+ (Figure 2-1) with chiral D-mandelic acid, suggesting an excess of the helix with one-handedness results.[98]

In the work described in the present chapter, we designed and synthesized a new *meta*-linked PPE featuring chiral and optically active ionic side groups based on L-alanine. The spectroscopic properties in different solvent systems were studied and the results demonstrated that the polymer undergoes a similar solvent driven folding like *m*PPE-SO_3^-. Circular dichroism spectroscopy provided direct evidence for the helix formation. Also, due to the similarity between our helical polymer and DNA, the interaction of the polymer with a well-known DNA intercalator, $[Ru(bpy)_2(dppz)]^{2+}$, was studied. And most interestingly, induced helical aggregation of cyanine dyes, such as 1,1′,3,3,3′,3′-hexamethylindodicarbocyanine iodide (HMIDC) and 3,3′-diethylthiadicarbocyanine ($DiSC_2(5)$) via "groove binding" to the helical polymer in water was also observed.

Results and Discussion

Synthesis

Figure 2-2 illustrates the synthetic scheme for the monomers. The synthesis started with commercially available 3,5-diaminobenzoic acid **1**, which was converted to 3,5-diiodobenzoic acid **2** in 65% yield through the in-situ formation of diazonium salt and subsequent reaction with

KI (Sandmeyer reaction).[104] Compound **2** was then reacted with benzyl ester protected L-alanine using carbodiimide-based condensation[105] to give compound **3** in a yield of 67%. The latter was then subjected to Sonogashira reaction with 2 eq. of trimethylsilyacetylene (TMSA) to give the protected acetylene derivative **4** in 74% yield. After desilylation with TBAF in THF, the desired monomer **5** was obtained in 86% yield. In another route, *tert*-butyl substituted 3,5-diiodobenzamide **7** was prepared via a two step process from **2**, which was converted to 3,5-diiodobenzoyl chloride using thionyl chloride and isolated as yellow crystal in 77% yield. The latter was then reacted with *tert*-butyl protected L-alanine in the presence of 2 eq. of 4-dimethyaminopyridine in dry methylene chloride to give compound **7** in an excellent 94% yield.

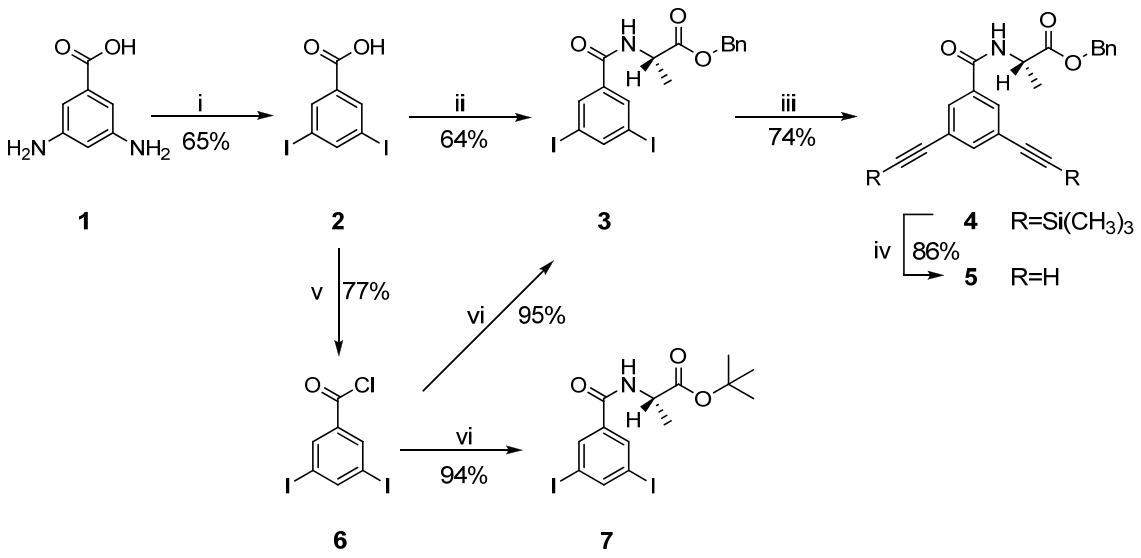

i. 1) $NaNO_2$, H_2SO_4; 2) KI,H_2O; ii. *L*-alanine benzyl ester, DPTS, DIPC, DMF, ambient;
iii. $Pd(PPh_3)_4$/CuI (cat.), trimethylsilylacetylene, THF/Et_3N, heat; iv. TBAF, ambient; v. $SOCl_2$, heat;
vi. DMAP, CH_2Cl_2, *L*-alanine benzyl ester/*L*-alanine *tert*-butyl ester, ambient.

Figure 2-2. Synthesis of monomers.

The synthesis of the model compound that contains the base chromophore resembling the repeat unit structure of the polymer is shown in Figure 2-3. Starting from either the benzyl (**3**) or *tert*-butyl (**7**) protected monomers, Sonogashira coupling with phenylacetylene gave the desired products in excellent yields. Then the benzyl ester was cleaved using 1 N NaOH in DMF to give

the water soluble model compound **9** in 90% yield; while the *tert*-butyl group was removed using a 1:1 mixture of trifluoroacetic acid (TFA)/CH_2Cl_2, further treatment with saturated aqueous Na_2CO_3 afforded the same compound in 92% yield.

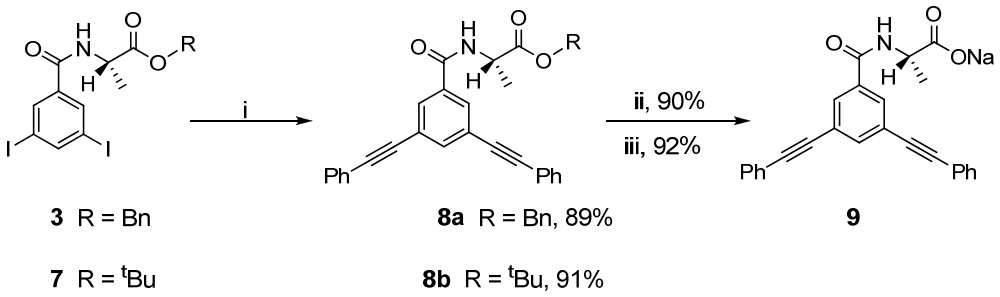

3 R = Bn

7 R = ^{t}Bu

8a R = Bn, 89%

8b R = ^{t}Bu, 91%

9

i. $Pd(PPh_3)_4$/CuI (cat.), phenylacetylene, THF/Et_3N; ii. NaOH (1N); iii. 1) TFA/CH_2Cl_2(1/1); 2) Na_2CO_3.

Figure 2-3. Synthesis of the model compound **9**.

The polymerization was first carried out between monomer **3** (AA) and monomer **5** (BB) to prepare the *meta*-linked homopolymer **P1** (Figure 2-4). Unfortunately even after optimizing the reaction solvents, temperature, amount of catalysts, the polymerization only led to a mixture of oligomeric species with an average length of 5 determined by gel permeation chromatography (GPC). Considering the mechanism of Sonogashira coupling,[24] we suspected that the presence of substituted side chains on each repeat unit in the oligomeric species during the reaction process raises the energy barrier for the *trans/cis* isomerization before the reductive elimination and thus prevents the efficient chain growth to give high molecular weight polymer. In response to the assumption, we carried out the polymerization between **3** (benzyl protected) and un-substituted 1,4-diethynylbenzene (**12**), as well as the polymerization between **7** (*tert*-butyl protected) and 1,4-diethylbenzene. The latter compound was prepared from commercially available 1,4-diiodobenzene following the procedure reported in the literature.[106]

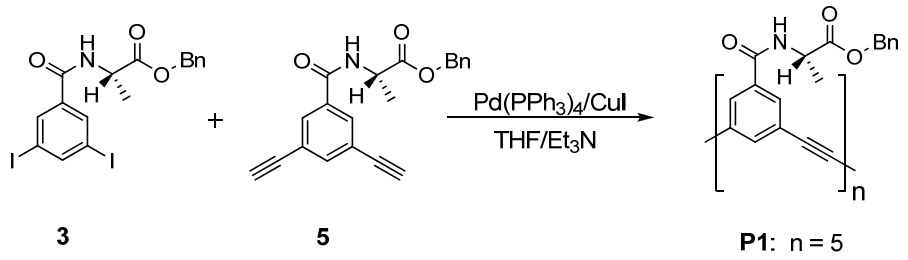

Figure 2-4. Synthesis of the homopolymer.

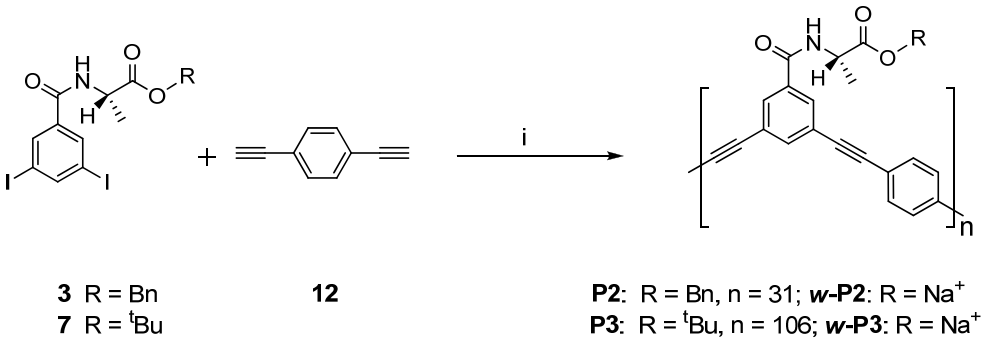

Figure 2-5. Synthesis of co-polymers.

Under the same conditions, both polymerizations afforded the alternating *meta*-/*para*-phenylene copolymers with considerably higher molecular weight than that of the homopolymer **P1**, as illustrated in Figure 2-5. The number-average molecular weight (M_n) of the polymer carrying benzyl protected ester is 12 kD, corresponding to 31 repeat units. Simply changing the protecting group from benzyl to *tert*-butyl, a polymer with average 106 repeat units (M_n = 39 kD) was obtained. Such an increase of molecular weight is most possibly due to the better solvation of the polymer with *t*-butyl side chains in THF. Besides THF, both polymers were found to be also soluble in chlorinated solvents such as chloroform and methylene chloride. The organic polymers (**P2** and **P3**) were hydrolyzed using the conditions which were used to hydrolyze the model compounds (**8a** and **8b**), respectively. After the hydrolysis, both polymers were isolated as yellow solids and could be dissolved in water and other polar solvents such as DMF and

DMSO. Final purification of the water-soluble polymers was done by dialysis of the aqueous solutions of the polymers against ultrapure water (18.2 MΩ) using a 12-14 kD molecular weight cut-off (MWCO) cellulose membrane.

Model Compound (9)

Figure 2-6 shows the absorption (a) and emission (b) spectra of the model compound **9** (Figure 2-3) in methanol (MeOH) and aqueous solutions, respectively. In general, the spectra do not vary much from methanol to aqueous solution. The absorption spectrum is characterized by two bands arising from the different vibronic modes of planar and twisted backbone structures, respectively. The absorption at 300 nm is assigned to the $\pi \rightarrow \pi^*$ transition of the planar structure due to its longer conjugation length. The emission features a strong band with λ_{max} = 352 nm for MeOH solution and λ_{max} = 361 nm for aqueous solution. The 9 nm red-shift of the emission maximum might be due to the change of polarity from methanol to water.

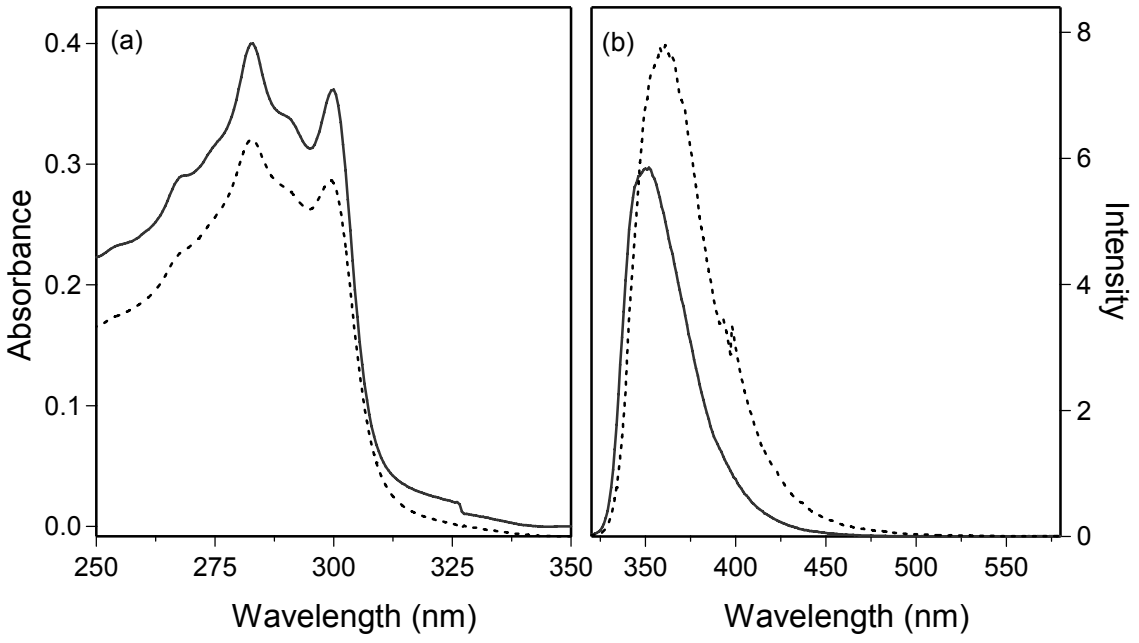

Figure 2-6. Absorption (a) and emission (b) spectra of model compound **9** in methanol (—) and water (---). [***9***] = 10 μM.

Solvatochromic Properties of *Meta*-Linked PPEs

UV-Vis absorption spectroscopy

Despite the difference in the molecular weight between ***w*-P2** and ***w*-P3**, they exhibit similar photophysical properties. In the following text, we will only present the results for ***w*-P2**. Figure 2-7 illustrates the UV region absorption spectra of ***w*-P2** in MeOH, in water, and in mixtures of these two solvents at various compositions. First, the absorption of the polymer in MeOH is characterized by a broad maximum at $\lambda_{max} \approx 326$ nm and a second band that appears as a shoulder at $\lambda \approx 350$ nm. These bands have been previously assigned as arising from the *cisoid* and *transoid* conformations of the *m*PPE backbone.[50,96] Interestingly, as the amount of water in the solvent mixture increases, the 328 nm absorption band blue-shifts (< 10 nm) and decreases in intensity (hypochromic effect), whereas the 350 nm shoulder red-shifts (< 5 nm) and decreases in intensity. The relative change in the A_{350}/A_{328} absorption ratio indicates a high population of *cisoid* conformation in the polymer helix (Figure 2-7, inset). The spectral changes for ***w*-P2** that are induced by the change of solvent from methanol to water are very similar, but slightly attenuated, relative to those observed for the sulfonate-substituted *meta*-linked PPE polymer (*m*PPE-SO_3^-).[96] By analogy to the previously studied system, the change in absorption that accompanies an increase in the volume fraction of water in the solvent is believed to arise due to an increase in the fraction of the polymer which exists in the helical conformation. Specifically, the absorption spectrum of ***w*-P2** exhibits a hypochromic effect with increasing water in the solvent; this effect is likely caused by π-stacking of the aromatic chromophores in the folded helical conformation. The solvent effects on the absorption of ***w*-P2** are attenuated relative to those reported previously for *m*PPE-SO_3^-,[96] presumably because in ***w*-P2** a significant fraction of the polymer exists in a helical conformation even in pure MeOH solution (*vide infra*).

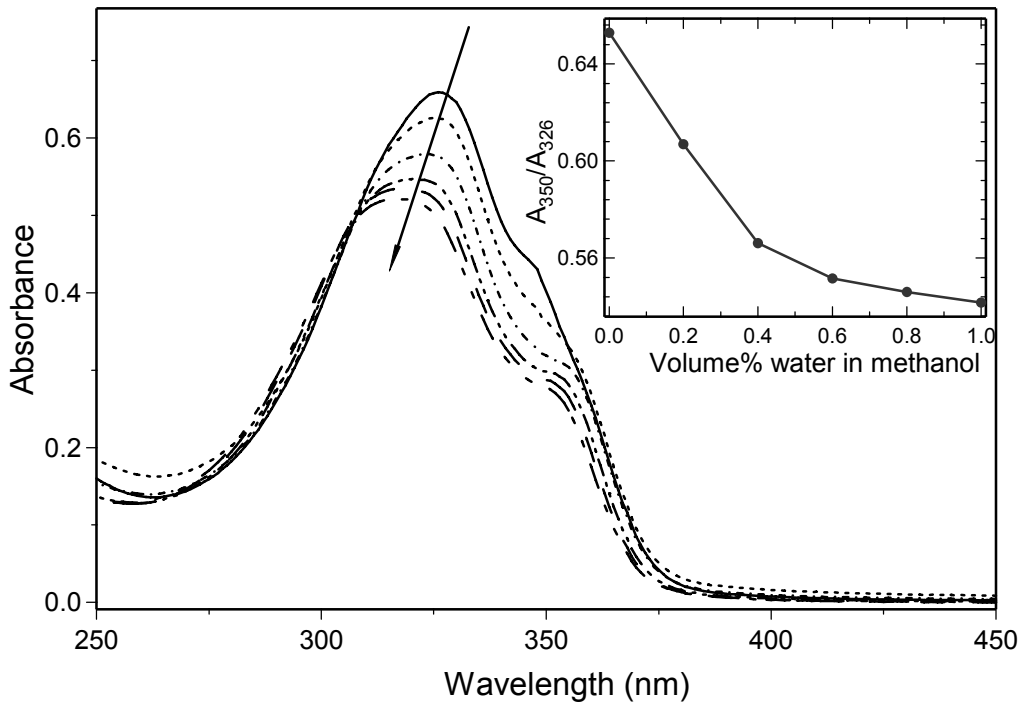

Figure 2-7. UV-Visible absorption of ***w*-P2** (c = 10 μM) in methanol, water and methanol/water mixtures. The arrow shows the direction of change with increasing volume % water. Inset shows the ratio of intensities of UV maxima at 350 nm and 326 nm (A_{350}/A_{328}) versus percent of water in MeOH (by volume).

Steady state fluorescence spectroscopy

Fluorescence spectra (Figure 2-8) of ***w*-P2** obtained in MeOH, water and MeOH/water mixtures provide additional information regarding the influence of solvent composition on the polymer's conformation. First, in pure MeOH, the fluorescence of ***w*-P2** is dominated by a structured band with a 0-0 transition at λ_{max} = 353 nm with weaker vibronic bands in the 360 – 400 nm region. In addition, the polymer also exhibits a weak and very broad emission band centered at $\lambda \approx 500$ nm. The structured near-UV emission is believed to emanate from the random coil conformation of the polymer, whereas the broad, structureless "excimer like" visible emission band likely arises from the folded, helical conformation of ***w*-P2**.[96] The fact that the structured emission dominates in MeOH solution, suggests that in this solvent ***w*-P2** exists

predominantly in the random coil conformation in this medium; however, the appearance of the broad excimer like emission indicates that even in MeOH a small fraction of ***w*-P2** is folded so that π-π stacking of adjacent chains is possible.

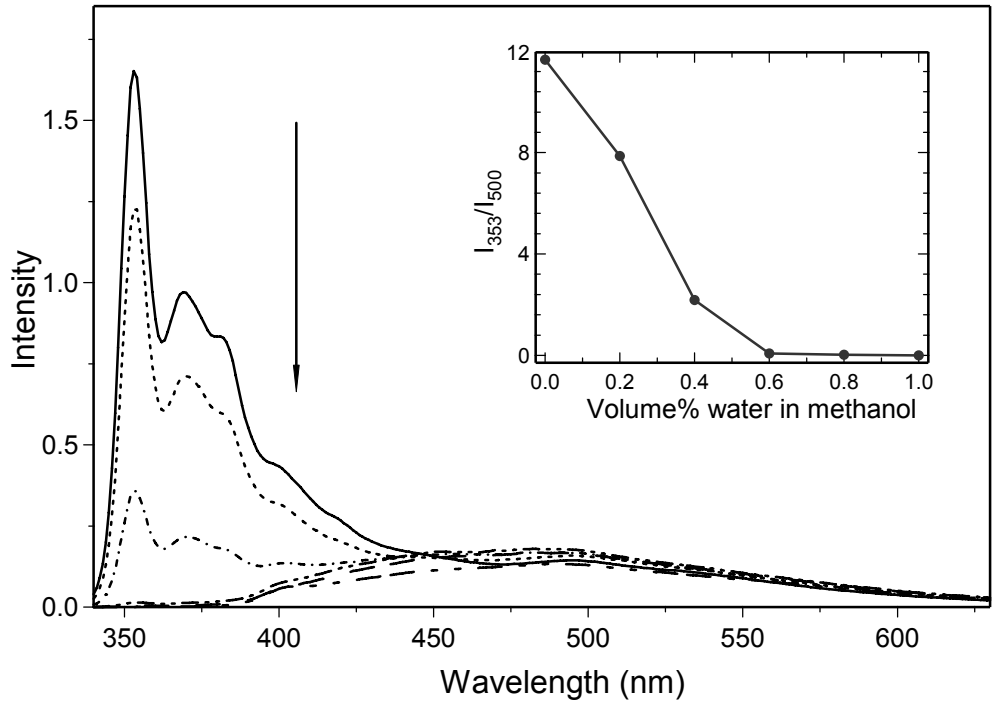

Figure 2-8. Fluorescence spectra (λ_{exc} = 320 nm) of ***w*-P2** (c = 10 μM polymer repeat units) in MeOH, water and MeOH/water mixtures. The arrow shows the direction of change with increasing volume % water. The spectra were obtained under the same conditions, so the spectral intensities reflect the approximate change in fluorescence quantum efficiency with solvent composition. Inset shows the ratio of intensities of emission at 363 nm and 500 nm (A_{363}/A_{500}) versus percent of water in MeOH (by volume).

Interestingly, as the volume fraction of water in the solvent increases, the intensity of the structured near-UV emission attributed to the random coil conformation decreases significantly (Figure 2-8 inset). For solutions that contain ≥ 60% water, the structured emission is completely quenched, and the only emission observed is the broad, visible region fluorescence. This observation is consistent with the conclusions based on the solvent-induced shift in the absorption spectrum, i.e., in MeOH ***w*-P2** exists mainly in a random coil conformation, whereas

in solvent mixtures that contain ≥ 60% water the polymer is mostly folded into the helical conformation.

Circular dichroism spectroscopy

The alanine-derived side group in ***w*-P2** is chiral and optically active, and we anticipated that its presence would induce an enantiomeric excess in the helical conformation of the *m*PPE backbone. In order to probe this effect, CD spectroscopy was used to study the optical activity of ***w*-P2** and the model compound **9** in solutions of methanol, water and methanol/water mixtures. Figure 2-9 shows the CD spectra of ***w*-P2** in a series of solvent mixtures along with the spectrum of **9** in water. First, it is quite evident that the model compound **9** is CD inactive. This finding is not surprising in view of the fact that the conjugated chromophore in ***w*-P2** is inherently achiral. It clearly shows that the perturbation provided by the chiral center in the alanine side group alone is insufficient to induce a measurable chiroptical effect on the conjugated chromophore.

By contrast to the model, ***w*-P2** exhibits a strong bisignate CD spectrum in methanol, water as well as in mixtures of the two solvents. Since the model compound **9** is CD-inactive, the bisignate CD signal observed for ***w*-P2** clearly arises because the conjugated *m*PPE backbone of the polymer is in a chiral conformation (i.e., a helix) and the chiral side group induces an enantiomeric excess in one of the helical conformers. The longer wavelength Cotton effect is negative ($\lambda \approx 368$ nm), whereas the short wavelength couplet is positive ($\lambda \approx 325$ nm). This relationship is termed "negative chirality", and suggests that the left-handed helical conformation (i.e., an M-helix) of the *m*PPE backbone is in excess.[107]

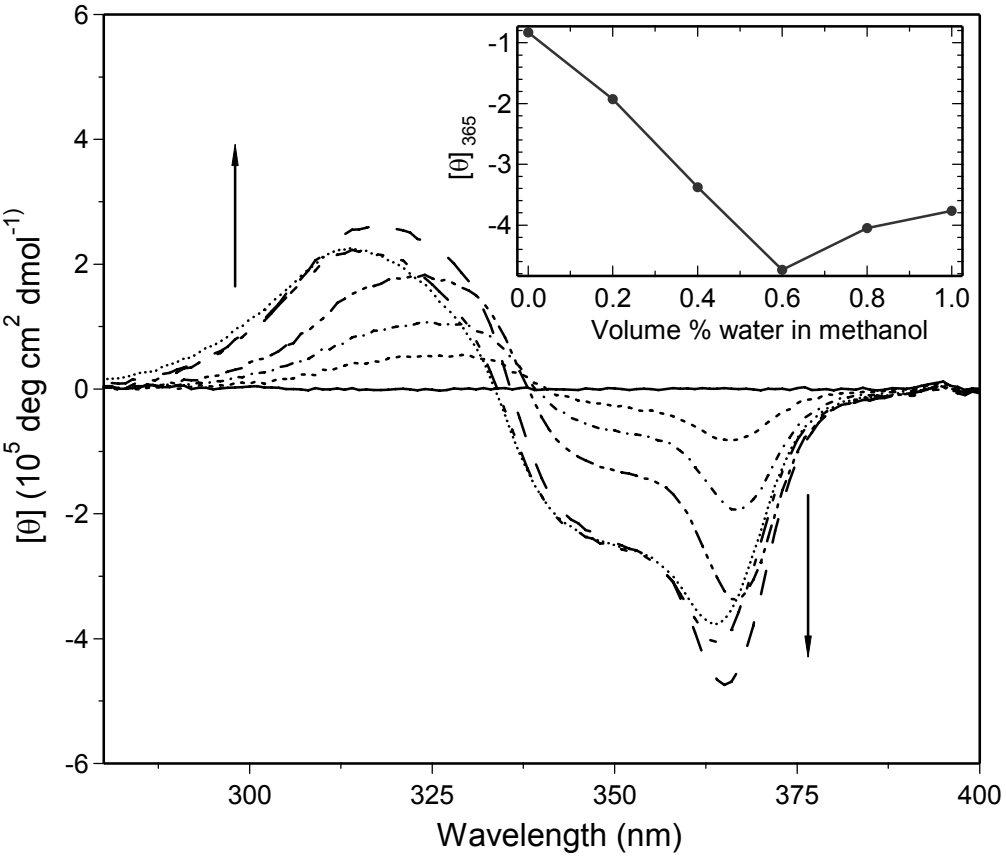

Figure 2-9. Circular dichroism spectra of model compound **9** in water (c = 15 μM, solid black line) and ***w*-P2** (c = 15 μM polymer repeat units) in methanol, water and in methanol/water mixtures. Arrows show the direction of change with increasing volume % water.

Interestingly, the amplitude of the CD signal for ***w*-P2** varies with solvent composition. In particular, the spectrum is relatively weak in MeOH, and it increases approximately 8-fold with increasing water content, reaching a maximum at 60 volume % water. Further addition of water results in a slight decrease (*ca.* 20%) in the amplitude of the CD signal. First, the observation of a CD signal for ***w*-P2** in MeOH indicates that in this solvent the polymer adopts a helical conformation to some extent. This fact is consistent with the fluorescence of the polymer in MeOH, where the excimer-like emission attributed to the helical conformation is observed. The fact that ***w*-P2** exists in part in a helical conformation in pure MeOH contrasts with the behavior of *m*PPE-SO_3^-,[96] which on the basis of fluorescence and absorption spectroscopy is believed to

exist exclusively in a random coil conformation in MeOH. The helical conformation in ***w*-P2** may be stabilized in MeOH by hydrogen bond formation between proximal amide units in the helix. The increase in CD intensity with increasing water content in the solvent indicates that the hydrophobic effect is important in inducing the polymer to adopt the helical conformation to a greater extent. The loss in CD intensity for volume fractions of water > 60% may signal a loss of helical conformation, or more likely it is due to a change in the structure of the helix (e.g., a decrease in the helical pitch) which leads to a change in the strength of the exciton coupling along the *meta*-linked π-system. Similar loss of helicity has been observed by Swager in the aggregate of conjugated polymers carrying chiral side groups.[108]

Guest Binding with *Meta*-Linked PPEs

Given the qualitative similarity between the secondary structure of the helical conformation of anionic, *m*PPEs and double-helical DNA (i.e., both are helical polyanions which feature aromatic units that are π-stacked along the helical axis), we have an interest in exploring whether cationic dyes will interact with *m*PPEs in a comparative manner.

Interaction of dyes with DNA has been intensively employed to probe the DNA structure.[109] There are three well-known binding modes for DNA helix, i.e., electrostatic binding, intercalation and groove binding. Electrostatic binding is simply the association between DNA (negatively charged) and positively charged small molecules via electrostatic interaction. This is the most common way that DNA interacts with metal ions. Intercalation is a binding mode that small molecules insert their planar aromatic functionality between the base pair of DNA helix. Thus, the binding is stabilized by π-π stacking. Many organic dyes that contain aromatic or hetero-aromatic rings have been proven to interact with DNA through intercalation, such as ethidium bromide,[110] acridine orange,[111] (9-anthrylmethyl)ammonium

chloride,[112] etc.[113,114] Metal complexes that contain fused aromatic ligands, such as dipyridophenazine (dppz),[115,116] 9,10-phenanthrenequinone diimine,[117] etc.[118] have also been widely studied as DNA intercalators. One well-known example is a ruthenium complex, $[Ru(bpy)_2(dppz)]^{2+}$, which becomes luminescent in water when intercalated into double-helical DNA.[119] Groove binding involves the assembly of guest molecules in the minor or major grooves of DNA. The binding is stabilized by a combination of many forces, such as hydrogen bonding, hydrophobic and electrostatic interactions. The most successful class of minor groove binding molecules is the hairpin polyamides[120] which mimic the structure of natural minor groove binder, distamycin.[121] For organic dyes, Armitage and co-workers[122-125] have shown that cationic cyanine dyes can assemble into the minor groove as dimers, which are further aligned in an end-to-end fashion to form helical aggregates. This work is important because it not only showed that cyanine dyes could be effective photocleavage agents for DNA but also present a good example of supramolecular helical assembly of achiral molecules.

In a previous report[96] we demonstrated that the complex $[Ru(bpy)_2(dppz)]^{2+}$ binds to the helical conformation of *m*PPE-SO_3^- via intercalation of the dppz ligand into the π-stack of the adjacent phenylene ethynylene units. Intercalation of $[Ru(bpy)_2(dppz)]^{2+}$ within the polymer helix is signaled by the appearance of the strong orange-red photoluminescence characteristic of the intercalated form of the complex.

In the present investigation we have explored the interaction of ***w*-P2** with $[Ru(bpy)_2(dppz)]^{2+}$ and the cationic cyanine dye HMIDC (Figure 2-10) in order to determine if these dyes will interact with the polymer via intercalation and/or groove-binding, and if so, if the chiral environment of the polymer helix will give rise to a CD transition for the intercalated dye.

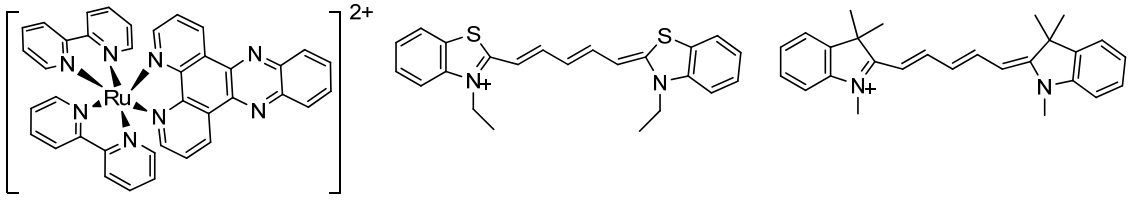

$[Ru(bpy)_2(dppz)]^{2+}$ $DiSC_2(5)$ HMIDC

Figure 2-10. Chemical structures of the organic dyes.

Intercalation of $[Ru(bpy)_2(dppz)]^{2+}$

First, we examined the effect of addition of ***w*-P2** on the photoluminescence of the cationic metallo-intercalator $[Ru(bpy)_2(dppz)]^{2+}$. As shown in Figure 2-11, in aqueous solution alone $[Ru(bpy)_2(dppz)]^{2+}$ (c = 15 μM) does not display any photoluminescence. The intensity of the photoluminescence increases very sharply over the polymer concentration range 0 – 50 μM, and then it increases more slowly until it saturates at [***w*-P2**] ≈ 150 μM (concentrations in polymer repeat units). This stoichiometry suggests that the "binding site size" for the intercalated metal complex is approximately three ***w*-P2** repeat units; moreover, since one turn of the helix requires *ca*. 6 polymer repeat units, this corresponds to two metal complexes bound per turn of the helix (e.g., one on either side as shown in Figure 2-12). Addition of polymer above the 50 μM level leads to an additional, but less pronounced increase in the $[Ru(bpy)_2(dppz)]^{2+}$ photoluminescence. The additional increase in emission intensity is likely due to a small increase in the number of bound complexes, but more importantly due to tighter intercalation of the complexes as they are able to bind less densely on the ***w*-P2** helix, as illustrated in Figure 2-12.

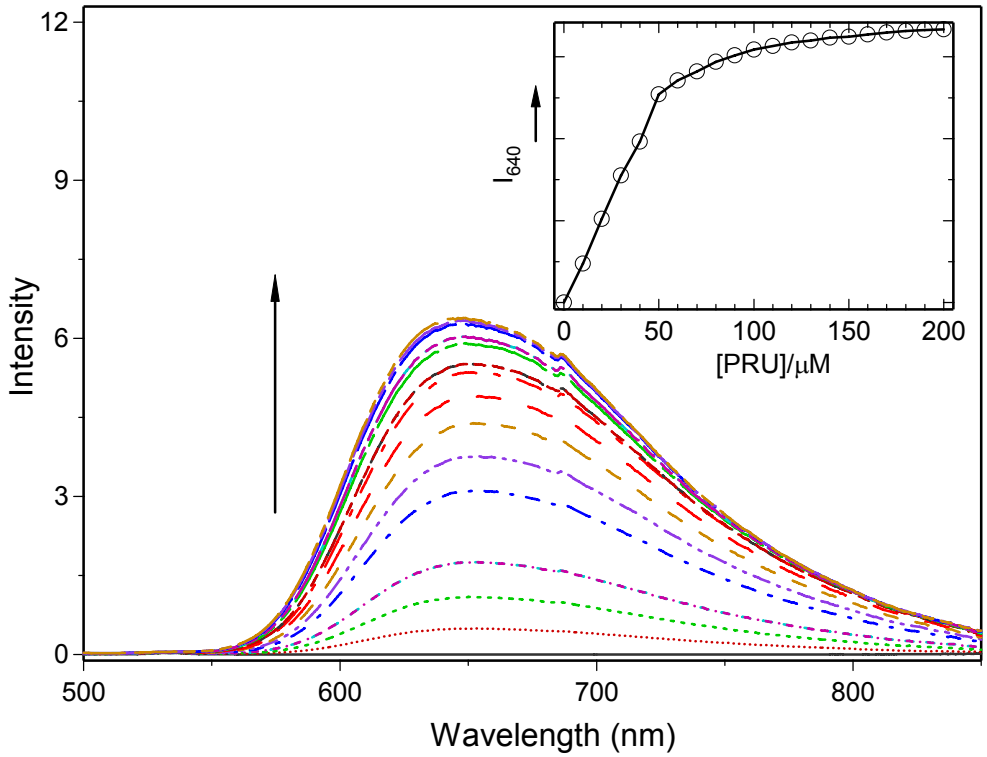

Figure 2-11. Emission spectra of $[Ru(bpy)_2(dppz)]^{2+}$ in the absence (solid black line) and presence of ***w*-P2** (concentration of ***w*-P2** ranges from 0 - 120 μM polymer repeat units, excitation wavelength is 450 nm). Solutions are deoxygenated by argon bubbling. The inset illustrates the variation of $[Ru(bpy)_2(dppz)]^{2+}$ emission intensity at 640 nm with increasing concentration of ***w*-P2**.

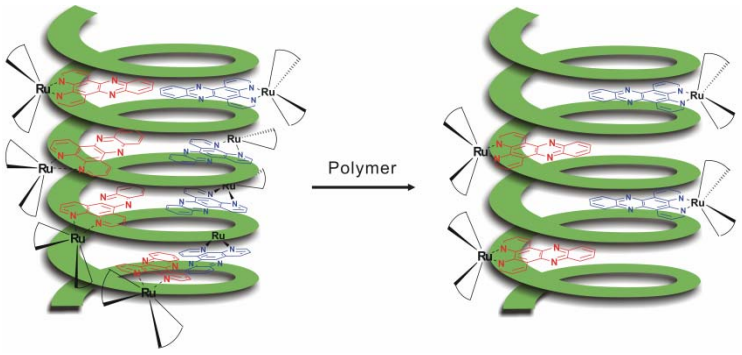

Figure 2-12. Schematic representation of the interaction between ***w*-P2** and $[Ru(bpy)_2(dppz)]^{2+}$.

An aqueous solution that contained 100 μM ***w*-P2** and 15 μM $[Ru(bpy)_2(dppz)]^{2+}$ was explored by using circular dichroism spectroscopy. This solution exhibited the near-UV

bisignate CD signal characteristic of the helical polymer, however, no CD was observed in the 400 – 500 nm region which corresponds to the metal-to-ligand charge transfer absorption (MLCT) of the metal complex. This finding indicates that the chiral environment provided by the helix is insufficient to induce a CD signal in the MLCT transition localized on the metal complex chromophore.

Groove binding of cyanine dyes

UV-Vis absorption

In a previous research,[126] we have shown that a *para*-linked CPE, PPE-SO_3^- could template the formation of *J*-aggregate of HMIDC when the polymer existed in the "aggregate state". Here, we explored the effect of addition of *meta*-linked CPE on the optical spectroscopy of two cationic cyanine dyes HMIDC and $DiSC_2(5)$ (Figure 2-10). In general, similar results were obtained for both dyes, so only results for the former dye are presented herein. Data for $DISC_5(5)$ interacting with ***w*-P2** is provided in the Appendix. In aqueous solution HMIDC features an absorption band due to the π,π^* transition of the polymethine chromophore at $\lambda_{max} \approx$ 635 nm. As shown in Figure 2-13, addition of ***w*-P2** to the aqueous solution of HMIDC induces significant changes in the dye's absorption. In particular, as ***w*-P2** is added, the 635 nm absorption decreases, and it is replaced by a red-shifted absorption at 660 nm. The red-shift of the HMIDC absorption upon addition of ***w*-P2** clearly signals that the dye binds to the polymer helix. A plot of the HMIDC absorbance at 660 nm as a function of the polymer:dye molar ratio reveals that dye binding is 80% complete at a 1:1 stoichoimetry and it is saturated at a ratio of *ca.* two ***w*-P2** repeat units per HMIDC (Figure 2-13 inset). The nearly stoichiometric binding ratio suggests that the dye-polymer interaction is driven by electrostatics (ion-pairing), and supports the notion that HMIDC binds to the periphery of the ***w*-P2** helix (i.e., "groove binding").

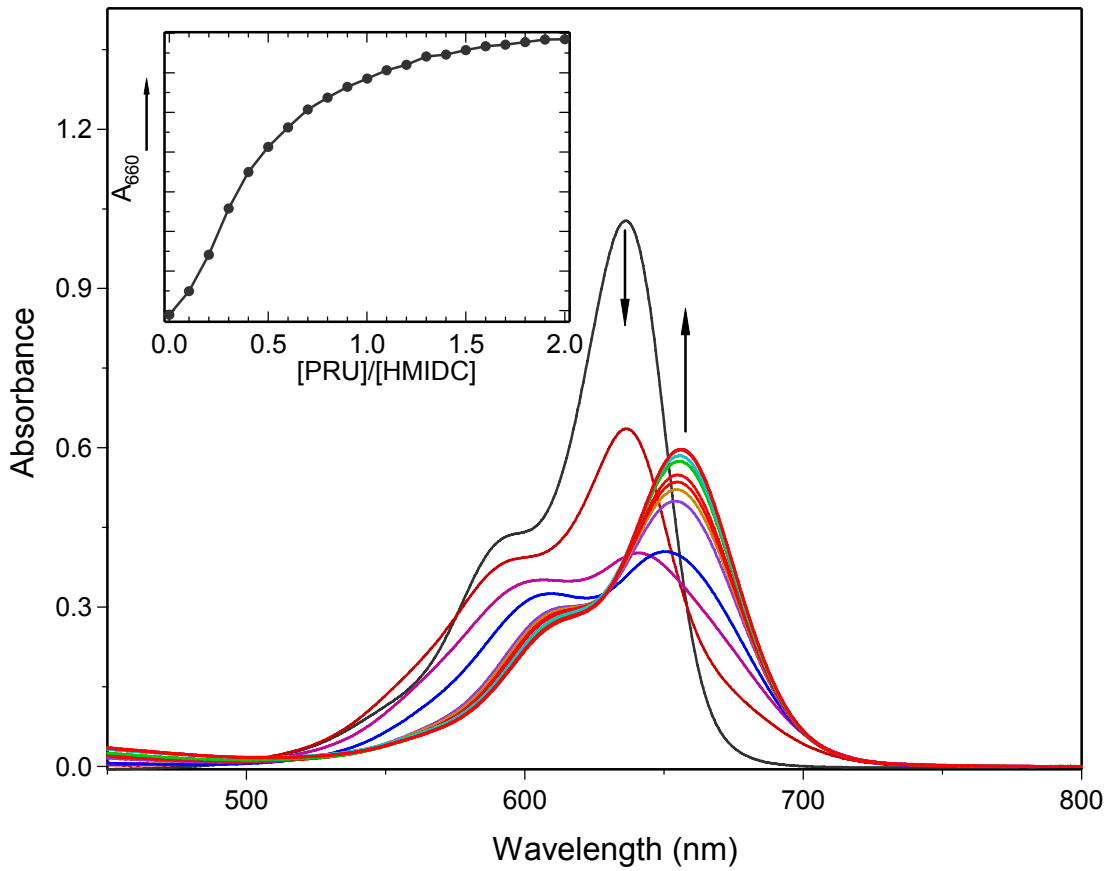

Figure 2-13. UV-Visible absorption of HMIDC in water (c = 5 μM) titrated with ***w*-P2**. Concentration range of ***w*-P2** is 0 – 5.0 μM polymer repeat units, in 0.5 μM increments. Arrows show direction of change of spectrum with increasing polymer concentration.

Fluorescence spectroscopy

Addition of ***w*-P2** to HMIDC also elicits changes in the dye's fluorescence. As shown in Figure 2-14, addition of ***w*-P2** to an aqueous solution of HMIDC leads to a decrease in the fluorescence from the free dye (λ_{em} = 667 nm), with concomitant appearance of a red-shifted fluorescence with $\lambda_{max} \approx$ 685 nm. Interestingly, the fluorescence of the free dye is completely quenched at relatively low polymer:dye ratio. This suggests that most of the HMIDC is bound to the polymer even at low polymer concentration, and that energy transfer occurs to the fully groove-bound dyes which emit at longer wavelength.

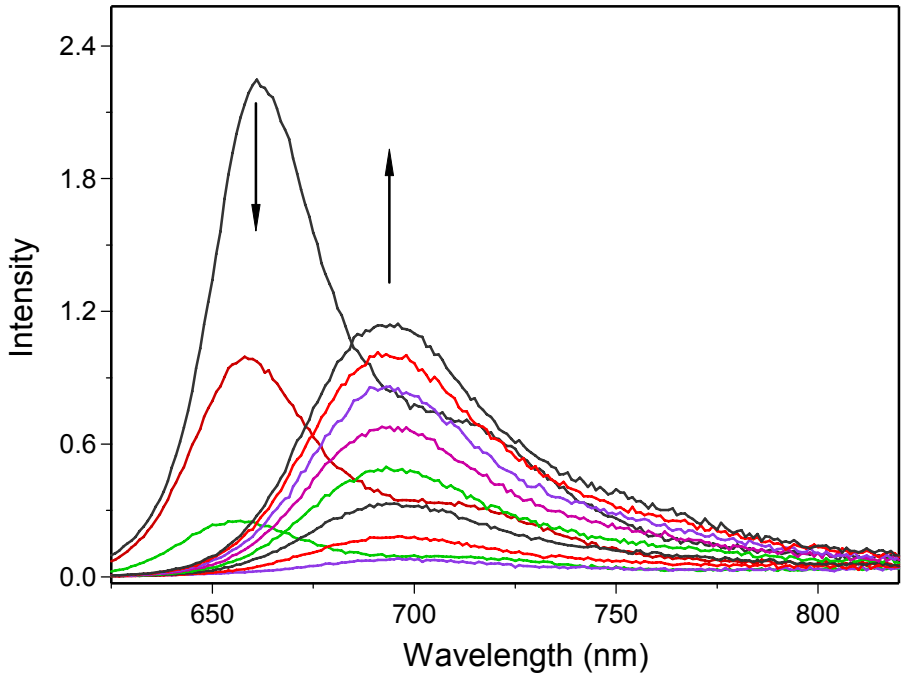

Figure 2-14. Fluorescence spectra of HMIDC (c = 5.0 μM) in water titrated with ***w*-P2**, excitation wavelength is 610 nm. Concentration range of ***w*-P2** is 0 – 5.0 μM polymer repeat units, in 0.5 μM increments. Arrows show direction of change of spectrum with increasing polymer concentration.

Circular dichroism spectroscopy

Figure 2-15 illustrates the circular dichroism spectrum obtained for solutions that contain HMIDC only (c = 7 μM) or HMIDC and ***w*-P2** (c = 7 μM and 10 μM, respectively). As expected, HMIDC alone features no CD signal; however, the polymer-HMIDC mixture features a distinct unsymmetrical, bisignate CD signal in the region corresponding to the absorption of the polymer-bound dye. Although the bisignate signal is unsymmetrical, we believe that it arises due to exciton coupling within a chiral, dye-chromophore aggregate that is formed as the dye molecules are oriented by the helical ***w*-P2** "template". Figure 2-16 shows an idealized model for this structure. Individual HMIDC molecules bound within the ***w*-P2** "groove" are oriented by the helical turn of the polymer. The individual HMIDC molecules are thus oriented relative to

one another such that the dipole-dipole coupling between them will follow a helical path, which affords the condition necessary for the exciton-coupled CD signal to be observed.

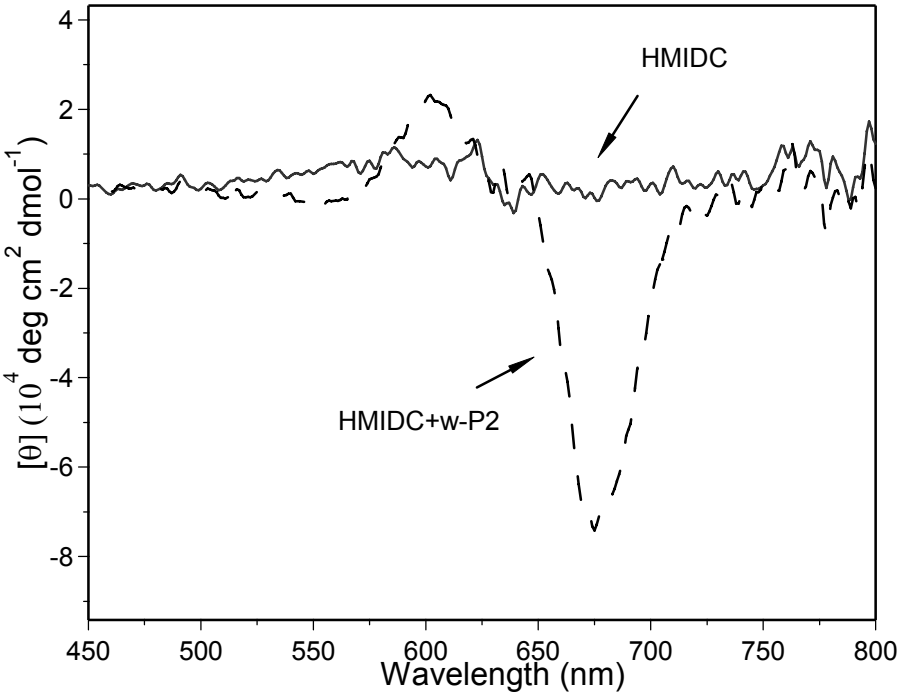

Figure 2-15. Circular dichroism spectra of HMIDC (c = 7.0 μM) alone and HMIDC with ***w*-P2** (c = 7 μM and 10.0 μM, respectively) in aqueous solution.

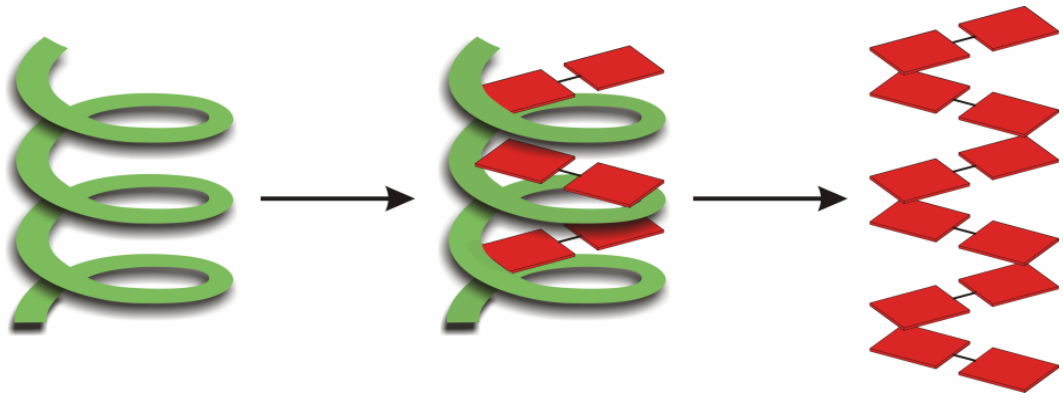

Figure 2-16. Schematic representation of the interaction between ***w*-P2** and HMIDC.

The importance of polymer helix to template the formation of HMIDC aggregates was further confirmed by the results of titration of ***w*-P2** into the methanol solution containing HMIDC. As seen from Figure 2-17, there is only a slight change of intensity in the absorption and emission spectrum of HMIDC with the addition of ***w*-P2**, indicating that the polymer helical conformation is crucial to the "groove binding" of HMIDC to form the chiral dye aggregates.

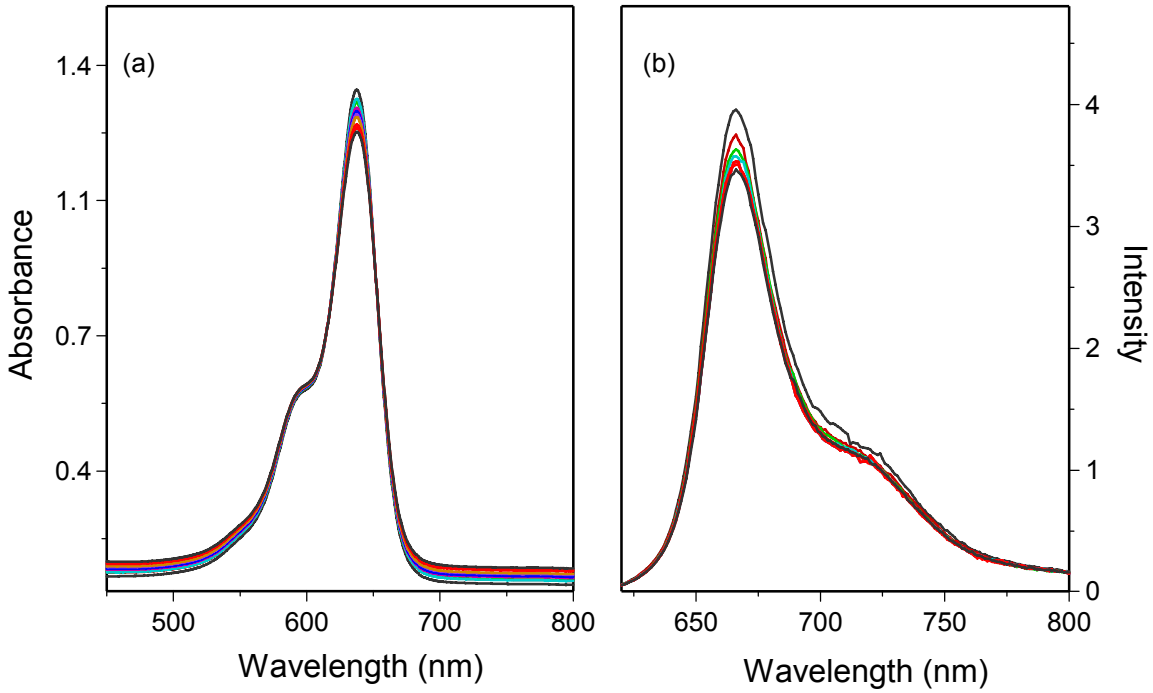

Figure 2-17. UV-Vis absorption (a) and fluorescence emission spectra (b) of HMIDC in methanol with titrations of ***w*-P2**. Fluoresence emission spectra were measured with excitation wavelength at 610 nm. [HMIDC] = 5.5 μM. ***w*-P2** solution was added in 0.5 μM aliquots, ranging from 0 to 6 μM.

Experimental

Materials

Palladium catalysts were used as received from Strem Chemical Co. Triethylamine and THF and CH_2Cl_2 were purified by distillation over sodium hydride. *N,N*′-Diisopropylcarbodiimide (DIPC) was bought from Aldrich Chemical Co. Anhydrous DMF was used as supplied by Acros Chemical Company. The cyanine dyes HMIDC, $DiSC_2(5)$ were

obtained from Acros and they were used as received. 4-(Dimethylamino)pyridinium 4-toluenesulfonate (DPTS),[105] 1,4-Diethynylbenzene were synthesized following the literature.[106] The ruthenium (II) complex $[Ru(bpy)_2(dppz)]^{2+}$ was synthesized from $RuCl_3 \cdot xH_2O$ in two steps.[127,128] All other chemicals were purchased from either Acors or Aldrich chemical Company and used as received.

Instrumentation

NMR spectra were recorded on a Varian VXR-300 FT-NMR, operating at 300 MHz for ^{1}H-NMR and at 75.4 MHz for ^{13}C-NMR. Chemical shifts were reported in ppm using $CHCl_3$ or C_2HD_5SO as internal reference. FTIR spectra were taken on a Perkin-Elmer 1600 spectrometer. Gel permeation chromatography (GPC) analyses were carried out on a system comprised of a Rainin Dynamax SD-200 pump and a Beckman Instruments Spectroflow 757 absorbance detector. UV-visible absorption spectra were obtained on Varian Cary 100 dual beam spectrophotometer, with a scan rate of 300 nm/min. Steady-state fluorescence spectra were recorded on a SPEX Fluorolog-2 or a SPEX Fluorolog-3 fluorescence spectrometer. Emission spectra were collected at 90 ºC relative to excitation. 1 cm square quartz cuvette were used for both absorption and emission measurements. CD spectra were recorded on an Aviv model 202 CD spectrometer, with temperature set at 25 ºC using 1-cm rectangular quartz cells.

General Methods

For optical measurements on polymer solutions, the reported concentrations refer to the concentration of polymer repeat units. Solutions for spectroscopic studies were prepared by dilution of stock solutions. Titrations were carried out by adding microliter aliquots of stock solutions to the sample solution that was contained in a quartz optical cuvette. Luminescence studies on $[Ru(bpy)_2(dppz)]^{2+}$ were carried out on samples that had been deoxygenated by bubbling with argon for 20 minutes.

Synthetic Procedures

3,5-Diiodobenzoic acid (2).[104] To an ice-cooled, stirred suspension of 3,5-diaminobenzoic acid (6.0 g, 39.5 mmol) in 90 ml of sulfuric acid and water (v/v = 2/1) mixture, sodium nitrite powder (6.5 g, 94 mmol) was added with the temperature controlled between -5 °C – 0 °C. After 1 h, urea (0.50 g, 8.3 mmol) was added, and then a cold solution of Potassium Iodide (65.6 g, 395 mmol) in 60 ml water was added drop by drop. An additional 3 hr was allowed to react before the reaction mixture was heated up. Then the warm suspension was poured into 300 ml ice-cold water and the brown precipitate was collected by vacuum filtration, dried and extracted using diethyl ether. The obtained dark brown diethyl ether solution was washed with $Na_2S_2O_3$ water solution until a pale yellow color was observed. After diethyl ether was removed *in vacuo*, the resulting yellow solid was purified by recrystallization from toluene. Yield: 9.6 g (65%). ^{1}H NMR (DMSO-d_6): δ = 8.30 (s, 1H, 4-H), 8.17 (s, 2H, 2, 6-H). ^{13}C NMR (DMSO-d_6): 165.35, 148.88, 137.68, 134.99, 96.84.

(S)-Benzyl 2-(3,5-diiodobenzamido)propanoate (3). 3, 5-diiodobenzoic acid (1.3 g, 3.5 mmol) was dissolved in 10 ml DMF, then 1.2 g DPTS (4.1 mmol) was added. Heat was applied to dissolve all the materials, and during the dissolution, 5 ml more DMF was added to the mixture. 0.59 g L-alanine benzyl ester (3.3 mmol) was added to the clear solution. Then DIPC (0.57 g, 4.6 mmol) was added, and the reaction was allowed to stir for 12 hr. The reaction was diluted with CH_2Cl_2, washed three times with H_2O and concentrated *in vacuo*. Flash chromatograph using CH_2Cl_2/hexane (v/v = 7:3) as the eluent afforded the pure product as a white solid. Yield: 1.2 g (64%), mp 143-144 ºC. ^{1}H NMR ($CDCl_3$, δ_{ppm}): 1.52 (d, 3H), 4.80 (q, 1H), 5.23 (d, 2H), 6.79 (d, 1H), 7.38 (m, 5H), 8.05 (s, 2H), 8.20 (s, 1H). ^{13}C NMR ($CDCl_3$, δ_{ppm}): 18.68, 48.99, 67.73, 95.03, 128.42, 128.83, 128.93, 135.30, 135.55, 137.39, 148.32, 164.01, 173.01. HR-MS (EI): Calcd for $C_{17}H_{16}I_2NO_3$ [M+H$^+$] 535.9214, found

535.9229. Elemental analysis: Calcd for $C_{17}H_{15}I_2NO_3$: C, 38.16; H, 2.83; N, 2.62. Found: C, 37.97; H, 2.51; N, 2.61. FT-IR (ν_{max}, KBr pellet): 3258, 3056, 2980, 1760, 1732, 1637, 1627, 1533, 1450, 1384, 1348, 1278, 1207, 1140, 1126, 1049, 959, 912, 861, 752, 696, 667.

(**S)-Benzyl 2-(3,5-bis((trimethylsilyl)ethynyl)benzamido)propanoate (4).** A solution of compound **3** (1.3 g, 2.4 mmol) in 20 ml dry THF/Et_3N (v/v = 2/1) was degassed for 15 minutes using argon. Then 50.5 mg $Pd(PPh_3)_2Cl_2$ (72 μmol) and 27.4 mg of CuI (144 μmol) was added into the solution under the protection of argon, followed by the addtion of 3 ml of trimethlysilylacetylene (21.3 mmol). The resulting mixture was stirred at room temperature for 3 hr. The brown suspension was filtrated and the filtrate was concentrated *in vacuo*. The residue was loaded on a silica column and eluted with a mixture of CH_2Cl_2/hexane (3/2) affording a yellow oil (yield: 0.85 g, 74%). ^{1}H NMR ($CDCl_3$, δ_{ppm}): 7.79 (d, 2H), 7.68 (t, 1H), 7.38 (s, 5H), 6.68 (d, 1H), 5.22 (d, 2H), 4.82 (q, 5H), 1.53 (d, 3H), 0.25 (s, 18H).

(S)-Benzyl 2-(3,5-diethynylbenzamido)propanoate (5). The yellow oil obtained as above (0.85 g, 1.8 mmol) was dissolved in 20 ml THF. The solution was acidified by adding 0.5 ml acetic acid before adding tetrabutylammonium fluoride (1M in THF, 5 ml). After stirred at room temperature for 30 minutes, the reaction mixture was diluted with 40 ml diethyl ether, then washed with 1 M HCl (60 ml × 1), aqueous $NaHCO_3$ (60 ml × 1) and water (60 ml × 1), then dried with $MgSO_4$. After the solvent was removed *in vacuo*, the crude product was purified by flash chromatography (silica gel, eluent: CH_2Cl_2/hexane = 9:1) to afford 0.51 g of **5** (yield: 86%). ^{1}H NMR ($CDCl_3$, δ_{ppm}): 7.86(d, 2H), 7.71(t, 1H), 7.39 (s, 5H), 6.79 (d, 1H), 5.21 (d, 2H), 4.82 (q, 1H), 3.14 (s, 2H), 1.53 (d, 2H).

3,5-Diiodobenzoyl chloride (6). Compound **2** (2.0 g, 5.3 mmol) and 5 ml thionyl chloride were placed in a 50 ml round bottom flask fitted with a condenser with a bubbler. The

suspension was heated at reflux for 30 minutes, at which time no more gas evolution was observed. Then the excess $SOCl_2$ was removed by vacuum distillation, the resulting residue was purified by crystallization from hexane. A white powder was obtained (yield: 1.6 g, 77%). ^1H NMR ($CDCl_3$, δ_{ppm}): 8.38 (d, 2H), 8.36 (t, 1H).

(S)-*tert*-Butyl 2-(3,5-diiodobenzamido)propanoate (7). A solution of L-alanine benzyl ester•HCl (1.04 g, 4.8 mmol) in 20 ml CH_2Cl_2 was added 0.62 g of 4-dimethylaminopyridine (5.0 mmol). Then 942 mg of **6** (2.4 mmol) was added. After 30 minutes, the solvent was removed *in vacuo*. The crude product was purified by flash chromatography (silica gel, eluent: CH_2Cl_2) to afford 1.13 g white wax-like product (yield: 94%). ^1H NMR ($CDCl_3$, δ_{ppm}): 8.18 (t, 1H), 8.07 (d, 2H), 6.73(d, 1H), 4.63 (q, 1H), 1.40 (s, 9H), 1.35 (d, 3H). ^{13}C NMR ($CDCl_3$, δ_{ppm}): 172.67, 163.94, 148.40, 137.82, 135.72, 95.21, 83.09, 49.67, 28.47, 19.18. LR-MS: Calcd for $C_{14}H_{17}I_2NO_3$ [M^+] 501 found 501.

(S)-Benzyl 2-(3,5-bis(phenylethynyl)benzamido)propanoate (8a). A solution containing 1 g of 3 (1.8 mmol), 0.95 g of phenylacetylene (93 mmol), 62 mg of tetrakis(triphenylphosphine)Palladium (54 μmol), 12 mg of copper(I) iodide (32 μmol) in 10 ml of a mixture of a THF/Et_3N was stirred at room temperature for 6 hr under argon. Then the solution was filtrated, the solvent was removed under reduced pressure, and the remaining solid was purified by flash chromatography. The product was isolated as a white solid, 0.79 g (91%), mp 180-181 ºC. ^1H NMR ($CDCl_3$, δ_{ppm}): 7.91 (d, 2H), 7.83 (t, 1H), 7.56 (m, 4H), 7.39 (m, 11H), 6.80 (d, 1H), 5.15 (t, 2H), 4.87 (q, 1H), 1.56 (d, 3H). ^{13}C NMR ($CDCl_3$): 173.15, 165.64, 137.33, 135.44, 134.80, 131.97, 129.89, 128.97, 128.92, 128.78, 128.68, 128.43, 124.57, 122.84, 91.26, 87.85, 67.65, 48.97, 18.84. FT-IR (ν_{max}, KBr pellet): 3435, 3278, 3056, 2932, 2210, 1736,

1645, 1599, 1543, 1490, 1452, 1409, 1387, 1348, 1312, 1224, 1151, 1109, 1071, 1027, 1109, 1071, 1027, 953, 910, 878, 754, 687.

(S)-*tert*-Butyl 2-(3,5-bis(phenylethynyl)benzamido)propanoate (8b). Compound **7** (0.6 g, 1.2 mmol) was dissolved in 12 ml of dry THF/Et_3N (3/1) and degassed with argon for 15 minutes. Then $Pd(PPh_3)_4$ (83 mg) and CuI (27 mg) were added to the solution, followed by the addition of 0.6 ml of phenylacetylene (5.5 mmol). The resulting mixture was slowly heated to 65 °C and stirred for 13 hr. After filtration, the solvent was removed *in vacuo*. The crude product was purified by flash chromatography (silica gel, eluent: CH_2Cl_2/hexane = 4/1). ^1H NMR ($CDCl_3$, δ_{ppm}): 7.92 (d, 2H), 7.82 (t, 1H), 7.55 (m, 4H), 7.39 (m, 6H), 4.69 (q, 1H), 1.52 (m, 12H). LR-MS: Calcd for $C_{30}H_{27}NO_3$ [M^+] 449 found 449.

Sodium (S)-2-(3,5-bis(phenylethynyl)benzamido)propanoate (9). Method 1: A solution of 0.2 g of **8a** in 5 ml DMF was added 5 ml 1 M NaOH solution, then left at room temperature under stirring for 15 minutes. Then the solvent was removed under reduced pressure, the residue was washed with CH_2Cl_2, acetone, cold water. Further purification could be applied by recrystallization from H_2O/MeOH (v/v = 7/3). 0.15 g white solid was obtained (yield: 87%). Method 2: Compound **8b** (0.5 g, 1 mmol) was dissolved in 5 ml CH_2Cl_2 and cooled down to 0 °C. Trifluoroacetic acid (TFA) (5 ml) was added drop-wise into the solution. After finishing the addition, the reaction mixture was allowed to warm to room temperature and stirred further for 2 hr. The solvent was removed *in vacuo*. The residue was dissolved in 20 ml DMF/H_2O (v/v = 1/1) and added 106 mg of Na_2CO_3. The solution was stirred at room temperature for 5hrand then precipitated into 200 ml of acetone. The product was isolated as a white solid. ^1H NMR (DMSO-d_6, δ_{ppm}): 8.27 (d, 1H), 7.99 (d, 2H), 7.86 (t, 1H), 7.61 (m, 4H), 7.45 (m, 6H), 4.05 (q, 1H), 1.30 (d, 3H). ^{13}C NMR (DMSO-d_6, δ_{ppm}): 175.29, 163.63, 136.89, 136.36, 132.26,

130.47, 129.88, 129.50, 123.83, 122.48, 91.27, 88.48, 51.18, 19.68. FT-IR (ν_{max}, KBr pellet): 3411, 3307, 3080, 3064, 2989, 2939, 2212, 1624, 1599, 1586, 1532, 1491, 1456, 1442, 1407, 1365, 1284, 1174, 1154, 1101, 1070, 1027, 958, 913, 886, 840, 757, 691, 670.

4-(Dimethylamino)pyridinium 4-Toluenesulfonate (DPTS) (10).[105] A 50 ml solution of 4-dimethylaminopyridine (2 N) was added slowly into a 50 ml solution of p-toluenesulfonic acid monohydrate (2 N) at room temperature under stirring. The resulting white precipitate was collected, washed with 100 ml of THF and dried under vacuum. ^{1}H NMR (DMSO-d_6): 8.22 (d, 2H), 7.50 (d, 2H), 7.14(d, 2H), 7.00 (d, 2H), 3.18 (d, 6H), 2.29 (s, 3H).

1,4-Bis((trimethylsilyl)ethynyl)benzene (11).[106] 1,4-Diiodobenzene (18.0 g, 54.6 mmol) was dissolved in 200 ml of THF/HN(i-Pr)$_2$ (4/1) in a Schlenk flask and degassed with argon for 30 minutes. The solution was cooled down to 5°C using an ice/water bath. Then 400 mg of $Pd(PPh)_2Cl_2$ (0.57 mmol) and 100 mg of CuI (0.53 mmol) were added, followed by the addition of 20 ml of trimethylsilylacetylene (141.8 mmol) via a syringe. A thick precipitate formed immediately (ensure efficient stirring!). After half an hour, the reaction mixture was allowed to warm to room temperature and stirred overnight. After filtering through a bed of celite, the solvent was removed *in vacuo*. The brown crude product was dissolved in a large amount of hexane and filtrated through a short plug of silica. Recrystallization from ethanol afforded a white flake crystalline product (yield: 10.4 g, 74%). ^{1}H NMR ($CDCl_3$, δ_{ppm}): 7.40 (s, 4H), 0.25 (s, 18H).

1,4-Diethynylbenzene (12). Compound **11** (2.0 g, 7.4 mmol) was dissolved in a minimum of dioxane (~ 20 ml) in a 250 ml beaker and acidified with 1 ml acetic acid. Then 18 ml of tetrabutylammonium fluoride (18 mmol) was added drop-wise. After 30 minutes, the volume of the solution was reduced to around 20 ml by flowing nitrogen above the surface. Then 200 ml of

H_2O/MeOH (9/1) was added to the reaction mixture. The product precipitated as a white solid and was collected on a büchnel funnel, washed with 50 ml of H_2O/MeOH (v/v = 9/1), dried in a desiccator loaded with 10 g of anhydrous $CaCl_2$. The dry product is usually pure enough for polymerization, but further purification could be done by dissolving in hexane and passing through a short plug of silica to improve the quality of the product. ^{1}H NMR ($CDCl_3$, δ_{ppm}): 7.45 (s, 4H), 3.18 (s, 2H).

$[Ru(Bpy)_2]Cl_2$ (13).[127] Commercial $RuCl_3 \cdot xH_2O$ (2.45 g, 11.8 mmol), bipyridine (3.75 g, 24 mmol) and LiCl (2.6 g, 61.5 mmol) were heated at reflux in 15 ml reagent grade DMF for 8 h. The reaction mixture was allowed to cool to room temperature, and then 100 ml cold acetone was added, the resulting suspension was kept in a refrigerator overnight. The purple solid was collected by vacuum filtration, washed with H_2O (20 ml × 3), cold acetone (20 ml × 3), diethyl ether (20 ml × 3), and then dried on the büchnel funnel by pulling with an aspirator. The obtained green-black solid was used for next step reaction without further purification.

$[Ru(bpy)_2(dppz)](BF_4)_2$ (14).[128] A mixture of $[Ru(bpy)_2]Cl_2$ (200 mg, 0.39 mmol) and dipyridophenazine (130 mg, 0.46 mmol) in 50 ml of MeOH/H_2O (v/v = 1/2) was heated at reflux for 4 hr. At that time, the original dark heterogeneous solution became red and clear. This solution was evaporated to 10% of its original volume then diluted with 30 ml H_2O and boiled for 10 minutes. After the solution was slowly cooled down using an ice-water bath, the formed pale yellow precipitate was removed by filtration. The clear red filtrate was treated with 5 ml 10% $NaBF_4$ solution. The orange precipitate was collected by vacuum filtration. After dried on the büchnel funnel for 2 hr, the precipitate was crystallized from absolute ethanol. ^{1}H NMR (Acetone-d_6, δ_{ppm}): 9.79 (d, 2H), 8.89 (t, 4H), 8.51 - 8.58 (m, 4H), 8.09 - 8.31 (m, 12H), 7.67 (t, 2H), 7.43 (t, 2H).

Polymerization Procedures

P1. (S)-benzyl 2-(3,5-diiodobenzamido)propanoate (**3**) (323 mg, 0.60 mmol) and (S)-benzyl 2-(3,5-diethynylbenzamido)propanoate (**5**) (200 mg, 0.60 mmol) were dissolved in 1 ml DMF/Et_3N (v/v = 3/1) and degassed with argon for 30 minutes. Another degassed solution containing 34.6 mg of $Pd(PPh_3)_4$ (30 μmol) and 5.7 mg of CuI (30 μmol) in 1 ml DMF/Et_3N (3/1) was added to the former solution via a syringe. The resulting mixture was heated to 70 °C and stirred for 24 hr. GPC (THF, polystyrene standards): M_w = 1,680, M_n = 1,550, PDI = 1.10.

P2. (S)-benzyl 2-(3,5-diiodobenzamido)propanoate **(3)** (535 mg, 1mmol) and 1,4-diethynyl-benzene **(12)** (126 mg, 1mmol) were dissolved in 10 ml of dry THF/Et_3N (v/v = 3:1) solution using a Schlenk flask and degassed for 30 minutes. Then 57.7 mg $Pd(PPh_3)_4$ (50 μmol) and 9.5 mg CuI (50 μmol) powder were added under the protection of Argon. The resulting solution was stirred at room temperature for 24 hr, and then poured into a large volume of methanol. The polymer precipitated as a yellow fine powder and it was further purified by several steps of dissolution in DMF followed with precipitation from methanol and acetone. Yield: 71%. GPC (THF, Polystyrene standards): M_w = 23,660, M_n = 12,710, PDI = 1.80. ^1H NMR (DMSO-d_6, δ_{ppm}): 9.11 (br, d, 1H), 8.10 (br, m, 2H), 7.95 (br, m, 1H), 7.68 (br, m, 4H), 7.36 (br, m, 6H), 5.16 (br, s, 2H), 4.58 (br, m, 1H), 1.45 (br, d, 3H).

P3. (S)-*tert*-butyl 2-(3,5-diiodobenzamido)propanoate **(7)** (501 mg, 1 mmol) and 1,4-diethynyl-benzene (**12**) (126 mg, 1 mmol) were dissolved in 5 ml dry THF/Et_3N (v/v = 3/1) mixture. The resulting solution was degassed with argon for 15 minutes. Another degassed solution containing 69 mg of $Pd(PPh_3)_4$ (60 μmol) and 23 mg of CuI (120 μmol) in THF/Et_3N (v/v = 3/1) was added to the former solution via a syringe. The resulting mixture was heated to 70 °C and stirred for 5 hr. The polymer was isolated as a yellow solid by precipitating into 400

ml of methanol and further purified by 2 cycles of dissolution in THF followed with precipitation from methanol. Yield: 72%. GPC (THF, polystyrene standards): M_w = 125,490, M_n = 39,510, PDI = 3.10.

Hydrolysis of the Neutral Polymers.

Method 1: **P2** (250 mg, 0.6 mmol) was dissolved in 30 ml of DMF, and then 10 ml of 1 N NaOH solution was added drop-wise. The resulting solution was stirred at room temperature. During the course of the polymer hydrolysis, a few drops of water were systematically added in order to keep the polymer in solution. After 30 minutes, the mixture was poured into 500 ml of methanol/acetone/ether (v/v/v = 1:4:5) mixture. The polymer precipitated as a light yellow solid. **Method 2**: **P3** (260 mg, 0.7 mmol) was dissolved in 30 ml CH_2Cl_2 and cooled down in an ice/water bath. 30 ml of trifluoroacetic acid (TFA) was added to the polymer solution drop-wise. Upon the completion of the addition, the reaction mixture was allowed to warm to room temperature and stirred for another 16 hr. The excess TFA and the solvent were removed *in vacuo*. The residue was treated with aqueous Na_2CO_3 solution (10 ml, 20%). After 6 hr, the solution was poured into 200 ml of acetone; the polymer precipitated as a yellow solid and was isolated by centrifuge. Final purification of the polymer was accomplished by dialysis of aqueous solution of the polymer against ultrapure water (Millipore Simplicity Water System) and using a 12 kD molecular weight cut-off (MWCO) cellulose membrane (Fisher Scientific). After dialysis, the polymer solution was filtered through a nylon membrane (pore size: 0.8 μm). The polymer was stored in this format and diluted as appropriate for spectroscopic studies. ^{1}H NMR (DMSO-d_6, δ_{ppm}): 8.05-8.10 (br, m, 1H), 8.00 (s, 2H), 7.75 (s, 4H), 4.0-4.08 (br, m, 1H), 1.24 (d, 3H).

CHAPTER 3
POLY(PHENYLENE ETHYNYLENE) CARBOXYLATE

Introduction

In a previous work,[71,126] we reported the synthesis of poly(phenylene ethynylene) (PPE) carrying sulfonate solubilizing groups. The polymer was synthesized in a direct fashion that the monomer carrying sulfonate and the other organic monomer were dissolved in an aqueous mixture of DMF/H_2O/i-Pr_2NH (3/2/1) and polymerized in the presence of a catalytic amount of $Pd(PPh_3)_4$ and CuI. Polymers prepared following this strategy are soluble in polar solvents, such as water, DMF and DMSO. Using techniques such as viscometry, ultrafiltration and pulsed field gradient NMR, the molecular weights of these polymers were estimated.[96,126] However, characterization of the molecular weights of such-prepared polymers using gel permeation chromatography (GPC) was unsuccessful, probably due to the strong aggregation tendency of this type of polymers. In addition to such a direct approach to prepare conjugated polyelectrolytes, another method involves the polymerization of monomers in which the ionic groups are protected; the ionic groups are produced in a subsequent reaction that is carried out on the polymer. [53,129] The precursor polymers obtained by this method are typically soluble in organic solvents such as THF, $CHCl_3$, which enables the determination of the molecular weights of these polymers by GPC.

As one of the most common ionic groups, carboxylate could be protected as carboxylic acid ester in various forms, such as methyl ester, ethyl ester, oxazoline ester, etc.[130] The ester groups can be cleaved quantitatively using either acid or base methodologies. Most interestingly, carboxylate group shows the ability to selectively bind some di- or trivalent metal ions to form coordination complexes. Conjugated polymers containing pendant carboxylate groups have been reported. For example, McCullough and co-workers synthesized regioregular

polythiophenes with carboxylate side groups and studied their ionchromatic sensing in water.[81,131] Also the association between carboxylate group and Ga^{3+} was used to develop highly sensitive assays for kinase and phosphatase based on conjugated polyelectrolyte-coated polystyrene microspheres.[132]

In the present chapter, we report the synthesis of monomers carrying carboxylic dodecyl ester groups. Two water-soluble PPEs were prepared by organic phase polymerization and subsequent base-promoted hydrolysis. These two PPEs share the same backbone structure (phenylene-ethynylene) but differ in the carboxylate substitution pattern. One contains two carboxylate side chains per repeat unit (one phenylene-ethynylene) and the other contains two carboxylate side chains for every two repeat units. The photophysical properties of these two CPEs were compared to each other and to those of PPE-SO_3^-. In the second part, the interaction between the latter polymer and 9 different divalent metal ions was studied in methanol (MeOH) and 4-(2-hydroxyethyl)-1-piperazine-1-ethanesulfonic acid (HEPES) buffer solution. Quenching of the polymer fluorescence by organic ions, such as methyl viologen (MV^{2+}) in MeOH was also studied. To the end, a fluorescence turn-on sensor that is highly selective and sensitive to pyrophosphate (PPi) was developed using a CPE-metal ion system.

Results and Discussion

Synthesis

The monomer that carries carboxylic dodecyl esters, didodecyl-2,2'-(2,5-diiodo-1,4-phenylene)bis(oxy)diacetate (**8**) was synthesized via two different routes, as shown in Figure 3-1. In route A, the monomer was synthesized from commercially available 1,4-dimethoxybenzene (**1**) in 4 steps with an overall yield of 33%. The route involves the preparation of 2,5-diiodohydroquinone (**3**) with procedures adapted from the literature.[27] Substitution reaction of 1 equivalent of 2,4-diiodohydroquinone (**3**) to 2 equivalents of bromoacetic acid afforded

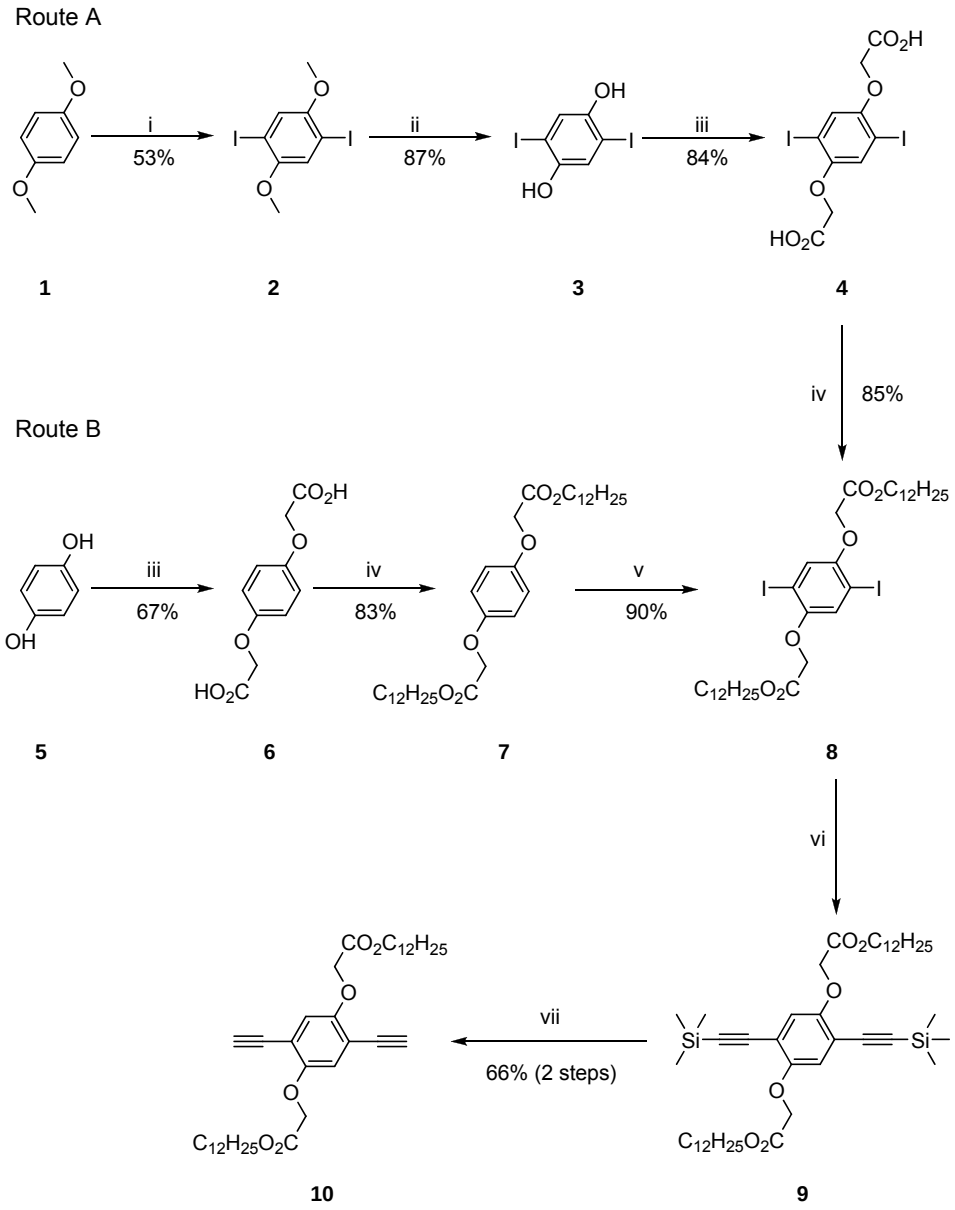

i. KIO_3, I_2, H_2SO_4, CH_3CO_2H, heat; ii. BBr_3, CH_2Cl_2, -78 $^oC \longrightarrow$ 0 ^oC; iii. 1) NaOH, $BrCH_2CO_2H$, heat; 2) 6 N HCl; iv. H_3PO_4, $C_{12}H_{25}OH$; v. $PhI(CO_2CF_3)_2$, I_2, CCl_4, RT; vi. Trimethylsilylacetylene, $Pd(PPh_3)_2Cl_2$, CuI, THF/Et_3N, heat; vii. TBAF, THF, RT.

Figure 3-1. Synthesis of monomers **8** and **10**.

compound **8** in 84% yield. Subsequent Fischer esterification between compound **4** and 1-dodecanol in the presence of a catalytic amount of H_3PO_4 gave the desired product **8**, which was isolated as a white crystalline solid in 85% yield. Following this procedure monomer **8** was prepared in a 10-20 g scale. However, the synthesis of 2,5-diiodohydroquinone involved the use

of boron tribromide in the second step. Although the demethylation works in a high yield (87%), the handling of boron tribromide needs special attention because of its high toxicity. In an effort to avoid using boron tribrimide, a 3-step procedure was developed to synthesize the monomers.

In route B, 1,4-hydroquinone (**5**) was first reacted with bromoacetic acid to afford 2,2'-(1,4-phenylenebis(oxy))diacetic acid (**6**) in 67% yield, which was then reacted with 1-dodecanol under Fischer esterification conditions. The product was then iodinated using 1.2 equivalents of a trivalent iodine compound, [bis(trifluoroacetoxy)iodo]benzene together with 1 equivalent of I_2 in an excellent yield of 90%. The overall yield of route B to produce monomer **8** is 50% with the same quality as a crystalline white solid. The diacetylene monomer **10** was prepared from monomer **8** following a standard Pd-catalyzed Sonogashira coupling and subsequent removal of the trimethylsilyl groups by tetrabutylammonium fluoride (TBAF). The yield for the two-step process is 66%; and monomer **10** was isolated as a slightly yellow powder.

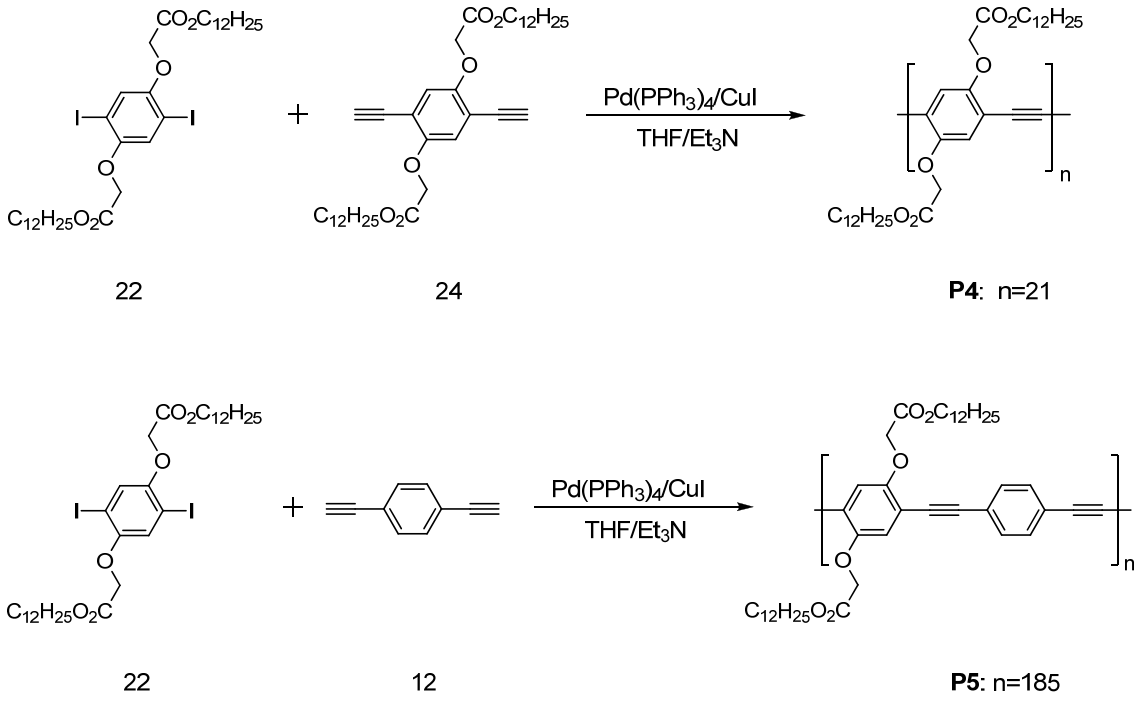

Figure 3-2. Synthesis of the neutral polymer precursors.

The polymers studied in this chapter were synthesized using polycondensation between bifunctional monomers based on Sonogashira coupling, as illustrated in Figure 3-2. Polymerization between **8** and **10** in THF/Et_3N (v/v = 3/2) afforded the homopolymer **P4** which carries the ester groups on each repeat unit. And, the copolymerization between **8** and 1,4-diethynylbenzene produced the polymer **P5** with carboxylic dodecyl ester groups every two repeat units. Both polymers are soluble in THF, CH_2Cl_2, $CHCl_3$, but not soluble in polar solvents, such as methanol, DMSO and DMF. The GPC chromatograms of **P4** and **P5** are shown in Figure 3-3, indicating a mono-modal distribution of the molecular weights for both polymers.

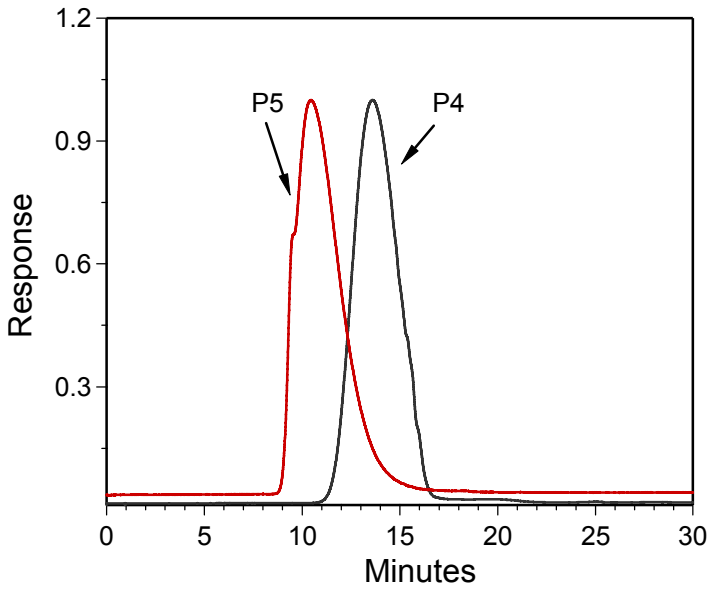

Figure 3-3. GPC chromatograms of **P4** and **P5**.

The number-average molecular weights determined against the polystyrene standard for **P4** and **P5** are 12 kD and 127 kD, respectively. The degrees of polymerization (DP or n) were calculated based on the number-average molecular weights. The polydispersity indices (PDI) for **P4** and **P5** were calculated to be 2.3 and 2.2 respectively, which are close to the theoretical value of 2.0 for ideal step-growth polycondensation.[133] The large difference in the molecular weights obtained for the homopolymer (**P4**) and copolymer (**P5**) is possibly due to the sterically

favorable transition state for the copolymer during the palladium-catalyzed polymerization. To date, the copolymer **P5** is one of the alkoxy-substituted PPEs with highest molecular weight that have been reported in the literature.[10]

The water-soluble PPEs were prepared by hydrolyzing the corresponding neutral polymers in dioxane using tetrabutylammonium hydroxide (TBAH) (1 M in methanol) with subsequent counter cation exchange by aqueous $NaClO_4$ solution, as shown in Figure 3-4. As confirmed by ^1H NMR and FT-IR, the base cleaved the carboxylic dodecyl ester group with a conversion yield higher than 95%. Since the conjugated backbone remained intact during the hydrolysis, thus the water-soluble polymers should have the same chain length as that of their neutral precursor polymers. Characterizations of **P4** and ***w*-P4** were reported previously by our group,[134] in the following context, we presented the characterization of the copolymer **P5** and the water-soluble polymer ***w*-P5**.

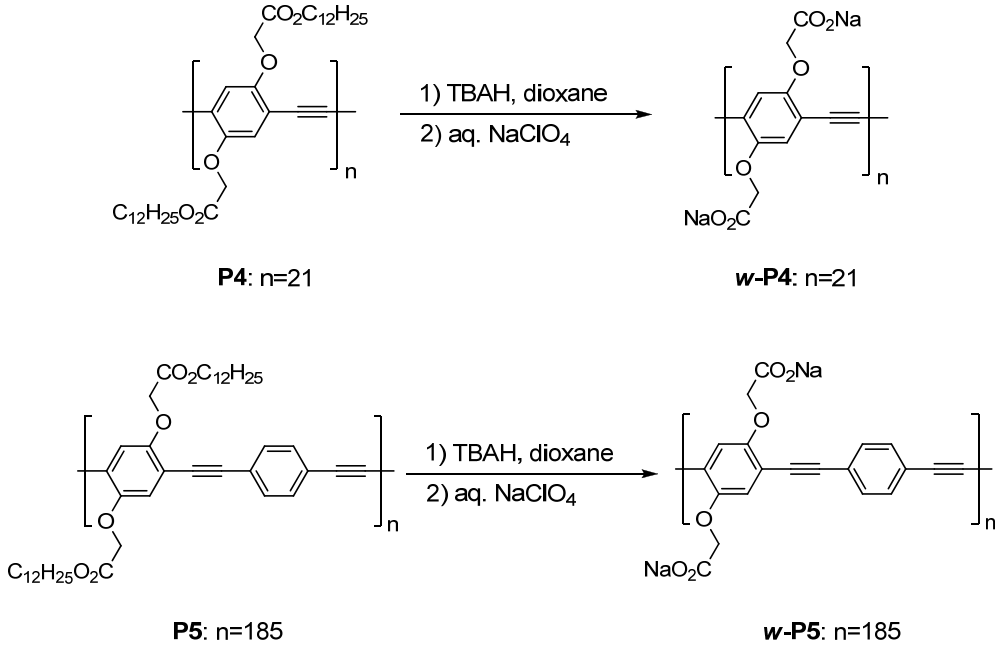

Figure 3-4. Hydrolysis of the neutral polymers to prepare the water-soluble polymers, ***w*-P4** and ***w*-P5**.

Polymer Characterization

^{1}H NMR spectra

Figure 3-5 shows the ^{1}H NMR spectra of monomer **8**, **P5** and ***w*-P5**. Due to its high molecular weight and strong tendency to aggregate in the solid state, the organic polymer, **P5** becomes barely soluble after complete drying, even in its good solvents, such as chloroform and THF (solubility is less than 2 mg/ml). Although in the ^{1}H NMR spectra of **P5**, the aromatic protons are hardly seen, the protons in the aliphatic area derived from monomer **8** can be clearly seen.

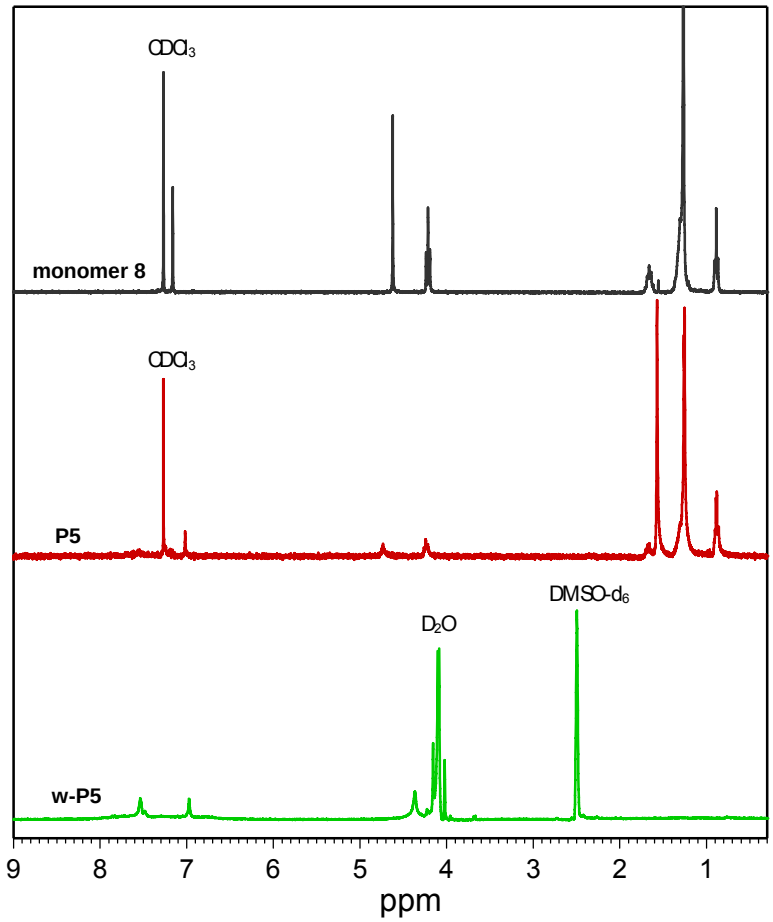

Figure 3-5. ^{1}H NMR spectra of monomer **8**, organic polymer **P5** and the water-soluble polymer ***w*-P5**.

After hydrolysis, the polyelectrolyte, ***w*-P5** is soluble in water (> 5 mg/ml). However, the ^{1}H NMR spectrum of ***w*-P5** in D_2O shows very broad signals, suggesting that the polymer is strongly aggregated in concentrated aqueous solutions (~ 5 mg/ml). DMSO-d_6 is a good solvent for polyelectrolytes and was used to obtain NMR spectra for many conjugated polyelectrolytes,[135] but the current polymer (***w*-P5**) only shows limited solubility in DMSO (< 1 mg/ml). Using a mixture of D_2O/DMSO-d_6 (v/v = 1:1), ^{1}H NMR spectrum of ***w*-P5** was finally obtained after intensive scanning (1024 scans) at 70 ºC. As shown in Figure 3-5, the singlet at δ = 4.37 ppm is assigned to the methylene groups (- O***CH*$_2$**CO_2Na –), which shifts upfield compared to the signals in the spectra of the monomer and the precursor polymer. In the aromatic region, two singlets are observed. The singlet at δ = 7.54 ppm is attributed to the 1,4-phenylene. And the other singlet at δ = 6.97 ppm is from the 2,5-disubstituted-1,4-phenylene protons on the polymer backbone derived from monomer **8**.

Infrared spectra

The hydrolysis was also confirmed by FT-IR spectra, as shown in Figure 3-6. The absorption at 1730 cm^{-1} in the IR spectra of the monomer **8** is assigned to the C=O stretching of the ester groups. For the organic polymer **P5**, the backbone C≡C stretching appears as a weak signal at 2208 cm^{-1}. The absorption at 1734 cm^{-1} is due to the ester groups. And the absorption at 1762 cm^{-1} that is absent in the monomer spectrum probably results from the Fermi resonance between the C=O stretching band and the first overtone band near 839 cm^{-1}.[136] After hydrolysis, the ester band at 1734 cm^{-1} disappears and two new bands appear at 1610 cm^{-1} and 1445 cm^{-1}, which are assigned to the asymmetric and symmetric CO_2^- stretching, respectively. The absorptions near 1200 cm^{-1} for all the samples in the spectra probably represent the asymmetric C-O-C stretching.

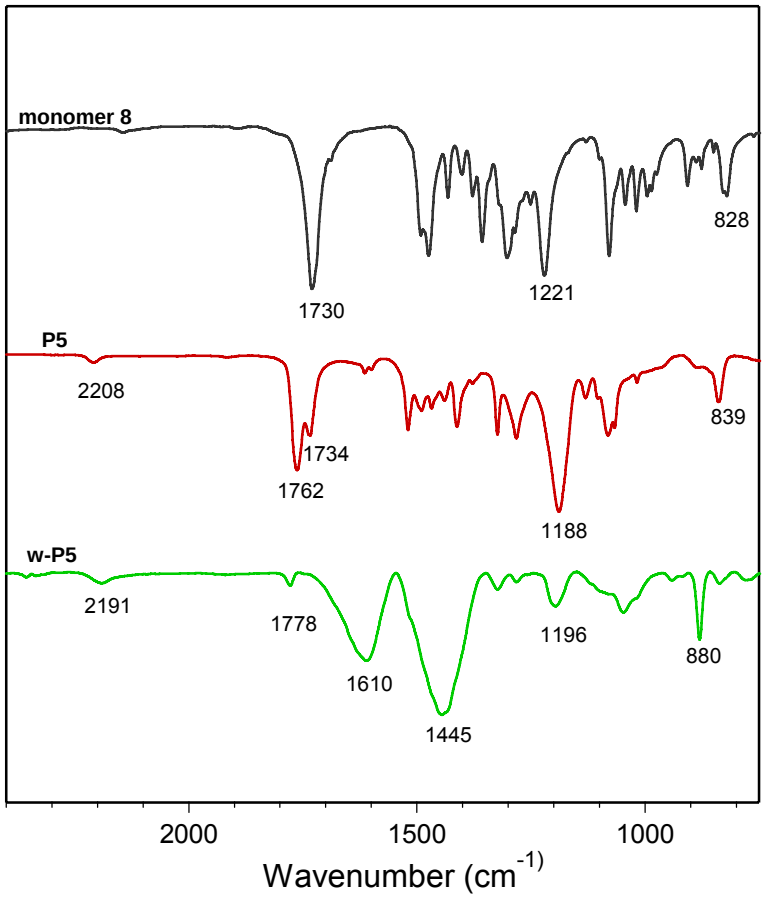

Figure 3-6. FT-IR spectra of monomer **8**, organic polymer **P5** and the water-soluble polymer ***w*-P5**. In these experiments, KBr pellets containing the samples were prepared and used.

Photophysical Characterization

Previously, we have reported the photophysical properties of a structure similar PPE, PPE-SO_3^- in different solvent mixtures.[71] The studies revealed that the absorption and fluorescence of the polymer are strongly solvent-dependent, which is due to aggregation of the polymer chains in different solvent environments. After hydrolysis, ***w*-P4** and ***w*-P5** bearing carboxylate groups have the same backbone structure as that of PPE-SO_3^-. As noted before, ***w*-P4** has two carboxylate side groups per repeat unit while ***w*-P5** has two carboxylate groups for every two repeat units, which is more like PPE-SO_3^-. These polymers show similar solubility in water and other polar solvents, such as MeOH, DMF and DMSO. Since aggregation is a

cooperative process driven by a combination of many forces, such as π-π stacking, hydrophobic and electrostatic interaction, the density of ionic groups on the hydrophobic backbone will play a key role in changing the polymer conformation and stabilizing/destabilizing the aggregate structure. In order to study this effect, the absorption and fluorescence spectra in different solvents were carefully examined for ***w*-P4** and ***w*-P5**.

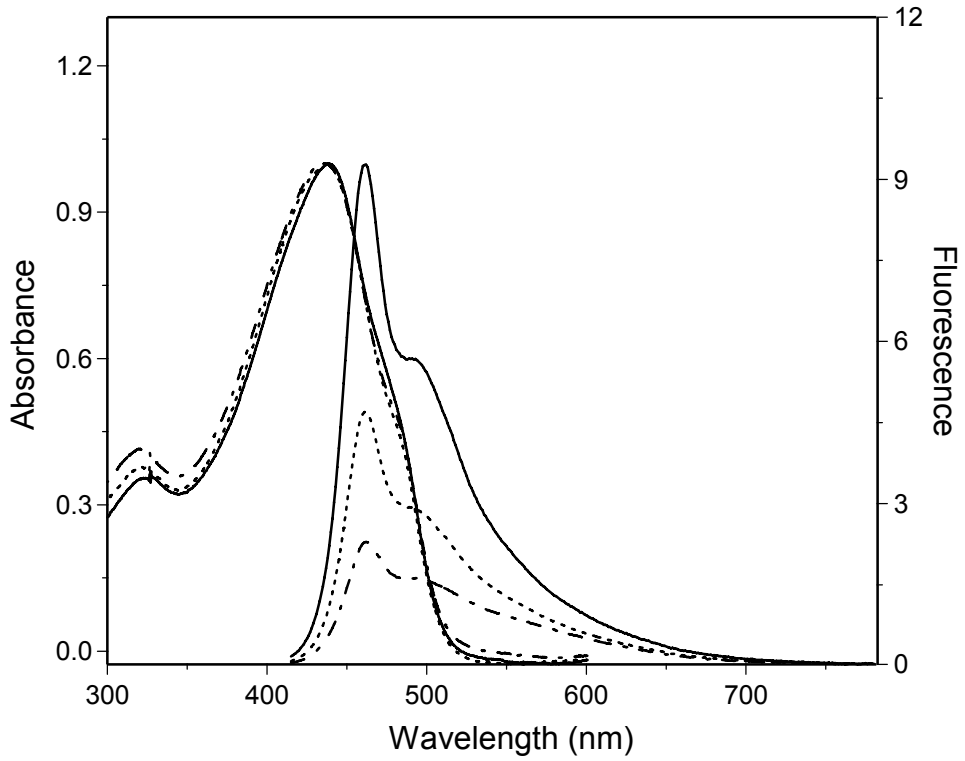

Figure 3-7. Normalized absorption (left) and fluorescence (right) spectra of ***w*-P4** in MeOH (—), (1:1) H_2O-MeOH (- - -) and H_2O (– -). Fluorescence spectra were measured with excitation at 400 nm and are intensity-normalized according to respective quantum yield.

As shown in Figure 3-7, in MeOH, ***w*-P4** has a major absorption band centering at 439 nm, which blue-shifts (<5 nm) with increasing volume of water in the mixture. In the fluorescence spectra, ***w*-P4** shows a structured blue emission at 462 nm (0-0 band) in MeOH and the emission intensity is continually quenched with increasing water. However, there is no observable emerging new band. The polymer maintains its blue emission even in water. By contrast, a new

red-shifted and narrow band appears in the absorption spectra of PPE-SO_3^- as the volume of water in the MeOH/water mixture increases. In the fluorescence spectra, the blue emission band observed in MeOH is completely quenched in water and a new broad and red-shifted band appears.[71] Compared to ***w*-P4**, ***w*-P5** is structurally more close to PPE-SO_3^- except they have different ionic groups. As expected, ***w*-P5** shows more similar spectral change as PPE-SO_3^- when its absorption and emission properties were studied in different solvent mixtures.

Figure 3-8 illustrates the absorption spectra of ***w*-P5** in different methanol/water mixtures along with the spectrum of its neutral precursor (**P5**) in THF. THF is a good solvent for the neutral polymer, in which the aggregation of **P5** is expected to be minimal. In the absorption spectrum of **P5** (Figure 3-8 a), there is a main absorption band with a maximum at 415 nm, which is assigned to the $\pi \rightarrow \pi^*$ transition of the un-aggregated conjugated polymer chains. As shown in Figure 3-8 (b), the absorption spectrum of ***w*-P5** in methanol shows a main absorption band at 415 nm (un-aggregated polymer chains) and a shoulder peak at 433 nm (aggregate band), which arises from the planarization of the conjugated backbone in the aggregate. As the volume fraction of H_2O increases, the absorbance of the maxima at the longer wavelength continually increases and becomes more pronounced. There is also a stepwise red-shift (< 7 nm) of the absorption maximum. The water-driven aggregation trend is clearly shown by plotting the ratio of the absorbance at the maximum divided by the absorbance at 415 nm to the volume of water in methanol (Figure 3-8 c).

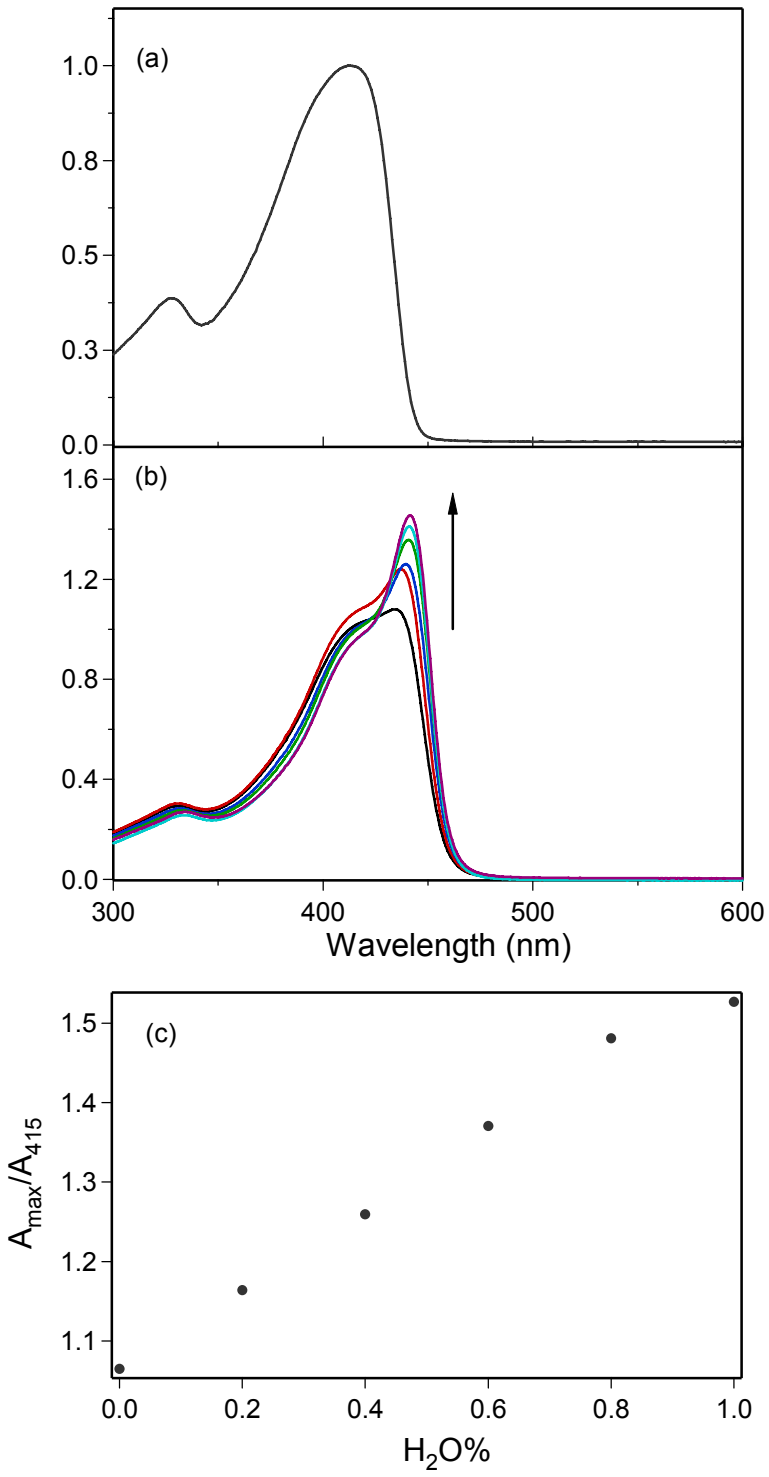

Figure 3-8. (a) Normalized absorption spectrum of **P5** in THF solution; (b) Normalized absorption spectra of ***w*-P5** in MeOH/H_2O mixtures, the arrow shows the direction of change with increasing volume % H_2O (c) Variation of A_{max}/A_{415} in the absorption spectra of ***w*-P5** with the volume % H_2O.

As expected, ***w*-P5** and PPE-SO_3^- that have the same backbone feature but different ionic groups show similar solvatochromic properties. However, the shoulder peak (433 nm) in the spectrum of ***w*-P5** in MeOH indicates that even in methanol there is already a small fraction of aggregated chains, which differs from PPE-SO_3^-. The latter polymer exhibits a major absorption at 425 nm without the apparent "aggregate band" in MeOH, which is similar to those of their organic analogues in good solvents (THF or $CHCl_3$).[10,73] This different behavior of ***w*-P5** and PPE-SO_3^- in methanol is related to the acid-base equilibrium of both materials in the neutral water in which the stock solutions were prepared and stored. Sulfonate (SO_3^-) is a weaker base with pK_a (R-SO_3H) ≈ - 2.6,[137] thus PPE-SO_3^- exists exclusively in its base form in the stock solution. Compared to sulfonate, carboxylate (CO_2^-) is a much stronger base, pK_a (R-CO_2H) ≈ 4.8).[137] Thus in its stock solution (pH = 5 – 6), a considerable fraction of the R-CO_2^- groups on the ***w*-P5** chains is protonated, which decreases the intrachain or interchain electrostatic repulsion and favors the aggregate formation. This assumption was further proven by a pH control experiment. When the pH of the stock solution was higher than pH = 8, it was found that the shoulder peak (433 nm) in the absorption spectra of ***w*-P5** in MeOH was obviated.

In the fluorescence spectra (Figure 3-9), in methanol, at 10 μM polymer repeat unit (PRU) concentration, the polymer features a structured fluorescence spectrum with a maximum intensity at 465 nm and a quantum yield of 0.24. At lower concentrations (less than 5 μM), the 0-0 emission band at 436 is actually the dominant peak, which is attenuated in concentrated solutions because of the self-absorption of the polymer (typically a small Stokes shift of 3 nm was observed for these polymer solutions). As can be seen in Figure 3-9, with increasing amount of water, a continuous decrease of the fluorescence intensity in the blue region is observed and finally in the water solution, a red-shifted and broad emission at 524 nm becomes the dominant

peak with a quantum yield of 7.5%. These results are quite similar to those of PPE-SO_3^-, implying that the electronic properties of these two polymers are predominantly determined by the conjugated backbones while the ionic side groups play a minor role. And the pronounced excimer-like band existing in both polymers indicates a strong excimer interaction in the aggregates due to the optimized π-π stacking between the polymer chains.

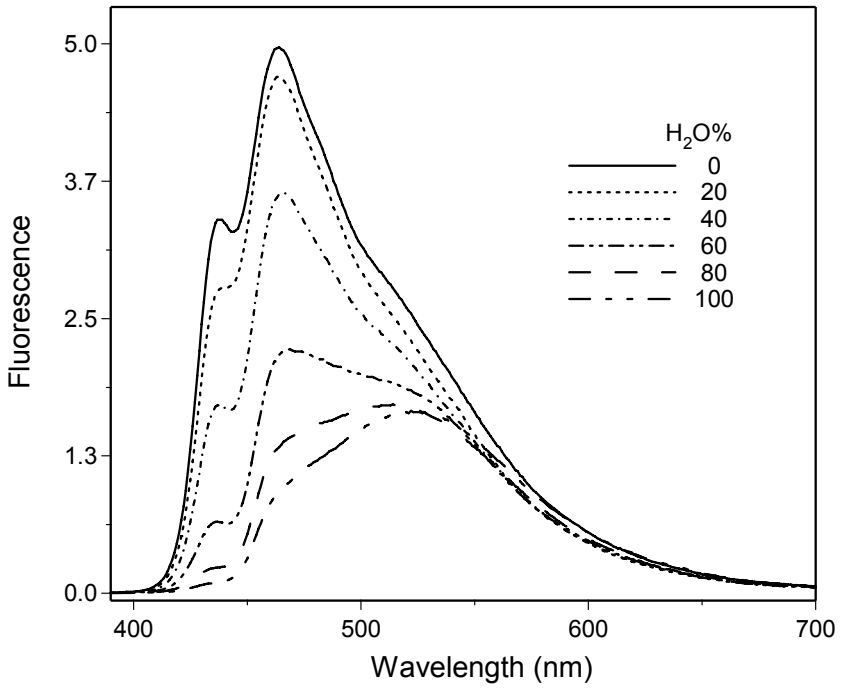

Figure 3-9. Fluorescence spectra (λ_{exc} = 380 nm) of ***w*-P5** (c = 10 μM polymer repeat units) in MeOH, water and MeOH/water mixtures. The spectra were obtained under the same conditions, so the spectral intensity reflects the approximate change in the fluorescence quantum efficiency with solvent composition. The data used in this graph was obtained by Hui Jiang in Schanze group.

Figure 3-10 (a) shows a schematic representation of π-π stacking of ***w*-P5** in the aggregate. Because of the combination of different forces including π-π stacking, hydrophobic and electrostatic interactions, a face-to-face stacking of the phenyl rings is realized and the ionic side chains are extended into the solvent. In such a way, the contact between the hydrophobic aromatic backbones with the aqueous environment is minimized. This proposed model is

consistent with some of the experimental results from Swager's research group. In a series of work, they studied the Langmuir monolayer of some amphiphilic PPEs. Their results reveal that the cofacial spacing of PPE chains less than about 4.3 - 4.5 Å leads to a dominant excimer-like emission band in the fluorescence spectra.[138-141] While in the aqueous solution of ***w*-P4**, because of the existence of carboxylate side chains on each repeat unit, the electronic repulsion (interchain and intrachain) between the ionic side groups prevents such a co-facial stacking. However, in the water-rich solutions of ***w*-P4**, agglomeration of polymer chains still occurs and generates some less ordered low-energy traps, which leads to the reduced quantum efficiency. This was also proven by the observation of pH-induced aggregation of ***w*-P4**.[134] In acidic conditions, the carboxylate groups are protonated, which enables the co-facial packing mode, thus similar absorption and fluorescence spectra as those of ***w*-P5** and PPE-SO_3^- were observed.

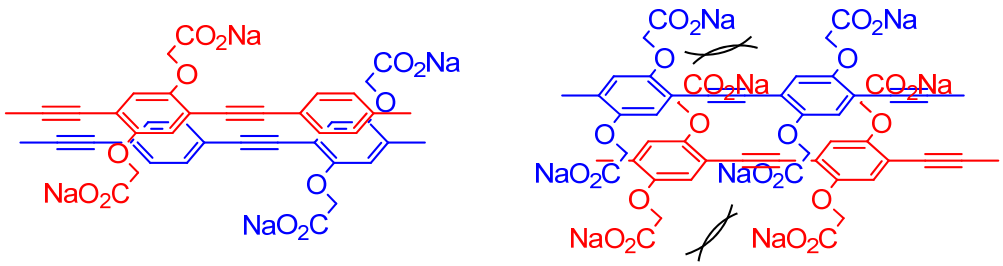

Figure 3-10. Schematic representation of the π-π stacking interaction in CPE aggregates.

Fluorescence Quenching Properties

Previously, we have studied the quenching of PPE-SO_3^- and ***w*-P4** by cationic electron acceptors with different charges and/or some cationic cyanine dyes, which can quench the polymer fluorescence via an energy transfer mechanism.[71,126,134] PPE-SO_3^- is quenched very efficiently by these molecules either in methanol or water in an amplified quenching process. The Stern-Volmer quenching constants (K_{sv}) are usually in the range of 10^6 M^{-1} to 10^7 M^{-1} in water. ***w*-P4** is found to be quenched less efficiently than PPE-SO_3^- by methyl viologen (MV^{2+}).

K_{sv} values are in the order of 10^5 M^{-1} in water. The less efficient quenching of ***w*-P4** is probably due to the lack of aggregate formation in water and/or the short chain length of the polymer.[55,71] However, the carboxylate groups of ***w*-P4** and ***w*-P5** provide the receptor sites for metal ions, which allows us to look at the perturbation of polymer fluorescence by different metal ions in either MeOH or water. Independently, Kim and Bunz recently also reported the results of fluorescence quenching of a carboxylate-substituted PPE with the same structure of ***w*-P4** by different metal ions.[142-144]

Quenching with metal ions in MeOH

The interaction of ***w*-P5** with divalent metal ions was first studied in methanol. This includes a series of 9 different metal ions, Ca^{2+}, Mn^{2+}, Co^{2+}, Ni^{2+}, Cu^{2+}, Zn^{2+}, Cd^{2+}, Hg^{2+} and Pb^{2+}. Addition of 1 equivalent of metal ions induced similar changes in the absorption and emission spectra of the polymer ([PRU] = 5μM) for all the metal ions except Cu^{2+}.

Figure 3-11 shows the absorption (a) and emission (b) spectra of ***w*-P5** at various concentrations of Ca^{2+}. Interestingly, addition of small amounts of Ca^{2+} induces spectroscopic changes that resemble those when the solvent is changed from MeOH to water. In the absorption spectra, the intensity of the shoulder peak (430 nm) increases gradually with the addition of Ca^{2+} and in the emission spectra, the strong structured emission at 436 nm decreases and is finally replaced by a red-shifted, structureless and broad emission band at 510 nm (aggregation band). Such observations indicates that Ca^{2+} and other metal ions (Mn^{2+}, Co^{2+}, Ni^{2+}, Zn^{2+}, Cd^{2+}, Hg^{2+} and Pb^{2+}) quenches the polymer fluorescence in methanol via an aggregation-inducing process. Since most divalent metal ions could coordinate up to 2 or 3 carboxylate groups, thus they can bridge different polymer chains and cause the aggregation of the polymer. For Cu^{2+}, although a similar change as the other metal ions is observed in the absorption spectra (Figure 3-11 c), the change in the fluorescence spectrum is different. As shown in Figure 3-11 (d), addition of Cu^{2+}

to the methanol solution of ***w*-P5** leads to the strong quenching of fluorescence intensity without appearance of the new emission band at 510 nm, which indicates that Cu^{2+} can quench the polymer fluorescence via a different mechanism, possibly a photo-induced electron transfer process (PET) or energy transfer (ET) process.[145]

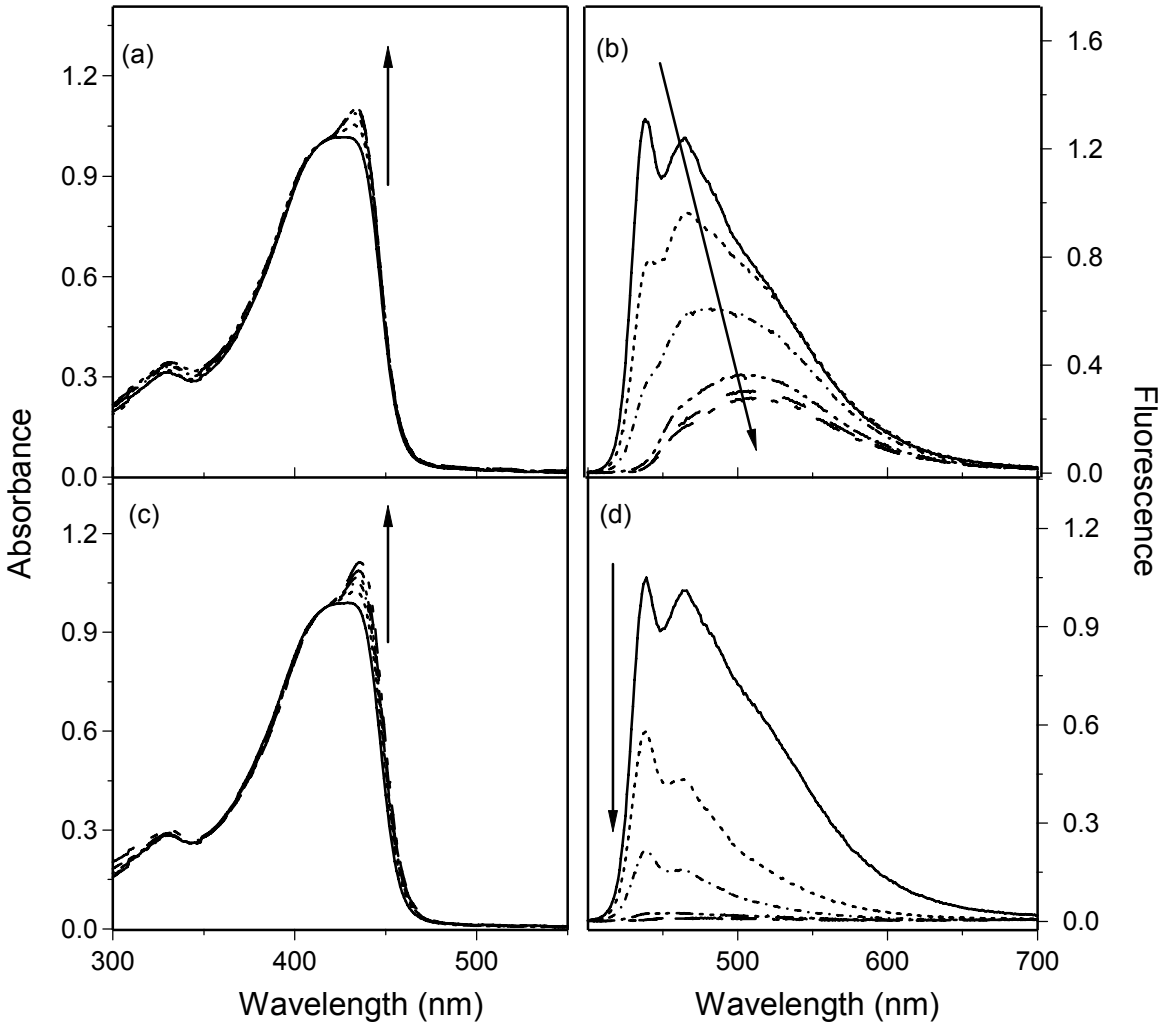

Figure 3-11. Absorption (a) and fluorescence (b) spectra of ***w*-P5** in MeOH with added Ca^{2+}, Ca^{2+} was added in 1 μM aliquots, [Ca^{2+}] ranges from 0 – 5 μM. Absorption (c) and fluorescence (d) spectra of ***w*-P5** in MeOH with added Cu^{2+}, Cu^{2+} was added in 1 μM aliquots, [Cu^{2+}] ranges from 0 – 5 μM. [***w*-P5**] = 5 μM. The arrow shows the direction of change with increasing amount of metal ions.

Quenching with metal ions in the HEPES buffer

We have demonstrated that the fluorescence of ***w*-P5** in methanol could be quenched by different metals via either induced aggregation (less efficient) process or PET/ET mechanisms (more efficient). In order to develop sensors for biological applications, it is more useful that all the experiments can be carried out in a buffer solution. Here we use 4-(2-hydroxyethyl)-1-piperazine-1-ethanesulfonic acid (HEPES) because it does not bind to metal ions and thus will not interfere with the interaction between the polymer and the metal ions. From the study of solvent effect on the optical properties of ***w*-P5**, we know that in water the polymer is aggregated. Figure 3-12 shows the absorption (left) and emission (right) spectra of ***w*-P5** in HEPES buffer (pH = 7.5), which are essentially the same as those of the polymer in pure water, indicating the polymer is also strongly aggregated in the HEPES buffer solution.

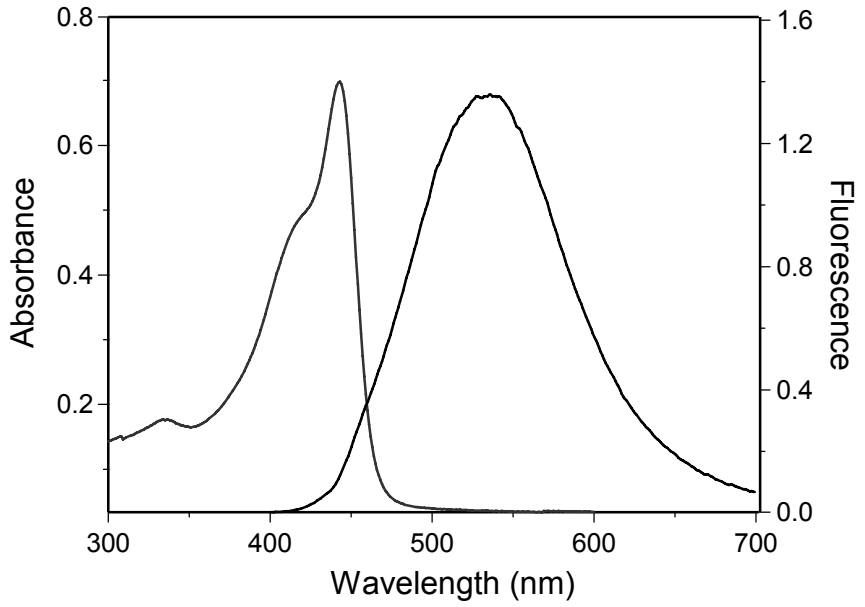

Figure 3-12. Absorption (Left) and emission (right) spectra of ***w*-P5** in 10 mM HEPES buffer solution. [***w*-P5**] = 5 μM. Excitation at 380 nm.

In the HEPES buffer, quenching experiments of ***w*-P5** with different metal ions were carried out. For all 9 metal ions, the absorption spectra show negligible change, indicating the

addition of metal ions does not lead to further aggregation or conformation changes of the polymer in the buffer solution. Figure 3-13 shows the absorption and emission spectra of ***w*-P5** in 10 mM HEPES buffer with the addition of either Ca^{2+} or Cu^{2+}.

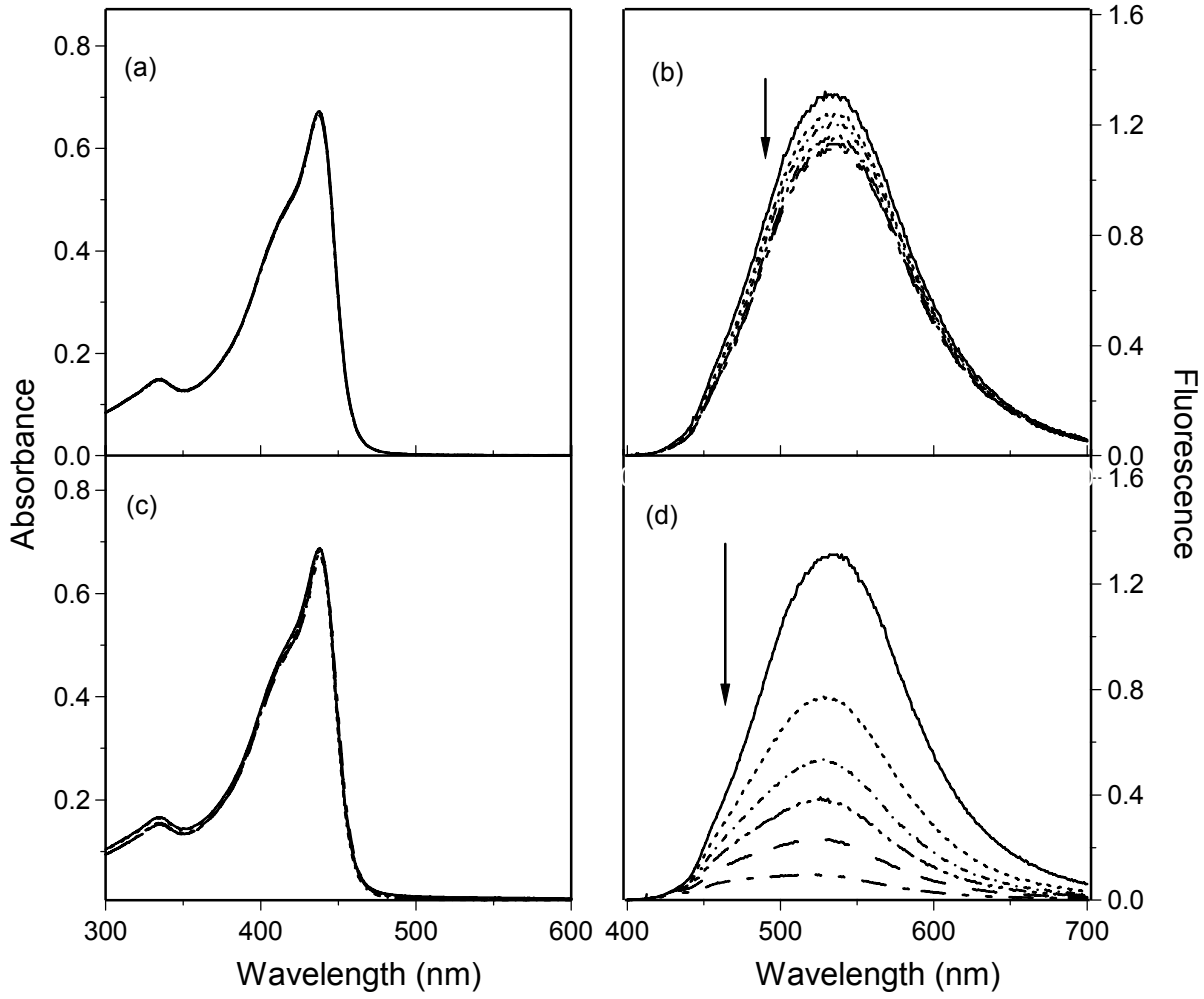

Figure 3-13. Absorption (a) and fluorescence (b) spectra of ***w*-P5** in the HEPES buffer (pH = 7.5) with added Ca^{2+}, Ca^{2+} was added in 1 μM aliquots, [Ca^{2+}] ranges from 0 – 5 μM. Absorption (c) and fluorescence (d) spectra of ***w*-P5** in the HEPES buffer with added Cu^{2+}, Cu^{2+} was added in 1 μM aliquots, [Cu^{2+}] ranges from 0 – 5 μM. [***w*-P5**] = 5 μM. The arrow shows the direction of change with increasing amount of metal ions.

In contrast to the strong quenching of the polymer fluorescence in methanol by Ca^{2+}, in the HEPES buffer where the polymer is already aggregated, adding 1 equivalent Ca^{2+} (5 μM) only quenches 15% of the original polymer fluorescence (Figure 3-13 b). While for Cu^{2+}, which can

quench the polymer fluorescence via PET/ET mechanisms, the addition of 5 μM Cu^{2+} (1 equivalent) quenches 90% of the original fluorescence (Figure 3-13 d).

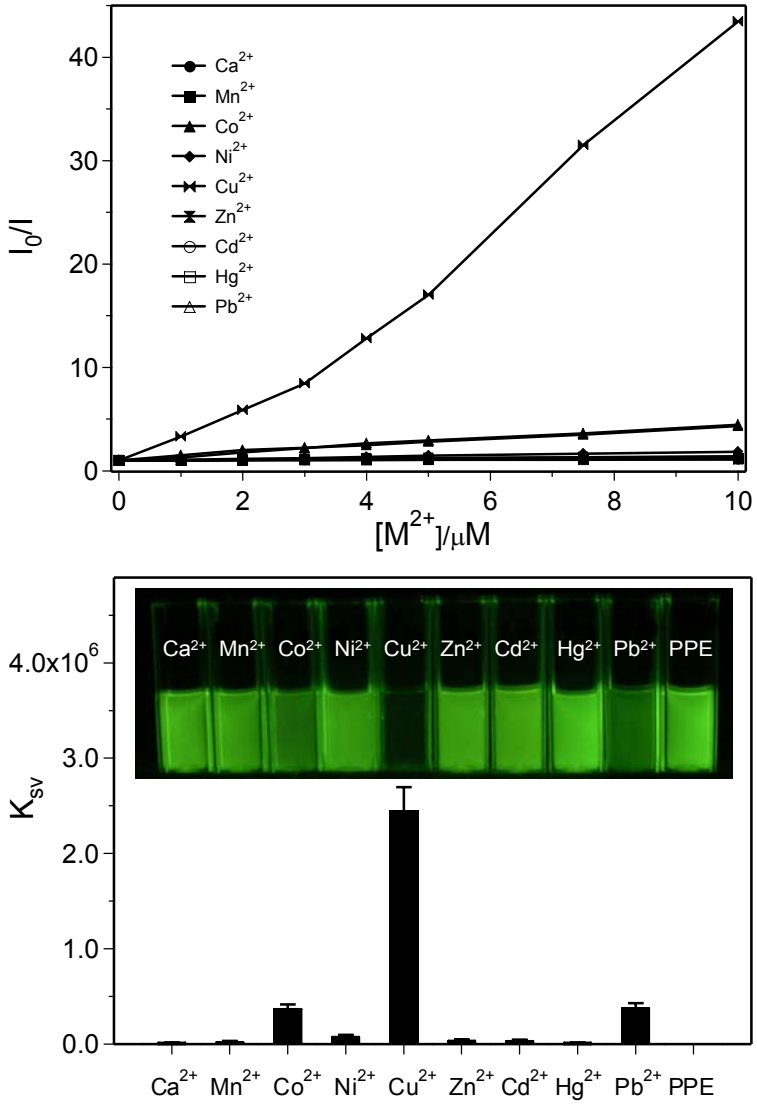

Figure 3-14. Stern-Volmer plots (upper) of ***w*-P5** emission quenching by different metal ions in 10 mM HEPES buffer and comparison of K_{sv} values for different metal ions (lower). The inset shows a photograph of ***w*-P5**/M^{2+} (5 μM/10 μM) solutions illuminated with a UV lamp.

The Stern-Volmer (SV) plots for all the 9 metal ions are shown in Figure 3-14 (upper). In the low concentration range (0-5 μM), a linear correlation is observed for all the metal ions except Cu^{2+}, for which an upward curvature occurs above the concentration of 3 μM. Stern-

Volmer quenching constants (K_{sv}) for all the metal ions were extrapolated by fitting the linear regions of their SV plots and are compared in the bar graph shown in Figure 3-14 (lower). For most of the metal ions (Ca^{2+}, Mn^{2+}, Ni^{2+}, Zn^{2+}, Cd^{2+}, Hg^{2+}), K_{sv} values in the range of 10^4 M^{-1} – 10^5 M^{-1} are observed. For Co^{2+} and Pb^{2+}, relatively larger K_{sv} values of 3.8×10^5 M^{-1} and 3.9×10^5 M^{-1} are obtained, respectively. The largest K_{sv} value is obtained for Cu^{2+} and is in the order of 10^6, which is comparable to the quenching of ***w*-P5** by MV^2. The inset in Figure 3-14 shows a photograph of the fluorescence from the ***w*-P5**/M^{2+} solutions acquired under UV-illumination. Clearly, the polymer fluorescence is strongly quenched by Cu^{2+}, but only slightly quenched by Co^{2+} and Pb^{2+} and all the other mixtures remain highly fluorescent.

Quenching by methyl viologen (MV^{2+}) in MeOH mediated by Ca^{2+}: an explanation of superlinear quenching behavior for CPE-quencher system.

Typically, in most of the CPE-quencher systems, the SV plots exhibit a linear correlation at low quencher concentration range and a superlinear behavior (upward curvature) at higher quencher concentrations. Several phenomena have been proposed to account for the superlinear SV quenching behavior, including ion-pair complex formation between the polymer and the quencher,[57,61,146] efficient singlet exciton migration within the polymer,[57,60] efficient long-range Förster energy transfer between the polymer and quencher,[146] and aggregation of polymer chains induced by the quencher.[57,71,126] As shown in previous sections, the fluorescence of **w-P5** is quenched by Ca^{2+} in methanol due to the metal ion induced aggregation of polymer chains. Consistent with the mechanism, in water where the polymer is already aggregated, there is not much quenching in the fluorescence intensity with the addition of Ca^{2+}. In view of this fact, in order to probe the effect of induced polymer aggregation on the quenching efficiency by oppositely charged quenchers, we carried out the experiments of fluorescence quenching by

MV^{2+} in methanol, in which the "aggregation state" of ***w*-P5** is systematically varied by adding different amount of Ca^{2+}.

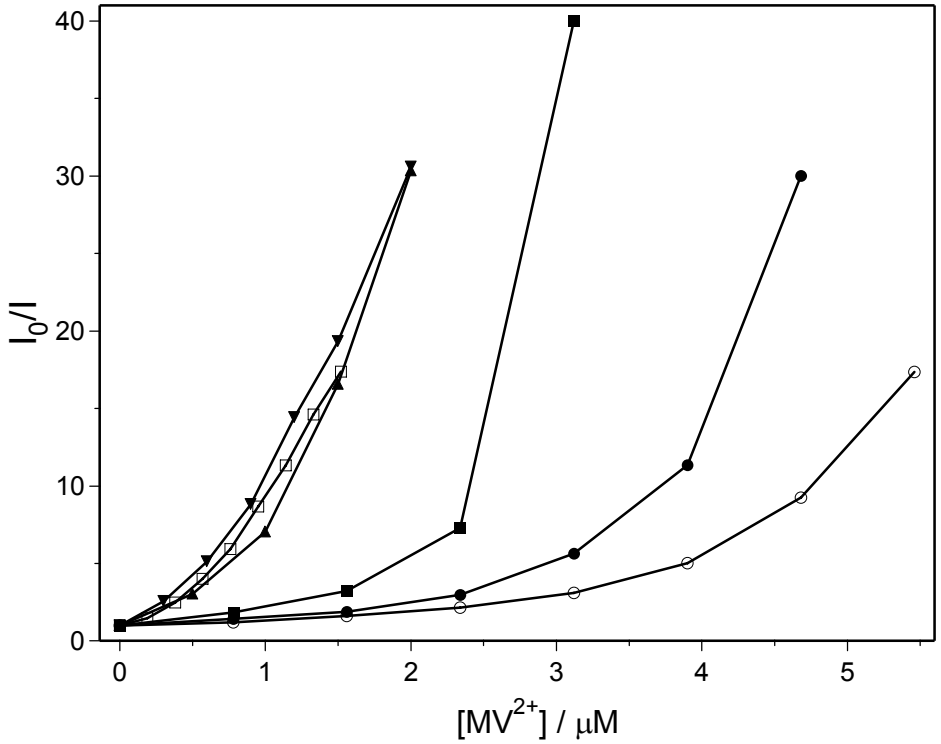

Figure 3-15. Stern-Volmer quenching of 10 μM ***w*-P5** emission by MV^{2+} in water (□) and in MeOH with 0 μM (○), 2.5 μM (●), 5.0 μM (■), 7.5 μM (▲) 10 μM (▼) $CaCl_2$. These experiments were carried out by Hui Jiang in Schanze group.

Figure 3-15 shows the SV plots of ***w*-P5** emission quenching by MV^{2+} in pure water, pure methanol and in methanol with added Ca^{2+} at different concentration. In all cases, a linear relationship is observed at low quencher concentration range, and an upward curvature occurs at certain quencher concentration. Similar to the quenching of PPE-SO_3^- with MV^{2+}, quenching of ***w*-P5** is more efficient in water than in methanol. For the aggregated polymer in water, the SV plot is superlinear even at very low quencher concentration ($c < 1\ \mu M$). By contrast, in methanol where the polymer is less aggregated, the SV plot features a distinct "induction region" wherein the correlation is nearly linear and the slope (K_{SV}) is significantly less than at higher MV^{2+} concentration ($c > 3\ \mu M$) where the correlation becomes superlinear. As also shown in Figure

3-15, addition of Ca^{2+} has a pronounced effect on the efficiency by which MV^{2+} quenches the ***w*-P5** fluorescence. In particular, the range of MV^{2+} concentrations corresponding to the "induction range" in the SV plot is compressed in the presence of Ca^{2+}. Remarkably, for methanol solutions that contain >7.5 μM Ca^{2+} (corresponding to approximately 1 equiv of Ca^{2+} per polymer repeat unit), the "induction range" in the SV plots is virtually eliminated, and MV^{2+} quenches ***w*-P5** emission with efficiency comparable to that seen in aqueous solution.

Taken together, these results clearly demonstrate the connection between cation-induced CPE aggregation and the superlinear quenching response typical of CPE-quencher systems. The current results also indicate that the "sphere-of-action" quenching model,[61] which has been applied to analyze the SV quenching data in CPE-quencher systems, is likely not valid with polyvalent quencher ions because the state of the system (i.e., effective exciton radius, effective CPE-quencher ion-pair binding constant) is strongly dependent on the relative concentrations of the CPE and quencher. Analysis of the quenching efficiency and dynamics by using a model that incorporates the possibility of 3-dimensional exciton diffusion within a polymer aggregate that contains many individual CPE chains is clearly more appropriate for the situation.

Application to Pyrophosphate (PPi) Sensing

Pyrophosphate ($P_2O_7^{4-}$, PPi) is an inorganic anion that is involved in many important biological processes such as cellular signal transduction and protein synthesis.[147] Fluorogenic sensors for detecting PPi in aqueous solution have been the focus of considerable research. "Fluorophore-spacer-receptor" sensors based on signal transduction mechanisms such as photoinduced electron transfer (PET)[148-152] or monomer-excimer formation[151] have been reported. "Turn-on" sensors that rely on indicator displacement have also been designed.[153-155] However, in these systems small molecule dyes were used as the indicators, therefore the

sensitivity to PPi is limited due to the comparatively inefficient quenching of the indicators by the receptors.

Because of their signal amplification property, conjugated polyelectrolytes have been used for sensing a variety of analytes, including heavy metal ions,[142,143] DNA,[18,58,59,78] RNA[18] and some proteins.[18,58,156] However, examples of using CPE to specifically sense pyrophosphate (PPi) have not yet been reported. Since many of the small molecule sensors for PPi were designed utilizing the binding of PPi to the metal-complex, we anticipated that the current CPE/metal ion system could provide a new platform to develop efficient sensors for pyrophosphate. Based on the results described above, we chose a composite system of ***w*-P5** and Cu^{2+}, in which the concentration ratio between the polymer and Cu^{2+} is 1:2 (with respect to carboxylate groups which are the actual binding sites for metal, the ratio is 1:1). At this ratio ([PRU]/[Cu^{2+}] = 5 μM/10 μM) , the intensity of polymer's fluorescence is quenched by more than 98% at λ_{max} = 530 nm compared to the intensity of a solution containing only polymer ([PRU] = 5 μM).

Figure 3-16 (a) illustrates the fluorescence intensity change of ***w*-P5**/Cu^{2+} in the HEPES buffer at pH 7.5 with the addition of various amount of PPi. Titration of PPi into the ***w*-P5**/Cu^{2+} (5 μM/10 μM) solution results in a continuous recovery of the polymer's fluorescence intensity, and at 10 μM of added PPi (1 equivalent relative to [Cu^{2+}]) a 17-fold enhancement of fluorescence intensity is observed. As shown in Figure 3-16 (b), the full titration curve of adding 0-100 μM PPi displays a sigmoidal progression indicating that multiple equilibria are involved in the process.[157] These equilibria likely involve dissociation of the ***w*-P5**/Cu^{2+} complex and formation of the Cu^{2+}/PPi complex. The most significant fluorescence increase is seen with addition of PPi up to 20 μM (30-fold enhancement). Above that concentration the increase

occurs more gradually, and at [PPi] = 50 μM (5 equivalents added) approximately 85% of the polymer's initial fluorescence intensity is recovered (38-fold enhancement) (nearly100% of the fluorescence intensity is recovered at 100 μM [PPi]). During the entire PPi titration, there is no shift of the emission maximum, and UV-Vis absorption exhibits only a small blue shift (< 5 nm). This finding suggests that PPi acts mainly by sequestering Cu^{2+}, and that there are not significant changes in the polymer aggregation state occur during the anion titration.

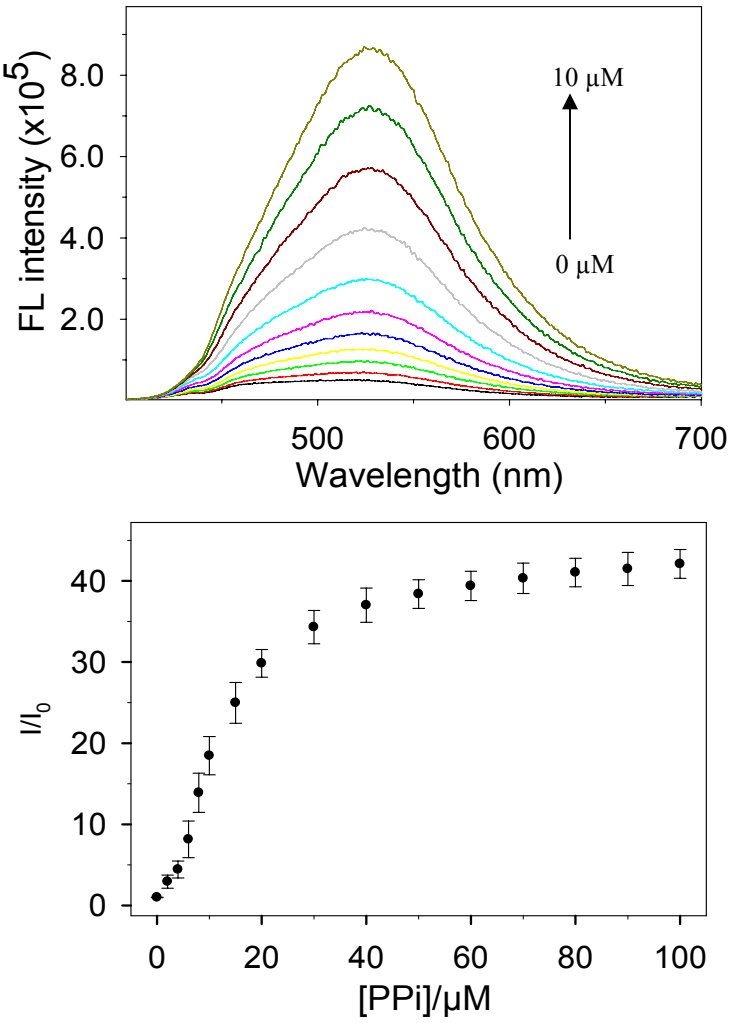

Figure 3-16. (a) Fluorescence spectra of a solution of ***w*-P5**/Cu^{2+} (5 μM/10 μM) titrated with PPi in 10 mM HEPES buffer at pH 7.5, 25 °C. [PPi] ranges from 0 – 10 μM. (b) Intensity enhancement (I/I_0) at 530 nm titrated with PPi (0-100 μM). Excitation at 380 nm.

Selectivity

The selectivity of the ***w*-P5**/Cu^{2+} sensor for PPi was evaluated by carrying out the same fluorescence titration with other anions including monovalent anions (F^-, Cl^-, Br^-, I^-, HSO_4^-, NO_3^-, HCO_3^-, $H_2PO_4^-$, $CH_3CO_2^-$) and divalent anions (SO_4^{2-}, CO_3^{2-}, HPO_4^{2-}). Addition of 50 μM any of these anions induced only a small change of the ***w*-P5** fluorescence intensity (typical change was less than 2%). In another experiment, two separate solutions were prepared; one contained 50 μM each anion (totally 12 anions) except PPi, the other contained all 13 anions. Only the latter solution showed fluorescence, demonstrating that PPi was specifically detected.

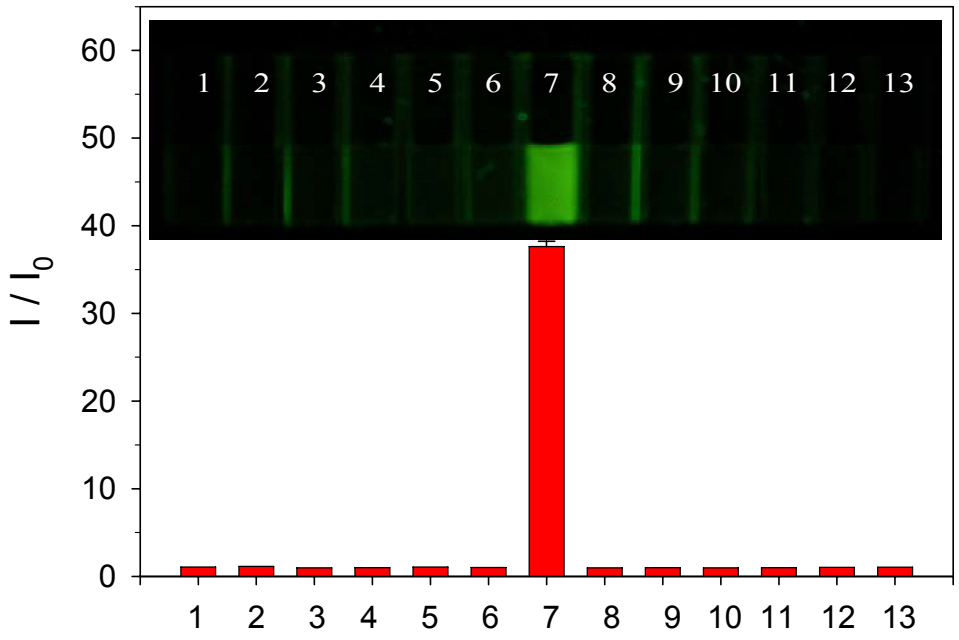

Figure 3-17. Fluorescence response of ***w*-P5**/Cu^{2+} (5 μM/10 μM) to various anions at 50 μM concentration in 10 mM HEPES buffer at pH 7.5, 25 °C (1, F^-; 2, Cl^-; 3, Br^-; 4, I^-; 5, HPO_4^{2-}; 6, $H_2PO_4^-$; 7, $P_2O_7^{4-}$; 8, $CH_3CO_2^-$; 9, HSO_4^-; 10, NO_3^-; 11, HCO_3^-; 12, SO_4^{2-}; 13, CO_3^{2-}). Inset shows a photograph of the sensor/anion solutions illuminated with a UV-lamp.

Figure 3-17 compares the response of ***w*-P5**/Cu^{2+} to the addition of 50 μM of 12 different anions. This presentation shows that the sensor is highly selective to PPi with an intensity enhancement of 40-fold, compared with all of the other the anions tested, including phosphate

(Pi: $H_2PO_4^-$ and HPO_4^{2-}). The inset shows a photograph of the fluorescence from the ***w*-P5**/Cu^{2+}/anion solutions acquired under UV-illumination. The photograph clearly shows that the fluorescence of the polymer is very strong in the presence of PPi, whereas it is very weak in the presence of the other anions.

Sensitivity

As mentioned, one of the advantages of CPE-based sensors over small organic dye-based sensors is the signal amplification imparted by the conjugated polymer because of the "molecular wire" effect. To date, the sensitivity for most PPi sensors achieved by small organic dyes in aqueous solution is still in the micromolar range. The sensitivity of the current sensor was determined by carrying out the titration of ***w*-P5**/Cu^{2+} with PPi in a concentration range of 0.1 - 10 μM.

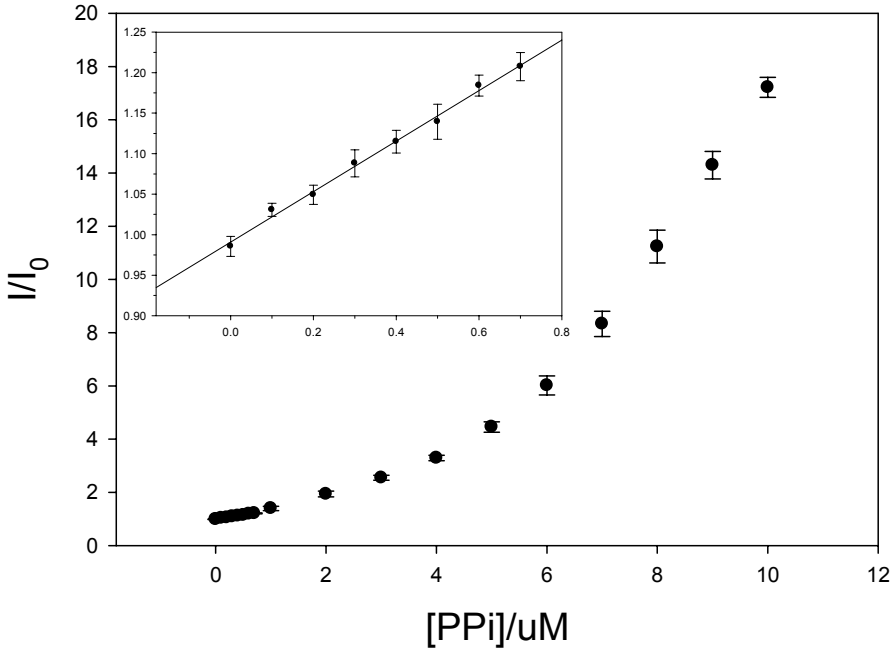

Figure 3-18. Intensity enhancement (I/I_0) at 530 nm of ***w*-P5**/Cu^{2+} (5 μM/10 μM) titrated with PPi (0-10 μM). The inset shows the emission enhancement at lower PPi concentrations.

As shown in Figure 3-18, an upward curvature occurs after adding very low concentration of PPi, which is consistent with the sigmoidal progression in the full titration curve (Figure 3-14). However, in the concentration range of 0.1 - 0.7 μM, a nearly linear relationship is obtained (Inset). The analytical detection limit is determined to be 80 nM using the following equation: D.L. = 3 δ_{bk}/m (δ_{bk} , standard deviation of the blank; m, slope of the curve).[158] This is the first CPE-based sensor for PPi with sensitivity higher than that of most PPi sensors based on organic dyes or small molecules and with a high selectivity over many other inorganic anions, including $H_2PO_4^-$ and HPO_4^{2-}.

Sensing mechanism

Based on the above studies of the sensing response to various anions, the selectivity of the current sensor for PPi is believed to arise from the ability of PPi to chelate Cu^{2+} via the diphosphate moiety.[159] The proposed sensing mechanism is shown in Figure 3-19.

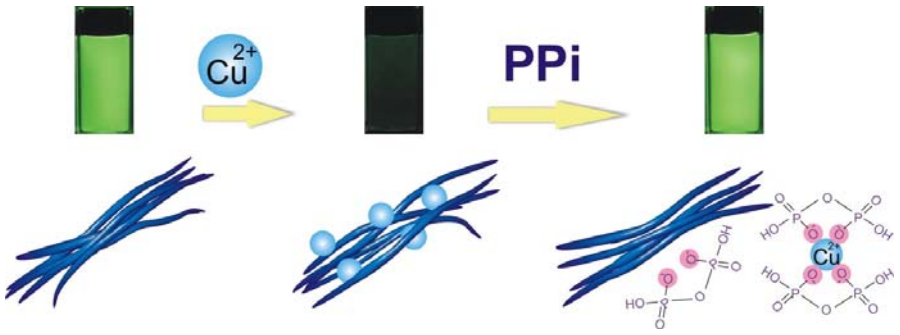

Figure 3-19. Schematic representation of the sensing of PPi by ***w*-P5**/Cu^{2+} system.

Initially the fluorescence of the polymer is quenched by Cu^{2+} through the formation of ***w*-P5**/Cu^{2+} weak complex by binding to the carboxylate groups, and then the fluorescence is turned on by the addition of PPi because the formation of PPi/Cu^{2+} complex (2/1 complex, most possibly) disrupts the binding of Cu^{2+} with the polymer carboxylate groups. The hypothesis that the diphosphate unit acts by binding to and sequestering Cu^{2+} is further supported by the observation that the addition of 10 μM (1 equivalent) of the strong chelator ethylenediamine

tetraacetic acid (EDTA) to the ***w*-P5**/Cu^{2+}/HEPES solution leads to the complete recovery of the polymer's fluorescence intensity.

As the last point, since the selective sensing of PPi in the presence of adenosine triphosphate (ATP), adenosine diphosphate (ADP) is important for some biosensor applications, the response of the current sensor to these two organic anions was also checked. Not surprisingly, addition of ATP elicits a very similar fluorescence response compared to PPi. However, the fluorescence response to ADP is markedly lower than that of PPi; at saturation, addition of ADP leads to only 25% recovery of the initial fluorescence intensity whereas as noted above addition of PPi leads to > 95% fluorescence recovery. Design of sensors based on CPEs that can discriminate PPi, ATP and ADP is the goal of future research.

Experimental

Materials

$Pd(PPh_3)_2Cl_2$ and $Pd(PPh_3)_4$ were purchased from Strem Chemical Company and used as received. 1,4-diiodo-2,5-dimethoxybenzene, bromoacetic acid, trimethylsilylacetylene (98%), 1-dodecanol, bis(trifluoroacetoxy)phenyliodine, tetrabutylammonium fluoride (1 M in THF) and tetrabutylammonium hydroxide (1 M in methanol) were purchased from Acros Chemical Company. Et_3N and THF used in the polymerization were purified by distillation over CaH_2. For all the metal ions, their chloride salts were used. For all the anions, their sodium salts were used. ATP and ADP were purchased from Aldrich chemical Co. and kept in a refrigerator. All the other chemicals were supplied by either Acros or Aldrich Chemical Company and used without further purification.

Instrumentation

NMR spectra were recorded on a Varian VXR-300 or Gemin-300 FT-NMR, operating at 300 MHz for ^{1}H-NMR and at 75.4 MHz for ^{13}C-NMR. High temperature NMR spectra were

recorded on a Varian Mercury 300 FT-NMR. Chemical shifts were reported in ppm using $CHCl_3$ or C_2HD_5SO as internal reference. FTIR spectra were taken on a Perkin-Elmer 1600 spectrometer. Gel permeation chromatography (GPC) analyses were carried out on a system comprised of a Rainin Dynamax SD-200 pump and a Beckman Instruments Spectroflow 757 absorbance detector. UV-visible absorption spectra were obtained on Varian Cary 100 dual beam spectrophotometer, with a scan rate of 300 nm/min. Steady-state fluorescence spectra were recorded on a PTi fluorescence spectrometer.

General Methods

Fluorescence quenching and absorption titration experiments were carried out by micro-titration in a fluorescence cuvette. In a typical titration experiment, 2 mL of a polymer solution was placed in a 1 cm quartz fluorescence cell with a small magnetic stir bar. The UV-Visible absorption and fluorescence spectra were recorded at room temperature. Then fluorescence and/or absorption spectra were repeatedly acquired subsequent to the addition of μL aliquots of a concentrated solution that contained the quencher. Quencher solution aliquots were delivered by using a calibrated Eppendorf micro liter pipetter. For anion sensing experiments, the ***w*-P5**/Cu^{2+} (1/2, concentration ratio) stock solution was prepared one night before the anion titration experiments. The photograph was taken using a Pentax Digital Camera (5 Megapixel) with a bandpass filter (LG 450).

Synthetic Procedures

1,4-Diiodo-2,5-dimethoxybenzene (2). In a 1000 ml three-necked flask fitted with a condenser and a mechanical stirring was charged with a mixture of glacial acetic acid (200 ml), H_2SO_4 (3 ml), H_2O (7 ml), KIO_3 (7.8 g, 36.5 mmol) and I_2 (19.3 g, 76.0 mmol). 1,4-Dimethoxybenzene (10.0 g, 72.4 mmol) was added to the mixture and the dark purple mixture was heated at 120 ºC and stirred for 15 h. Then the purple solution was poured into 200 ml of

$NaHSO_3$ (10%). The grey precipitate was collected on a Büchnel funnel, washed with 200 ml of cold water and dried overnight in the hood. The solid was dissolved in 200 ml of THF/$CHCl_3$ (1/1) and treated with activated carbon. After filtering through a bed of celite, a nice yellow crystalline solid was obtained after the solvent was removed under reduced pressure (Yield: 53%). ^{1}H NMR ($CDCl_3$, δ_{ppm}): 7.17 (s, 2H), 3.81 (s, 6H).

2, 5-Diiodohydroquinone (3).[27] This compound was synthesized using a literature procedure modified for easier work-up. Compound **2** (10.0 g, 38 mmol) was dissolved in 300 ml of dry CH_2Cl_2 in a 1000 ml round bottom flask fitted with a condenser and the resulting mixture was cooled to -78 °C (dry ice/acetone bath). Boron tribromide (14 ml, 148 mmol) was added slowly through the condenser in 1 hr. Upon the completion of the addition, the yellow suspension was stirred at -78 °C for 2 h and then allowed to warm to room temperature. The brown solution was further stirred for 48 h. Then the reaction was quenched by adding 15 ml of cold water (Violent gas evolution!). After the gas evolution subsided, 300 ml of water was poured into the flask. With the addition of 100 ml acetone, the white precipitate formed during the addition of water was re-dissolved in the solution. The bottom layer was collected and the solvent was removed *in vacuo*. Dissolution of the crude product in a minimum of CH_2Cl_2 followed with precipitation into hexane afforded a slight yellow powder (yield: 12.0 g, 87%). ^{1}H NMR (DMSO-d_6, δ_{ppm}): 9.78 (s, 2H), 7.14 (s, 2H).

2,2'-(2,5-Diiodo-1,4-phenylene)bis(oxy)diacetic acid (4). In a 100 ml of three-necked round bottom flask purged with argon, a solution of 2.6 g of NaOH (66 mmol) in 10 ml of water was added drop-wise to a stirred solution of 5.4 g of **3** and 5.0 g of bromoacetic acid (36 mmol) in 25 ml of water. The reaction mixture was heated at reflux for 4 h. At which time, there was a lot of white precipitate formed. The reaction flask was then placed in a refrigerator overnight.

The settled precipitate was collected by vacuum filtration, then re-dissolved in 60 ml of water and acidified with 20 ml of 6 N HCl. The white solid obtained was collected by vacuum filtration, dried under the vacuum. Yield: 6.0 g, 84%. ^{1}H NMR (DMSO-d_6, δ_{ppm}): 13.07 (s, br, 2H), 7.25 (s, 2H), 4.74 (s, 4H). ^{13}C NMR (DMSO-d_6, δ_{ppm}): 169.76, 151.78, 122.28, 86.13, 66.03.

2,2'-(1,4-Phenylenebis(oxy))diacetic acid (6). A solution of 5.0 g (125 mmol) of sodium hydroxide in 20 ml of water was added drop-wise to a stirred solution of 3.3 g (30 mmol) of hydroquinone and 9.2 g (66 mmol) of bromoacetic acid in 30 ml water. The resulting solution was refluxed for 4 hr, then cooled to 2-5 °C whereupon the sodium salt of **6** settled at the bottom of the flask. The white solid was collected on a Büchnel funnel, washed with 60 ml of water, 60 ml of methanol, dried and dissolved in 30 ml of hot water, then acidified with 6 N HCl. The white precipitate was collected by vacuum filtration, rinsed with cold water and dried under vacuum. Yield: 4.5 g, 67%. ^{1}H NMR (DMSO-d_6, δ_{ppm}): 12.94 (s, br, 2H), 6.83 (s, 4H), 4.60 (s, 4H). ^{13}C NMR (DMSO-d_6, δ_{ppm}): 140.32, 122.06, 85.25, 34.96.

Didodecyl 2,2'-(1,4-phenylenebis(oxy))diacetate (7). A mixture of 1.5 g (6.6 mol) of **6**, 25 g (134 mmol) of dodecyl alcohol and 1 ml of 85% phosphoric acid was heated at 150 °C in a two-necked round bottom flask with a magnetic stirring bar. The water formed during the esterification was removed by flowing nitrogen slowly through the top of the reaction flask. After 6 hr, the clear solution was poured into 300 ml of hot hexane. The resulting mixture was cooled in a refrigerator overnight. The obtained white solid was collected by vacuum filtration; further recrystallization from isopropanol affording a white crystalline product (yield: 3.1 g, 84%). ^{1}H NMR ($CDCl_3$, δ_{ppm}): 6.86 (s, 4H), 4.57 (s, 4H), 4.20 (t, 4H). 1.65 (m, 4H), 1.27 (m,

36H), 0.89 (t, 6H). ^{13}C NMR ($CDCl_3$, δ_{ppm}): 169.12, 115.80, 66.17, 65.46, 31.93, 29.65, 29.36, 19.21, 28.54, 25.80, 22.71, 14.14.

Didodecyl 2,2'-(2,5-diiodo-1,4-phenylene)bis(oxy)diacetate (8). Route A: A mixture of 5.0 g (10.5 mmol) of **4**, 37.2 g (0.2 mol) of dodecyl alcohol and 0.5 g of phosphoric acid was heated at 150 °C in a two-necked round bottom flask with magnetic stirring for 6 h. The water formed during the esterification was removed by flowing nitrogen slowly through the top of the reaction flask. After 6 hr, the clear solution was poured into 300 ml of hot hexane. The resulting mixture was cooled in a refrigerator overnight. The obtained white solid was collected by vacuum filtration; further purification was done by recrystallization from iso-propanol (yiled: 85%). Route B: compound **7** (5.2 g, 9.2 mmol) , iodine (2.3 g, 9.2 mmol) and bis(trifluoroacetoxy)phenyliodine (4.3 g, 9.0 mmol) were mixed in 25 ml CCl_4. The purple suspension was stirred at room temperature for 6 h, and then diluted with 75 ml CH_2Cl_2, washed with 5% $NaHSO_3$ till the purple color disappeared. The solution was then dried with anhydrous $MgSO_4$ and the solvent was removed under reduced pressure. The obtained yellow solid was further purified by recrystallization from 25 ml isopropanol, white crystal product was obtained (yield: 6.8 g, 90%). ^{1}H NMR ($CDCl_3$, δ_{ppm}): 7.16 (s, 2H); 4.62 (s, 4 H); 4.22 (t, 4H); 1.67 (m, 4H), 1.27 (m, 36 H); 0.89 (t, 6H). ^{13}C NMR ($CDCl_3$, δ_{ppm}): 168.53, 153.23, 124.03, 86.61, 67.75, 32.37, 30.09, 29.97, 29.81, 29.67, 28.99, 26.28, 23.15, 14.59.

Didodecyl 2,2'-(2,5-bis((trimethylsilyl)ethynyl)-1,4-phenylene)bis(oxy)diacetate (9). Compound of **8** (814 mg, 1 mmol) was dissolved in 10 ml of dry THF/Et_3N (3/1, v/v) in a Schlenk flask and degassed with argon for 15 minutes. Then 21 mg of $Pd(PPh_3)_2Cl_2$ (30 μmol) and 12 mg of CuI (63 μmol) were added, followed with the addition of 0.7 ml of trimethylsilylacetylene (5 mmol). The reaction was stirred at room temperature for 22 hr. After

filtration through a bed of celite (~ 10 cm), the solvent was removed *in vacuo*. The crude product was used for next step without further purification.

Didodecyl 2,2'-(2,5-diethynyl-1,4-phenylene)bis(oxy)diacetate (10). The crude product obtained as above was dissolved in 10 ml of THF. Tetrabutylammonium fluoride (3 ml of a 1 M solution in THF) was added and the resulting mixture was stirred at room temperature for 1 hr. Then the solution was diluted with 20 ml of ethyl ether, poured into a seperatory funnel and washed with water (30 ml × 1). The organic layer was collected and the water layer was extracted with ethyl ether (30 ml × 1). The organic solutions were combined and removal of the solvent afforded a brownish crude product. It was dissolved in a minimum of CH_2Cl_2 and loaded on the top of silica column. The column was first eluted with 300 ml CH_2Cl_2/hexane (v/v = 1/2), then with a mixture of CH_2Cl_2/hexane (v/v = 3/1). A slight yellow solid was obtained (yield: 400 mg, 66% for 2 steps). ^{1}H NMR ($CDCl_3$, δ_{ppm}): 6.95 (s, 2H), 4.66 (s, 4H), 4.18 (s, 4H), 3.37 (s, 2H), 1.56 (m, 4H), 1.26 (s, 36H), 0.87 (t, 6H). ^{13}C NMR ($CDCl_3$, δ_{ppm}): 168.44, 153.69, 118.65, 114.01, 83.53, 78.95, 66.82, 65.64, 31.97, 29.69, 29.68, 29.62, 29.55, 29.40, 29.25, 28.57, 25.85, 22.74, 14.16.

General polymerization procedure for the preparation of P4 and P5. A solution of 2,5-bis(dodecyloxycarbonylmethoxy)-1,4-diiodobenzene (204 mg, 0.25 mmol) (**8**) and didodecyl 2,2'-(2,5-diethynyl-1,4-phenylene)bis(oxy)diacetate (153 mg, 0.25 mmol) (**10**) or 1,4-diethynylbenzene (32 mg, 0.25 mmol) in 10 mL of dry THF/Et_3N (v/v = 2/1) was degassed with argon for 15 minutes. Then 8.7 mg of $Pd(PPh_3)_4$ (7.5 μmol) and 4 mg of CuI (7.5 μmol) were added under argon. The reaction was stirred at 60 ºC for 18 hr. The obtained viscous suspension was poured into 150 mL of methanol, resulting in the precipitation of the ester precursor polymers (**P4** or **P5**) as orange powders and light yellow fibers, respectively. The polymers were

further purified by two repeated cycles of dissolution in THF and precipitation into methanol. A small amount (~30 mg) of each polymer was dried completely under vacuum and used for NMR study immediately (note that after complete drying these polymers are barely soluble in their good solvents, such as THF and $CHCl_3$ and the solubility becomes worse with storing). The rest of the polymer was kept as a THF solution till the next step.

Hydrolysis. To a solution of **P4** (117 mg, 0.20 mmol) or **P5** (135 mg, 0.20 mmol) in 30 mL of dioxane/THF (v/v = 5/1) was added 1.5 mL of 1 M $(n\text{-}Bu)_4NOH$ in methanol, and the resulting mixture was stirred at room temperature for 24 hr. During the course of the hydrolysis reaction, 2 mL of water were systematically added in order to keep the solution clear. Then a solution of 0.20 g of $NaClO_4$ (1.6 mmol) in 3 mL of water was added to the hydrolyzed polymer solution, and the resulting mixture was poured into 400 mL of cold acetone, resulting in the precipitation of ***w*-P4** and ***w*-P5** as fine orange and yellow powders, respectively. The polymer (***w*-P4** or ***w*-P5**) was then dissolved in 50 mL of deionized water (several drops of 1 N NaOH solution were added) and was purified by dialysis against deionized water using a regenerated cellulose membrane (12 kD molecular weight cut-off). After dialysis, the polymer solution was filtered through 1.0 μm glass fiber filter (Fisher Scientific) and stored as the stock solution in the refrigerator.

P4. GPC (THF, polystyrene standard): M_w = 26, 790, M_n = 12, 420, PDI = 2.10. ***w*-P4**. ^1H NMR (D_2O, δ_{ppm}): 7.22 (br, s, 2H), 4.56 (br,s, 4H).

P5. ^1H NMR($CDCl_3$, δ_{ppm}): 7.56 (br, s, 4H), 7.02 (br, s, 2H), 4.74 (br, s, 4H), 4.24 (br, m, 4H), 1.68 (br, m, 4H), 1.25 (br, m, 36H), 0.88 (br, t, 6 H). GPC (THF, polystyrene standard): M_w = 285, 390; M_n = 126, 680, PDI = 2.30. FT-IR (ν_{max}, KBr pellet): 3117, 3039, 2924, 2853, 2208, 1763, 1732, 1598, 1518, 1489, 1467, 1440, 1411, 1282, 1185, 1079, 836, 721, 600, 544.

***w*-P5**. ^{1}H NMR (D_2O/DMSO-d_6 = 1/1, δ_{ppm}): 7.53 (br, s, 4H), 6.97 (br, s, 2H), 4.37 (s, 4H). FT-IR (ν_{max}, KBr pellet): 3332, 2924, 2191, 1778, 1610, 1445, 1323, 1282, 1196, 1047, 941, 880, 837, 779, 700, 668, 600, 544.

CHAPTER 4
VARIABLE CHAIN LENGTH POLY(PHENYLENE ETHYNYLENE) CARBOXYLATE

Introduction

The relationship between the length of conjugated molecules and their optical and electronic properties has been studied intensively.[43,160-162] Most of the research has been focused on the synthesis of monodisperse oligomers with precisely defined length to obtain such information. Unfortunately, preparing these oligomers often requires many synthetic steps and tedious separation and purification.[163-165] Although conjugated oligomers provide excellent model systems for interpreting the electronic and optical properties of their polymeric analogues, study of the chain length dependence in polymeric systems could be more useful in a practical point of view. Molecular weight of conjugated polymer has been shown to play an important role in determining the chain conformation, solid state morphology and thus optical and electronic properties of conjugated polymer thin films. For example, Koynov *et al.*[166] found that the refractive index and birefringence of poly(2-methoxy-5-(2'-ethyl-hexyloxy)-1,4-phenylene vinylene) thin films are strongly dependent on the molecular weight of the polymers. Goh *et al.*[167] also reported that the hole mobility of regioregular poly(3-hexyl-thiophene) in field-effect transitors increases almost 4 orders of magnitude when the molecular weight is varied from 3.2 kD to 36.5 kD.

As mentioned earlier in Chapter 1, amplified fluorescence quenching is an inherent property of conjugated polymers due to the efficient exciton migration along the polymer chain. Thus the signal enhancement of the polymer relative to the small model compound will be a factor that depends on the chain length of the polymer. Swager and co-workers[55] compared the quenching constants of their receptor poly(phenylene vinylene)s with 3 different molecular weights by methyl viologen and pointed out that the increase in molecular weight can produce

greater enhancement only when the chain length of polymer is smaller than the diffusion length of the exciton. For conjugated polyelectrolytes, several researchers have also pointed out that chain length has a big effect on the quenching efficiency of CPEs, but their results were based on comparing only two different molecular weight samples, one extremely low, one substantially high.[60,168]

In this chapter, we present a systematic study of the relationships between photophysical properties, quenching behaviors of CPEs and their molecular weights. The successful synthesis of anionic poly(p-phenylene ethynylene) (PPE)s with 5 different chain lengths was realized via the "precursor route".[129] The molecular weight of the organic soluble polymer precursors was varied in a well-controlled manner by changing the loading amount of a monofunctional monomer, 1-iodo-4-(trifluoromethyl)benzene, in the mixture of bifunctional monomers, 2,5-bis(dodecyloxycarbonylmethoxy)-1,4-diiodobenze (AA-type) and 1,4-diethynylbenzene (BB-type). The molecular weight of each polymer was determined by gel permeation chromatography (GPC), as well as NMR end-group analysis. The series of water-soluble conjugated PPEs with the same chain length as derived from their organic-soluble analogues were obtained by base-catalyzed hydrolysis. Then we carried out a systematic photophysical investigation of the series in methanol and water. To the end, the electron transfer quenching behavior of the series of CPEs with methyl viologen (MV^+, MV^{2+}) and heptyl viologen (HV^+ and HV^{2+}) were explored in methanol.

Results and Discussion

Synthesis

The structures of the monomers and polymers used in the current work are shown in Figure 4-1. 2,5-Bis(dodecyloxycarbonylmethoxy)-1,4-diiodobenze (**1**) and 1,4-diethynylbenzene (**2**) were synthesized following the procedures reported in the previous chapters. 1-Iodo-4-

(trifluoromethyl)benzene (**3**) was purchased from Aldrich and used as the monofunctional monomer. Its reaction with the growing polymer can generate chain ends devoid of the reactive functional group (the iodide group), making the chain incapable of further reaction. Thus the monofunctional monomer is often referred as the end-capper for the polymer chains. In such a polymerization, the amount of the monofunctional monomer in the initial reaction mixture controls and limits the polymerization of bifunctional monomers, which leads to polymers with varied molecular weights. In order to minimize the influence of the polymerization by other factors, such as catalyst loading, monomer concentration, etc., all the polymerizations were carried out in the mixture of THF/Et_3N (v/v, 3/2) with monomer concentrations for the bifunctional monomers kept at 25 mM in the presence of $Pd(PPh_3)_4$ and CuI catalysts.

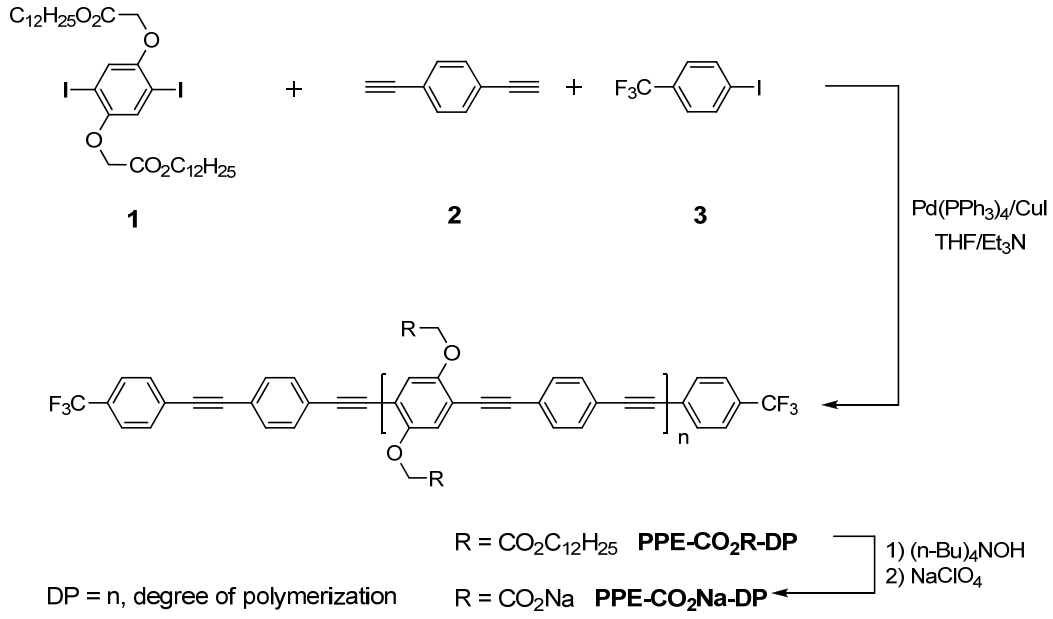

Figure 4-1. The synthetic route for conjugated polyelectrolytes with different chain lengths

Since polycondensation based on Sonogashira coupling follows the step-growth polymerization mechanism, the resulting degree of polymerization (DP) is related inversely to the extent of the reaction (p) by the equation:[133]

$$DP = 1/(1-p) \qquad (4\text{-}1)$$

if the two reactive monomers are present in a stoichiometric balance. In view of this, first we carried out a polymerization using a stoichiometric amount of monomer **1** and **2** in the absence of monofunctional monomer **3**. The polymerization process was monitored using GPC and indeed we observed typical GPC traces characteristic of the step-growth polymerization. The number-average molecular weight of the final polymer is 127 kD corresponding to a DP of 187, as determined by GPC using polystyrene as the standard in THF. The extent of polymerization (p) is estimated to be 0.995 by a reverse calculation using the equation of p = 1-1/DP. Assuming a similar p for all the reactions under the same polymerization conditions, the expected molecular weights of the other polymers by polymerizing **1** and **2** in the presence of varying amounts of **3** (from 25% to 1%) were predicted using the Carothers equation[133] and listed as column 3 in Table 4-1.

Table 4-1. GPC and ^{1}H NMR end-group analysis of the precursor polymers.

	End-capper (%)[a]	[DP][b]	GPC			NMR
			M_n	DP	PDI	DP
PPE-CO_2R-7	25	9	5,390	7	1.80	7
PPE-CO_2R-13	15	14	9,040	13	2.30	12
PPE-CO_2R-35	5	33	24,390	35	2.30	21
PPE-CO_2R-49	3	51	33,760	49	2.30	28
PPE-CO_2R-108	1	100	74,350	108	2.70	85
PPE-CO_2R-187	0	—	127,950	187	2.90	—

Note: [a] molar percent; [b]DP calculated using Carothers equation:[133] DP = (1+r)/(1+r-2rp); r, stoichiometric imbalance; p, extent of reaction.

Polymer Characterization

Gel permeation chromatography

The molecular weights (MWs) of all the polymers were measured in THF solutions using GPC with a UV detector. The GPC chromatograms of all the polymers are shown in Figure 4-2,

indicating monomodal distributions of molecular weights for all the polymers. The number-average molecular weights (M_n) obtained from GPC (column 4 in Table 4-1) correspond well with the predicted M_n, suggesting that all the polymers with controlled chain length are functionalized at both ends with the end-capper. The polydispersity indices (PDIs) of all the polymers are ~ 2, which is in agreement with Flory-Schulz distribution of the molecular weight for ideal step-growth polycondensation.[169] For clarity, all the polymers are named in this format, PPE-CO_2X-DP (X = R for organic precursors and X = Na for CPEs).

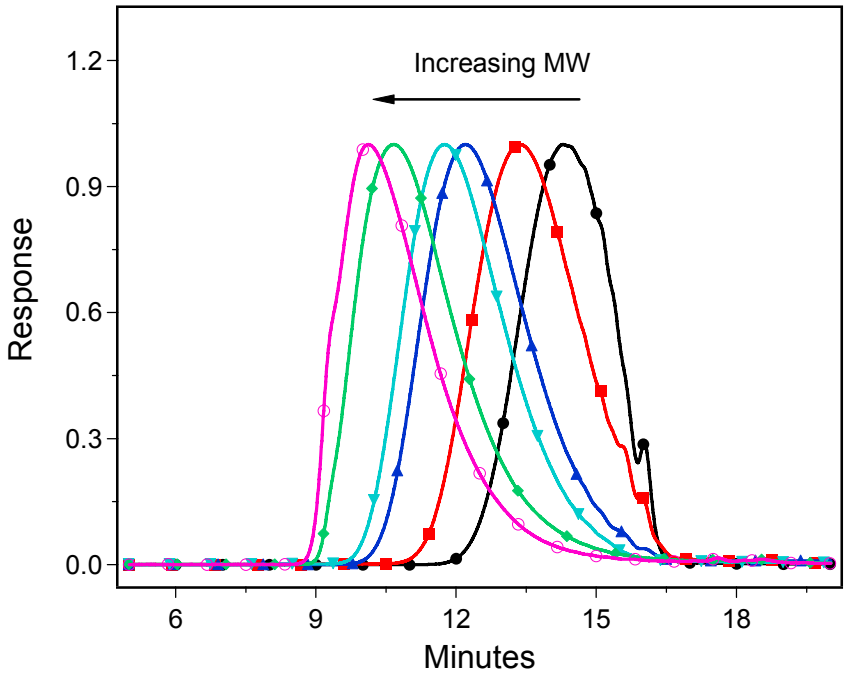

Figure 4-2. GPC chromatograms of the precursor polymers, PPE-CO_2R-7 (●), PPE-CO_2R-13 (■), PPE-CO_2R-35 (▲), PPE-CO_2R-49 (▼), PPE-CO_2R-108 (♦) and PPE-CO_2R-187 (○). Symbols were added to delineate different curves.

NMR spectra

Each polymer was characterized by ^{1}H NMR spectroscopy in order to examine the purity and prove the existence of the end groups. As an example, the ^{1}H NMR spectrum of PPE-CO_2R-7 is shown in Figure 4-3. The singlet at δ = 4.73 ppm (d) is assigned to the methylene group protons (– O***CH₂***$CO_2C_{12}H_{25}$) and the other signals in the aliphatic area (e, f, g, h) are

caused by the dodecyl groups. The inset shows the expansion of the aromatic region. The aromatic protons of the end groups (trifluoromethylbenzene) appear as a singlet at δ = 7.64 ppm (a)[170] and the aromatic protons of the 1,4-phenylene and 2,5-disubstituted-1,4-phenylene on the backbone appear at δ =7.56 ppm (b) and δ =7.02 ppm (c), respectively.

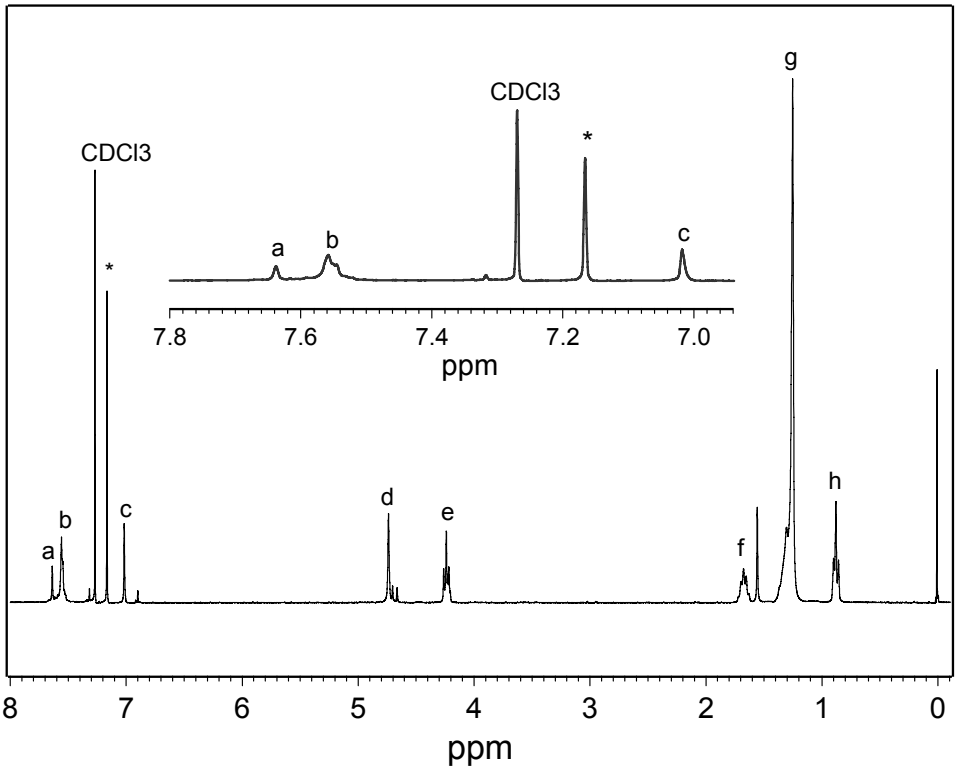

Figure 4-3. ^{1}H NMR spectrum of PPE-CO_2R-7 in $CDCl_3$. The starred signal at 7.17 ppm is from octafluoro[2.2]paracyclophane added as the internal standard for ^{19}F NMR study. Analysis of the molecular weight using ^{19}F NMR was unsuccessful due to the distinct relaxation behavior of the polymer and the small fluorinated compound.

End group analysis by NMR

The GPC method used to determine the molecular weights of our polymers is sensitive to the employed calibration standards.[169] It has been proven that using the polystyrene calibration to evaluate the GPC of rigid-rod polymers (like ours) overestimates the molecular weight by a factor of 1.4 ~ 2.0.[10] Since the aromatic protons from the end group phenyl (a) and backbone phenyl (b and c) can be discriminated in the ^{1}H NMR spectra, the average number of repeat units

(n or DP) can be determined by comparing the integrations of proton signals from the end group and the main chain .

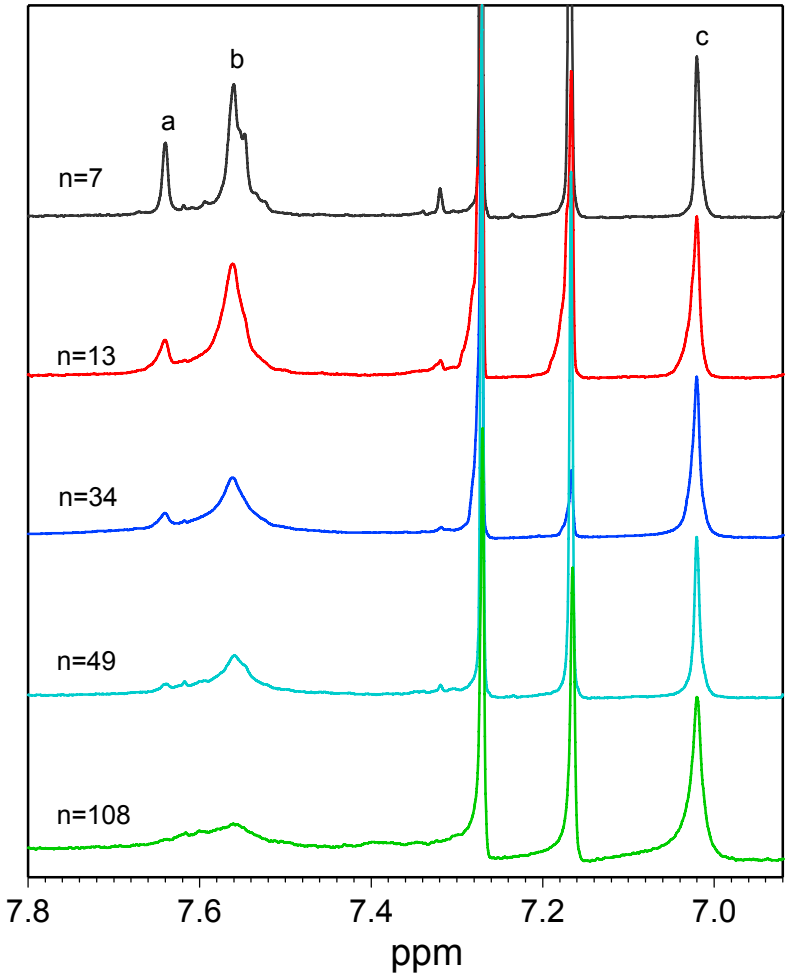

Figure 4-4. The aromatic region in the ^{1}H NMR spectra of the precursor polymers with variable chain length in $CDCl_3$.

As shown in Figure 4-4, with the increase of the molecular weight, the signal at δ =7.56 ppm (b) corresponding to the 1,4-phenylene on the backbone becomes broader and begins to overlap the signal for the end groups (a, δ = 7.64 ppm). By contrast, another signal from the polymer backbone protons at δ =7.02 ppm (c, 2,5-disubstituted-1,4- phenylene) is well separated from the end group signal. Thus the DPs of the polymers were extrapolated by comparing the integration at δ = 7.64 ppm (a) to the integration at δ =7.02 ppm (c) and the results are listed in

Table 4-1. The values obtained by ^{1}H NMR are close to the values determined by GPC for low-MW samples (PPE-CO_2Na-7 and PPE-CO_2Na-13). For medium-MW samples (PPE-CO_2Na-35 and PPE-CO_2Na-49), the values calculated by ^{1}H NMR differ by a factor of 1.7-1.8 compared to the values by GPC. And a smaller factor of 1.3 is resulted for high-MW sample, PPE-CO_2Na-108. These results are consistent with other observations made for rigid-rod oligomers and high-MW PPEs.[10,46,171] Since GPC is an indirect measure of the molecular weight based on the hydrodynamic volume,[169] the rigidity of the PPE chains has a strong effect on the accuracy of the molecular weight obtained by GPC using randomly coil polystyrene as the standard. In the low-MW region, prior to significant coiling of polystyrene chains, GPC gives accurate measurement of molecular weight for rigid-rod like PPEs. For medium-MW PPEs, the molecular weights by GPC are largely exaggerated because of the significant coiling of polystyrene chains. However, for high-MW PPEs, the polymer chains become considerably more flexible, which makes polystyrene a better standard again.

Structural characterization of water-soluble polymers

The water-soluble polyelectrolytes of different chain length were prepared following the procedure used in Chapter 3 for hydrolyzing the dodecyl ester groups. After hydrolysis, the polymers were characterized by ^{1}H NMR and IR, as shown in Figure 4-5. The ^{1}H NMR spectra of all the polymers in the D_2O/DMSO-d_6 mixture (v/v, 1/1) show only one signal in the aliphatic area at δ = 4.35 ppm corresponding to the methylene groups (– O***CH*****$_2$**CO_2Na –), which confirms the complete cleavage (> 95%) of the ester groups. In the aromatic region, the protons from the polymer backbone are observed. Similar to the changes in the ^{1}H NMR spectra of their organic precursor polymers, with the increase of the molecular weight, the signal for the end groups becomes weak and is barely detectable for high-MW polymers.

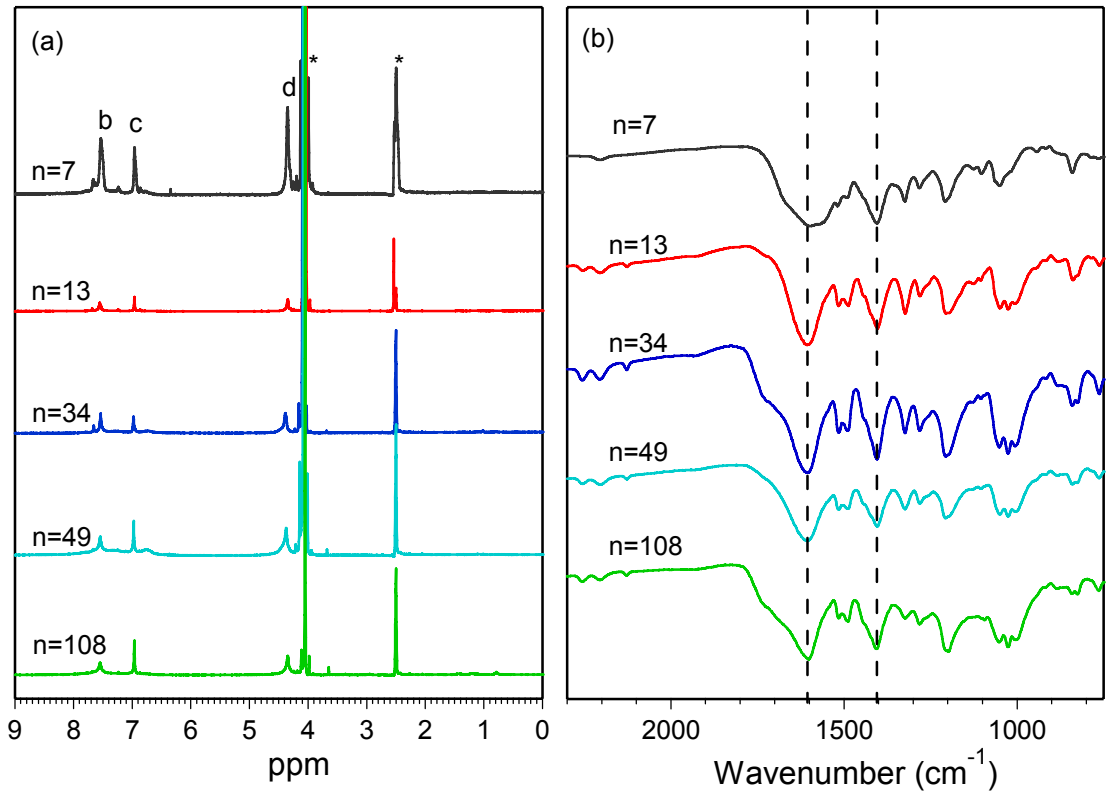

Figure 4-5. ^{1}H NMR (a) and IR (b) spectra of the water-soluble polymers with different chain length. The starred signals at 4.05 ppm and 2.50 ppm in the ^{1}H NMR spectra are due to DMSO-d_6 and D_2O, respectively.

Infrared spectra for all the water-soluble polymers are shown in Figure 4-5 (b). As there is no structural difference between these polymers except for the molecular weight, IR spectra of these polymers are very similar to each other. The absorption at 1600 cm^{-1} and 1400 cm^{-1} can be attributed to the symmetrical and unsymmetrical vibration of the carboxylate (CO^{2-}) group, respectively. Another strongly absorption at 1205 cm^{-1} for all the polymers arises most possibly from the unsymmetrical stretching of C-O-C bond.

Photophysical Characterization

In methanol

Figure 4-6 (a) illustrates the absorption and emission spectra of the five CPEs in MeOH. Across the series, the absorption maximum ($\pi \rightarrow \pi^*$) shifts from 404 nm (PPE-CO_2Na-7),

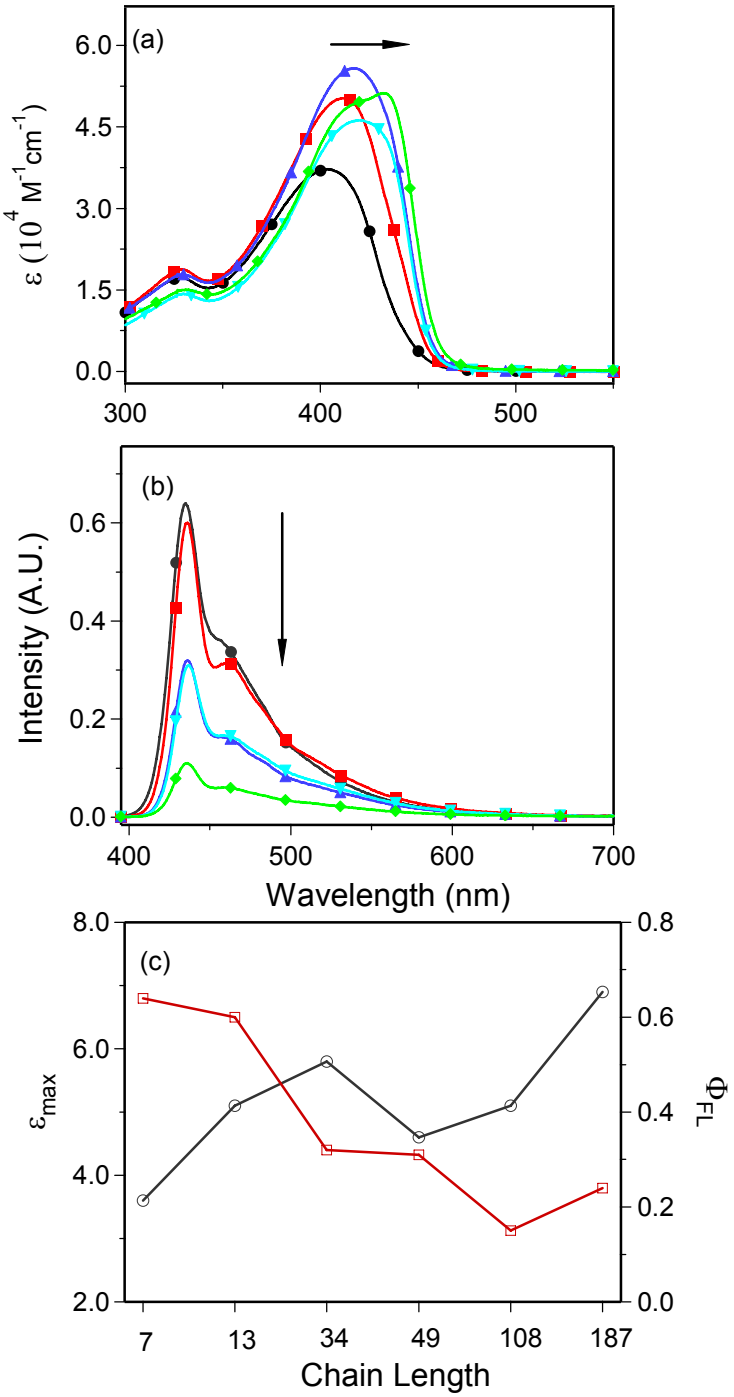

Figure 4-6. Absorption (a) and emission spectra (b) of the series in methanol, PPE-CO_2Na-7 (●), PPE-CO_2Na-13 (■), PPE-CO_2Na-35 (▲), PPE-CO_2Na-49 (▼), PPE-CO_2Na-108 (♦). Symbols were added to delineate different curves. (c) Dependence of molar extinction coefficient (○) and fluorescence quantum yield (□) on the polymer chain length. Arrows show the direction of change with increasing chain length.

411 nm (PPE-CO_2Na-13) to 417 nm (PPE-CO_2Na-49) due to the fact that conjugation length increases when chain length increases. This effect has been well documented by the intensive studies of well-defined oligomers.[43,160] For the current series, the extension of conjugation saturates at this point, further increase of molecular weight of the polymer leads to the appearance and the growing of the shoulder absorption (432 nm) and eventually the shoulder becomes the maximum absorption peak (PPE-CO_2Na-108). Based on our studies on PPEs with sulfonate[71] and carboxylate side groups[172] and other people's work,[140] this peak at 432 nm is assigned to planarization of PPE chains due to aggregation. Besides the change of wavelength for samples with different chain lengths, the trend of increasing molar extinction coefficient from 3.6×10^4 $M^{-1}\cdot cm^{-1}$ (PPE-CO_2Na-7) to 5.8×10^4 $M^{-1}\cdot cm^{-1}$ (PPE-CO_2Na-35) and 6.9×10^4 $M^{-1}\cdot cm^{-1}$ (PPE-CO_2Na-187) is also evident. The "less-than-expected" molar extinction coefficients for PPE-CO_2Na-49 and PPE-CO_2Na-108 might be due to the emerging new band because of aggregation.

In contrast to the clear red-shift of the absorption maximum depending on the chain length, all the polymers emit at the same wavelength of 436 nm (0-0 band), as shown in Figure 4-6 (b). This can be explained by the fact that these polymers are poly-dispersed (PDI ≈ 2) and efficient energy transfer could occur among segments of different conjugation length for each polymer sample. Eventually, the emission is from the segments with the longest conjugation length (lowest energy). As also seen in Figure 4-6 (b) in which the emission spectra are normalized according to respective quantum yield, it is obvious that the quantum efficiency decreases dramatically when the polymer chain length increases from low-MW polymers (PPE-CO_2Na-7 and PPE-CO_2Na-13) to medium-MW polymers (PPE-CO_2Na-35 and PPE-CO_2Na-49), and eventually to the large-MW polymer (PPE-CO_2Na-108). This effect is due to two possible

reasons. First, the chain length increase adds more freedom of conformational, vibrational and rotational changes to the polymer chain, therefore increases the possibility of non-radiative decay. Second, aggregate formation in high-MW polymers creates the "excimer-like" state, which competes with the radiative decay process from the excited state of the free polymer chains.

The molar extinction coefficients and quantum yields of the series are plotted versus the chain length together with those of PPE-CO_2Na-187, as shown in Figure 4-6 (c). The trends for decreasing molar extinction coefficients and increasing quantum yields with the chain length as described above are clearly evident. The little increase of quantum yield of PPE-CO_2Na-187 compared to PPE-CO_2Na-108 might arise from the absence of the end groups (a potential electron acceptor) on the polymer chains of PPE-CO_2Na-187.

In water

In comparison with their photophysical properties in methanol, the absorption and emission spectra of these CPEs in water are predominantly determined by the aggregation of the polymer chains. As shown in Figure 4-7 (a), the absorption of PPE-CO_2Na-7 shows a major absorption band centered at 409 nm and a shoulder band at 437 nm. Further increase of molecular weight leads to a negligible wavelength shift of the absorption band at 409 nm, rather a continuous increase of the shoulder intensity is observed. For PPE-CO_2Na-35, PPE-CO_2Na-49 and PPE-CO_2Na-108, the band at 437 nm becomes the major absorption. The molar extinction coefficients of the series in water show an increasing trend with the increase of molecular weight ($7 < 13 < 35 < 49$, $108 < 187$).

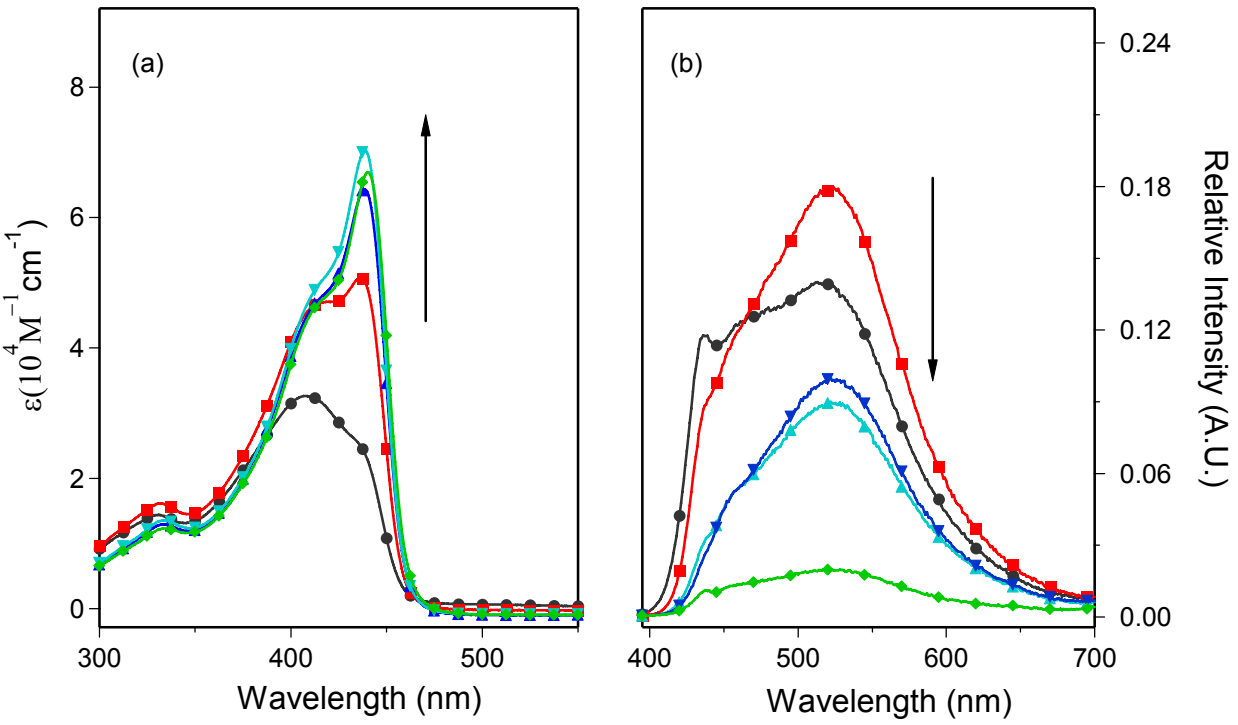

Figure 4-7. (a) Absorption and (b) emission spectra of the series in water, PPE-CO_2Na-7 (●), PPE-CO_2Na-13 (■), PPE-CO_2Na-35 (▲), PPE-CO_2Na-49 (▼), PPE-CO_2Na-108 (♦). Arrows shows the change direction with increasing chain length. Symbols were added to delineate different curves.

Figure 4-7 (b) illustrates the fluorescence spectra in water for polymers with different molecular weights. Similar to the earlier results for PPE with pendant carboxylate side chains (chapter 3) without any special end groups , the fluorescence spectra of the current CPEs with different chain length in water show a broad, red-shifted and structureless band at 520 nm with significantly lower quantum yield (4% - 18%), which confirms the aggregate formation. Table 4-2 summarizes the photophysical data of all the polymers in methanol and water. Three trends are clearly evident from these data. First, all the polymers feature a blue emission at 436 in methanol and a green emission at 520 nm in water regardless of their chain length; second, the molar extinction coefficient increases with the increasing chain length in both methanol and water; third, the quantum yield decreases with the increasing chain length in both solvents.

Table 4-2. Photophysical properties of the CPEs with different chain lengths in methanol and water.

	In methanol				In water			
	λ_{max}^{ab} (nm)	ε_{max} ($\times 10^4$) $M^{-1}\cdot cm^{-1}$	λ_{max}^{em} (nm)	Φ_{FL}[a]	λ_{max}^{a} [b] (nm)	ε_{max} ($\times 10^4$) $M^{-1}\cdot cm^{-1}$	λ_{max}^{em} (nm)	Φ_{FL}[a]
PPE-CO_2Na-7	404	3.6	436	0.64	408	3.3	520	0.14
PPE-CO_2Na-13	411	5.1		0.60	436	5.1		0.18
PPE-CO_2Na-35	417	5.8		0.32	438	6.5		0.09
PPE-CO_2Na-49	419	4.6		0.31	439	7.0		0.1
PPE-CO_2Na-108	432	5.1		0.15	440	6.8		0.04
PPE-CO_2Na-187[b]	433	6.9		0.23	441	9.1		0.07

[a] Coumarin 102 in EtOH as standard, $\Phi_{FL} = 0.95$.[173] [b] This is the polymer obtained when no end-capper was added in the reaction mixture.

Fluorescence Quenching with Electron Acceptors

Previously, we and others have studied the fluorescence quenching of anionic conjugated polyelectrolytes with methyl viologen carrying different charges.[126,134] It was found that K_{sv} increases when the charge on the quencher is increased, which is ascribed to the stronger complexation and/or induced-aggregation for quenchers with greater charger.[61,126,134]

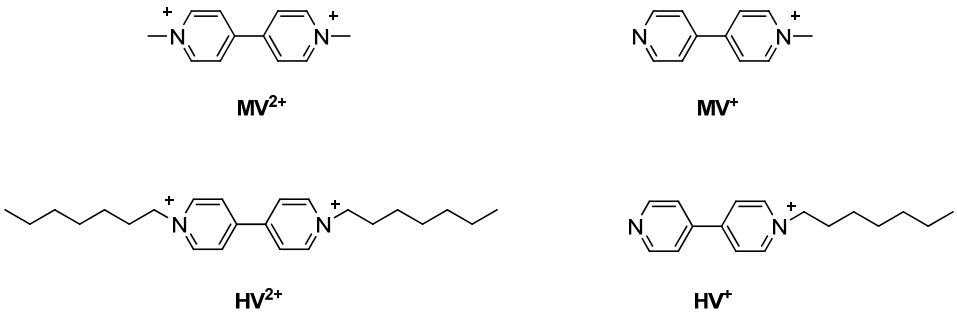

Figure 4-8. Molecular structures of the quenchers used in the current study.

Here, we studied the quenching of the PPE series with different chain lengths by 4 different quenchers, including methyl viologen (MV^+, MV^{2+}) and heptyl viologen (HV^+ and HV^{2+}). Their structures are shown in Figure 4-8. In order to examine the effect of chain length

on the quenching constants, all the experiments were carried out in methanol, in which the PPEs are believed to predominantly exist in a "molecularly dissolved" state.

Quenching of PPE-CO_2Na-7 by MV^+ and MV^{2+}

First we compared the quenching of PPE-CO_2Na-7 in methanol by MV^+ and MV^{2+}. The polyelectrolyte concentrations were kept at 5.0 μM (polymer repeat unit) to prevent possible concentration-dependent aggregation.

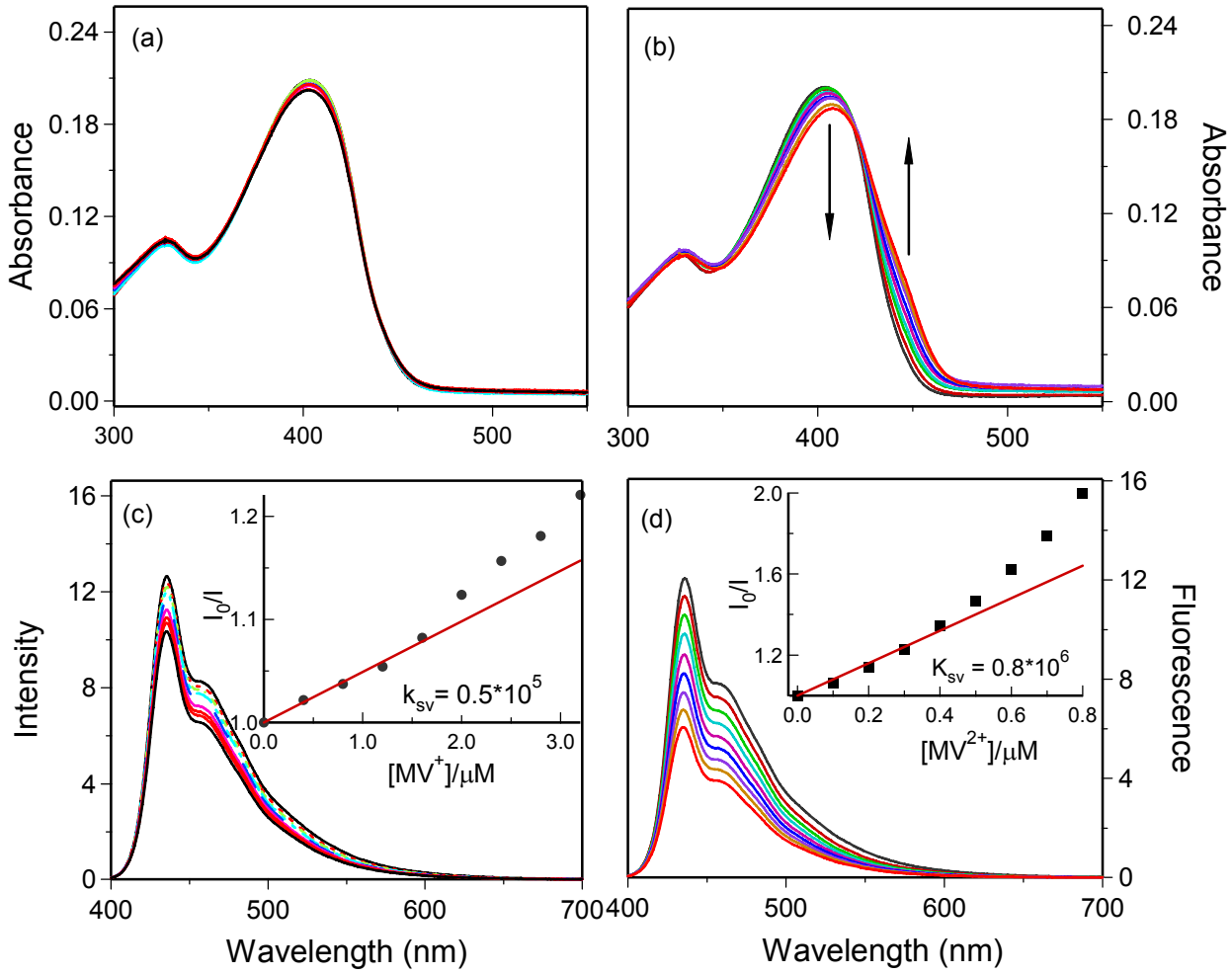

Figure 4-9. Absorption (a) and emission (c) spectra of PPE-CO_2Na-7 with the addition of MV^+, [MV^+] ranges from 0.4 μM to 3.2 μM. Absorption (b) and emission (d) spectra of PPE-CO_2Na-7 with the addition of MV^{2+}, [MV^{2+}] ranges from 0.1 μM to 0.8 μM. Emission intensity decreases with increasing quencher concentration. [PPE-CO_2Na-7] = 5 μM. Emission spectra were measured with excitation at 380 nm. Insets of c and d show the SV-plots of each quencher and the linear fits.

Figure 4-9 illustrates the absorption and emission spectra of PPE-CO_2Na-7 upon the addition of MV^+ and MV^{2+}. The insets in both fluorescence spectra (c and d) are the Stern-Volmer (SV) plots obtained by plotting the fluorescence intensity ratio (monitored at 436 nm) as a function of quencher concentration. From the spectral comparison, two trends are evident. First, the addition of even very small amount of the divalent cationic quencher (MV^{2+}) induces continuous absorption intensity decreases and red-shifts of the absorption spectra (Figure 4-9 b), indicating the aggregation of the polymer chains. Second, quenching of the polymer fluorescence is more efficient for MV^{2+} than MV^+. The Stern-Volmer constants (K_{sv}) for both quenchers were extrapolated by fitting the linear region of the SV plot. The K_{sv} value for MV^{2+} is 0.8×10^6 M^{-1}, which is 10 times larger than the value for MV^+, which is 0.5×10^5 M^{-1}. Based on our earlier results and other people's work,[61,172] we attribute the enhanced quenching by MV^{2+} to the ability of the divalent cation to induce the aggregation of the polymer chains.

Quenching of the series by monovalent cationic quenchers.

In order to explore the chain length effect on the amplified fluorescence quenching, first the quenching of the series by two monovalent cationic methyl viologen derivatives (MV^+ and HV^+) was investigated. Similar to PPE-CO_2Na-7 (Figure 4-9 a), there is also no spectral shift in the absorption spectra of PPE-CO_2Na-13, PPE-CO_2Na-35 and PPE-CO_2Na-49 with the addition of quencher (MV^+ or HV^+), indicating that the quencher-induced aggregation of polymer chains is a minor process when monovalent cationic quenchers are used. For PPE-CO_2Na-108 which shows a strong tendency to aggregate even in MeOH, adding monovalent cationic quenchers (MV^+ or HV^+) helps to break the polymer aggregate, which will be discussed in the following section. The quenching effects were all evaluated using the Stern-Volmer (SV) equation with the fluorescence intensity monitored at 436 nm. As shown in Figure 4-10 (a), the SV quenching plots for the series with MV^+ exhibit nearly linear correlations within the quencher concentration

range from 0 μM to 3.2 μM. The K_{sv} values for the series of different chain lengths were extrapolated by fitting the linear region of the SV plots. It increases from 0.5×10^5 M^{-1} (PPE-CO_2Na-7) to 2.1×10^5 M^{-1} (PPE-CO_2Na-49), then drops down to 1.4×10^5 M^{-1} (PPE-CO_2Na-108).

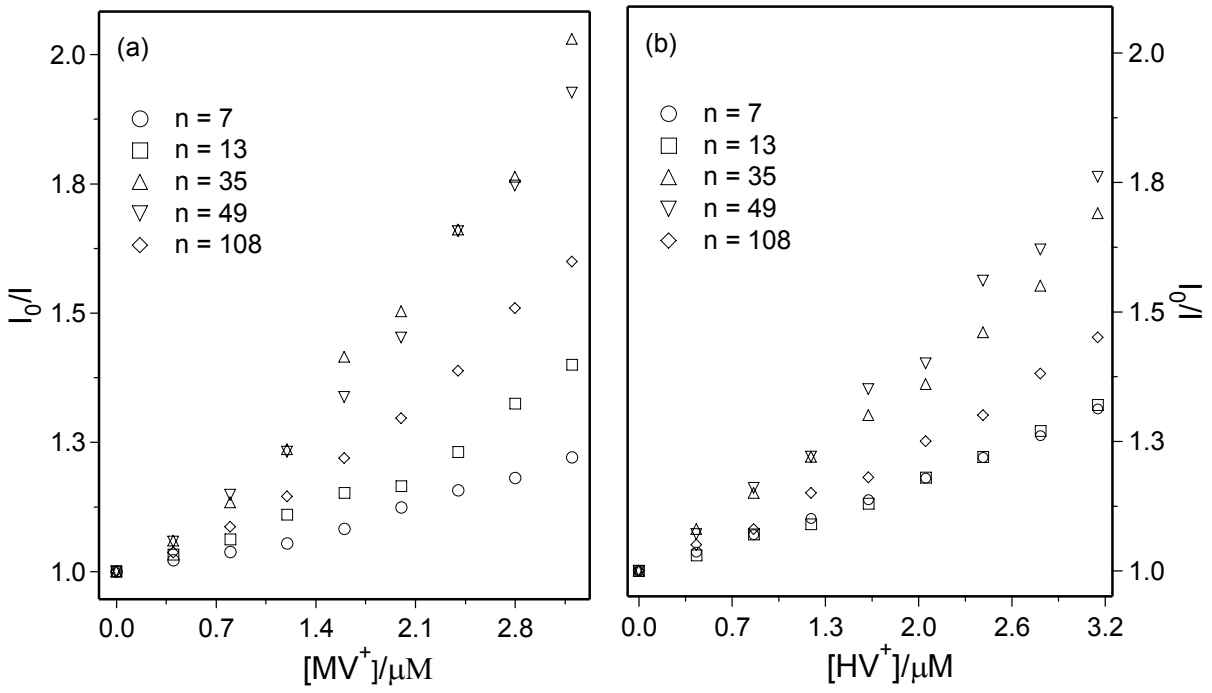

Figure 4-10. SV Plots of the series in MeOH quenching by MV^+ (a) and HV^+ (b), respectively. [Polymer] = 5 μM. MV^+ or HV^+ was added in 0.4 μM aliquots, ranging from 0 μM to 3.2 μM. The emission intensity was monitored at 436 nm.

Figure 4-10 (b) illustrates the SV quenching plot of the series by HV^+. Similar dependence of quenching efficiency on polymer chain length is observed. The K_{sv} values were also obtained from the slopes of the linear fits of their SV plots, ranging from 0.9×10^5 M^{-1} (PPE-CO_2Na-7) to 2.2×10^5 M^{-1} (PPE-CO_2Na-49). For PPE-CO_2Na-108, a smaller value of 1.3×10^5 M^{-1} is obtained for K_{sv}. In general, for the same polymer, HV^+ shows a higher quenching efficiency than MV^+ (larger K_{sv} values), which is due to the more hydrophobic nature of HV^+ compared to MV^+.

Quenching of the series by divalent cationic quenchers

In the second line of the investigation, we carried out the fluorescence quenching of the series by two different divalent cationic quenchers, MV^{2+} and HV^{2+}.

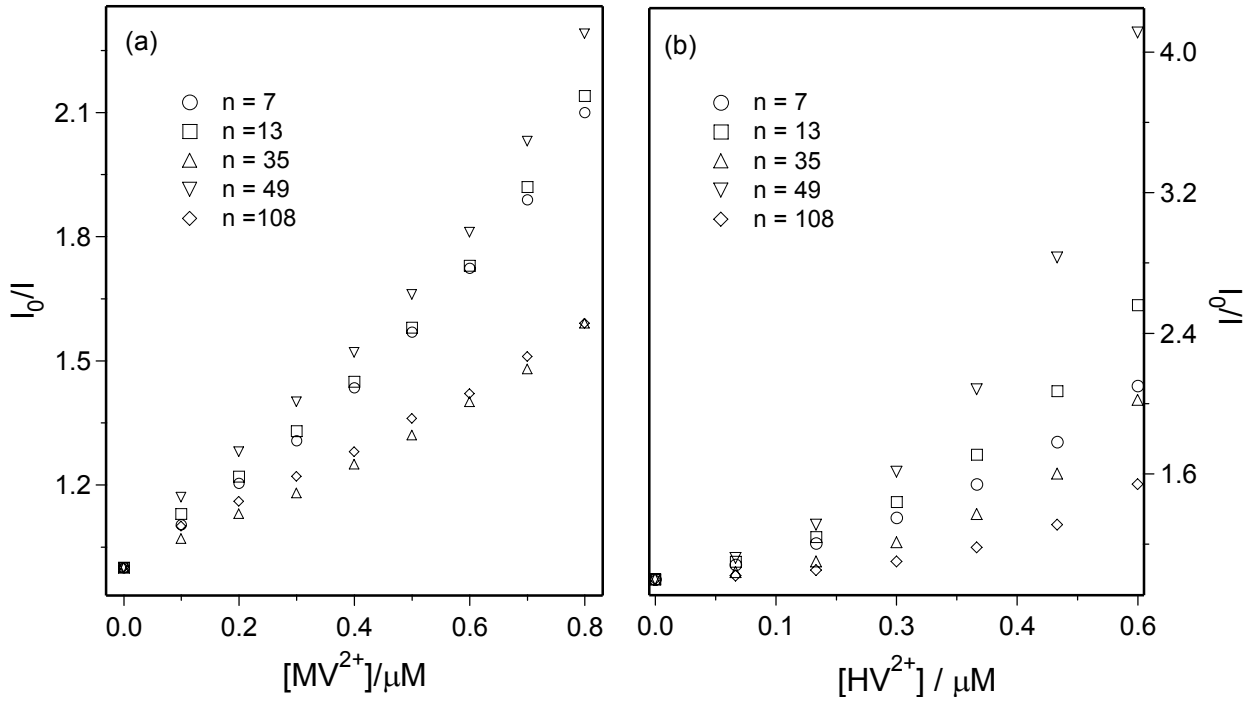

Figure 4-11. SV plots of the series quenching in MeOH by MV^{2+} (a) and HV^{2+} (b), respectively. [Polymer] = 5 μM. MV^{2+} or HV^{2+} was added in 0.1 μM aliquots, ranging from 0 μM to 0.8 μM. The emission intensity was monitored at 436 nm.

As shown earlier in the quenching of PPE-CO_2Na-7 by MV^{2+}, the divalent cationic quencher shows higher quenching efficiency compared to the monovalent cationic quencher, MV^{+}. The enhanced quenching efficiency is attributed to the ability of the divalent cationic quencher to induce the aggregation of the polymer chains.[71,172] During the fluorescence quenching experiments by MV^{2+} and HV^{2+} of the series, we monitored the UV-Vis absorption spectra of each polymer in the course of quencher titration. It was observed that bathochromic shift is a common feature for all the polymers, indicating that the aggregation is induced by the divalent cationic quenchers. Figure 4-11 shows the SV quenching plots of the series by MV^{2+}

(Figure 4-11 a) and HV^{2+} (Figure 4-11 b). In the concentration range of 0 - 0.4 μM, a linear SV relationship is observed for the fluorescence quenching by both quenchers. The K_{sv} values obtained for the polymers by either MV^{2+} or HV^{2+} are all in the order of 10^6 M^{-1} and follow the following order: PPE-CO_2Na-49 > PPE-CO_2Na-7, PPE-CO_2Na-13 > PPE-CO_2Na-35, PPE-CO_2Na-108.

Quenching of PPE-CO_2Na-108 by MV^+ and MV^{2+}

As noted earlier in the study of absorption and emission spectra of the series in different solvents, it was observed that for PPE-CO_2Na-108, there is a pronounced contribution from the aggregated polymer chains to both spectra even in methanol. When the quenching experiments by MV^+ or MV^{2+} were carried out, different spectral changes were observed in the absorption spectra.

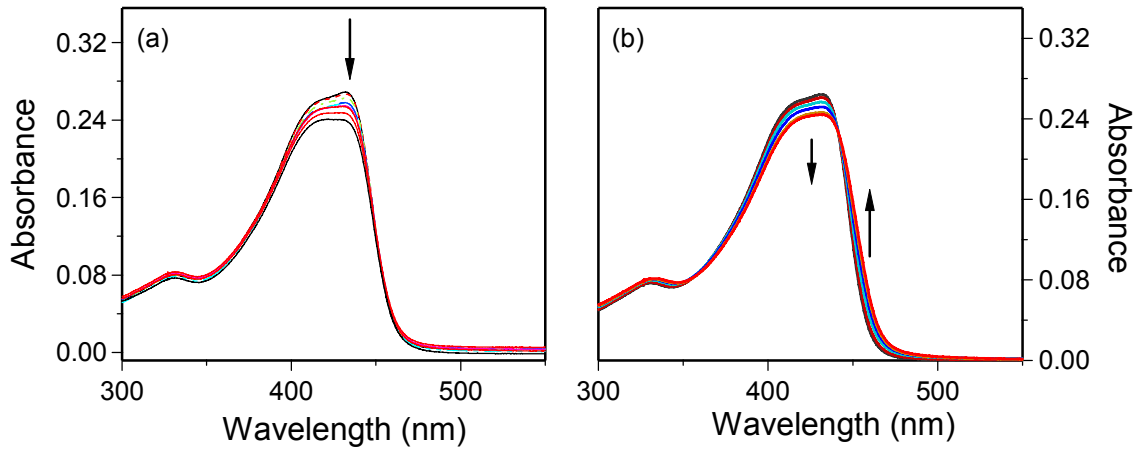

Figure 4-12. UV-visible absorption spectra of PPE-CO_2Na-108 in MeOH with the addition of MV^+ (a) and MV^{2+} (b). [PPE-CO_2Na-108] = 5 μM. MV^+ was added in 0.4 μM aliquots, [MV^+] ranges from 0 μM – 3.2 μM. MV^{2+} was added in 0.1 μM aliquots, [MV^{2+}] ranges from 0 μM -0.5 μM. Arrows show the direction of change with the addition of quenchers.

As shown in Figure 4-12 (a and b), with the addition of MV^+, the absorption intensity of the shoulder (432 nm) is attenuated in a stepwise manner; while a continuous intensity decrease and red-shift of the absorption are resulted with increasing MV^{2+}. Because the shoulder peak

arises from the planarization of PPE backbone in the aggregate, the decrease of the shoulder intensity signals that some of the aggregated chains are de-aggregated after forming the weak complex with MV^{+}. In contrast, during the titration of MV^{2+}, the bathochromic shift suggests that more chains are aggregated with the addition of divalent cationic quencher as observed for other polymers with shorter chain lengths.

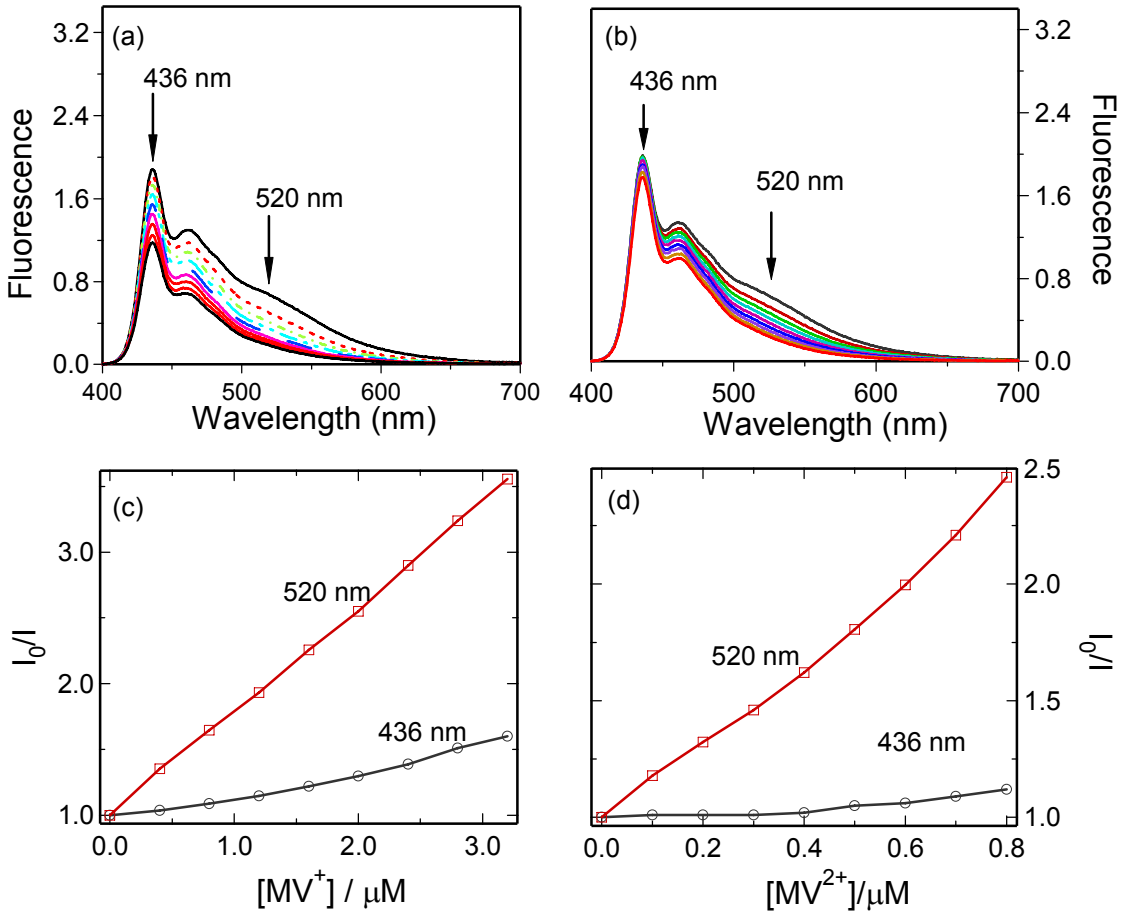

Figure 4-13. Emission spectra (a) and SV-plot (c) of PPE-CO_2Na-108 in MeOH with the addition of MV^{+}. [PPE-CO_2Na-108] = 5 μM. MV^{+} was added in 0.4 μM aliquots, [MV^{+}] ranges from 0 μM - 3.2 μM. Emission spectra (b) and SV-plot (d) of PPE-CO_2Na-108 with the addition of MV^{2+}. MV^{2+} was added in 0.1 μM aliquots, [MV^{2+}] ranges from 0 μM - 0.8 μM.

As shown in Figure 4-13 (a, b), although the emission at 436 nm is still the dominant band in the fluorescence spectrum of PPE-CO_2Na-108 in methanol, the band at 520 nm due to the aggregate can be readily seen (upper). With the addition of either MV^{+} or MV^{2+}, the emission

band at 520 nm (aggregate) decreases in intensity prior to the band at 436 nm (free polymer chain). The difference in the quenching efficiency for the two bands is clearly revealed by the slope of the SV plots obtained by monitoring the emission intensity at different wavelengths (Figure 4-13 c, d). The K_{sv} values calculated for MV^+ are 7.9×10^5 M^{-1} (aggregate) and 1.4×10^5 M^{-1} (free polymer chain), respectively. For MV^{2+}, K_{sv} values of 1.7×10^6 M^{-1} and 1.3×10^5 M^{-1} are obtained for the aggregates and free polymer chains, respectively. One conclusion that can be drawn from the result is that there is a competing quenching by the quencher molecule between the free polymer chains and the aggregates of PPE-CO_2Na-108 in MeOH. And the emission from the aggregates is quenched more efficiently by the quencher molecules compared to the emission from the free chains.

Chain length dependence of K_{sv}

Taken together, the current research shows that there is a correlation between the SV quenching constant (K_{sv}) and the chain length of the PPEs. In our study, using the monovalent cationic methyl viologen derivatives (MV^+ and HV^+) as the quenchers, we were able to clarify the influence of the chain length on the quenching constant. For the two monovalent quenchers, the SV constants obtained from the quenching experiments in methanol are plotted versus the chain length as a bar graph, which is shown in Figure 4-14.

For MV^+, the K_{sv} value is tripled when the chain length is increased from 8 to 35, and further increase of the chain length (n = 49) only results in a slight improvement (15%) indicating that the chain length effect saturates around this point. Since each polymer repeat unit contains two phenylene ethynylene moieties; the exciton diffusion length of the current polymers can be estimated to be about 98 phenylene ethynylene units based on GPC or 56 phenylene ethynylene units based on NMR. The drop of K_{sv} values for PPE-CO_2Na-108 is most probably due to the fact that the aggregates existing in the polymer solution compete with the free polymer

chains for the quencher molecules (as shown in Figure 4-13 c). Thus the actual number of quencher molecules that can quench the fluorescence of the free polymer chain (intensity at 436 nm) is much smaller than the number of quencher molecules added. Since the K_{sv} value is calculated based on the total concentration of the quencher molecules, it underestimates the K_{sv} value for PPE-CO_2Na-108.

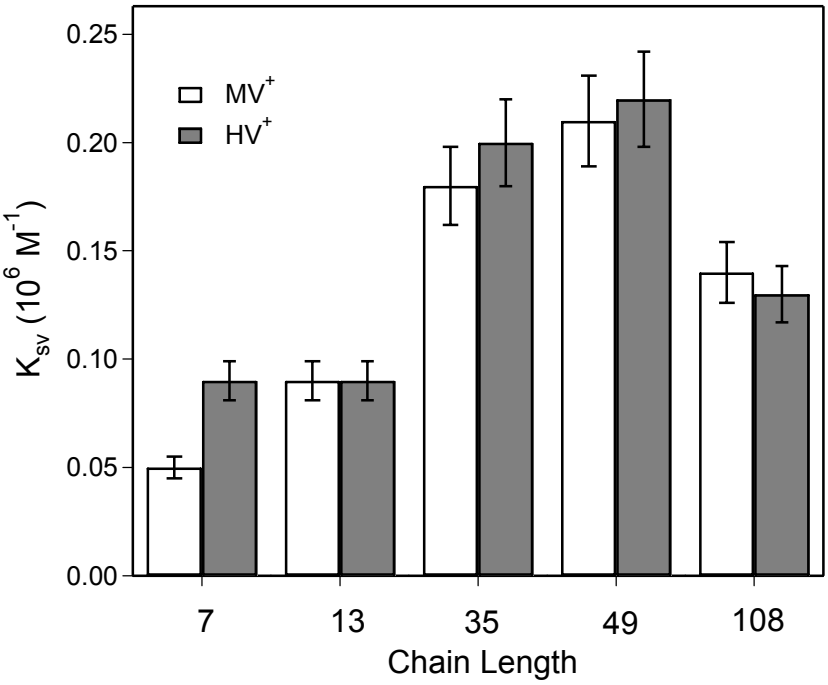

Figure 4-14. Comparison of the K_{sv} values obtained from SV plots for the series quenching with MV^+ and HV^+ in MeOH.

Another conclusion that can be drawn from the present study is that the aggregation of the polymer chains plays a key role in determining the quenching efficiency of CPEs and it overwhelms the effect of chain length on K_{sv} whenever aggregation occurs in the polymer solution. It has been proven that interchain exciton migration takes place on a time scale of a few picoseconds, while intrachain exciton migration occurs on a time scale of a few hundred picoseconds.[174] Because of the fast kinetics of interchain exciton migration, any polymer aggregation or quencher-induced polymer aggregation will have a strong effect on the K_{sv}. Then

the evaluation of chain length effect on K_{sv} will have to discriminate the contributions from both intrachain and interchain exciton migrations. Otherwise there will be no clear correlation between chain length and K_{sv} in such circumstances, as observed in our experiments when divalent quenchers were used.

Experimental

Materials

$Pd(PPh_3)_4$ catalyst was used as received from Strem Chemical Company. Triethylamine and THF were purified by distillation over sodium hydride. 1-Iodo-4-(trifluoromethyl)benzene, coumarin 102, N,N-dimethyl-4,4'-bipyridinium chloride (MV^{2+}), N,N-heptyl-4,4'-bipyridinium bromide (HV^{2+}) were purchased from Sigma-Aldrich and used without further purification. N-Heptyl-4,4'-bipyridinium bromide (HV^{+}) was purchased from Sigma-Aldrich and further purified by recrystallization from acetone.[175] N-Methyl-4,4'-bipyridinium iodide (MV^{+}) was synthesized following the literature procedure.[176] Octafluoro[2.2]paracyclophane was kindly provided by Prof. William R. Dolbier.

Instrumentation

NMR spectra were obtained with a Varian Mecury-300 or a Varian Gemini-300 and chemical shifts were reported in ppm using $CHCl_3$ or C_2HD_5SO as internal reference. GPC analyses were carried out on a system comprised of a Rainin Dynamax SD-200 pump and a Beckman Instruments Spectroflow 757 absorbance detector. UV-Visible absorption spectra were recorded using a Lambda 25 spectrophotometer from PerkinElmer. Steady-state fluorescence spectra were obtained with a Fluorolog-3 spectrofluorometer from Jobin Yvon. A 1-cm square quartz cuvette was used for all spectral measurements.

General Methods

Stern-Volmer quenching. A polymer solution (2 ml, c = 5 μM) was placed in a rectangular quartz cell and titrated with different quenchers. The absorption and fluorescence spectra were measured after each addition of the quencher. Fluorescence peak intensities were used for the construction of the Stern-Volmer (SV) plots if not specifically mentioned. The ratio of initial fluorescence to observed fluorescence was plotted *versus* the quencher concentration. By fitting of the linear region of SV plots, K_{sv} values were obtained.

Quantum yield measurements. Quantum yields of the series were measured by a relative method using Coumarin 102 as the standard (QY = 0.95 in EtOH solution)[173] and were corrected for solvent refractive index. The absorbance at the excitation wavelength (λ = 380 nm) were kept between 0.1 - 0.12 to reduce the inner filter effect.

Synthetic Procedures

General procedure for polymerization. Monomer **1** (407.3 mg, 0.50 mmol), monomer **2** (63.1 mg, 0.50 mmol) and a certain amount of **3**, (1-iodo-4-(trifluoromethyl)benzene, varying from 1% to 25%, molar ratio) were dissolved in 20 ml of dry THF/Et_3N (v/v = 3/2) mixture in a Schlenk flask. The solution was deoxygenated with argon for 15 minutes at 55 °C. Then 16.2 mg (0.014 mmol) $Pd(PPh_3)_4$ and 5.0 mg (0.026 mmol) of CuI were added into the solution under the protection of argon. The resulting mixture was heated to 60 °C and stirred for 24 hr. The obtained yellow solution was poured into 200 ml of methanol, which caused the precipitation of the polymer. The precipitate was collected by vacuum filtration and further purified by two repeated cycles of dissolution in THF and precipitation into a large volume of methanol. All these polymers can be dissolved in THF or CHCl3 after complete drying under vacuum. However, with storing, the polymers with longer chain length (n = 108 or n = 187) became barely soluble. Typical reaction yield is 75%-85%.

Hydrolysis. A small amount (~ 30 mg) of each polymer was taken from the obtained organic soluble polymers and used for GPC and NMR characterization. The rest of the polymers were dissolved in 40 ml of 1,4-dioxane. To the solution, 4 ml of n-Bu_4NOH (1 M in MeOH) was added. The solution became turbid immediately upon the addition of the base. Water (4 ml) was added at this stage; the mixture became clear and was stirred at room temperature for 24 hr. Then a solution of sodium perchlorate (480 mg, 4 mmol) dissolved in 1 ml of water was added to the hydrolyzed polymer solution and the resulting mixture was poured into 500 ml of cold acetone, whereupon the water soluble polymer precipitated as a fine yellow powder. Final purification of the polymers was accomplished by dialysis of the aqueous solution of the polymers against nanopure water (Millipore Simplicity water system). Regenerated cellulose membranes (Fisher Scientific) with 12 kD molecular weight cut-off (MWCO) were used for all the polymer samples including PPE-CO_2Na-7 and PPE-CO_2Na-13. During the dialysis, several drops of NaOH (1 N) was added to the polymer solution to prevent the precipitation of the polymer. After dialysis, the solution was filtered through a 1.0 μm glass fiber membrane and the concentration of the aqueous solution was calibrated using gravimetric analysis. The polymers were stored in this format and diluted as appropriate for spectroscopic studies. Typical reaction yield is 85%-95%. The polymer samples for NMR studies were prepared in the following way: the polymer was isolated by precipitating its aqueous solution into acetone, dried in an oven (heated at 100 – 120 °C) and then dissolved in 1 ml of DMSO-d_6/D_2O mixture (v/v = 1/1). The NMR spectra were acquired at 70 °C with at least 128 scans.

PPE-CO_2R-7. GPC (THF, polystyrene standard): M_w = 9,500, M_n = 5,390, PDI = 1.80. ^{1}H NMR ($CDCl_3$, δ_{ppm}): 7.64 (end groups), 7.56 (br, m, 4H), 7.02 (s, 2H), 4.74 (s, 4H), 4.24 (t, 4H), 1.68 (m, 4H), 1.31-1.25 (m, 36H), 0.90 (t, 6H). ^{19}F NMR ($CDCl_3$, δ_{ppm}): -63.22, -118.63

(internal standard). FT-IR (ν_{max}, KBr pellet): 3041, 2925, 2854, 2208, 1762, 1733, 1614, 1520, 1489, 1468, 1439, 1412, 1323, 1282, 1188, 1081,839, 722, 598, 544.

PPE-CO_2Na-7. ^{1}H NMR (D_2O/DMSO-d_6 = 1/1, δ_{ppm}): 7.66 (end groups), 7.54 (s, 4H), 7.02 (s, 2H), 4.35 (s, 4H). FT-IR (ν_{max}, KBr pellet): 3383, 2204, 1599, 1404, 1324, 1282, 1208, 1125, 1104, 1051, 943, 840, 765, 677, 597, 547.

PPE-CO_2R-13. GPC (THF, polystyrene standard): M_w = 20,640, M_n = 9,040, PDI = 2.30. ^{1}H NMR ($CDCl_3$, δ_{ppm}): 7.64 (end groups), 7.56 (br, m, 4H), 7.02 (s, 2H), 4.74 (s, 4H), 4.24 (t, 4H), 1.68 (m, 4H), 1.31-1.26 (m, 36H), 0.90 (t, 6H). ^{19}F NMR ($CDCl_3$, δ_{ppm}): -63.22, -118.63 (internal standard). FT-IR (ν_{max}, KBr pellet): 3040, 2925, 2854, 2207, 1761, 1738, 1615, 1520, 1490, 1467, 1440, 1412, 1377, 1323, 1282, 1188, 1130, 1082, 1017, 837, 722, 544.

PPE-CO_2Na-13. ^{1}H NMR (D_2O/DMSO-d_6 = 1/1, δ_{ppm}): 7.68 (end groups), 7.55 (s, 4H), 6.96 (s, 2H), 4.34 (s, 4H). FT-IR (ν_{max}, KBr pellet): 3401, 2927, 2255, 2205, 2127, 1607, 1515, 1488, 1404, 1323, 1281, 1205, 1126, 1104, 1049, 1025, 882, 838, 763, 703, 591, 541.

PPE-CO_2R-35. GPC (THF, polystyrene standard): M_w = 56,980, M_n = 24,390, PDI = 2.30. ^{1}H NMR ($CDCl_3$, δ_{ppm}): 7.64 (end groups), 7.56 (br, m, 4H), 7.02 (s, 2H), 4.74 (s, 4H), 4.24 (t, 4H), 1.68 (m, 4H), 1.31-1.26 (m, 36H), 0.90 (t, 6H). ^{19}F NMR ($CDCl_3$, δ_{ppm}): -63.22, -118.63 (internal standard).

PPE-CO_2Na-35. ^{1}H NMR (D_2O/DMSO-d_6 = 1/1, δ_{ppm}): 7.66 (end groups), 7.54 (s, 4H), 6.98 (s, 2H), 4.39 (s, 4H). FT-IR (ν_{max}, KBr pellet): 3394, 2929, 2256, 2205, 2128, 1607, 1515, 1489, 1404, 1323, 1281, 1206, 1105, 1051, 1026, 1006, 882, 840, 825, 763, 721, 703, 614, 596, 546

PPE-CO_2R-49. GPC (THF, polystyrene standard): M_w = 78,750, M_n = 33,760, PDI = 2.30. ^{1}H NMR ($CDCl_3$, δ_{ppm}): 7.56 (br, m, 4H), 7.02 (s, 2H), 4.74 (s, 4H), 4.24 (t, 4H), 1.68 (m,

4H), 1.31-1.26 (m, 36H), 0.90 (t, 6H). ^{19}F NMR ($CDCl_3$, δ_{ppm}): -63.22, -118.63 (internal standard).

PPE-CO_2Na-49. ^{1}H NMR (D_2O/DMSO-d_6 = 1/1, δ_{ppm}): 7.54 (s, 4H), 6.97 (s, 2H), 4.37 (s, 4H). FT-IR (ν_{max}, KBr pellet): 3384, 2934, 2255, 2204, 2127, 1604, 1515, 1488, 1404, 1323, 1281, 1207, 1104, 1050, 1026, 1005, 884, 840, 825, 763, 720, 704, 629, 595, 545.

PPE-CO_2R-108. GPC (THF, polystyrene standard): M_w = 202,890, M_n = 74,350, PDI = 2.70. ^{1}H NMR ($CDCl_3$, δ_{ppm}): 7.55 (br, m, 4H), 7.02 (s, 2H), 4.74 (s, 4H), 4.24 (t, 4H), 1.68 (m, 4H), 1.31-1.26 (m, 36H), 0.90 (t, 6H). ^{19}F NMR ($CDCl_3$, δ_{ppm}): -63.22, -118.63 (internal standard).

PPE-CO_2Na-108. ^{1}H NMR (D_2O/DMSO-d_6 = 1/1, δ_{ppm}): 7.55 (s, 4H), 6.96 (s, 2H), 4.34 (s, 4H). FT-IR (ν_{max}, KBr pellet): 3398, 2930, 2256, 2205, 2128 1602, 1515, 1489, 1406, 1323, 1281, 1198, 1094, 1051, 1026, 1004, 885, 841, 825, 764, 721, 700, 631, 617, 544.

CHAPTER 5
VARIABLE BAND GAP POLY(ARYLENE ETHYNYLENE)S

Introduction

Reduction of the band gap (E_g) of conjugated polymers (CPs) has been the objective of polymer chemists since the discovery of conductivity of doped polyacetylene.[177,178] The decrease of E_g can lead to intrinsic conducting polymers which do not need additional chemical or electrical doping. And the continuous reduction of E_g will give CPs that can continuously absorb and emit light in the visible and near-IR spectral range. These materials will be useful for the fabrication of multicolor LEDs, sensing arrays and solar cells.[179-181] Two general approaches have been widely used to reduce the E_g of conjugated polymers, i.e., minimization of bond-length alternation and alternation of electron-donor and electron-acceptor in the main chain.[178] As the most common type of poly(arylene ethynylene)s (PAEs), poly(phenylene ethynylene) (PPE)s have a optical band gap of ~ 2.4 eV.[10] Because the frequently used Sonogashira coupling is compatible to a wide variety of functionalities, numerous PAEs with variable band gaps that are soluble in organic solvents have been synthesized using the donor-acceptor repeating unit strategy.[10] We reported the first synthesis of a homologous family of PAE-based CPEs that differ widely in HOMO-LUMO band gap.[135] In that work, the band gap was tuned by copolymerizing diiodophenylene carrying sulfonate (SO_3^-) or alkyl ammonium groups (NR_3^+) with 5 different arylene ethynylenes in DMF/water mixtures.

In the present chapter, we report the synthesis of variable band gap PAEs that feature carboxylate (CO_2^-) and ammonium (NH_3^+) side groups. For PAEs that carry linear carboxylate ($-OCH_2CO_2^-Na$) side chains, four polymers that incorporate 1,4-phenyl, 2,5-thienyl (TH), 2,5-(3,4-ethylenedioxy)thienyl (EDOT), and 1,4-benzo[2,1,3]- thiodiazole (BTD) in the repeat unit were synthesized. To provide conjugated polyelectrolytes that can retain high quantum

efficiency in water and solid state films, two dendritic side chains that can sterically hinder the aggregation of the polymer chains were designed and synthesized. Conjugated polymers that incorporate these dendritic ionic side chains were prepared and their photophysical properties were studied in different solvents. Effects of acidity and ionic strength on the polymer optical properties were also studied in an aqueous environment. To the end, the potential applications of these PAEs that have linear carboxylate side groups in Grätzel type solar cells were discussed.

Results and Discussion

Synthesis of PAEs with Linear Side Chains

The tuning of the PAE band gap was realized by copolymerizing 2,5-bis(dodecyloxycarbonylmethoxy)-1,4-diiodobenze **1** with different trimethylsilyl (TMS) protected diacetylene compounds. The synthetic routes used to prepare the polymers are shown in Figure 5-1. 2,5-Bis((trimethylsilyl)ethynyl)thiophene (TH) **3** was prepared by coupling trimethysilylacetylene (TMSA) to commercially available 2,5-dibromothiophene under Sonogashira conditions in 95% yield. 2,5-Diiodo-3,4-ethylenedioxythiophene (EDOT)[135] and 4,7-dibromobenzo[c][1,2,5]thiadiazole (BTD)[163] were prepared following the procedures reported in the literature. They were then reacted with TMSA respectively to give the protected diacetylene monomers in moderate yields. Although the deprotection of the TMS group for all the monomers was successful, we found that these deprotected monomers are extremely unstable and change their color quickly if stored even for relatively short periods of time (from white or yellow color to brownish). Thus for making these PAEs containing heteroaromatic rings, a different strategy was used. In a typical polymerization, a stoichiometric quantity of 2,5-bis(dodecyloxycarbonylmethoxy)-1,4-diiodobenze **1** and the stable TMS-protected monomer was dissolved in a THF/Et_3N mixture (v/v, 3/1) and carefully degassed with argon. Then tetrabutyl ammonium fluoride (TBAF) was added to the mixture following with the addition of a

catalytic amount of $Pd(PPh_3)_4$ and CuI. The polymerization usually required 20– 24 hours at 60 ºC. The number-average molecular weights of **PPE, TH-PPE**, **EDOT-PPE** and **BTD-PPE** determined by GPC are 36 kD, 30 kD, 11 kD and 16 kD, respectively. These polymers are soluble in most non-polar solvents, such as CH_2Cl_2, $CHCl_3$ and THF. After confirming the structure of these polymers by ^1H NMR in $CDCl_3$, they were subjected to the base-promoted hydrolysis that was used to prepare water-soluble PPEs in the earlier chapters. Using tetra-*n*-butyl ammonium hydroxide (TBAH), we were able to obtain the water-soluble polymers from **PPE**, **TH-PPE** and **EDOT-PPE** (Note that **PPE-CO_2Na** has the same chemical structure of the polymer that we studied in chapter 3 but with lower molecular weight). However, when we tried to hydrolyze the **BTD-PPE**, a material with the maximum absorption at 322 nm was resulted. The big blue shift (~ 180 nm) comparing the unknown material to **BTD-PPE** indicates that the backbone of the polymer was destroyed probably by the attack of BTD ring by the base. Through a different route, the water-soluble counterpart of **BTD-PPE**, **BTD-PPE-CO_2Na** was prepared from the hydrolyzed bis(dodecyloxycarbonylmethoxy)-1,4-diiodobenze and 4,7-bis((trimethylsilyl)ethynyl)benzo[c][1,2,5]thiadiazole **8** in a DMF/water/diisopropylamine mixture (9/6/2) under the same polymerization conditions. The solubility of these polymers in water is about 3 - 5 mg/mL. The same as what we found for PPE-SO_3^-, these polymers can not be re-dissolved even in water or other polar solvents, such as DMF and DMSO after complete drying, which is probably due to the strong tendency of these polymers to aggregate in the solid state. Thus these polymers were stored in their water solutions after final purification using membrane dialysis. To prevent the precipitation during the storage, the pH of the stock solution was kept between pH = 8 - 10.

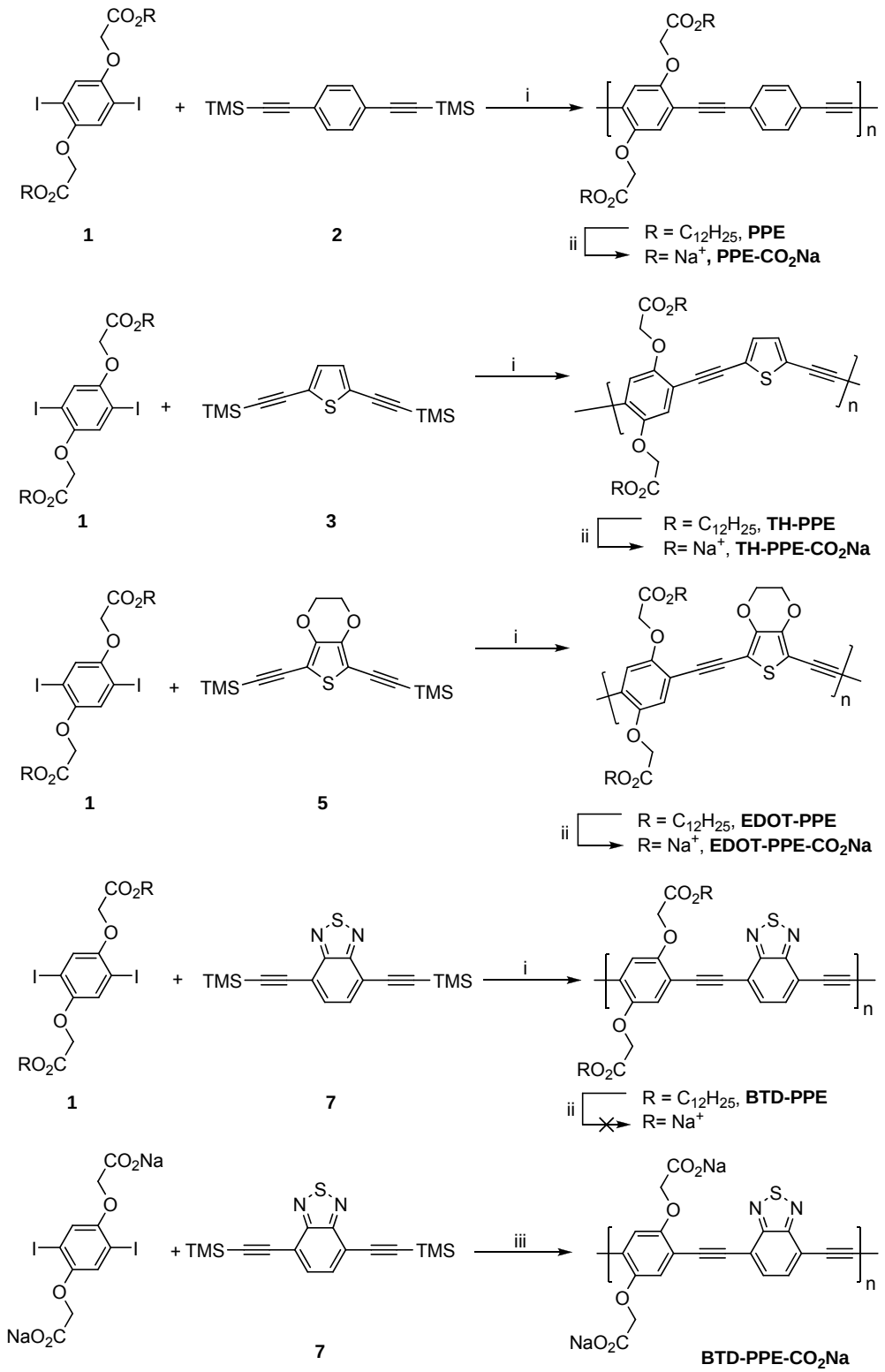

i. $Pd(PPh_3)_4$, CuI, THF/Et_3N, 60 °C, TBAF, 24 hr; ii. 1) $(n\text{-}Bu)_4NOH$, dioxane, ambient, 12 hr; 2) a.q. $NaClO_4$; iii. $Pd(PPh_3)_4$, CuI, $DMF/H_2O/i\text{-}Pr_2NH$, 60 °C, 24 hr.

Figure 5-1. Synthesis of variable band gap PAEs with linear carboxylate side chains.

Synthesis of PAEs with Dendritic Side Chains

In a series of studies,[64,71,126,172] we have investigated the effect of aggregation on the photophysical properties of PAE-based conjugated polyelectrolytes. And aggregation has also been shown to strongly influence the optical properties of other types of conjugated polyelectrolytes in aqueous solution, such as poly(2-methoxy-5-propyloxy sulfonate phenylene vinylene) (MPS-PPV),[57] poly[9,9-bis(6´-N,N,N-trimethylammoniumhexyl)fluorene diiodide][75] and etc.[182] Attaching dendritic side groups to rigid conjugated polymer chains to prevent their aggregation in thin films have been populated in the literature.[183-185] However, there were only two examples of using dendritic side chains to disrupt the aggregation of CPEs in aqueous solution.[186,187] Here we present our results of synthesizing two new dendritic side chains and PAEs carrying the first generation of these dendritic groups.

Monomer synthesis

Figure 5-2 shows the synthetic routes of monomers **19**, **20** that carry the dendritic side chains. A convergent strategy was used. The triester compound **11** was prepared from *tert*-butyl acrylate in two steps with an overall yield of 63%. In parallel, compound **16** was synthesized in 4 steps. Starting from commercially available 4-(2-carboxyethyl)-4-nitroheptanedioic acid **12**, it was converted to 4-(3-chloro-3-oxopropyl)-4-nitroheptanedioyl dichloride **13** in nearly quantitative yield by treating with thionyl chloride ($SOCl_2$). The latter was then reacted with trimethylsilyl azide to give 3-(2-aminoethyl)-3-nitropentane-1,5-diamine•HCl salt **14** in 81% yield. After reacting with 3 equivalents di-*tert*-butyl dicarbonate, compound **15** was obtained in 85% yield. The nitro group in compound **15** was then hydrogenated (60 ºC, 100 psi) in the presence of T-1 Raney nickel[188] to give compound **16** in 93% yield. Dendritic monomers **19** and **20** were prepared by the coupling of either 2,2'-(2,5-diiodo-1,4-phenylene)bis(oxy)diacetic acid **17** or its chloride **18** with **11** or **16**. However, the direct reaction between **17** and **11** using

4-(dimethylamino)pyridinium 4-toluenesulfonate (DPTS)[105] and diisopropylcarbodiimde (DIPC) as coupling reagents only gave the desired monomer **19** in 38% yield. To improve the yield, compound **17** was converted to **18** by reacting with $SOCl_2$. Compound **18** was found to be fairly stable and purified by recrystallization. Then reactions of **18** with **11** or **16** afforded monomer **19** and **20** in 76% and 50% yield, respectively. The purity of these monomers was proven by ^{1}H and ^{13}C NMR spectroscopy, elemental analysis and mass spectroscopy.

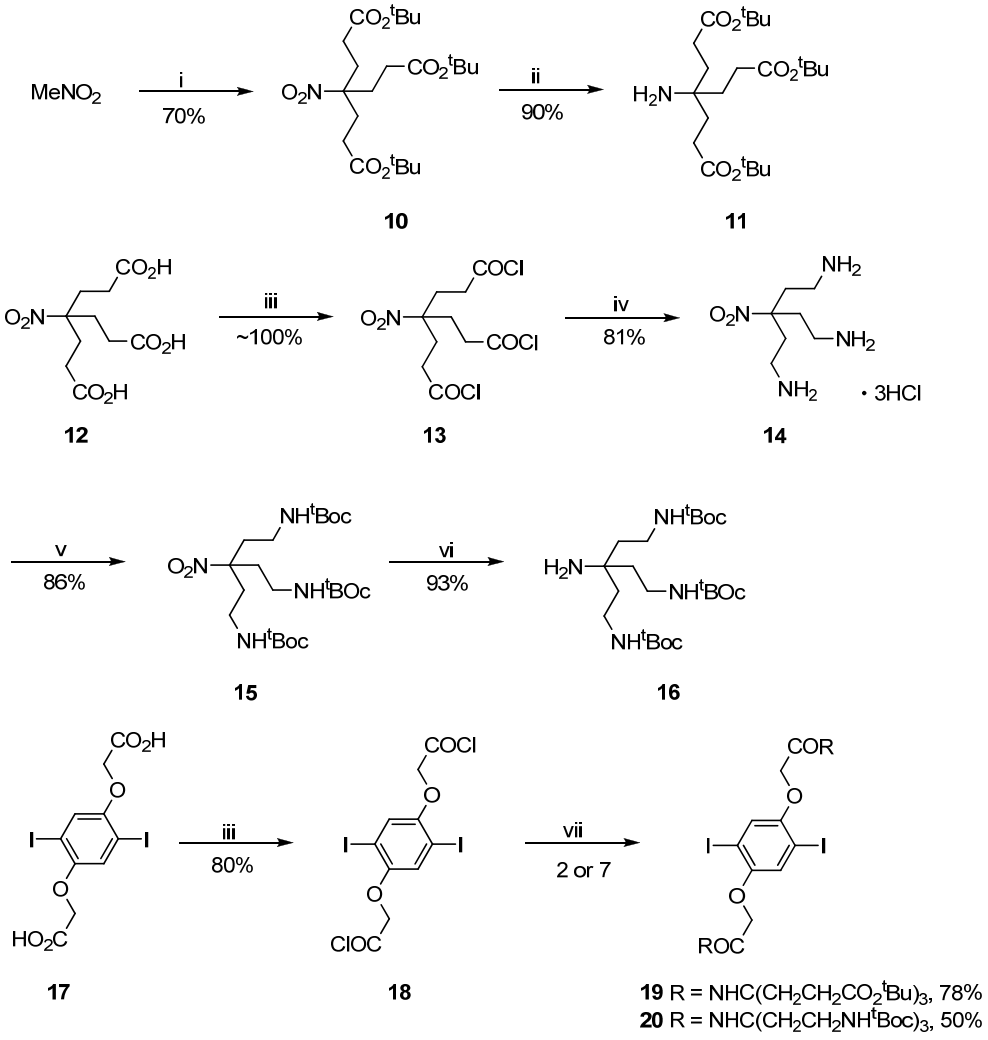

i. DME, Triton-B, $CH_2{=}CH_2CO_2$-^{t}Bu, 70-80 °C; ii. T-1 Raney nickel, EtOH, H_2 (balloon), ambient, 48 hr; iii. $SOCl_2$, DMF (cat.), reflux, 2 hr; iv. 1) $(CH_3)_3SiN_3$, dioxane, 80 °C, 2 hr; 2) Acetone, HCl (12 N), 50 °C, 1 hr; v. Boc_2O, Et_3N, CH_3CN, reflux, 7 hr; vi. T-1 Raney nickel, EtOH, H_2, 100 psi, 70 °C, 36 hr; vii. Et_3N, CH_2Cl_2, 5 °C ⟶ ambient, 24 hr.

Figure 5-2. Synthesis of monomers (**19**, **20**) carrying dendritic side chains.

Synthesis of PAEs carrying anionic side chains

The synthetic procedures used to prepare the PAEs that carry anionic dendritic side chains are shown in Figure 5-3.

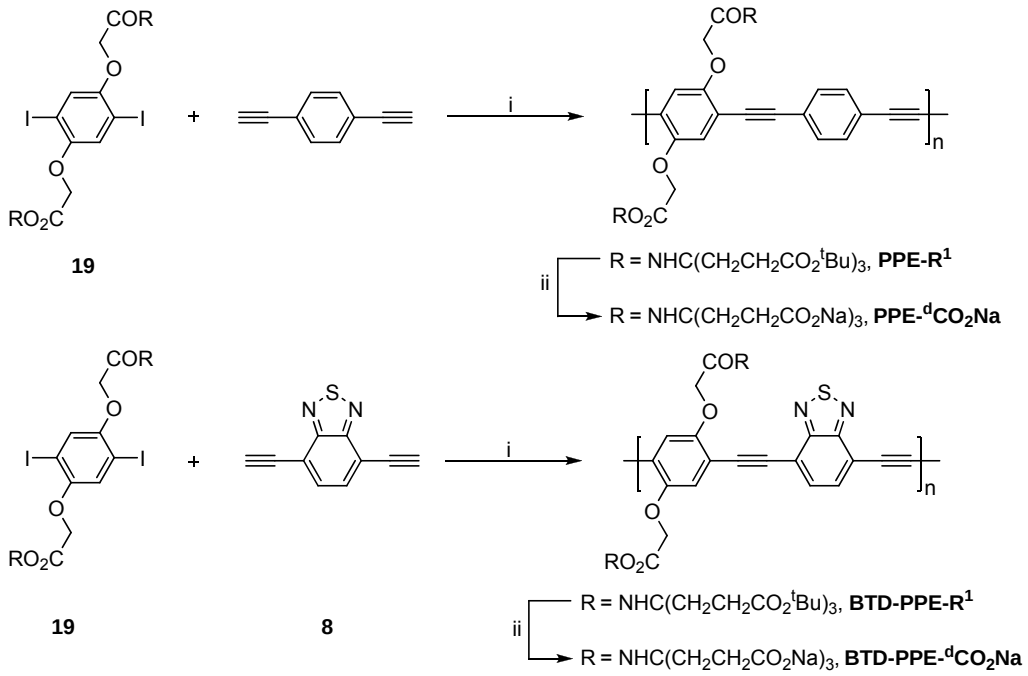

i. $Pd(PPh_3)_4$, CuI, THF/Et_3N, 60 °C, 24 hr; ii) 1). TFA/CH_2Cl_2 (1/1), ambient, 24 hr; 2). a.q. Na_2CO_3, 24 hr.

Figure 5-3. Synthesis of PAEs carrying dendritic anion side groups.

The Sonogashira polycondensation of an stoichiometric amount of monomer **19** and 1,4-diethynylbenzene was carried out in a mixture of THF/Et_3N (3:1) with $Pd(PPh_3)_4$/CuI as catalysts. After the reaction was stirred at 60 ºC for 24 h, the polymer (**PPE-R^1**) was isolated as a yellow solid and purified by repeated precipitation from THF solutions into methanol. The number-average molecular weight of **PPE-R^1** determined by GPC against polystyrene standards is 33 kD (PDI = 3.1), corresponding to 29 repeat units. The ester groups of **PPE-R^1** was hydrolyzed using a CH_2Cl_2/trifluoacetic acid (TFA) mixture (v/v = 1/1) at room temperature. After removal of the solvent, the residue was treated with saturated aqueous Na_2CO_3 and then dialyzed against deionized (DI) water using 12 kD molecular-weight-cutoff (MWCO) dialysis

cellulose membranes. The water-soluble polymer (**PPE-^{d}CO$_2$Na**) was isolated as a pale yellow solid by precipitation from the aqueous solution into acetone, and then dried in a vacuum oven for at least 2 days.

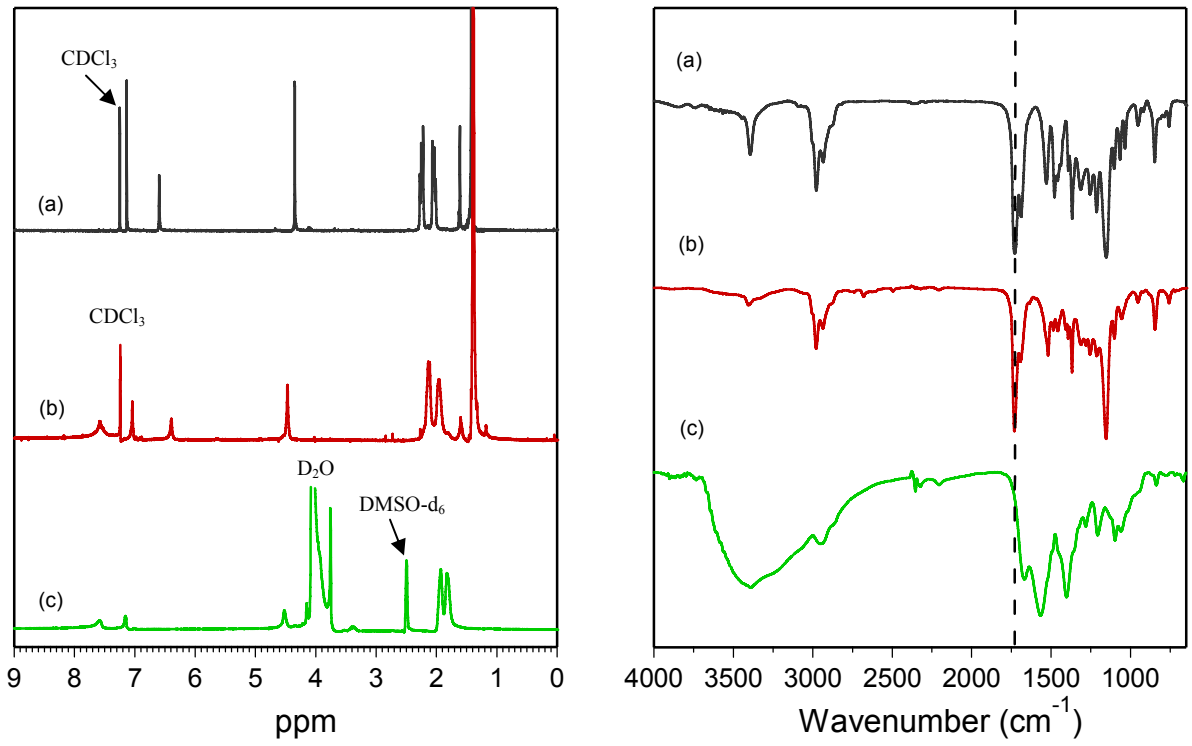

Figure 5-4. ^{1}H NMR (left) and FT-IR (right) spectra of monomer **19** (a), **PPE-R^{1}** (b) and **PPE-^{d}CO$_2$Na** (c).

The ^{1}H NMR and FT-IR spectra of the dendritic monomer **19**, the neutral polymer **PPE-R^{1}** and the water-soluble polymer PPE-^{d}CO$_2$Na are shown in Figure 5-4. Comparison between the spectra of monomer **19** and **PPE-R^{1}** reveals that there is only one new resonance peak at δ = 7.58 ppm, which is assigned to the aromatic protons of 1,4-phenylene on the polymer backbone. The *tert*-butyl protons appear as a strong singlet at δ = 1.42 ppm in the spectra of monomer **19** and **PPE-R^{1}**. After hydrolysis, the ^{1}H NMR spectroscopy of **PPE-^{d}CO2Na** was accomplished in a mixture of DMSO-d$_6$/D$_2$O (v/v = 1/1). There are no signals in the 1.4 – 1.5 ppm range, indicating that the *tert*-butyl groups were cleaved with an excellent yield (> 95%).

Figure 5-4 (right) shows the IR spectra of **PPE-R^1** and **PPE-^{d}CO$_2$Na**, the spectrum of monomer **19** is also shown for the purpose of comparison. The IR spectrum of the neutral polymer (**PPE-R^1**) is very similar to the spectrum of monomer **19** except that a very weak absorption at 2205 cm^{-1} due to C≡C stretching is seen for the polymer. The absorption bands, which can be attributed to the ester and amide groups in the spectra of **19** and **PPE-R^1**, occur at 1728 cm^{-1} and 1688 cm^{-1}, respectively. After hydrolysis, the absorption at 1728 cm^{-1} disappears, indicating the removal of the *tert*-butyl ester groups. The absorption bands associated with the carboxylate groups (CO_2^-) appear at 1566 cm^{-1} and 1403 cm^{-1}. The strong broad absorption ranging from 3000 cm^{-1} to 3500 cm^{-1} implies the existence of H_2O in the sample, due to the strong hydrophilicity of **PPE-^{d}CO$_2$Na**.

Using a similar procedure, one PAE that incorporates the strong electron acceptor, benzo[c][1,2,5]thiadiazole (BTD) into the backbone, was also synthesized. The number-average molecular weight determined by GPC for the neutral polymer (**BTD-PPE-R^1**) is 12 kD (PDI = 1.4). The water-soluble polymer, **BTD-PPE-^{d}CO$_2$Na** was obtained using the same hydrolysis condition used for **PPE-^{d}CO$_2$Na**. Characterizations of **BTD-PPE-R^1** and **BTD-PPE-^{d}CO$_2$Na** by NMR spectroscopy and IR spectroscopy are consistent with their proposed structures.

Synthesis of PAEs carrying cationic side chains

Figure 5-5 shows the synthetic routes to make PAEs that carry dendritic charged amino groups. The polymerizations of monomer **20** with 1,4-diethynylbenzene or 4,7-diethynylbenzo[c][1,2,5]thiadiazole **8** were carried out under the Sonogashira coupling conditions. But because of the richness of amide functionality in the polymers (2 amide and 6 carbamate groups per repeat unit), these polymers are more polar than the previous polymers (**PPE-R^1** and **BTD-PPE-R^1**) and were purified by repeated precipitation from THF solutions into hexane, instead of methanol. **PPE-R^2** was isolated as a yellow fiber and has a number-

average molecular weight of 24 kD (PDI = 4.3). Deprotection of the Boc group was accomplished using 4 N HCl/dioxane. The polymer was obtained as a pale yellow solid after precipitation from acetone in a quantitative yield. After washing with a large amount of cold hexane, the polymer was dried in a vacuum oven.

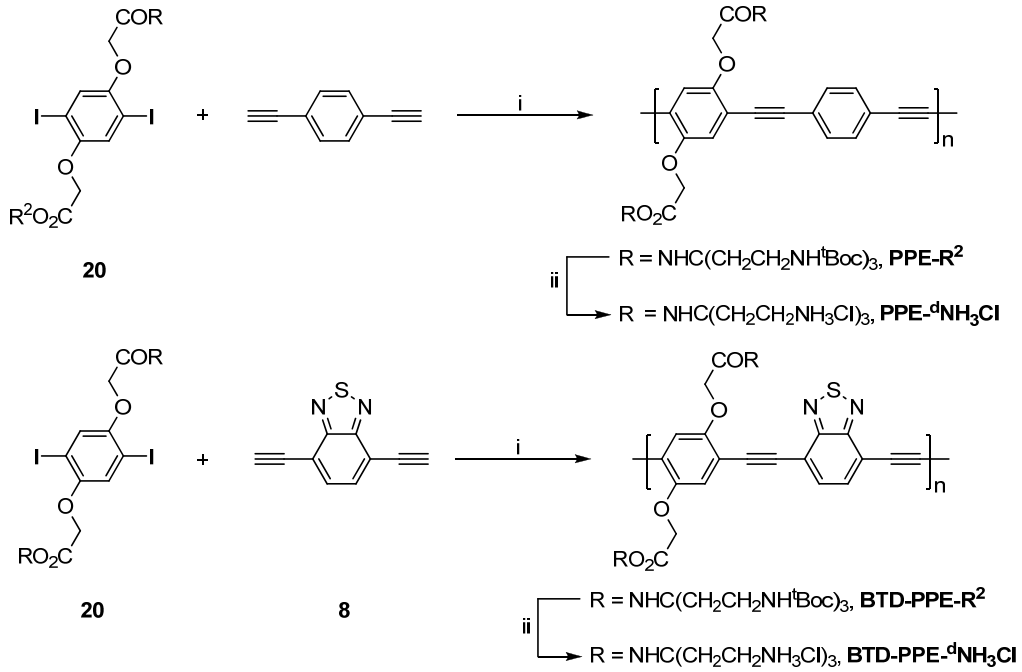

i. $Pd(PPh_3)_4$, CuI, THF/Et_3N, 60 °C, 24 hr; ii. 1) 4 N HCl, dioxane, ambient, 24 hr.

Figure 5-5. Synthesis of PAEs carrying dendritic cationic side groups.

The structures of the neutral polymer **PPE-R^2** and the water-soluble polymer **PPE-^{d}NH$_3$Cl** were confirmed by ^{1}H NMR and FT-IR spectroscopy, as shown in Figure 5-6. For the purpose of comparison, the ^{1}H NMR and IR spectra of monomer **20** are also shown. In the ^{1}H NMR spectrum of monomer **20**, the phenylene protons appear as a singlet at δ = 7.14 ppm. Two broad singlets at δ = 6.71 and δ = 4.80 ppm are assigned to the amide protons of –OCH$_2$CO***NH***– and -CH$_2$CH$_2$***NH***COOtBu, respectively. The singlet signal at δ = 4.34 ppm is due to the methylene group of –O***CH$_2$***CO*NH*–. Signals for the methylene groups of -C(***CH$_2$CH$_2$***NH^{t}Boc)$_3$– appear at δ = 2.02 ppm and δ = 3.20 ppm, respectively. The *tert*-butyl protons appear as a strong

singlet at δ = 1.40 ppm. The ^{1}H NMR spectrum of the neutral polymer (**PPE-R^2**) is very similar to that of monomer **20**, except that there is one new signal at δ = 7.60 ppm due to the protons of 1,4-phenylene on the polymer backbone. As can be seen from the spectrum of water-soluble polymer (**PPE-^{d}NH$_3$Cl**) in DMSO-d_6/D_2O (1/1) after deprotection, the peaks at δ = 4.80 and δ = 1.40 ppm disappear, indicating the removal of the ^{t}Boc group. The occurrence of signals for all the other protons confirms that there were no other side reactions.

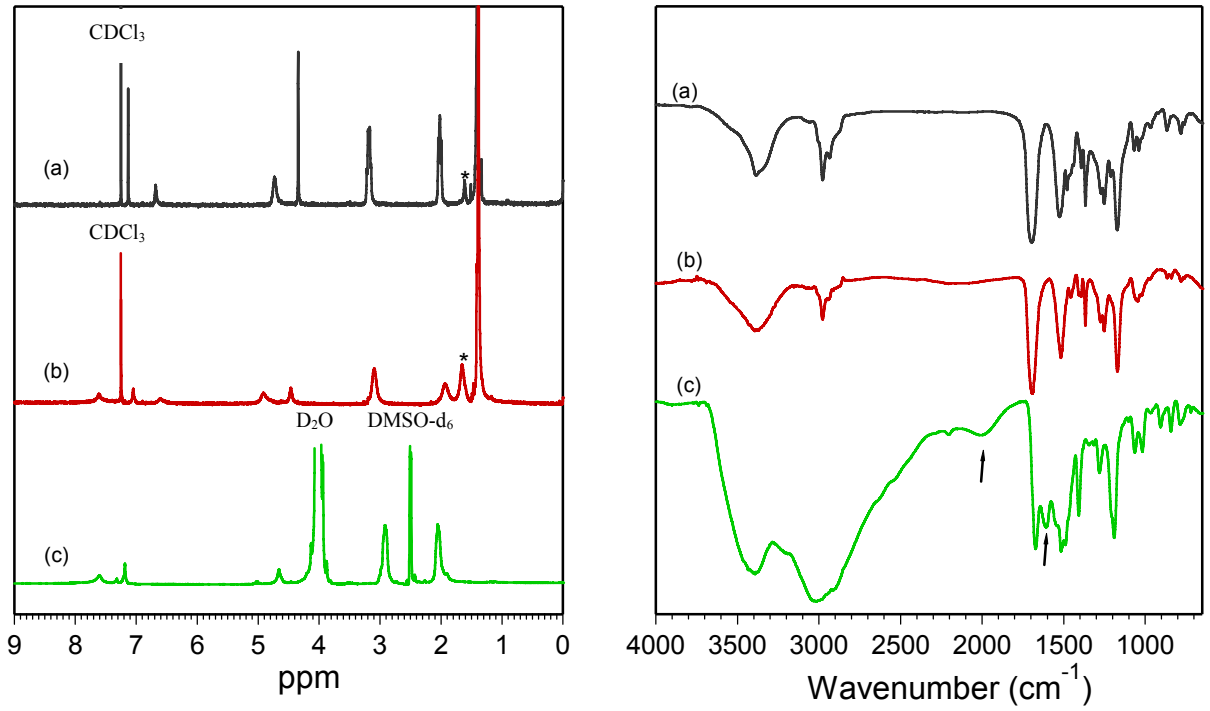

Figure 5-6. ^{1}H NMR (left) and FT-IR (right) spectra of monomer **20** (a), **PPE-R^2** (b) and **PPE-^{d}NH$_3$Cl** (c). The starred signals are due to H_2O in the solvent or the sample.

The IR spectra of monomer **20** and the neutral polymer are also very similar. The absorption at 1692 cm^{-1} is due to the C=O stretching of carbamate groups, which overlaps the absorption of C=O stretching of the amide groups. In the spectrum of water-soluble polymer, **BTD-PPE-^{d}NH$_3$Cl**, three new absorptions associated with NH_3^+ groups appear at 1607 cm^{-1}, 2008 cm^{-1} and 3015 cm^{-1}, which can be assigned to the bending vibration, combination and stretching bands of NH_3^+, respectively. The absorption at 1692 cm^{-1} due to carbamate groups

disappears, the absorption band of amide at 1672 cm^{-1} is observed. In all the spectra, the absorption bands around 3400 cm^{-1} are assigned to the N-H stretching of the amide groups.

The other organic polymer, **BTD-PPE-R^2** was isolated as a red solid and has a number-average molecular weight of 12 kD (PDI = 3.6). The water-soluble polymer was obtained after hydrolyzing **BTD-PPE-R^2** with 4 N HCl. The structures of both polymers were confirmed by ^{1}H NMR and FT-IR spectroscopy.

Optical Properties of PAEs with Linear Carboxylate Side Chains

In our previous studies of PPE-SO_3^- and PPE-CO_2^-,[71,172] we found that the optical properties of these polymers in solution are strongly dependent on the solvents. In methanol, the absorption and emission spectra of these conjugated polyelectrolytes correspond well with the spectra of their structurally analogous polymers that contain alkyl or alkoxy-solubilizing groups in good solvents. In water, the spectra of the CPEs display spectral changes that are characteristic of aggregate formation as seen in the solid films of the structurally similar organic polymers.[189] Here, we present our studies of the absorption and fluorescence spectra of **TH-PPE-CO_2Na**, **EDOT-PPE-CO_2Na** and **BTD-PPE-CO_2Na** (the spectra of **PPE-CO_2Na** are also shown for comparison) in methanol and water.

Figure 5-7 illustrates the absorption and fluorescence spectra of the series in MeOH. The wavelength maxima of the absorption and fluorescence spectra systematically red-shift in the order of phenyl < TH < EDOT < BTD. Across the entire series, the absorption maximum shifts from 417 nm (**PPE-CO_2Na**) to 520 nm (**BTD-PPE-CO_2Na**), whereas the fluorescence maximum shifts from 430 nm (**PPE-CO_2Na**) to 665 nm (**BTD-PPE-CO_2Na**). The origin of the red-shifts in the absorption and fluorescence likely arise from several factors that vary with the structure of the heterocyclic ring in the PAE backbone. Specifically, the red-shift for the 2,5-thienyl- (TH) and 3,4-ethylenedioxy-2,5-thienyl- (EDOT) polymers likely arises because the

HOMO level of the polymer is increased because of the electron-donor characteristic of the TH and EDOT units.[190] The increase in the HOMO energy reduces the HOMO-LUMO gap, thereby reducing the energy of the lowest singlet excited state. In contrast to the TH and EDOT polymers, in the 2,1,3-benzothiadiazole (BTD) polymer the nitrogen-containing heterocycles likely act as electron acceptors thereby reducing the LUMO level of the polymer.[191,192] In effect, the dialkoxybenzene units act as donors and the BDT groups act as electron acceptors giving rise to charge transfer character in the lowest excited state. The existence of charge transfer character in the singlet state of **BTD-PPE-CO_2Na** polymer is evidenced by the relatively large Stokes shift (*ca.* 150 nm) and combined with the broad, structureless band shape of the fluorescence spectra.

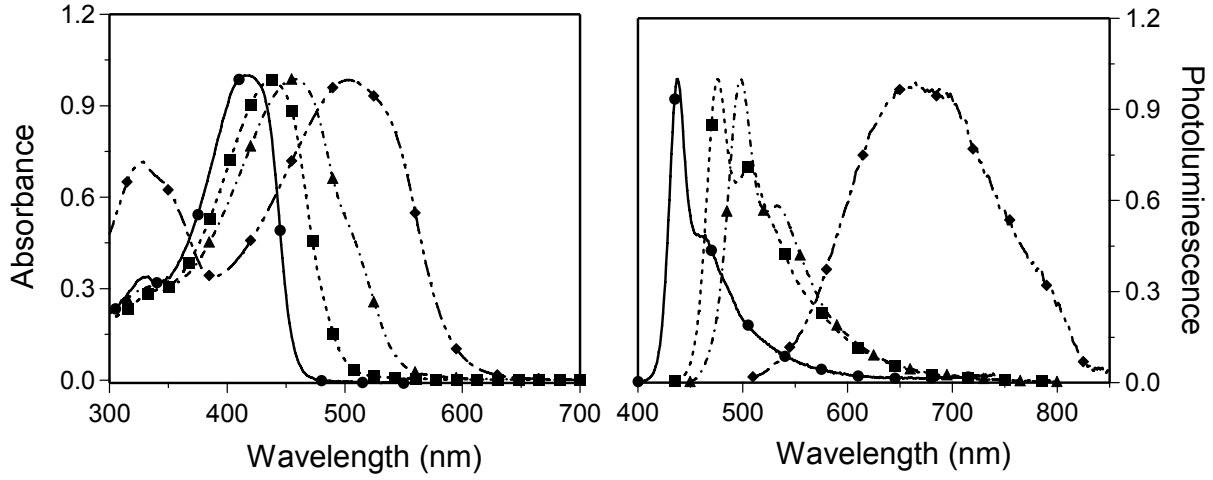

Figure 5-7. Absorption (a) and Emission (b) of PAEs containing linear carboxylate side chains in MeOH. **PPE-CO_2Na** (●), **TH-PPE-CO_2Na** (■), **EDOT-PPE-CO_2Na** (▲),**BTD-PPE-CO_2Na** (♦).

Similar to **PPE-CO_2Na**, these polymers also show a strong tendency to aggregate in water (spectra are not shown here). Aggregation of these polymers is signaled by a red-shift and narrowing of the polymer's absorption spectrum, a significant red-shift and broadening of the fluorescence spectrum, and a decrease in Φ_{PL}.

Table 5-1. UV-Vis absorption and photoluminescent properties of PAEs containing linear carboxylate side chains.

Polymers	solvent	$\lambda_{max,}^{abs}$ (nm)	$\lambda_{max,}^{em}$ (nm)	Φ_{PL}
PPE-CO_2Na	MeOH	417	437	0.23[a]
	H_2O	435	520	0.07[a]
TH-PPE-CO_2Na	MeOH	438	476	0.15[a]
	H_2O	447	512	0.06[a]
EDOT-PPE-CO_2Na	MeOH	457	498	0.09[a]
	H_2O	468	527	0.04[a]
BTD-PPE-CO_2Na	MeOH	504	650	0.002[b]
	H_2O	519	668	N/A

[a] Coumarin 102 in EtOH as the standard, $\Phi_{FL} = 0.95$.[173] [b] $Ru(bpy)_3Cl_2$ in H_2O as the standard, $\Phi_{PL} = 0.036$.[193,194]

Table 5-1 compiles the optical data, including the maximum absorption and emission wavelength, PL quantum efficiency (Φ_{PL}) of these CPEs in MeOH and H_2O. There are several trends that are clearly evident in the data. First, the absorption and emission maxima shift to longer wavelength when the solvent is changed from MeOH to H_2O. The origin of this effect is attributed to the aggregation-induced planarization of polymer backbone, which leads to increased conjugation length. Second, across the series, the Φ_{fl} values systematically decrease in the sequence Ph > Th > EDOT > BDT. Interestingly, this ordering correlates approximately with the emission energy, i.e., Φ_{fl} generally decreases with decreasing emission energy. The third effect is that the Φ_{fl} values are dramatically lower for all of the polymers in H_2O solution. This effect has been previously observed for PPE-SO_3^- and **PPE-CO_2Na**, and is attributed to aggregation-induced quenching of the intrachain singlet exciton.[71,172]

Optical Properties of PAEs Featuring Dendritic Side Chains

Compared with the PAEs containing linear carboxylate side chains, these polymers having either dendritic carboxylate or charged amino groups exhibit much better solubility (> 8 mg/ml in water). After complete drying under vacuum, the solid materials are able to be re-dissolved in

water, indicating the charged dendritic groups reduce the intermolecular interaction of the polymer chains in the solid state. To fully explore the potential of these dendritic side groups in preparing a new generation of water-soluble conjugate polymers, a comprehensive study was carried out in which the absorption and fluorescence spectra of the four CPEs were measured when the solution conditions, such as solvent, pH and ionic strength were varied.

Absorption and fluorescence properties

Figure 5-8 illustrates the absorption and fluorescence spectra of these CPEs carrying dendritic ionic side chains in MeOH. In general there is a very close correspondence between the wavelength maxima and band shape for the corresponding pairs of anionic and cationic PAE-type CPEs. This is not surprising in view of the fact that the polymers' optical properties are mainly determined by the structure of the π-conjugated backbone. In comparison with the absorption of **PPE-CO_2Na**, the absorption of **PPE-$^dCO_2Na$** and **PPE-$^dNH_3Cl$** that have the same π-conjugated backbone blue-shifts 15 nm; while the absorption of **BTD-PPE-$^dCO_2Na$** and **BTD-PPE-$^dNH_3Cl$** also blue-shifts 13 nm compared to the absorption of **BTD-PPE-CO_2Na**. The conjugated length of PPE-type polymers is determined to be 10 ~ 12 phenylene ethynylene units.[160] Since the degrees of polymerization (DP) for all these polymers are larger than 10 (~ 20 arylene ethynylene units), we believe that this effect (blue-shift of absorption maximum) for PAEs with dendritic side groups is due to the more twisted backbone conformation in the methanol solutions of these polymers because of the increased electronic repulsion between the charged dendritic groups. In the fluorescence spectra, for the blue-emitting polymers, there is a negligible shift in the maximum emission wavelength (< 3 nm) comparing **PPE-$^dCO_2Na$** or **PPE-$^dNH_3Cl$** to **PPE-CO_2Na**. However, for the red-emitting polymers, the broad emission spectra of **BTD-PPE-$^dCO_2Na$** and **BTD-PPE-$^dNH_3Cl$** center at 600 nm, which blue-shifts about

50 nm comparing to the emission of **BTD-PPE-CO_2Na**. One possible reason for this effect is the decrease of contact between methanol and the conjugated backbone of PAEs with dendritic side groups.

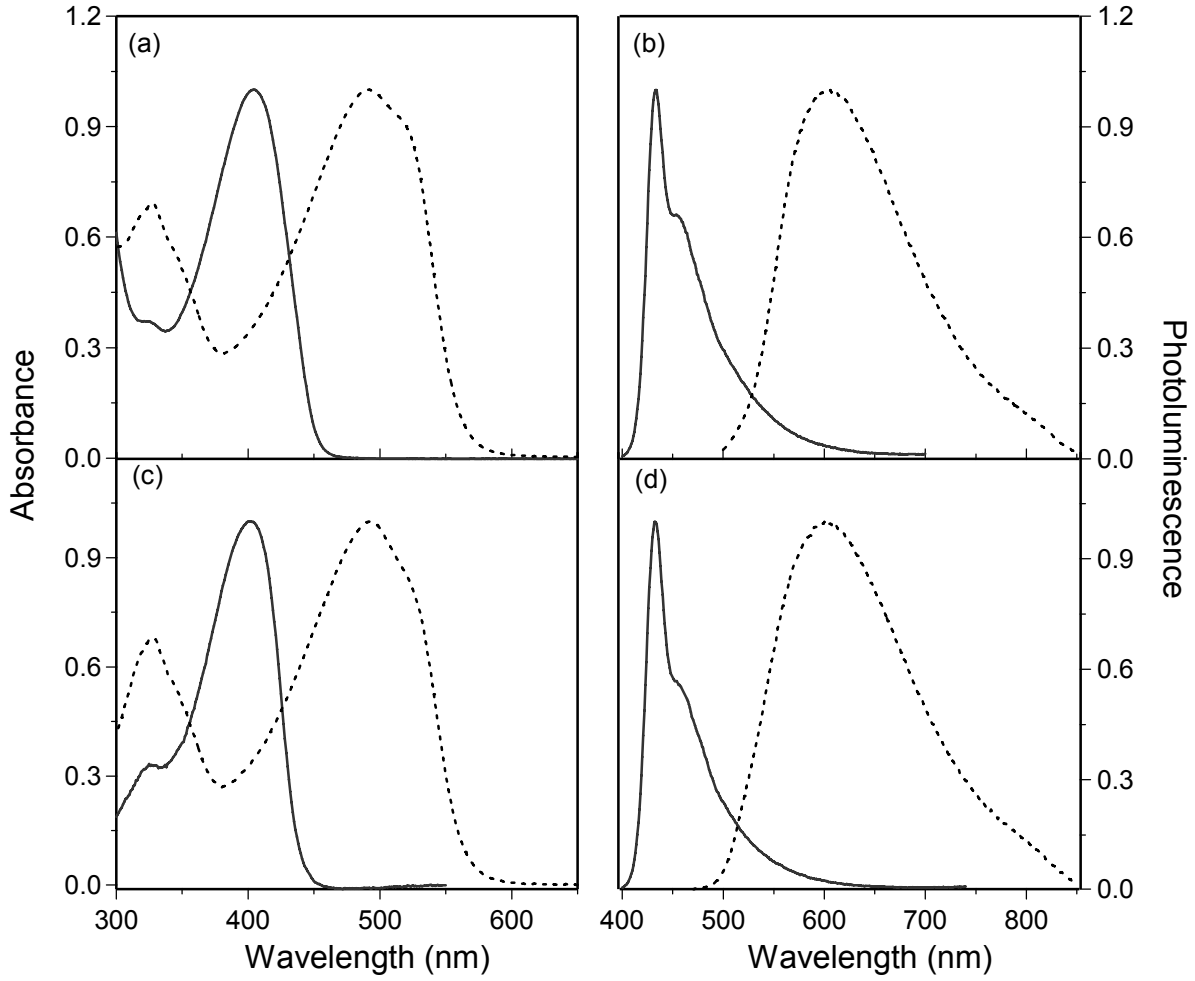

Figure 5-8. Normalized absorption (a) and fluorescence (b) spectra of **PPE-$^dCO_2Na$** (solid line) and **BTD-PPE-$^dCO_2Na$** (dotted line) in MeOH. Normalized absorption (c) and fluorescence (d) spectra of **PPE-$^dNH_3Cl$** (solid line) and **BTD-PPE-$^dNH_3Cl$** (dotted line) in MeOH.

Solvent effects on absorption and fluorescence

In order to explore how effectively these dendritic side groups can disrupt the intermolecular interaction of the polymer chains, a series of experiments were carried out in

which the absorption and fluorescence spectra of all of the CPEs were studied in MeOH/H_2O mixtures of varying composition.

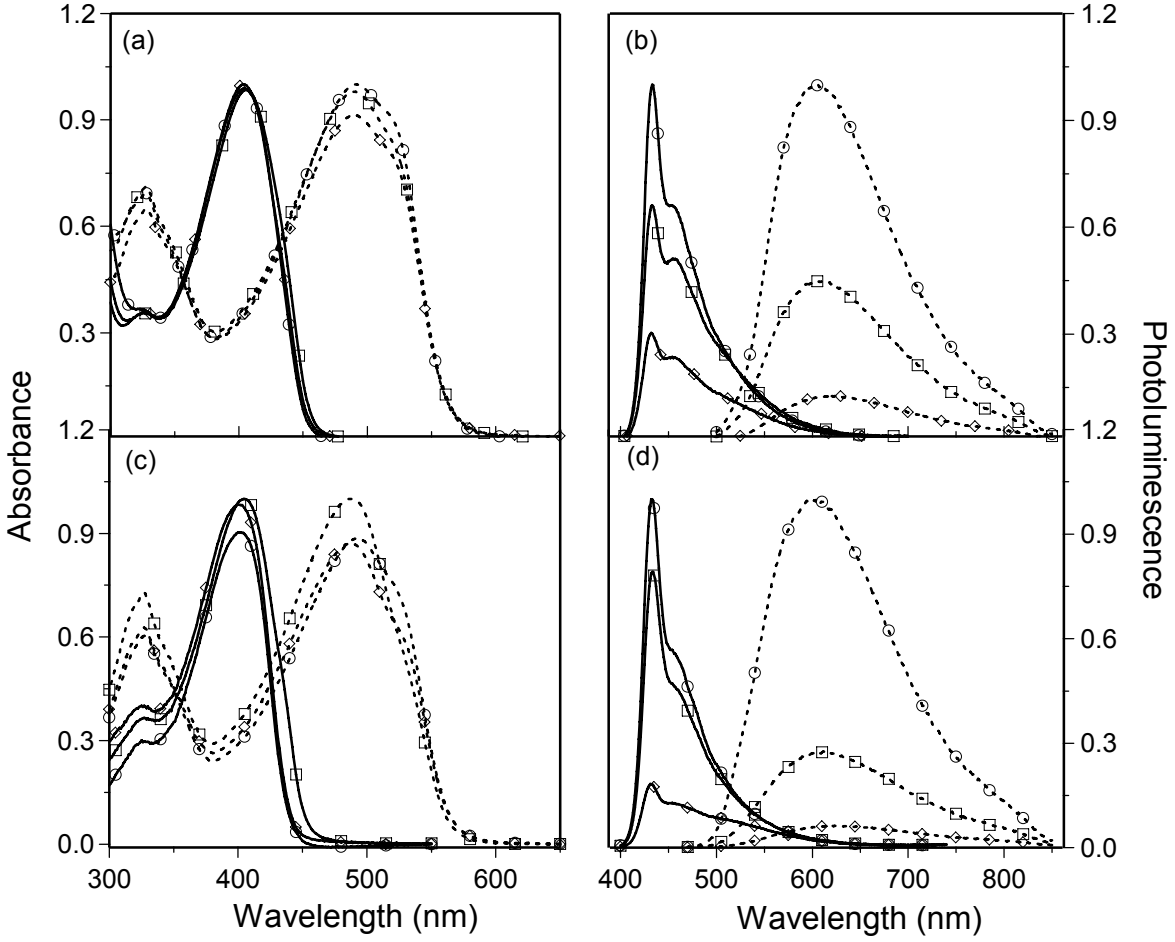

Figure 5-9. Absorption (a) and fluorescence (b) spectra of **PPE-$^{d}CO_2Na$** (solid line) and **BTD-PPE-$^{d}CO_2Na$** (dotted line). Absorption (c) and fluorescence (d) spectra of **PPE-$^{d}NH_3Cl$** (solid line) and **BTD-PPE-$^{d}NH_3Cl$** (dotted line). 0% H_2O (○), 50% H_2O (□) and 100% H_2O (◊). All the spectra were collected continuously and symbols were added to delineate different curves.

Figure 5-9 illustrates the absorption and fluorescence spectra of the anionic PAEs (upper) and cationic PAEs (lower) in MeOH/H_2O mixtures. As the volume fraction of H_2O in the solvent increases, the absorption spectra of these PAEs show little changes; while for the PAEs with linear carboxylate groups, a significant red-shift and narrowing of the absorption spectra is generally resulted. The fluorescence of **PPE-$^{d}CO_2Na$** or **PPE-$^{d}NH_3Cl$** decreases in intensity but

maintains their blue emission (~ 435 nm) as the volume fraction of H_2O increases. By contrast, for **PPE-CO_2Na**, the structured blue emission band is replaced by a broad and red-shifted fluorescence band as shown in chapter 3. For the red-emitting polymer (**BTD-PPE-^{d}CO_2Na** and **BTD-PPE-^{d}NH_3Cl**), their fluorescence also decrease significantly in intensity with increasing volume fraction of H_2O. But in comparison with **BTD-PPE-CO_2Na**, their fluorescence remains relatively efficient even in water. Taken together, the interchain aggregation in the aqueous solutions of these polymers (**PAE-^{d}CO_2Na** and **PAE-^{d}NH_3Cl**) is attenuated by attaching these bulky ionic groups, as evidenced by relative high quantum efficiencies in their H_2O solutions (Table 5-2). And the current results also suggest that to fully disrupt the interchain aggregation, synthesis of PAEs carrying higher generation dendritic side groups is needed.

Table 5-2. UV-Vis absorption and photoluminescent properties of PAEs containing dendritic carboxylate side groups.

	MeOH			H_2O		
	λ_{max}^{abs} (nm)	λ_{max}^{em} (nm)	Φ_{PL}	λ_{max}^{abs} (nm)	λ_{max}^{em} (nm)	Φ_{PL}
PPE-^{d}CO_2Na	403	433	0.31[a]	404	432	0.12[a]
BTD-PPE-^{d}CO_2Na	491 530 (sh)	605	0.04[b]	490 530(sh)	623	0.007[b]
PPE-^{d}NH_3Cl	402	432	0.45[a]	405	432	0.13[a]
BTD-PPE-^{d}NH_3Cl	487	604	0.04[b]	489 530 (sh)	620	0.003[b]

[a] Coumarin 102 in EtOH as the standard, $\Phi_{FL} = 0.95$.[173] [b] $Ru(bpy)_3Cl_2$ in H_2O as the standard, $\Phi_{PL} = 0.036$.[193,194]

Acidity effects on the absorption and fluorescence

Figure 5-10 shows the absorption and emission spectra of **PPE-^{d}CO_2Na** and **PPE-^{d}NH_3Cl** in water as a function of pH. The pH of the polymer-water solution was adjusted with HCl

and/or NaOH using a pH meter. In general, a strong dependence of absorption and emission on the pH is observed for both polymers.

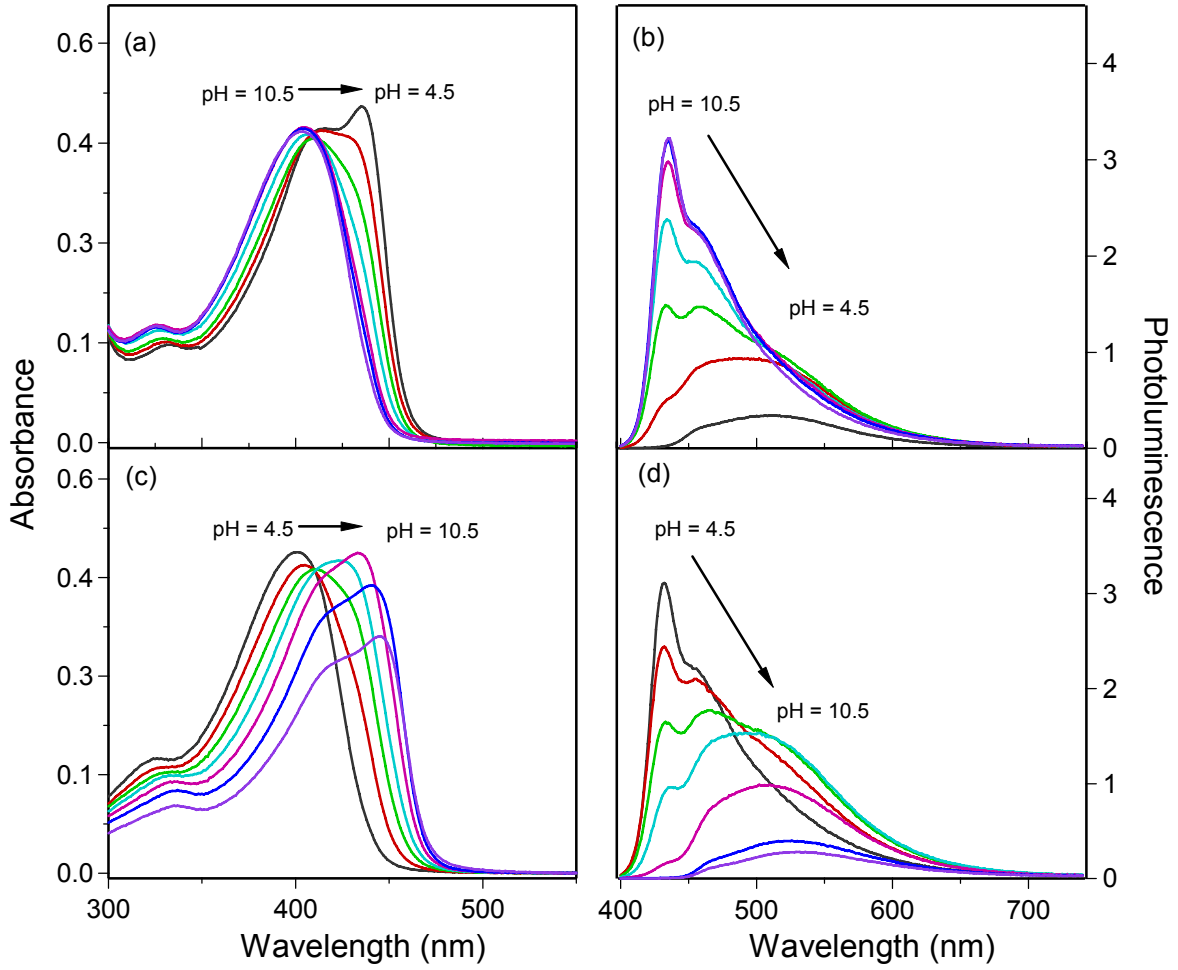

Figure 5-10. Absorption (a) and emission spectra (b) of **PPE-^{d}CO$_2$Na** in aqueous solutions as a function of pH. [**PPE-^{d}CO$_2$Na**] = 5 μM. Absorption (c) and emission spectra (d) of **PPE-^{d}NH$_3$Cl** in aqueous solutions as a function of pH. [**PPE-^{d}NH$_3$Cl**] = 5 μM. pH range from 4.5 to 10.5 in 0.5 pH unit intervals.

In the basic solution of **PPE-^{d}CO$_2$Na** (pH = 10.5), the absorption shows one band centered at 404 nm and the emission shows a structured band at 435 nm. When the pH is adjusted from 10.5 to 4.5, a continuous growing of the shoulder band at 435 nm in the absorption spectra is observed. The largest change in the absorption is visible at pH = 4.5, in line with the pK_a value of propionic acid, with pK_a = 4.88.[137] At this point, approximately 70% of the carboxylate

groups on the polymer chains are protonated. Based on our previous research on several other CPEs and other groups' study,[71,135,140,172] we believe that the red-shift of the absorption spectra arises from the conformation change of the polymer backbone. When the pH is above 7.5, the neighboring phenylene ethynylene groups are twisted in the polymer to minimize the electrostatic repulsion between the negatively charged carboxylate side groups. As the carboxylate is protonated (decreasing pH), the decreased repulsion between the side groups and the desolvation of the neutral and hydrophobic polymer lead to the planarization of the conjugated backbone. It is also very important to note that the series of absorption spectra define an isosbestic point at 410 nm, suggesting that the pH-induced change is between two distinct types of chromophores, which are probably the neutral and charged segments. Concomitant with the absorption changes, the fluorescence of **PPE-^{d}CO$_2$Na** undergoes a quenching of the blue emission band as the pH is decreased. At pH = 4.5, the blue emission is completely replaced by a red-shifted and broad band at 415 nm. Similar to the solvatochromism effect observed for **PPE-CO$_2$Na**,[172] we believe that this low-energy band also arises from the π-π stacking of the polymer chains.

A similar change of absorption and emission spectra is observed for **PPE-^{d}NH$_3$Cl** when the pH was varied from 4.5 to 10.5. The conformation change of the polymer backbone and the aggregation of the polymer chains are tuned by the protonation and deprotonation of the amino groups. Although ethylamine, an analogue of the **PPE-^{d}NH$_3$Cl** side chains, has a p*Ka* of 10.7.[137] the polymer began to precipitate out of the solution when the pH was brought up to 8.5. As shown in Figure 5-10 (c), the oscillator strength can be compared relatively by integrating the absorption band. A significant decrease occurs when the pH increases from 8.5 to 9.5, probably indicating that at this point, precipitation of the polymer chains occurs.

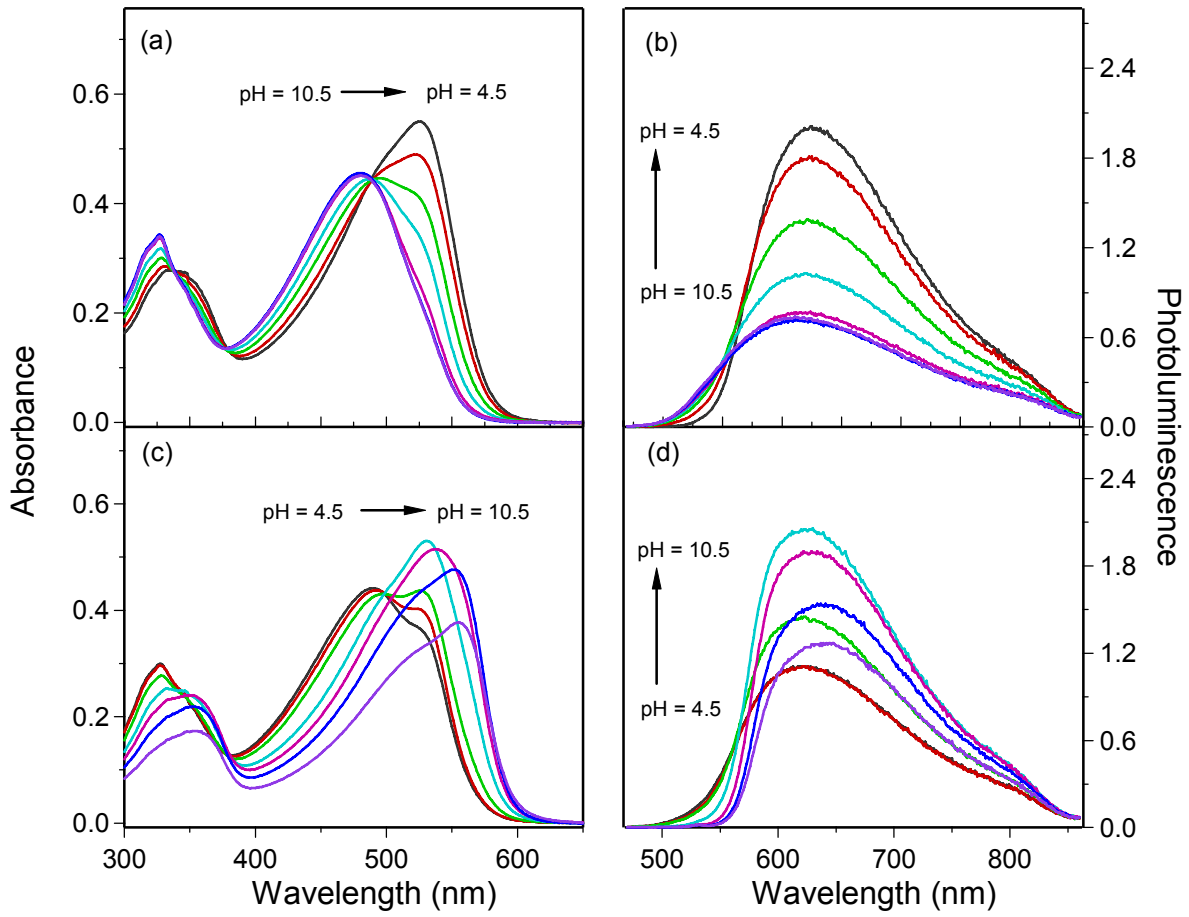

Figure 5-11. Absorption (a) and emission spectra (b) of **BTD-PPE-$^{d}CO_2Na$** in aqueous solutions as a function of pH. [**BTD-PPE-$^{d}CO_2Na$**] = 5 μM. Absorption (c) and emission spectra (d) of **BTD-PPE-$^{d}NH_3Cl$** in aqueous solutions as a function of pH. [**BTD-PPE-$^{d}NH_3Cl$**] = 5 μM. pH range from 4.5 to 10.5 in 0.5 pH unit intervals.

Figure 5-11 illustrates the absorption and emission spectra of **BTD-PPE-$^{d}CO_2Na$** and **BTD-PPE-$^{d}NH_3Cl$** in water when the pH is varied. In the absorption spectra, similar changes are observed as in the spectra of the blue-emitting polymers (**PPE-$^{d}CO_2Na$** and **PPE-$^{d}NH_3Cl$**). Interestingly, a distinct different behavior is observed in the emission spectra of **BTD-PPE-$^{d}CO_2Na$** and **BTD-PPE-$^{d}NH_3Cl$** compared to those of the blue-emitting polymers. For **BTD-PPE-$^{d}CO_2Na$**, at pH ≥ 8.5, there is little change of the emission spectra. When the pH is further decreased, the emission band narrows and increases gradually in intensity. At pH = 4.5, a 3-fold increase of the emission intensity is resulted. We believe that this aggregation-enhanced

emission effect is due to the shielding of BTD unit from water within the polymer aggregates. Recently, a similar effect was observed by Bazan and co-workers.[195] The possibility that protonation of the nitrogen atom in the BTD units causes the emission enhancement is ruled out by observing the same effect when **PPE-^{d}NH$_3$Cl** aggregate is formed by de-protonation of the amino groups.

Salt Effects on the absorption and fluorescence

The pH-induced absorption and fluorescence changes show that the charge density on the polymer side chains is very important to regulate the optical properties of conjugated polyelectrolytes in solution. Another important factor in the aqueous solution is the ionic strength and its effect on the photophysical properties of several different conjugated polyelectrolytes has been studied by several research groups.[66,196] Our polymers with dendritic ionic side groups show relative high quantum efficiencies in water compared to other PAE-based conjugated polyelectrolytes reported in the literature.[53] A detailed study of the effect of ionic strength on their optical properties is necessary for a full understanding of their behavior in the aqueous environment and will be potentially important for their future biosensor applications.

Figure 5-12 illustrates the absorption and fluorescence spectra of **PPE-^{d}CO$_2$Na** and **PPE-^{d}NH$_3$Cl** at varied concentrations of NaCl in water. The results clearly show that aggregation of the polymer chains takes place for both polymers when the NaCl concentration is increased, which is consistent with many observations made for other conjugated polyelectrolytes.[66,196] Since the polymers retain their charged groups, the aggregation of the polymers chains is enabled by the effective screening of the electrostatic repulsion between the pendant charged groups by the Na^+ and/or Cl^- ions in solution. Consequently, after the barrier for planarization is overcome, aggregation is facilitated in order to minimize the contact between

the hydrophobic backbone and water. For **BTD-PPE-$^{d}CO_2Na$** and **BTD- PPE-$^{d}NH_3Cl$**, similar effects were observed.

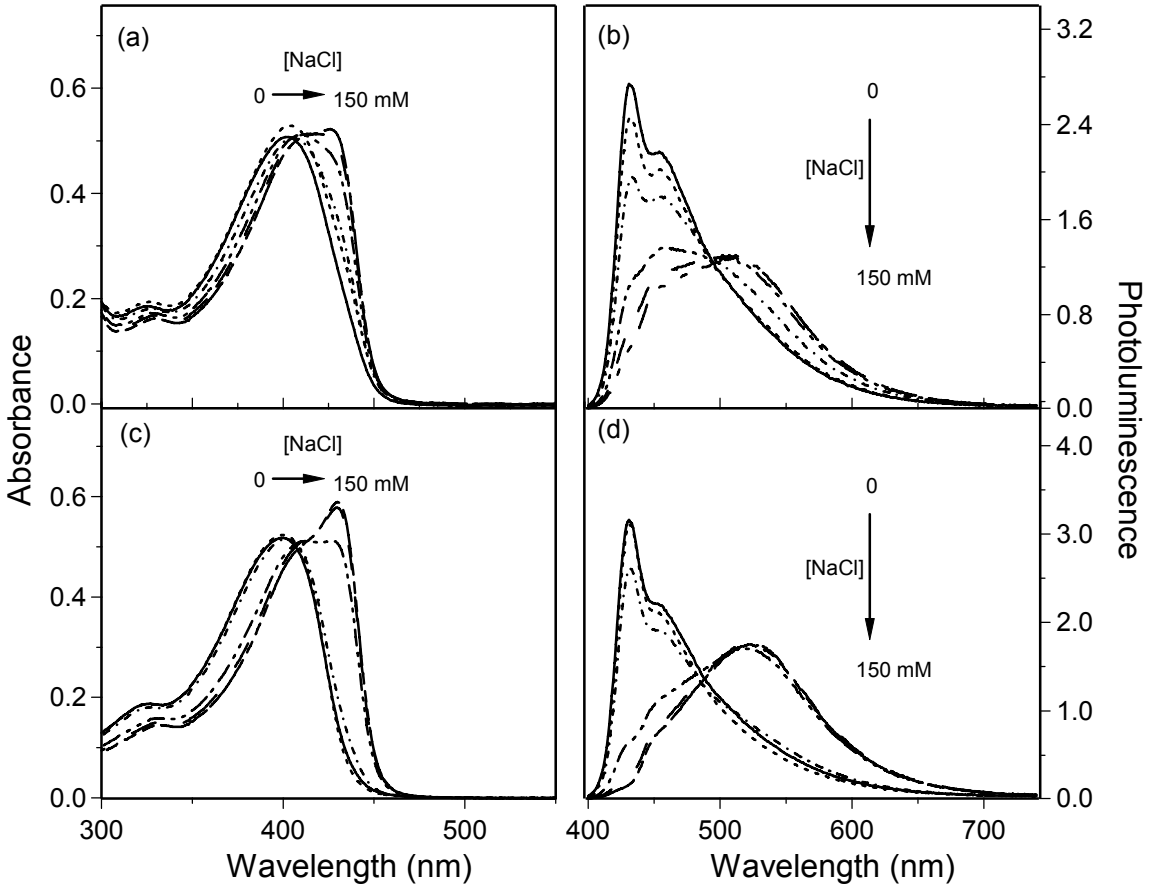

Figure 5-12. Absorption (a) and emission spectra (b) of **PPE-$^{d}CO_2Na$** in aqueous solutions as a function of NaCl concentration, [**PPE-$^{d}CO_2Na$**] = 5 μM. Absorption (c) and emission spectra (d) of PPE-$^{d}NH_3Cl$ in aqueous solutions as a function of NaCl concentration, [**PPE-$^{d}NH_3Cl$**] = 5 μM. [NaCl] = 0, 1, 5, 10, 100, 150 mM. The arrows show the direction of change with increasing NaCl concentration.

Applications of PAEs containing Linear Carboxylate Groups in Dye-sensitized Solar Cells.

One of the many applications of conjugated polyelectrolytes (CPEs) is to use them to replace their organic analogues to fabricate opto-electronic devices. There are several advantages for conjugated polyelectrolytes. First, CPEs exhibit similar electronic properties as their organic analogues but distinct solubility behavior, which enables the construction of heterostructures simply using spin coating; second, their solubility in water and alcohols could

eventually allow the processing of these materials in environment-friendly solvents; third, the existence of ionic side groups in CPEs allows the control of film structure in the molecular level by layer-by-layer (LbL) film deposition method. In a previous report, we described the fabrication of photovoltaic devices in which PAEs with pendant sulfonate groups and a water-soluble C_{60} derivative were assembled in a LbL fashion.[197] As mentioned in chapter 1, CPEs carrying carboxylate groups can be used as the sensitizer to construct TiO_2 based solar cells in the absence of the ruthenium complexes. Using one of the polymers synthesized in this chapter, **PPE-CO_2Na**, combined with a commercial polythiophene (PT-CO_2^-, Rieke Metals, Inc.), we have demonstrated that cell performance can be enhanced by broadening the absorption spectra of the polymer sensitizer (a dual-polymer system in this case).[198]

As our continuing investigations, we constructed DSSCs using the series of PAEs with linear carboxylate side chains and studied the correlation between cell performance and polymer band gap. As shown by many research groups, carboxylic acid functionality is critical for anchoring sensitizer onto the porous nanocrystalline TiO_2 surface.[87,199] To ensure the adsorption of the polymer to the TiO_2, the carboxylate groups in the polymer chains were protonated using 3 N HCl. The current series of PAEs with carboxylic acid groups were completely dried in a vacuum oven at 60 °C. They were then dissolved in dry DMF (solubility is less than 0.2 mg/ml due to the strong aggregation of the polymers in the solid state) and used for the immersion deposition into porous TiO_2 films. Usually, it takes 12 to 14 hours for the polymer adsorption process to saturate as proven by absorption measurements of the films. At saturation, the optical densities of the films for all the polymers are close to 1.0. Then the films were used to fabricate the solar cells, of which the cell performances were tested immediately.

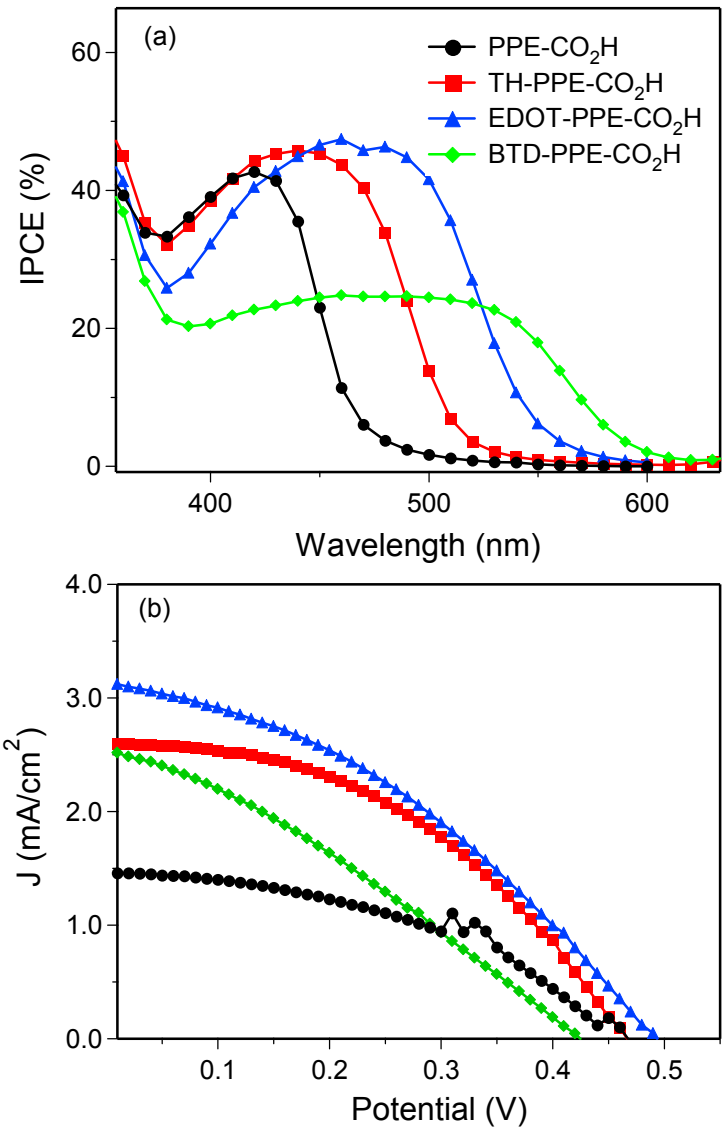

Figure 5-13. IPCE spectra (a) and Current-potential (I-V) curves (b) for CPE-sensitized solar cells under AM 1.5 condition. These experiments were carried out by Hui Jiang in Schanze group.

Figure 5-13 (a) shows the incident photo to current efficiency (IPCE) of the CPE sensitized solar cells as a function of wavelength. The IPCE values at the maxima for **PPE-CO_2H**, **TH-PPE-CO_2H** and **EDOT-PPE-CO_2H** are in the range of 42% to 47% and match very well with their absorption spectra. Since all the films for different polymers have very close absorbance at the absorption maxima, the IPCE value at the maximum for **BTD-PPE-CO_2H** is expected to be

in the same range. However, the IPCE values in the full range of the polymer's absorption are lower than 25%.

The current density - voltage (*J* - *V*) characteristics for the CPE sensitized cells are shown in Figure 5-13 (b). These cells' performance in terms of short circuit current (J_{sc}), open circuit voltage (V_{oc}), fill factor (*FF*), and power conversion efficiency (η) are summarized in Table 5-3, along with the maximum IPCE values. Consistent with the IPCE results, the overall power conversion efficiencies show the order of **PPE-CO_2H** < **TH-PPE-CO_2H** < **EDOT-PPE-CO_2H**, which can be ascribed to the enhanced solar energy harvesting due to the continuous red-shift of their absorption spectra. However, the performance of the cell utilizing the most red-absorbing polymer, **BTD-PPE-CO_2H** in the series is only comparable to that of the cell based on **PPE-CO_2H**.

Table 5-3. Summary of solar cell performance.

Device	IPCE (%)	J_{sc} (mA/cm^2)	V_{oc} (V)	*FF* (%)	η (%)
PPE-CO_2H	42.7 @420 nm	1.46	0.47	49.2	0.34
TH-PPE-CO_2H	45.8 @440 nm	2.60	0.47	43.4	0.53
EDOT-PPE-CO_2H	47.4 @460 nm	3.12	0.50	37.2	0.58
BTD-PPE-CO_2H	24.7 @480 nm	2.52	0.43	30.5	0.33

Note: these data were obtained by Hui Jiang in Schanze group.

To further understand the correlation between the cell performance and the electronic properties of current polymers, we measured the oxidation potentials of the excited state of the series in solution by cyclic voltammetry (CV) and differential pulse voltammetry (DPV). Due to the solubility issue, the dodecyl ester protected precursors (**PPE**, **TH-PPE** and **EDOT-PPE**) in dichloromethane and **BTD-PPE-CO_2H** in DMSO were used. Based on the optical band gap energy extracted from the cross point of absorption and fluorescence spectra, the oxidation

potentials of the ground state of the CPEs are also estimated. The results are summarized in Table 5-4. These results clearly show that the energies of the excited state and the ground state of all the polymers match very well with those of TiO_2 conduction band and redox pair I^-/I_3^-, indicating favorable driving forces for charge injections. Another reason that might explain the poor cell performance for **BTD-PPE-CO_2H** is that the charge injection occurs from the charge transfer band, while the other polymers inject electrons to the conduction band of TiO_2 from their π^* excited states. Thus a competing intramolecular/intermolecular charge transfer process takes place when the polymers are adsorbed on the surface of TiO_2, which decreases the efficiency of charge injection to the TiO_2 and thus the cell performance.

Table 5-4. Redox potentials of studied conjugated polyelectrolytes.

	Excited State Oxidation Potential [a] (V vs. SCE)	Optical Band Gap [b] (eV)	Ground State Oxidation Potential (V vs. SCE)
PPE	-1.12	2.89	1.77
TH-PPE	-1.12	2.65	1.53
EDOT-PPE	-0.87	2.53	1.66
BTD-PPE-CO_2H	-1.02	2.19	1.17

[a] Measured using ferrocene as the internal standard. [b] Optical band gap based on cross point of absorption and emission spectra. These data were obtained by Katsu Ogawa in Schanze group.

Experimental

Materials

$Pd(PPh_3)_2Cl_2$ and $Pd(PPh_3)_4$ were purchased from Strem Chemical Company and used as received. Triethyamine and THF used in the polymerization were purified by distillation over CaH_2. Iodine monochloride-pyridine complex and 4-(2-carboxyethyl)-4-nitroheptanedioic acid were purchased from Aldrich Chemical Company. All the other chemicals were supplied by

either Acros or Aldrich Chemical Company and used without further purification. Fluorine-doped tin oxide (FTO, TEC 8) glass substrates were purchased from Harford Glass, and nanocrystalline TiO_2 paste (12% wt., average particle size about 13 nm) was purchased from a Switzerland based company, Solaronix SA.

Instrumentation

NMR spectra were recorded on a Varian VXR-300 or Gemin-300 FT-NMR, operating at 300 MHz for ^{1}H-NMR and at 75.4 MHz for ^{13}C-NMR. High temperature NMR spectra were recorded on a Varian Mercury 300 FT-NMR. Chemical shifts were reported in ppm using $CHCl_3$ or C_2HD_5SO as internal reference. FT-IR spectra were taken on a Perkin-Elmer 1600 spectrometer. Gel permeation chromatography (GPC) analyses were carried out on a system comprised of a Rainin Dynamax SD-200 pump and a Beckman Instruments Spectroflow 757 absorbance detector. UV-Visible absorption spectra were recorded with a Lambda 25 spectrophotometer from PerkinElmer. Steady-state fluorescence spectra were obtained with a Fluorolog-3 spectrofluorometer from Jobin Yvon. The cyclic voltammetry (CV) and differential pulse voltammetry (DPV) experiments were performed on a Bioanalytical Systems CV50 electrochemical analyzer at a scan rate of 50 mV/s. Measurements were carried out in nitrogen-degassed solutions with 0.1 M tetrabutylammonium hexafluorophosphate ($TBAPF_6$) as the supporting electrolyte and ferrocene as the internal standard (0.43 V vs SCE in dry dichloromethane).

General Methods

Photovoltaic device fabrication and characterization. *All the solar cells were fabricated and characterized by Hui Jiang in Schanze group*. The DSSCs were fabricated by following the published procedures. Briefly, TiO_2 paste was spread out on a FTO substrate and sintered at 450 ºC for 30 min. The TiO_2 film thickness was about 5 μm. The film was immersed

in a polymer solution for about 14 hours for adsorption. To assemble the cell, 5 nm Pt coated FTO was used as the counter electrode and a propylene carbonate solution of 0.05 M I_2 / 0.5 M LiI was applied as the electrolyte. The active solar cell area was about 1.0 cm^2.

The current–voltage characteristics were measured with a Keithley SMU 2400 source meter under the illumination of AM 1.5 (100 mW/cm^2) using a 150 W Xe arc lamp (Oriel instruments). For IPCE measurements, the device was illuminated by monochromatic light from an Oriel Cornerstone™ 130 1/8 m spectrometer, and the current response under short circuit condition was recorded at 10 nm intervals using a Keithley SMU 2400 source meter. The intensity of the light source at each wavelength was determined using an energy meter (S350, UDT Instruments) equipped with a calibrated silicon detector (Model 221, UDT Instruments).

Synthetic Procedures

2,5-Bis((trimethylsilyl)ethynyl)thiophene (3) 2,5-Dibromothiophene (1.2 g, 5 mmol) was dissolved in a mixture of 25 ml of THF/$(i\text{-}Pr)_2NH$ (v/v, 4/1) and degassed with argon for 15 minutes. Then under the protection of argon, 70 mg of $Pd(PPh_3)_2Cl_2$ (10 mmol)and 20 mg (10 mmol) of CuI were added, followed by the addition of 2.1 mg of trimethylsilyacetylene (15 mmol). The resulting mixture was stirred at room temperature for 5 hr, then filtrated. After removal of the solvent, the brown oil was purified by chromatography on silica gel eluting with hexane to afford a yellow solid (yield: 1.5 g, 95%). ^1H NMR ($CDCl_3$, δ_{ppm}): 7.04 (s, 2H), 0.25 (s, 18H).

2,5-Diiodo-3,4-ethylenedioxythiophene (4). A solution of 5.6 g (40.0 mmol) of 3,4-ethylenedioxythiophene and 23.0 g (90.0 mmol) of iodine monochloride-pyridine complex in 150 mL of dry dichloromethane was stirred at room temperature for 1 hr. A precipitate of pyridinium salt that was produced during the reaction was removed by vacuum filtration, and the filtrate was evaporated. The remained solid residue was rinsed with a mixture of water/methanol

(1:1) and it was recrystallized twice from acetone. The product was obtained as greenish white crystals (yield: 14.8 g, 93%). ^{1}H NMR (DMSO-d_6; δ_{ppm} from TMS): 4.25 (s, 4H). ^{13}C NMR (DMSO-d_6; δ_{ppm}): 143.84, 64.83, 54.08.

2,5-Bis(trimethylsilylethynyl)-3,4-ethylenedioxythiophene (5). A deoxygenated solution of 3.93 g (10.0 mmol) of **2**, 6 mL (42.6 mmol) of trimethylsilylacetylene, 580 mg (0.5 mmol) of $Pd(PPh_3)_4$ and 95 mg (0.5 mmol) of CuI in 20 mL of THF/Et_3N (2/1) mixture was stirred at room temperature under argon for 2 hr. The triethylammonium salt which precipitated during the reaction was removed by filtration and the filtrate was evaporated *in vacuo*. The remaining dark oil was eluted through a silica gel column with hexanes. The pale yellow hexane solution was evaporated and the solid obtained was recrystallized two times from 90% methanol. The product was obtained as a fine light yellow solid (yield: 1.27 g, 38%). ^{1}H NMR ($CDCl_3$, δ_{ppm}): 4.26 (s, 4H), 0.24 (s, 18H). ^{13}C NMR ($CDCl_3$, δ_{ppm}): 143.79, 103.12, 99.91, 94.39, 64.97, 0.12.

2,5-Diethynyl-3,4-ethylenedioxythiophene (6). A solution of 1.0 g (3.0 mmol) of **3** in 20 mL of dioxane was acidified with 2 mL of 50% acetic acid and was deoxygenated with purging argon for 10 minutes. Then 25 mL of a solution of *n*-Bu_4NF in THF (c = 1 M) was added and the resulting mixture was stirred for 30 minutes at room temperature. Half of the solution volume was evaporated and the resulting solution was poured into 300 mL of ice water. The precipitated solid was collected by vacuum filtration, dissolved in 50 mL of hexanes and eluted through a short plug of silica gel. The solvent was evaporated and the solid obtained was stored in refrigerator for a few hours prior to use. ^{1}H NMR ($CDCl_3$; δ_{ppm}): 4.30 (s, 4H), 3.50 (s, 2H),. ^{13}C-NMR ($CDCl_3$; δ_{ppm}): 65.04, 73.96, 85.06, 98.70, 144.37.

4,7-Bis((trimethylsilyl)ethynyl)benzo[c][1,2,5]thiadiazole (7). 4,7-Dibromobenzo[c][1,2,5]thiadiazole (1.5 g, 5.1 mmol) was dissolved in a mixture of 50 ml of THF / $(i\text{-}Pr)_2NH$ (v/v, 3/1) and degassed by argon for 15 minutes. Then 1.5 g of trimethylsilyacetylene (15.3 mmol) was added using a syringe and followed by the addition of 107 mg (0.16 mmol) of $Pd(PPh_3)_2Cl_2$ and 29 mg (0.15 mmol) of CuI. The resulting mixture was heated at 55 °C for 12 h, then filtrated. After the removal of the solvent, the residue was purified by chromatography on silica gel eluting with CH_2Cl_2/hexane (v/v, 1/2) to afford a yellow solid (yield: 1.65 g, 98%). ^1H NMR ($CDCl_3$, δ_{ppm}): 7.71 (s, 2H), 0.34 (s, 18 H).

4,7-Diethynylbenzo[c][1,2,5]thiadiazole (8). Compound **7** (164 mg, 0.5 mmol) was dissolved in 10 ml THF/MeOH (v/v, 4/1). To the solution, 62 mg of KOH (1.1 mmol) in 0.5 ml of H_2O was added. The reaction mixture was stirred at room temperature for 1 hr and then poured into 60 ml of H_2O. A crystalline yellow solid was obtained and washed with cold MeOH/H_2O (1/1, 20 ml). After drying under vacuum, the solid was stored in the refrigerator for a very short period before using (yield: 81 mg, 87%). ^1H NMR ($CDCl_3$, δ_{ppm}): 7.76 (s, 2H), 3.68 (s, 2H).

Di-*tert*-butyl 4-Nitro-4-(3-tert-butoxy-3-oxopropyl)heptanedioate (10).[200] A stirred solution of $MeNO_2$ (6.1 g, 100 mmol), Triton B (benzyltrimethylammonium hydroxide, 40% in MeOH; 1.0 ml) in dimethoxyethane (DME, 20 ml) was heated to 65-70 °C. To the mixture, *tert*-butyl acrylate (39.7 g, 310 mmol) was added drop-wise. Additional triton B (1.0 ml ×2) was added after 15 minutes and the reaction was kept at 70-75 °C for 1 hr. After concentrated *in vacuo*, the residue was dissolved in $CHCl_3$ (200 ml), washed with 10% HCl (100 ml × 1) and brine (100 ml × 1), and dried with anhydrous $MgSO_4$. After removal of the solvent, the crude product was purified by crystallizing from ethanol (95%), which afforded a white crystalline

solid (yield: 70%). ^{1}H NMR ($CDCl_3$, δ_{ppm}): 2.18 (s, 12H), 1.42 (s, 27H). ^{13}C NMR ($CDCl_3$, δ_{ppm}): 171.04, 92.17, 81.16, 30.34, 29.80, 28.04.

Di-*tert*-butyl 4-Amino-[2-(*tert*-butoxycarbonyl)ethyl]-heptanedioate (11).[200] A solution of nitro ester **(10)** (4.46 g, 10 mmol) in absolute ethanol (100 ml) with T-1 Raney Ni (4.0 g) was hydrogenated at room temperature with a balloon filled with hydrogen for 48 hr. The catalyst was cautiously filtered away through a bed of celite. The solvent was removed *in vacuo*, affording a viscous liquid, which was purified by column chromatograph (silica gel, EtOAc/hexane (v/v, 1/1)) to give a clear yellow oil (4.0 g, 93%). The oil solidified after standing in the hood overnight, affording a white solid. ^{1}H NMR ($CDCl_3$, δ_{ppm}): 2.21 (t, 6H); 1.58 (t, 6H), 1.41 (s, 27H). ^{13}C NMR ($CDCl_3$, δ_{ppm}): 172.97, 80.26, 52.26, 34.33, 29.92, 28.01.

4-(3-Chloro-3-oxopropyl)-4-nitroheptanedioyl dichloride (13). A 100 ml round bottom flask was charged with 4.44 g of 4-(2-carboxyethyl)-4-nitroheptanedioic acid (16 mmol) and 30 ml thionyl chloride ($SOCl_2$). Two drops of DMF was added to the suspension and the mixture was then slowly heated up to reflux. After 1 hr, the solution became clear and there was no more gas evolution. The excess $SOCl_2$ was removed by vacuum distillation. The yellow residue solidified after flushing with nitrogen and used without further purification. ^{1}H NMR ($CDCl_3$, δ_{ppm}): 2.96 (t, 6H), 2.30 (t, 6H). ^{13}C NMR ($CDCl_3$, δ_{ppm}): 172.46, 89.91, 41.29, 30.16.

3-(2-Aminoethyl)-3-nitropentane-1,5-diamine•HCl salt (14). The acid chloride obtained from last step was dissolved in 30 ml dioxane in a three-necked round bottom flask protected with argon. Trimethylsilyl azide (6.3 ml, 48 mmol) was added to the solution at room temperature. The solution was then slowly heated up to 80 ºC. When there was no more gas evolution, the reaction mixture was allowed to cool down to 45 ºC and then added 20 ml of acetone. Concentrated HCl (12 ml) was added to the mixture drop-wise. White precipitate

formed immediately following the addition. After 1 hr, the reaction mixture was allowed to cool down to room temperature. The white precipitate was collected by vacuum filtration and washed with 200 ml cold acetone. After drying in the hood overnight, a slightly yellow solid was obtained (yield: 3.86 g, 81%). ^{1}H NMR (DMSO-d_6): 8.39 (s, 9H), 2.81 (t, 6H), 2.33 (t, 6H).

Compound (15). 3-(2-Aminoethyl)-3-nitropentane-1,5-diamine•HCl salt (**14**) (3.0 g, 10.0 mmol)was dissolved in 100 ml of Et_3N/CH_3CN (v/v, 1/3). Then 10.2 g of di-*tert*-butyl dicarbonate (46.8 mmol) was added. The mixture was heated at reflux for 7 hr and then diluted with 150 ml of ethyl acetate. The mixture was washed with H_2O (250 ml × 1). Then the aqueous phase was extracted with ethyl acetate (150 ml × 1). The organic phase was combined and dried with anhydrous $MgSO_4$. After the filtration, the solvent was removed *in vacuo*, affording a yellow oil which solidified under vacuum (yield: 4.2 g, 86%). ^{1}H NMR ($CDCl_3$, δ_{ppm}): 4.81 (s, 3H), 3.13 (m, 6H), 2.16 (t, 6H), 1.40 (s, 27H). ^{13}C NMR ($CDCl_3$, δ_{ppm}): 155.84, 90.59, 79.63, 35.79, 35.59, 28.34. LR-MS: calcd for $C_{22}H_{42}N_4O_8$[M+H] = 491.6, found 491. Elemental analysis: Calcd for $C_{22}H_{42}N_4O_8$: C, 57.86; H, 8.63; N, 11.42. Found: C, 53.78; H, 9.03; N, 11.24.

Compound (16).[201] A solution of 3.1 g of compound **15** (6.3 mmol) in 200 ml of ethanol with T1 Raney Nickel (3.0 g) was hydrogenated at 100 psi and 70 °C for 36 hr. The catalyst was removed by filtering the reaction mixture through a bed of celite. The solvent was removed *in vacuo*, affording a slightly yellow oil, which solidified as a fluffy white solid under vacuum (yield: 90%). ^{1}H NMR ($CDCl_3$, δ_{ppm}): 5.06 (s, 3H), 3.18 (m, 6H), 1.78 (s, 2H), 1.56 (t, 6H), 1.41 (s, 27H). ^{13}C NMR ($CDCl_3$, δ_{ppm}): 155.99, 79.22, 52.96, 39.37, 36.14, 28.41. LR-MS: calcd for $C_{22}H_{44}N_4O_6$ [M+H] = 461.6, found 461.

2,2'-(2,5-Diiodo-1,4-phenylene)bis(oxy)diacetyl chloride (18). 2,2'-(2,5-Diiodo-1,4-phenylene)bis(oxy)diacetic acid (5.8 g, 12 mmol) was suspended in 30 ml of $SOCl_2$. After adding 2 drops of DMF, the reaction mixture was heated up and stirred at reflux for 2 hr. then the excess $SOCl_2$ was removed by vacuum distillation and the resulting off-white solid was crystallized from 200 ml of heptane/toluene (v/v, 10/1), affording a slightly yellow crystalline solid (yield: 5.0 g, 80%). ^{1}H NMR ($CDCl_3$, δ_{ppm}): 7.15 (s, 2H), 4.92 (s, 4H). ^{13}C NMR ($CDCl_3$, δ_{ppm}): 152.58, 124.41, 113.62, 86.44, 74.05.

Compound (19). Di-*tert*-butyl 4-Amino-[2-(*tert*-butoxycarbonyl)ethyl]-heptanedioate (**11**) (1.2 g, 2.9 mmol), 0.4 ml of Et_3N and 25 ml of dry CH_2Cl_2 were placed in a 50 ml round bottom flask and cooled with an ice/water bath. Then 0.67 mg of 2,2'-(2,5-diiodo-1,4-phenylene)bis(oxy)diacetyl chloride (**9**) (1.3 mmol) in 15 ml of CH_2Cl_2 was added via a syringe. After 2 hr, the reaction mixture was allowed to warm to room temperature and further stirred for 24 hr. The solvent was removed *in vacuo*, the crude product was purified by flash chromatography (silica gel, EtOAc/hexane (1/3)) to give a white solid (yield: 1.4 g, 78%). ^{1}H NMR ($CDCl_3$, δ_{ppm}): 7.13 (S, 2H), 6.60 (s, 2H), 4.35 (s, 4H), 2.25 (m, 12H), 2.03 (m, 12H), 1.42 (s, 27H). ^{13}C NMR ($CDCl_3$, δ_{ppm}): 172.19, 165.73, 151.57, 122.63, 86.29, 80.63, 68.83, 57.80, 30.17, 29.74, 28.09. HR-MS: calcd. for $C_{54}H_{86}I_2N_2O_{16}$ [M+Na] = 1295.3959, found 1295.3966.

Compound (20). Compound **16** (1.5 g, 3.3 mmol), 0.45 ml of Et_3N (3.2 mmol) and 30 ml of dry CH_2Cl_2 were placed in a 50 ml round bottom flask, which was cooled in an ice/water bath. To the mixture, a solution of 0.76 g of 2,2'-(2,5-diiodo-1,4-phenylene)bis(oxy)diacetyl chloride (**9**) (1.5 mmol) was added via a syringe. After 2 hr, the reaction mixture was allowed to warm to room temperature and further stirred for 24 hr. The solvent was removed *in vacuo*, the crude product was purified by flash chromatography on silica gel with EtOAc/hexane (1/1) to give a

colorless oil, which solidified as a white solid under vacuum (yield: 1.0 g, 50%). The ^{1}H NMR ($CDCl_3$, δ_{ppm}): 7.15 (s, 2H), 6.71 (s, 2H), 4.80 (s, 6H), 4.36 (s, 4H), 3.19 (m, 12H), 2.03 (m, 12H), 1.42 (s, 27H). ^{13}C NMR ($CDCl_3$, δ_{ppm}): 166.38, 155.94, 151.61. 122.72, 86.43, 79.33, 68.71, 59.92, 35.76, 35.60, 28.39. HR-MS: calcd for $C_{54}H_{92}I_2N_8O_{16}$ [M+Na] = 1385.4613, found 1385.4613.

General polymerization procedure for PPE with linear side chains. 2,5-Bis(dodecyloxycarbonylmethoxy)-1,4-diiodobenze (814.6 mg, 1mmol) and 1 mmol of the other monomer (1,4-bis((trimethylsilyl)ethynyl)benzene or 2,5-bis((trimethylsilyl)ethynyl)thiophene or 2,5-bis(trimethylsilylethynyl)-3,4-ethylenedioxythiophene) were dissolved in 30 ml of THF/Et_3N (v/v. 3/2) in a Schlenk flask sealed with a septum. The resulting solution was deoxygenated by purging with argon for 15 minutes. Then 0.25 ml of TBAF (1 M in THF) was added to the solution via a syringe, followed by the addition of $Pd(PPh_3)_4$ (34.8 mg, 0.03 mmol) and CuI (12.6 mg, 0.06 mmol). The reaction mixture was then heated to 60 °C and stirred for 24 hr. Then the solution was poured into 300 ml methanol. The precipitate was collected by vacuum filtration and further purified by dissolution in THF and precipitation into methanol. Typical yields of these polymerization are 80% - 90%. A small amount (~30 mg) of each polymer was dried completely under vacuum and used for NMR study immediately. The rest of the polymer was hydrolyzed following the procedure described in Chapter 3.

PH-PPE. GPC (THF, polystyrene standard): M_w = 131, 560, M_n = 36, 820, PDI = 3.60.

TH-PPE. ^{1}H NMR ($CDCl_3$, δ_{ppm}): 7.22 (s, 2H), 6.97 (s, 2H), 4.72 (s, 4H), 4.24 (t, 4H), 1.68 (m, 4H), 1.30-1.25 (m, 36H), 0.88 (t, 6H). GPC (THF, polystyrene standard): M_w = 108, 980, M_n = 30, 300, PDI = 3.60.

TH-PPE-CO_2Na. ^1H NMR (D_2O/DMSO-d_6 = 1/1): 7.28 (s, 2H), 6.92 (s, 2H), 4.34 (s, 4H).

EDOT-PPE. ^1H NMR ($CDCl_3$, δ_{ppm}): 6.96 (s, 2H), 4.70 (s, 4H), 4.34 (s, 4H), 4.22 (t, 4H), 1.67 (m, 4H), 1.30-1.25 (m, 36H), 0.88 (t, 6H). GPC (THF, polystyrene standard): M_w = 26, 380, M_n = 10, 570, PDI = 2.50.

EDOT-PPE-CO_2Na. ^1H NMR (DMSO-d_6): 7.05 (s, 2H), 4.78 (s, 4H), 4.38 (s, 4H).

BTD-PPE-CO_2Na. A solution of sodium 2,2'-(2,5-diiodo-1,4-phenylene)bis(oxy)diacetate (521.9 mg, 1.0 mmol) and compound **7** (328.6 mg, 1.0 mmol) in 85 ml of DMF/H_2O/i-Pr_2NH (v/v/v = 9/6/2) was deoxygenated with argon for 30 minutes. Then 0.25 ml of TBAF (1 M in THF) was added under argon, followed by the addition of $Pd(PPh_3)_4$ (70 mg, 0.06 mmol) and CuI (22 mg, 0.12 mmol). The resulting brownish solution was heated at 60 ºC for 24 hr. The reaction mixture was then poured into 600 ml of acetone. The resulting reddish precipitate was collected by vacuum filtration and further purified by two repeated cycles of dissolution in H_2O and precipitation into acetone. Then the solid was dissolved in 75 ml of deionized H_2O and dialyzed against a large amount of water. After dialysis, the polymer was stored as its aqueous solution. During the storage, the solution pH was controlled in the range of 8-10. ^1H NMR (DMSO-d_6): 7.88 (br, s, 2H), 7.22 (br, s, 2H), 4.83 (s, 4H).

General polymerization procedure for PAEs with dendritic anionic side chains. Monomer **19** (318.3 mg, 0.25 mmol) and 0.25 mmol of the other monomer (1,4-diethynylbenzene or 4,7-diethynylbenzo[c][1,2,5]thiadiazole) were dissolved in 16 ml of THF/Et_3N (v/v, 3/1). The resulting solution was deoxygenated with argon for 15 minutes. Then 17.3 mg of $Pd(PPh_3)_4$ (15 μM) and 5.7 mg of CuI (30 μM) were added to the stirred solution under the protection of argon. The reaction mixture was then heated up to 60 ºC – 65 ºC and

stirred for 24 hr. The viscous solution was then poured into 200 ml of methanol. The precipitate was collected by vacuum filtration and washed with methanol (200 ml). After dried under vacuum, the polymer was stored as a solid. Typical reaction yields for the polymerization are 80% - 90%. For the hydrolysis, the organic polymer was dissolved in 20 ml CH_2Cl_2 and cooled in an ice/water bath. 20 ml of trifluoroacetic acid (TFA) was added to the polymer solution drop-wise. Upon the completion of the addition, the reaction mixture was allowed to warm to room temperature and stirred for another 12 hr. The excess of TFA and the solvent were removed *in vacuo*. The residue was treated with saturated aqueous Na_2CO_3 solution (10 ml) and stirred at room temperature for 3 hr. The solution was then poured into 200 ml of acetone. The polymer precipitate was then dissolved in water and purified by dialysis using 12 kD MWCO regenerated cellulose membranes (yield: 90% - 100%). The water-soluble polymers could be either stored as aqueous solutions or as solid powders.

PPE-R[1]. ^{1}H NMR ($CDCl_3$, δ_{ppm}): 7.57(br, s, 4H), 7.04 (s, 2H), 6.39 (s, 2H), 4.47 (s, 4H), 2.13 (br, m, 12H), 1.96 (br, s, 12H), 1.39 (s, 54 H). GPC (THF, polystyrene standard): M_w = 33, 230, M_n = 101, 210, PDI = 3.00. FT-IR (ν_{max}, KBr pellet): 3403, 2978, 2935, 2205, 1731, 1692, 1532, 1512, 1484, 1456, 1410, 1393, 1368, 1312, 1282, 1256, 1214, 1154, 1101, 1051, 954, 891, 848, 758.

PPE-^{d}CO$_2$Na. ^{1}H NMR (D_2O/DMSO-d_6 = 1/1): 7.58 (br, 4H), 7.16 (s. 2H). 5.25 (s, 4H). FT-IR (ν_{max}, KBr pellet): 3391, 2937, 2202, 1665, 1564, 1404, 1283, 1208, 1099, 1053, 892, 847, 675.

BTD-PPE-R[1]. ^{1}H NMR ($CDCl_3$, δ_{ppm}): 7.91 (br, s, 2H), 7.19 (s, 2H), 6.51 (s, 2H), 4.59 (s, 4H), 2.12 (br, m, 12H), 1.94 (br, s, 12H), 1.39 (br, s, 54H). GPC (THF, polystyrene standard): M_w = 16, 250, M_n = 11, 690, PDI = 1.40. FT-IR (ν_{max}, KBr pellet): 3405, 2978, 2936, 2679,

2494, 2204, 1731, 1693, 1519, 1486, 1457, 1393, 1368, 1312, 1281, 1256, 1213, 1154, 1101, 1056, 954, 847, 758, 721.

BTD-PPE-$^{d}CO_2Na$. ^{1}H NMR (D_2O/DMSO-d_6 = 1/1): 7.88 (br, s, 2H), 7.22 (br, s, 2H), 4.83 (s, 4H). FT-IR (ν_{max}, KBr pellet): 3391, 2951, 2204, 1667, 1566, 1403, 1283, 1207, 1097, 1061, 838, 778, 721, 667.

General polymerization procedure for PAEs with dendritic cationic side chains. Monomer **20** (340.8 mg, 0.25 mmol) and 0.25 mmol of the other monomer (1,4-diethynylbenzene or 4,7-diethynylbenzo[c][1,2,5]thiadiazole) were dissolved in 25 ml of THF/Et_3N (v/v, 4/1). The resulting solution was deoxygenated with argon for 15 minutes. Then 17.3 mg of $Pd(PPh_3)_4$ (15 μM) and 5.7 mg of CuI (30 μM) were added to the stirred solution under the protection of argon. The reaction mixture was then heated up to 55 ºC - 60 ºC and stirred for 20 hr. The viscous solution was then poured into 200 ml of hexane. The precipitate was collected by vacuum filtration and washed with hexane (200 ml). After dried under vacuum, the polymer was stored as a solid. Typical reaction yields for the polymerization are 80% - 90%. For the hydrolysis, the organic polymer was dissolved in 20 ml of dioxane. The polymer solution was then cooled to 0 ºC - 5 ºC using an ice/water bath. Concentrated HCl (7 ml, 12 N) was added to the stirred solution drop-wise. Upon the completion of the addition, the reaction mixture was allowed to warm to room temperature and stirred for another 12 hr. The polymer was then precipitated by pouring the solution into a large amount of acetone (200 ml). The precipitate was collected, washed with acetone (100 ml) and finally dried under vacuum (yield: 90% - 100%). No further purification was done on these polymers and they were stored as solid powders in a desiccator and can be re-dissolved in water easily.

PPE-R^2. ^{1}H NMR ($CDCl_3$, δ_{ppm}):7.61 (br, s, 4H), 7.05 (s, 2H), 6.60 (br, s, 2H), 4.92 (s, 6H), 4.46 (s, 4H), 3.09 (br, s, 12H), 1.93 (br, 2, 12H), 1.39 (s, 54H). GPC (THF, polystyrene standard): M_w = 105, 640, M_n = 24, 080, PDI = 4. 40). FT-IR (ν_{max}, KBr pellet): 3393, 2977, 1691, 1517, 1457, 1392, 1367, 1274, 1252, 1170, 1046, 866, 839, 781, 637, 601.

PPE-^{d}NH$_3$Cl. ^{1}H NMR (D_2O/DMSO-d_6 = 1/1): 7.61 (br, s, 4H), 7.18 (s, 2H), 4.66 (s, 4H), 2.92 (br, s, 12H), 2.05 (br, 2, 12H). FT-IR (ν_{max}, KBr pellet): 3392, 3031, 2202, 2002, 1672, 1607, 1516, 1489, 1407, 1281, 1191, 1063, 1017, 966, 906, 842, 786, 721, 548.

BTD-PPE-R^2. ^{1}H NMR ($CDCl_3$, δ_{ppm}): 7.94 (br, s, 2H), 7.25 (br,s, 2H), 4.97 (s, 6H), 4.58 (s, 4H), 3.09 (s, 12H), 1.94 (s, 12H), 1.40 (s, 54H). GPC (THF, polystyrene standard): M_w = 44, 700, M_n = 12, 320, PDI = 3.60). FT-IR (ν_{max}, KBr pellet): 3350, 2977, 2939, 2679, 2490, 2203, 1693, 1570, 1458, 1392, 1366, 1279, 1252, 1171, 1041, 966, 892, 866, 780, 634, 564.

BTD-PPE-^{d}NH$_3$Cl. ^{1}H NMR (D_2O/DMSO-d_6 = 1/1): 8.01 (br, s, 2H), 7.36 (s, 2H), 4.78 (s, 4H), 2.94 (s, 12H), 2.07 (s, 12H). FT-IR (ν_{max}, KBr pellet): 3394, 3035, 2202, 2011, 1672, 1610, 1542, 1509, 1409, 1342, 1281, 1191, 1067, 1020, 965, 893, 852, 786, 632, 563, 509.

CHAPTER 6
CONCLUSIONS

In the previous chapters, the synthesis, characterization and photophysical properties (absorption, emission and fluorescence quenching) of poly(arylene ethynylene)-based conjugated polyelectrolytes (CPEs) were described. In chapter 2, *meta*-linked poly(phenylene ethynylene)s (PPEs) carrying chiral side groups were synthesized and their self-assembly behavior in solution was investigated. In chapter 3, two types of *para*-linked poly(phenylene ethynylene) carrying carboxylate side groups were synthesized and their photophysical properties were studied. Based on the results of fluorescence quenching by divalent metal ions, a highly selective and sensitive sensor was developed for pyrophosphate, a biologically important inorganic anion. In chapter 4, a group of anionic poly(*p*-phenylene ethynylene)s with 5 different chain lengths was synthesized and characterized. The relationship between photophysical properties and chain length was investigated. In chapter 5, in the first part, the band gap of poly(arylene ethynylene)s (PAEs) with linear carboxylate side chains was tuned by incorporating different heteroaromatic units; in the second part, to disrupt the interchain interaction, PAEs with dendritic anionic and cationic side groups were synthesized. The photophysical properties of these PAEs in solution were systematically studied and the application of PAEs with linear carboxylate side chains in dye-sensitized solar cells was also explored.

Helical Self-assembly

Meta-linked poly(phenylene ethynylene)s carrying ionic side groups can fold into a helical conformation in water, which is stabilized by favorable π-π stacking and hydrophobic interactions. To probe the helical folding process, *meta*-linked PPEs featuring carboxylate groups based on *L*-alanine (***w*-P2** and ***w*-P3**) were synthesized. The molecular weight of the polymer was varied by using different protecting groups for carboxylic acid functionalities and

showed a negligible effect on the polymer folding process. The presence of the chiral and optically active ionic side groups induced the formation of left-handed helix of ***w*-P2** in enantiomeric excess, as evidenced by the circular dichroism spectroscopy. The helical conformation of ***w*-P2** bears some structural similarity to double-strand DNA. Specifically, the π-π stacks in the polymer helical conformation resemble the π-stacked base pairs in DNA. And their helical structures are both stabilized by negatively charged side groups that are extended to the surrounding environment. Interactions of small dye molecules with the helical conformation of the polymer could take place via different binding modes. DNA metallointercalator, $[Ru(bpy)_2(dppz)]^{2+}$, interacts with the ***w*-P2** in a similar mode compared to DNA, leading to the "turn on" of the emission from the metal complex. Cationic cyanine dyes assemble into the "grooves" of the helical polymer and form chiral and optically active supramolecular aggregates induced by the polymer template.

Aggregation & Chain Length

Rigid rod-like *para*-linked poly(phenylene ethynylene)s carrying ionic groups exist in an aggregated state in water and a random monomeric state in MeOH. The aggregation is believed to occur through the planarization of the conjugated backbone and the formation of cofacial π-π stacking of phenylene rings. It is characterized by the appearance of red-shifted band in the absorption spectrum and also a red-shifted broad excimer-like band with less quantum efficiency in the emission spectrum. Two types of PPEs which have the same backbone structure but different substitution patterns of carboxylate groups were synthesized and studied. It was found that the carboxylate-substitution pattern has a strong effect on the aggregate formation. For the polymer that carries carboxylate per repeat unit (one phenylene ethynylene), ***w*-P4**, the aggregation is suppressed by the increased electronic repulsion in the π-π stacks. While for the

polymer that carries carboxylate for every two repeat units, ***w*-P5**, the π-π stacks are formed between carboxylated 2,5-disubstituted-1,4-phenylene and 1,4-phenylene, which minimizes the electronic repulsion. Fluorescence quenching studies of ***w*-P5** by MV^{2+} in water and in methanol in the presence of different amount of Ca^{2+} reveal that the superlinear quenching behavior in many CPE-quencher systems arises from the aggregation and/or quencher-induced aggregation of conjugated polyelectrolyte chains. A careful study of the influence of molecular weight of ***w*-P5** on the photophysical properties of the polymer indicates that high-MW polymers tend to form aggregates even in methanol. A maximum of 4-fold enhancement of the Stern-Volmer constant is observed for high-MW polymers compared to low-MW samples when mono-valent viologen quenchers were used. Whenever aggregation or quencher-induced aggregation occurs, the influence of aggregation on the quenching efficiencies overwhelms the influence of chain length. These results indicate that the best sensing response could be attained by designing CPEs that can retain high quantum efficiencies in their aggregate state, which at the same time still facilitates the exciton diffusion.

Anion Sensing

The fluorescence of ***w*-P5** is most efficiently quenched by cupric ion (Cu^{2+}) both in methanol and in 4-(2-hydroxyethyl)-1-piperaziethanesulfonic acid (HEPES) buffer solution among 9 different divalent metal ions that were examined. In methanol, all the other metal ions induced the aggregation of ***w*-P5,** evidenced from the red-shifted band in the absorption spectra and the red-shifted broad excimer-like band in the emission spectra. But for Cu^{2+}, a complete quenching of the polymer fluorescence was observed, which indicates that the quenching by Cu^{2+} follows different mechanisms. In the HEPES buffer, Cu^{2+} was the most efficient quenching metal ion. The K_{sv} value for Cu^{2+} is in the order of 10^6 M^{-1}, which is comparable to the

quenching of ***w*-P5** by MV^{2+}. Taking advantage of the efficient fluorescence quenching of ***w*-P5** by Cu^{2+}, a system consisting of ***w*-P5** /Cu^{2+} (5 μM/10 μM) was used as a fluorescence turn-on sensing platform and shows high selectivity for pyrophosphate over 12 other anions. The selectivity is believed to arise from the ability of pyrophosphate to form a complex by chelation of the diphophate moiety to Cu^{2+}. The analytical detection limit is determined to be ~ 80 nM. The current research presented the first example of CPE-based sensor for PPi with sensitivity higher than that of most PPi sensors which are based on organic dyes or small molecules.

Dye-sensitized Solar Cells

The application of poly(arylene ethynylene)s with carboxylic acid functionalities in TiO_2 based dye-sensitized solar cells was also explored. These polymers feature a backbone consisting of a carboxylated bis(alkoxy)phenylene-1,4-ethynylene unit alternating with a second arylene ethynylene moiety. For nanocrystalline TiO_2 solar cells, the IPCE (maximum ~ 50%) and power conversion efficiency increase with the reduction of band gap of the polymers except that for the most red-absorbing polymer, **BTD-PPE-CO_2H,** a lower cell performance results. This polymer exhibits a donor-accepter charge-transfer band, which is evidenced by the relatively large Stokes shift (*ca.* 150 nm) and the broad, structureless band shape of the fluorescence spectra. The poor cell performance for **BTD-PPE-CO_2H** is likely due to the strong competition of intramolecular/intermolecular charge transfer process with the desired charge injection to TiO_2. Although the overall power conversion efficiencies of the cells using these PAEs are relatively low, these results indicate that the usage of donor-acceptor interaction to reduce the band gap of conjugated polymer for applications in solar cells might have to consider its negative effect, i.e, the competition between the intramolecular/intermolecular charge transfer and the charge injection from the polymer to the electron acceptor.

APPENDIX A
HELICAL FOLDING OF *META*-LINKED POLY(PHENYLENE ETHYNYLENES)

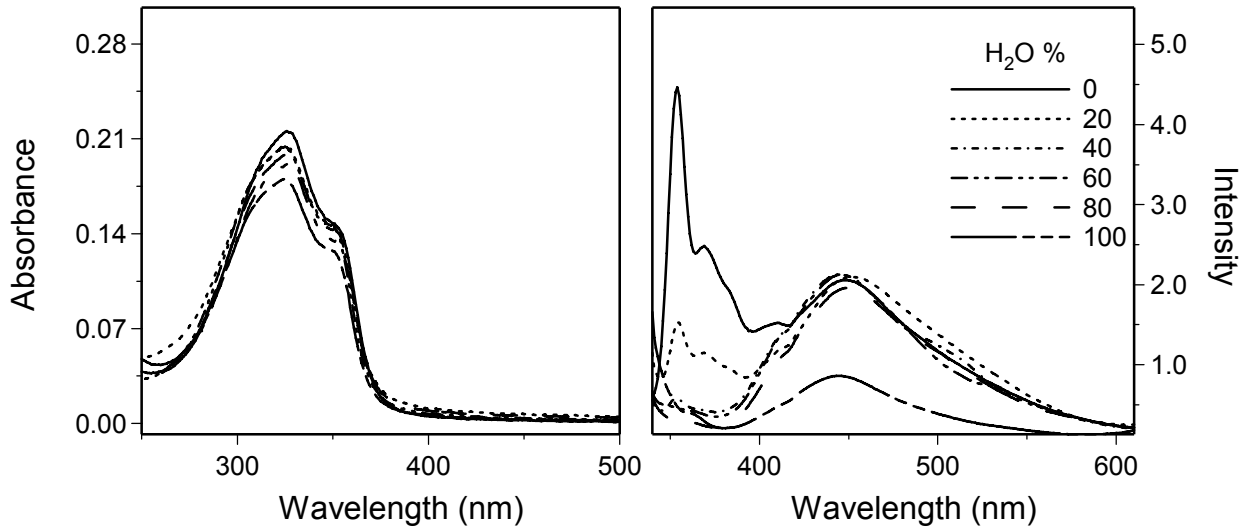

Figure A-1. Absorption (left) and fluorescence (right) of ***w*-P3** (DP = 39 kD) (c = 10 μM polymer repeat units, path length 1 cm) in methanol, water and methanol/water mixtures.

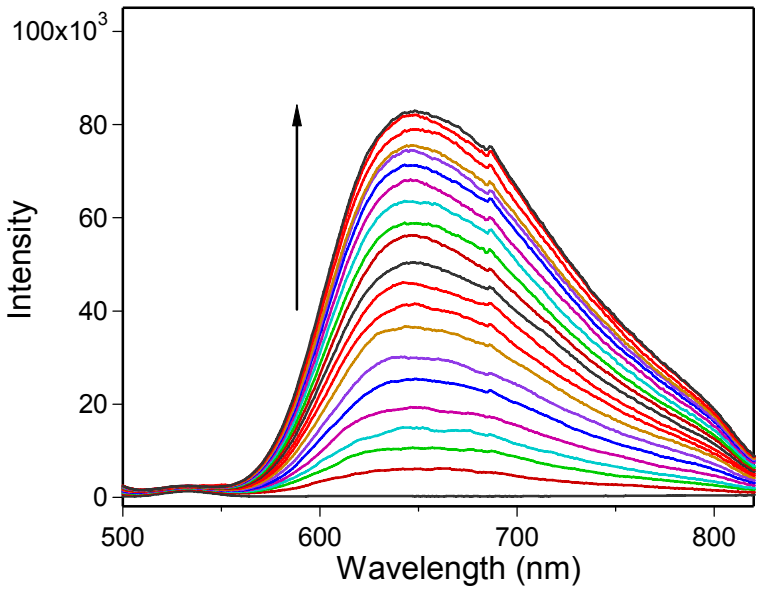

Figure A-2. Emission spectra of $[Ru(bpy)_2(dppz)]^{2+}$ in the absence (solid black line) and presence of ***w*-P3** (concentration of ***w*-P3** ranges from 0 - 120 μM polymer repeat units, excitation wavelength is 450 nm). Solutions are deoxygenated by argon bubbling.

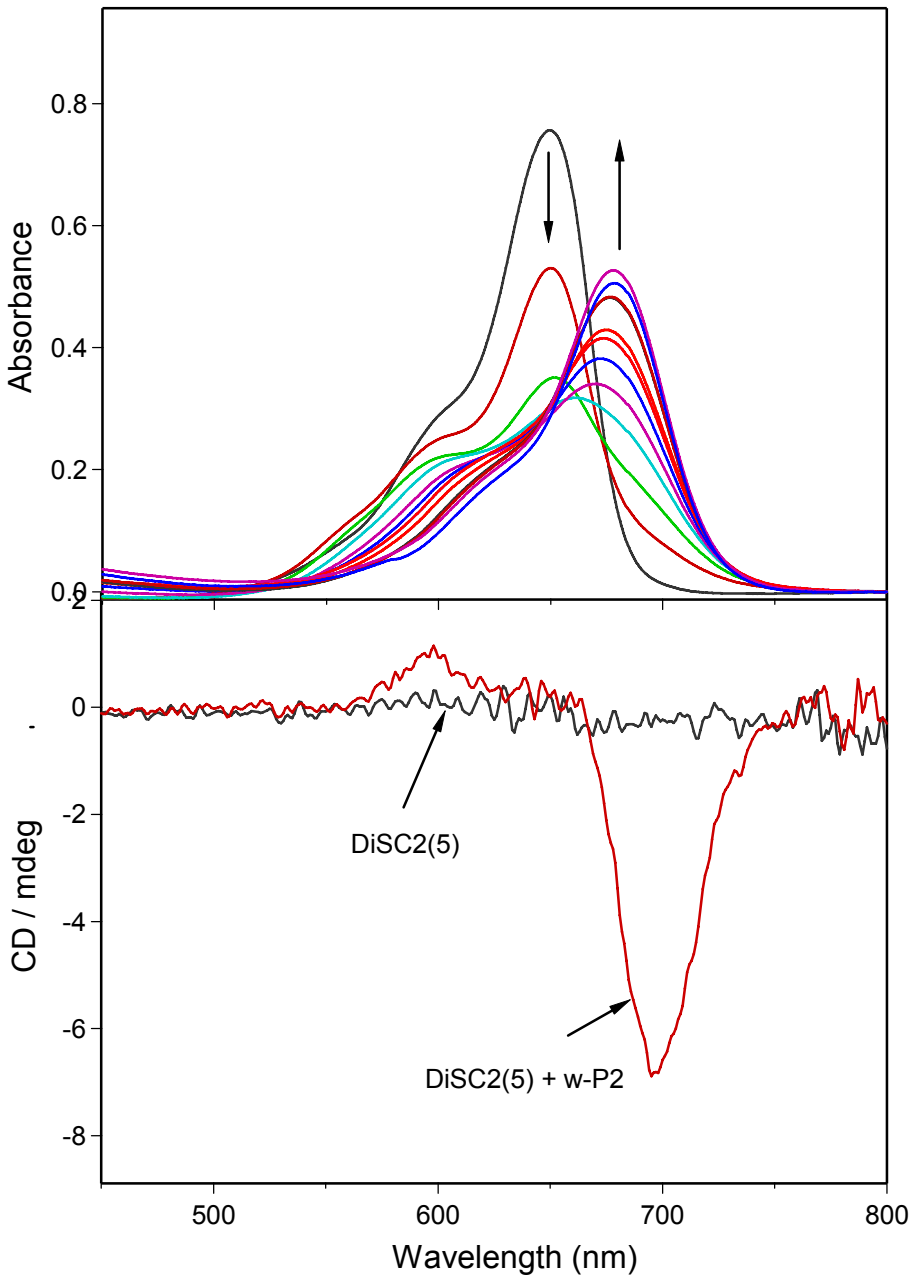

Figure A-3. TOP: UV-visible absorption of $DiSC_2(5)$ in water titrated with ***w*-P2**. [$DiSC_2(5)$] = 5.0 μM and ***w*-P2** was added in 0.5 μM aliquots. BOTTOM: Circular dichroism spectra of $DiSC_2(5)$ in water (c = 7.0 μM) and $DiSC_2(5)$ in water (c = 7.0 μM) mixed with ***w*-P2** (c = 10.0 μM).

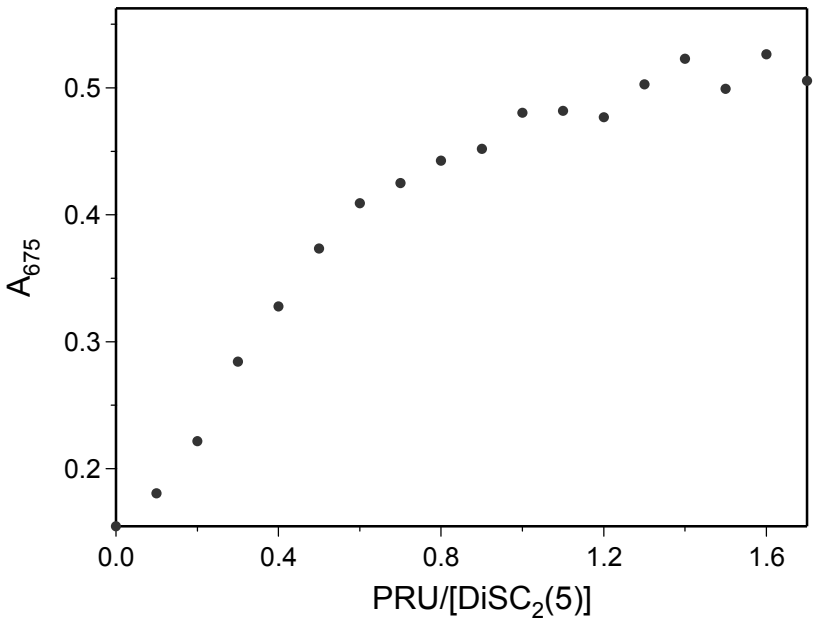

Figure A-4. Plot of absorbance at 675 nm (A_{675}) vs. [PRU]/[DiSC$_2$(5)] ratio, where [PRU] is the repeat unit concentration of ***w*-P2** added to the DiSC$_2$(5) solution in water.

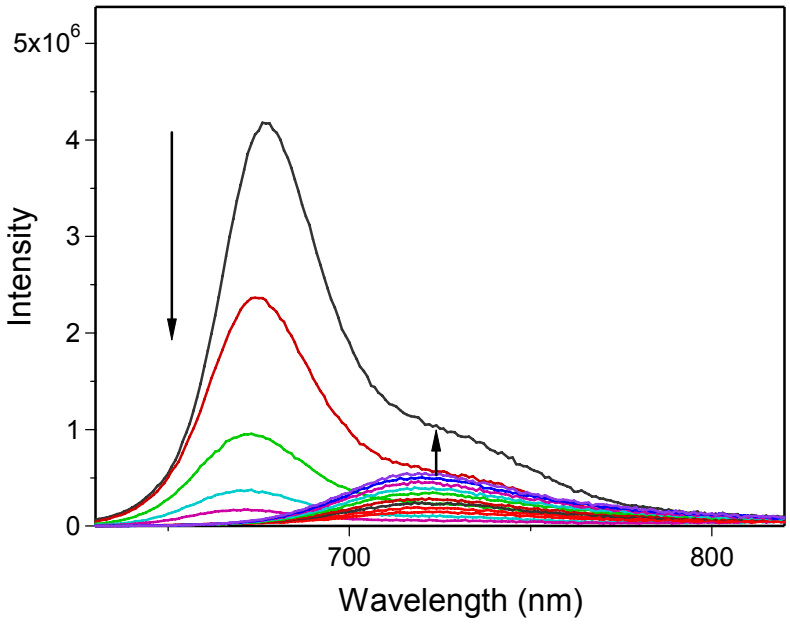

Figure A-5. Fluorescence spectra of DiSC$_2$(5) ([DiSC$_2$(5)] = 5.0 μM) in water titrated with ***w*-P2** recorded with excitation at 610 nm. ***w*-P2** was added in 0.5 μM aliquots.

APPENDIX B
NMR SPECTRA

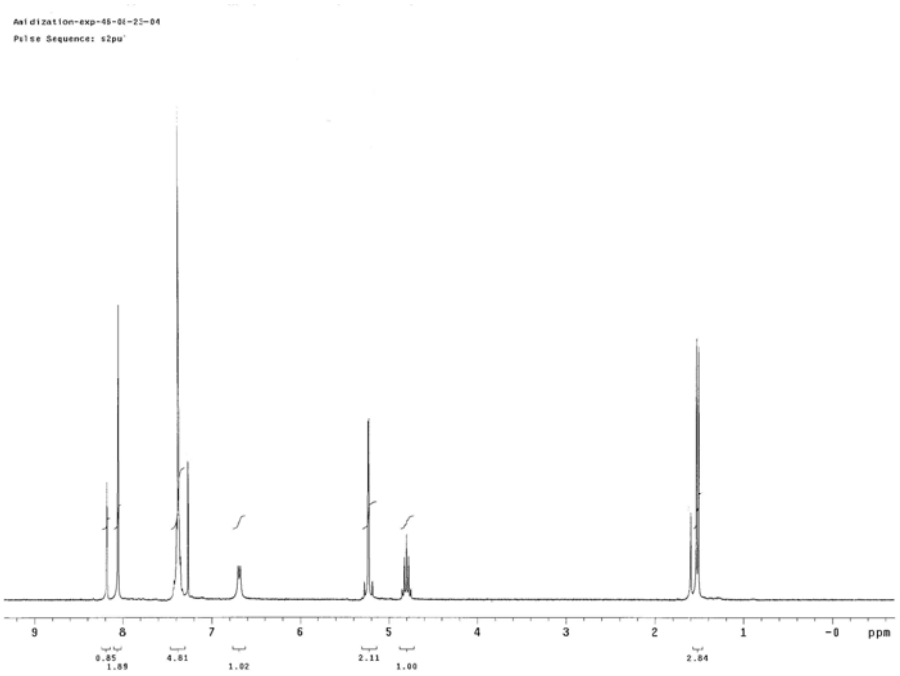

Figure B-1. ^{1}H NMR (300 M Hz, $CDCl_3$) spectrum of monomer **3** (chapter 2).

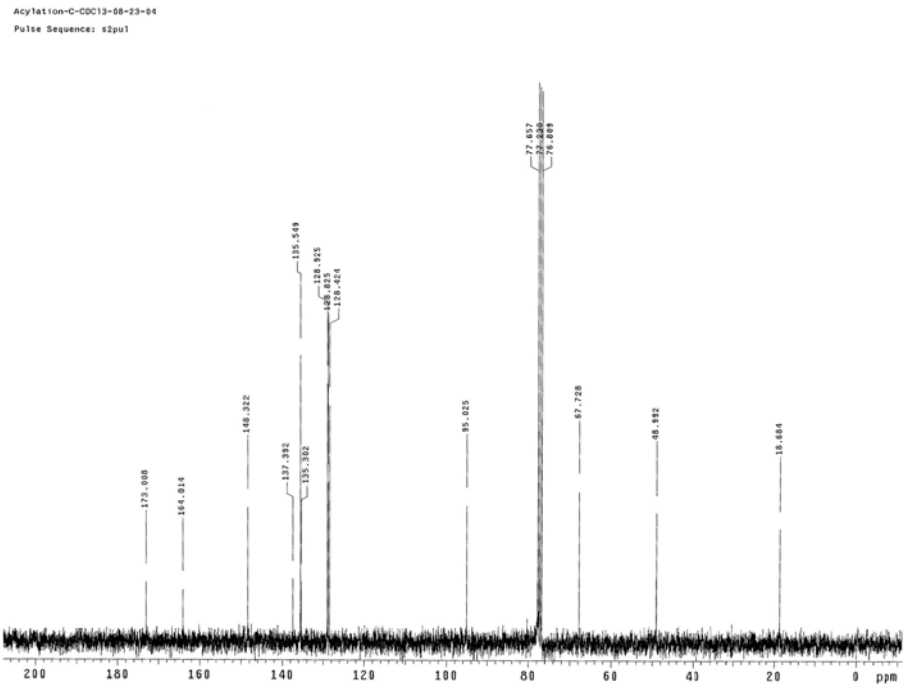

Figure B-2. ^{13}C NMR (75 MHz, $CDCl_3$) sepctrum of monomer **3** (chapter 2).

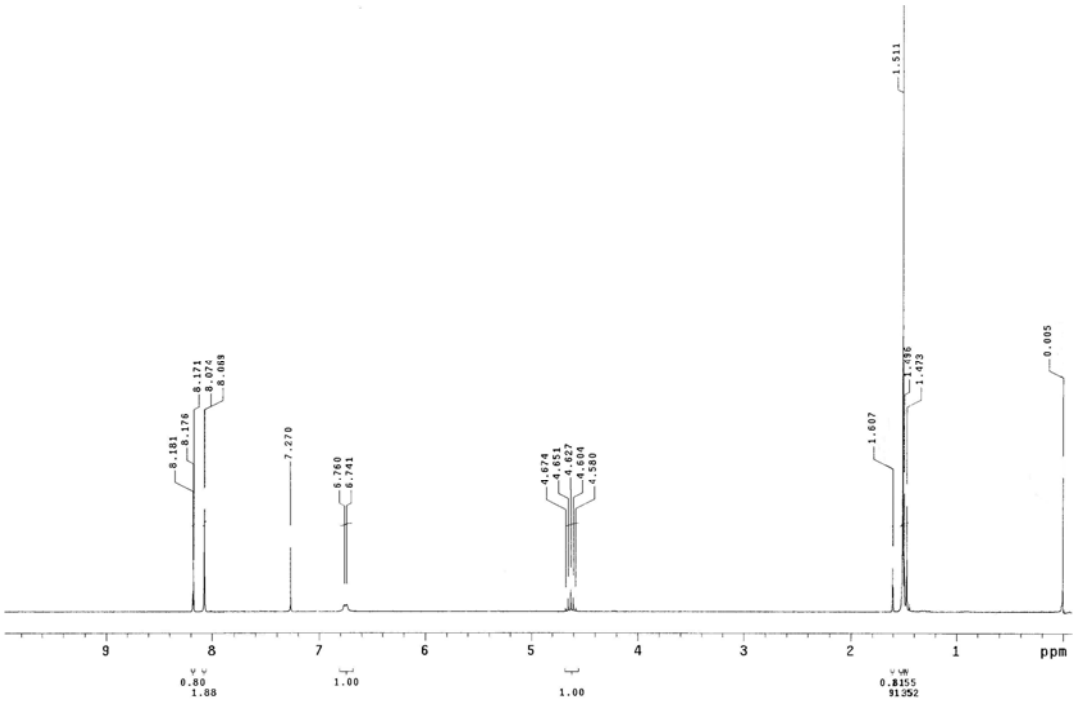

Figure B-3. ^{1}H NMR (300 M Hz, $CDCl_3$) spectrum of monomer **7** (chapter 2).

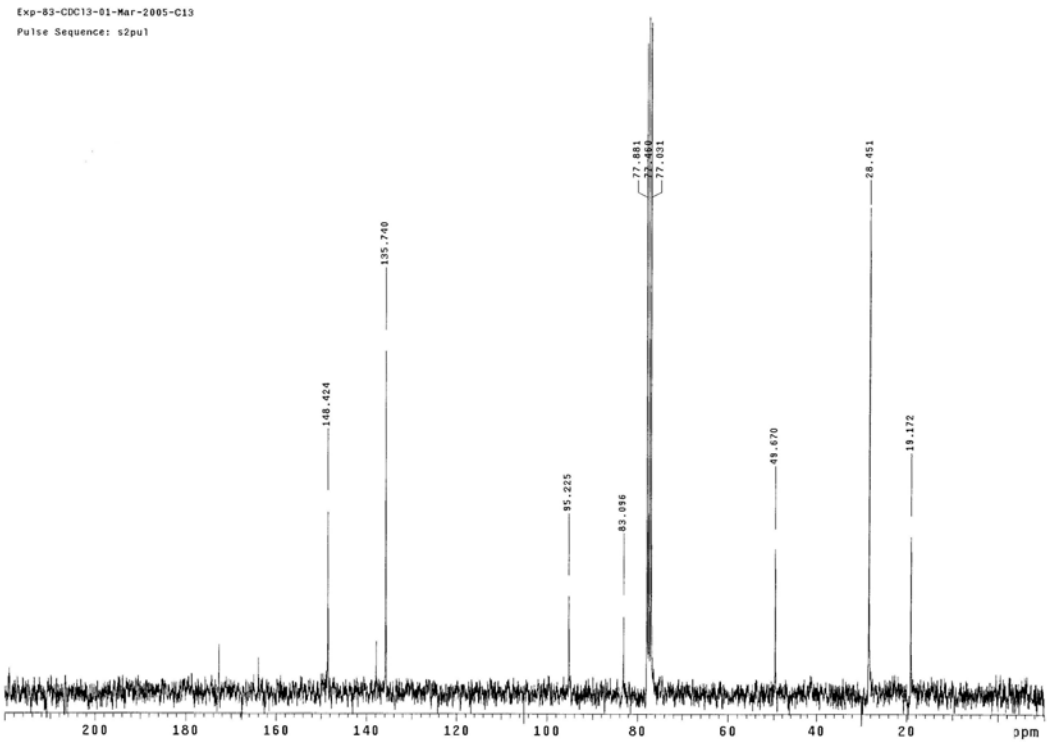

Figure B-4. ^{13}C NMR (75 MHz, $CDCl_3$) sepctrum of monomer **7** (chapter 2).

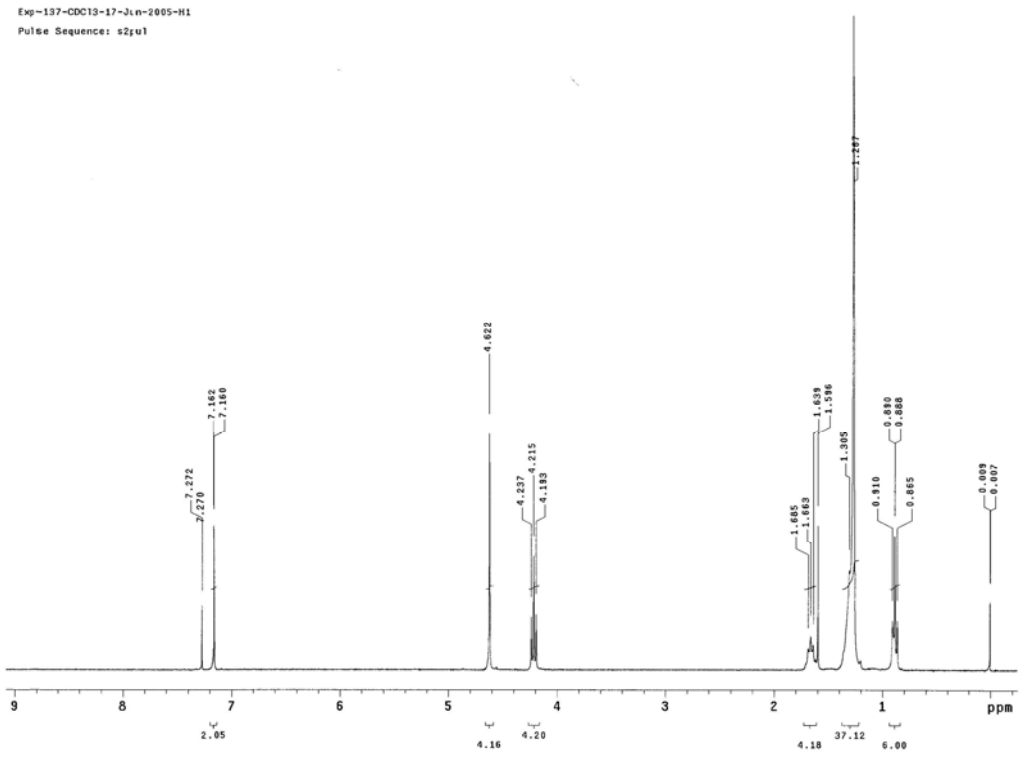

Figure B-5. ^{1}H NMR (300 M Hz, $CDCl_3$) spectrum of monomer **8** (chapter 3).

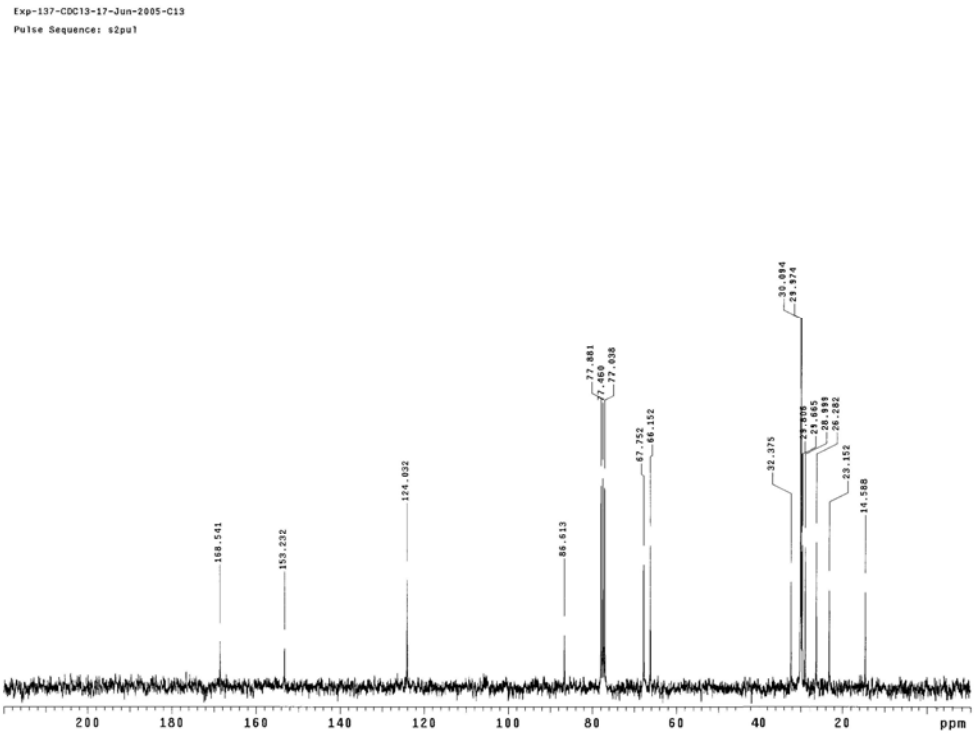

Figure B-6. ^{13}C NMR (75 MHz, $CDCl_3$) sepctrum of monomer **8** (chapter 3).

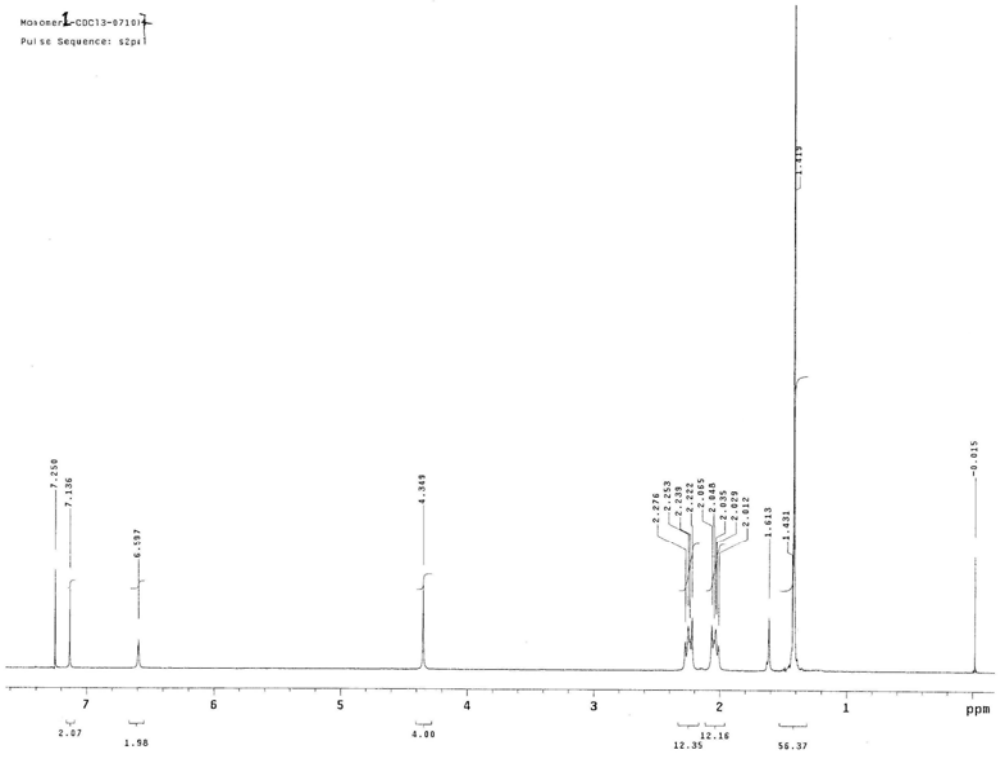

Figure B-7. ^{1}H NMR (300 M Hz, $CDCl_3$) spectrum of monomer **19** (chapter 5).

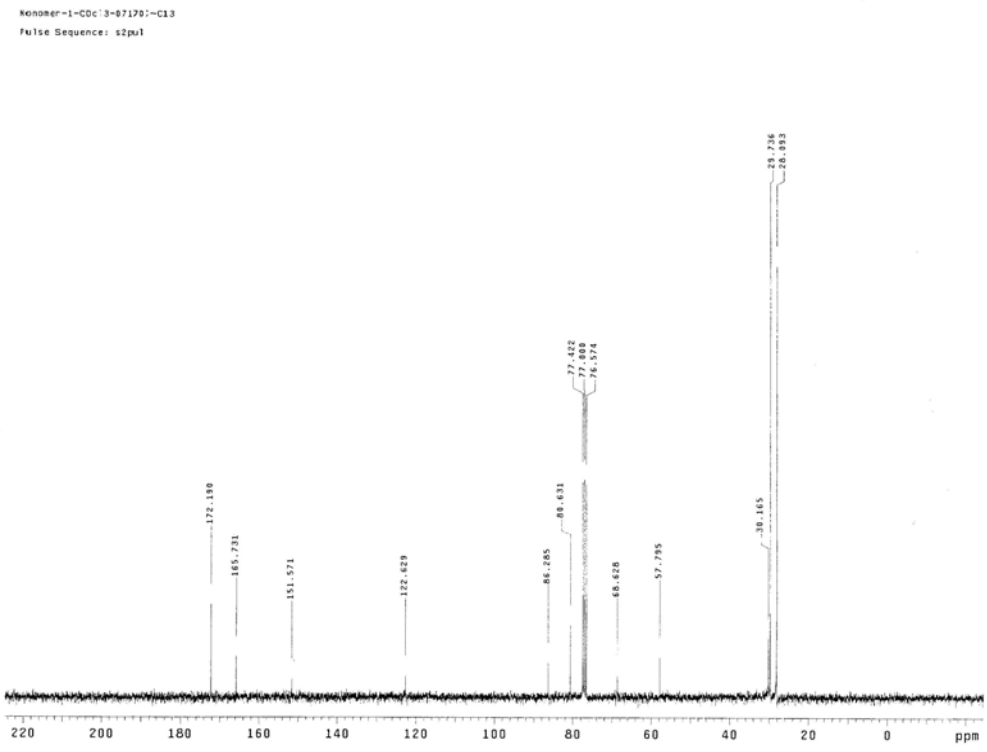

Figure B-8. ^{13}C NMR (75 MHz, $CDCl_3$) sepctrum of monomer **19** (chapter 5).

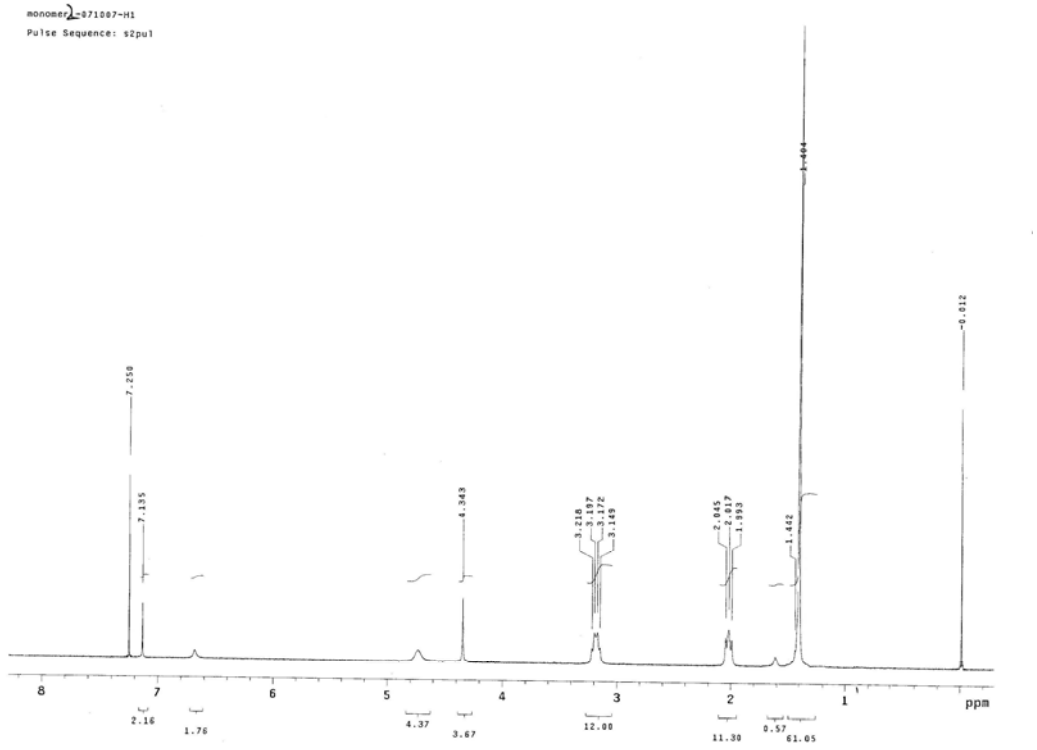

Figure B-9. ^{1}H NMR (300 M Hz, $CDCl_3$) spectrum of monomer **20** (chapter 5).

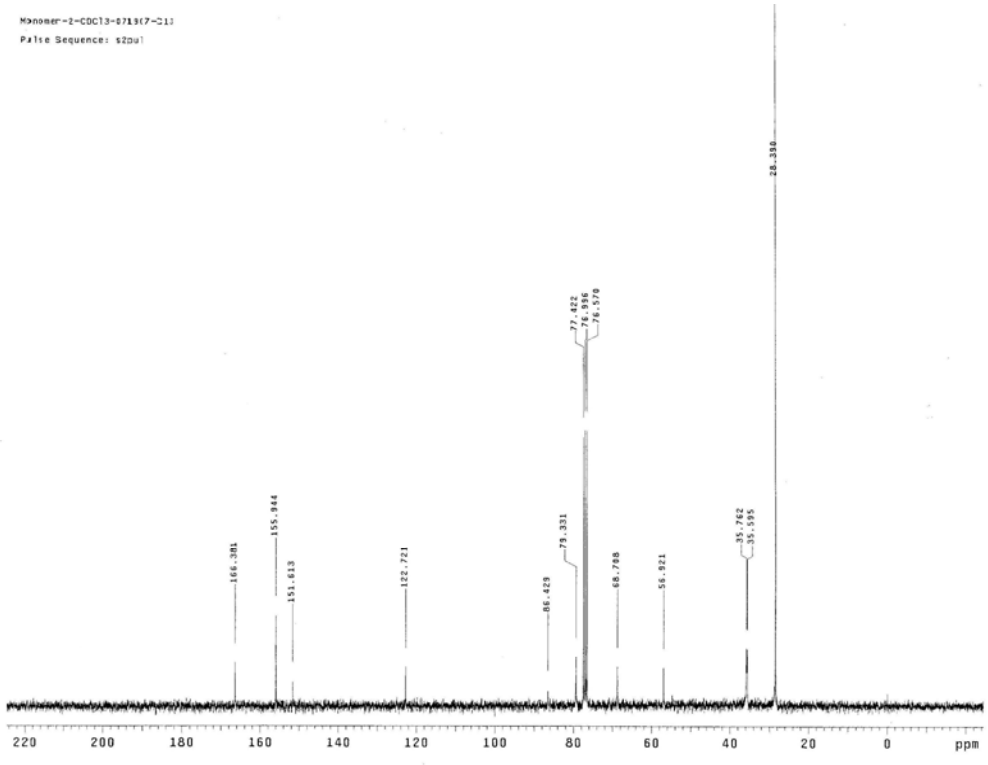

Figure B-10. ^{13}C NMR (75 MHz, $CDCl_3$) sepctrum of monomer **20** (chapter 5).

LIST OF REFERENCES

(1) Hall, N. *Chem. Commun.* **2003**, 1-4.

(2) Shirakawa, H.; Louis, E. J.; Macdiarmid, A. G.; Chiang, C. K.; Heeger, A. J. *J. Chem. Soc., Chem. Commun.* **1977**, 578-580.

(3) Shirakawa, H. *Angew. Chem., Int. Ed.* **2001**, *40*, 2575-2580.

(4) Heeger, A. J. *Angew. Chem., Int. Ed.* **2001**, *40*, 2591-2611.

(5) Patil, A. O.; Heeger, A. J.; Wudl, F. *Chem. Rev.* **1988**, *88*, 183-200.

(6) Grimsdale, A. C.; Mullen, K. *Emiss. Mater., Nanomater.* **2006**, *199*, 1-82.

(7) Perepichka, I. F.; Perepichka, D. F.; Meng, H.; Wudl, F. *Adv. Mater.* **2005**, *17*, 2281-2305.

(8) MacDiarmid, A. G. *Angew. Chem., Int. Ed.* **2001**, *40*, 2581-2590.

(9) Kraft, A.; Grimsdale, A. C.; Holmes, A. B. *Angew. Chem., Int. Ed.* **1998**, *37*, 402-428.

(10) Bunz, U. H. F. *Chem. Rev.* **2000**, *100*, 1605-1644.

(11) Scherf, U.; List, E. J. W. *Adv. Mater.* **2002**, *14*, 477-487.

(12) Burroughes, J. H.; Bradley, D. D. C.; Brown, A. R.; Marks, R. N.; Mackay, K.; Friend, R. H.; Burns, P. L.; Holmes, A. B. *Nature* **1990**, *347*, 539-541.

(13) Heeger, A. J. *Solid State Commun.* **1998**, *107*, 673-679.

(14) Hide, F.; DiazGarcia, M. A.; Schwartz, B. J.; Heeger, A. J. *Acc. Chem. Res.* **1997**, *30*, 430-436.

(15) Gunes, S.; Neugebauer, H.; Sariciftci, N. S. *Chem. Rev.* **2007**, *107*, 1324-1338.

(16) Sirringhaus, H. *Adv. Mater.* **2005**, *17*, 2411-2425.

(17) McQuade, D. T.; Pullen, A. E.; Swager, T. M. *Chem. Rev.* **2000**, *100*, 2537-2574.

(18) Thomas, S. W.; Joly, G. D.; Swager, T. M. *Chem. Rev.* **2007**, *107*, 1339-1386.

(19) Yang, J. S.; Swager, T. M. *J. Am. Chem. Soc.* **1998**, *120*, 11864-11873.

(20) Bumm, L. A.; Arnold, J. J.; Cygan, M. T.; Dunbar, T. D.; Burgin, T. P.; Jones, L.; Allara, D. L.; Tour, J. M.; Weiss, P. S. *Science* **1996**, *271*, 1705-1707.

(21) Weder, C.; Sarwa, C.; Montali, A.; Bastiaansen, G.; Smith, P. *Science* **1998**, *279*, 835-837.

(22) Montali, A.; Bastiaansen, G.; Smith, P.; Weder, C. *Nature* **1998**, *392*, 261-264.

(23) Sonogashira, K.; Tohda, Y.; Hagihara, N. *Tetrahedron Lett.* **1975**, 4467-4470.

(24) Chinchilla, R.; Najera, C. *Chem. Rev.* **2007**, *107*, 874-922.

(25) Dieck, H. A.; Heck, F. R. *J. Organomet. Chem.* **1975**, *93*, 259-263.

(26) Cassar, L. *J. Organomet. Chem.* **1975**, *93*, 253-257.

(27) Zhou, Q.; Swager, T. M. *J. Am. Chem. Soc.* **1995**, *117*, 12593-12602.

(28) Bunz, U. H. F. *Acc. Chem. Res.* **2001**, *34*, 998-1010.

(29) Goodson, F. E.; Wallow, T. I.; Novak, B. M. *J. Am. Chem. Soc.* **1997**, *119*, 12441-12453.

(30) Furstner, A.; Davies, P. W. *Chem. Commun.* **2005**, 2307-2320.

(31) Mortreux, A.; Blanchar.M *J. Chem. Soc., Chem. Commun.* **1974**, 786-787.

(32) Schrock, R. R. *Acc. Chem. Res.* **1986**, *19*, 342-348.

(33) Weiss, K.; Michel, A.; Auth, E. M.; Bunz, U. H. F.; Mangel, T.; Mullen, K. *Angew. Chem., Int. Ed.* **1997**, *36*, 506-509.

(34) Brizius, G.; Kroth, S.; Bunz, U. H. F. *Macromolecules* **2002**, *35*, 5317-5319.

(35) Zhang, W.; Kraft, S.; Moore, J. S. *Chem. Commun.* **2003**, 832-833.

(36) Zhang, W.; Kraft, S.; Moore, J. S. *J. Am. Chem. Soc.* **2004**, *126*, 329-335.

(37) Zhang, W.; Moore, J. S. *Macromolecules* **2004**, *37*, 3973-3975.

(38) Zhang, W.; Moore, J. S. *Adv. Synth. Catal.* **2007**, *349*, 93-120.

(39) Mori, A.; Kondo, T.; Kato, T.; Nishihara, Y. *Chem. Lett.* **2001**, 286-287.

(40) Wang, Y. F.; Watson, M. D. *J. Am. Chem. Soc.* **2006**, *128*, 2536-2537.

(41) Woody, K. B.; Bullock, J. E.; Parkin, S. R.; Watson, M. D. *Macromolecules* **2007**, *40*, 4470-4473.

(42) Moroni, M.; Lemoigne, J.; Luzzati, S. *Macromolecules* **1994**, *27*, 562-571.

(43) Tour, J. M. *Chem. Rev.* **1996**, *96*, 537-553.

(44) Cravino, A.; Zerza, G.; Neugebauer, H.; Maggini, M.; Bucella, S.; Menna, E.; Svensson, M.; Andersson, M. R.; Brabec, C. J.; Sariciftci, N. S. *J. Phys. Chem. B* **2002**, *106*, 70-76.

(45) Cotts, P. M.; Swager, T. M.; Zhou, Q. *Macromolecules* **1996**, *29*, 7323-7328.

(46) Ricks, H. L.; Choudry, U. H.; Marshall, A. R.; Bunz, U. H. F. *Macromolecules* **2003**, *36*, 1424-1425.

(47) Teraoka, I. *Polymer Solutions: An Introduction to Physical Properties*; John Wiley & Sons, Inc.: New York, 2002.

(48) Samori, P.; Francke, V.; Mullen, K.; Rabe, J. P. *Chem.- Eur. J.* **1999**, *5*, 2312-2317.

(49) Nelson, J. C.; Saven, J. G.; Moore, J. S.; Wolynes, P. G. *Science* **1997**, *277*, 1793-1796.

(50) Prince, R. B.; Saven, J. G.; Wolynes, P. G.; Moore, J. S. *J. Am. Chem. Soc.* **1999**, *121*, 3114-3121.

(51) Blatchly, R. A.; Tew, G. N. *J. Org. Chem.* **2003**, *68*, 8780-8785.

(52) Jones, T. V.; Slutsky, M. M.; Laos, R.; de Greef, T. F. A.; Tew, G. N. *J. Am. Chem. Soc.* **2005**, *127*, 17235-17240.

(53) Pinto, M. R.; Schanze, K. S. *Synthesis-Stuttgart* **2002**, 1293-1309.

(54) Lakowicz, J. R. *Principles of Fluorescence Spectroscopy*; 2nd ed.; Kluwer Academic/Plenum Publishers, 1999.

(55) Zhou, Q.; Swager, T. M. *J. Am. Chem. Soc.* **1995**, *117*, 7017-7018.

(56) Swager, T. M. *Acc. Chem. Res.* **1998**, *31*, 201-207.

(57) Chen, L. H.; McBranch, D. W.; Wang, H. L.; Helgeson, R.; Wudl, F.; Whitten, D. G. *Proc. Natl. Acad. Sci. U. S. A.* **1999**, *96*, 12287-12292.

(58) Achyuthan, K. E.; Bergstedt, T. S.; Chen, L.; Jones, R. M.; Kumaraswamy, S.; Kushon, S. A.; Ley, K. D.; Lu, L.; McBranch, D.; Mukundan, H.; Rininsland, F.; Shi, X.; Xia, W.; Whitten, D. G. *J. Mater. Chem.* **2005**, *15*, 2648-2656.

(59) Ho, H. A.; Bera-Aberem, M.; Leclerc, M. *Chem.- Eur. J.* **2005**, *11*, 1718-1724.

(60) Gaylord, B. S.; Wang, S. J.; Heeger, A. J.; Bazan, G. C. *J. Am. Chem. Soc.* **2001**, *123*, 6417-6418.

(61) Wang, D. L.; Wang, J.; Moses, D.; Bazan, G. C.; Heeger, A. J. *Langmuir* **2001**, *17*, 1262-1266.

(62) Fan, C. H.; Hirasa, T.; Plaxco, K. W.; Heeger, A. J. *Langmuir* **2003**, *19*, 3554-3556.

(63) Jiang, H.; Zhao, X. Y.; Schanze, K. S. *Langmuir* **2007**, *23*, 9481-9486.

(64) Pinto, M. R.; Kristal, B. M.; Schanze, K. S. *Langmuir* **2003**, *19*, 6523-6533.

(65) Fan, Q. L.; Zhou, Y.; Lu, X. M.; Hou, X. Y.; Huang, W. *Macromolecules* **2005**, *38*, 2927-2936.

(66) Wang, J.; Wang, D. L.; Miller, E. K.; Moses, D.; Bazan, G. C.; Heeger, A. J. *Macromolecules* **2000**, *33*, 5153-5158.

(67) Chen, L. H.; McBranch, D.; Wang, R.; Whitten, D. *Chem. Phys. Lett.* **2000**, *330*, 27-33.

(68) Chen, L. H.; Xu, S.; McBranch, D.; Whitten, D. *J. Am. Chem. Soc.* **2000**, *122*, 9302-9303.

(69) Dalvi-Malhotra, J.; Chen, L. H. *J. Phys. Chem. B* **2005**, *109*, 3873-3878.

(70) Abe, S.; Chen, L. H. *J. Polym. Sci. Pol. Phys.* **2003**, *41*, 1676-1679.

(71) Tan, C. Y.; Pinto, M. R.; Schanze, K. S. *Chem. Commun.* **2002**, 446-447.

(72) Muller, J. G.; Atas, E.; Tan, C.; Schanze, K. S.; Kleiman, V. D. *J. Am. Chem. Soc.* **2006**, *128*, 4007-4016.

(73) Halkyard, C. E.; Rampey, M. E.; Kloppenburg, L.; Studer-Martinez, S. L.; Bunz, U. H. F. *Macromolecules* **1998**, *31*, 8655-8659.

(74) Birks, J. B. *Photophysics of Aromatic Molecules*; Wiley-Inter-Science: London, 1970.

(75) Wang, S.; Bazan, G. C. *Chem. Commun.* **2004**, 2508-2509.

(76) Liu, B.; Bazan, G. C. *J. Am. Chem. Soc.* **2004**, *126*, 1942-1943.

(77) Dore, K.; Dubus, S.; Ho, H. A.; Levesque, I.; Brunette, M.; Corbeil, G.; Boissinot, M.; Boivin, G.; Bergeron, M. G.; Boudreau, D.; Leclerc, M. *J. Am. Chem. Soc.* **2004**, *126*, 4240-4244.

(78) Liu, B.; Bazan, G. C. *Chem. Mater.* **2004**, *16*, 4467-4476.

(79) Liu, B.; Bazan, G. C. *Proc. Natl. Acad. Sci. U. S. A.* **2005**, *102*, 589-593.

(80) Leclerc, M. *Adv. Mater.* **1999**, *11*, 1491-1498.

(81) McCullough, R. D.; Ewbank, P. C.; Loewe, R. S. *J. Am. Chem. Soc.* **1997**, *119*, 633-634.

(82) Ho, H. A.; Boissinot, M.; Bergeron, M. G.; Corbeil, G.; Dore, K.; Boudreau, D.; Leclerc, M. *Angew. Chem., Int. Ed.* **2002**, *41*, 1548-1551.

(83) Karlsson, K. F.; Asberg, P.; Nilsson, K. P. R.; Inganas, O. *Chem. Mater.* **2005**, *17*, 4204-4211.

(84) Herland, A.; Nilsson, K. P. R.; Olsson, J. D. M.; Hammarstrom, P.; Konradsson, P.; Inganas, O. *J. Am. Chem. Soc.* **2005**, *127*, 2317-2323.

(85) Gaylord, B. S.; Heeger, A. J.; Bazan, G. C. *Proc. Natl. Acad. Sci. U. S. A.* **2002**, *99*, 10954-10957.

(86) O'Regan, B.; Gratzel, M. *Nature* **1991**, *353*, 737-740.

(87) Hagfeldt, A.; Gratzel, M. *Acc. Chem. Res.* **2000**, *33*, 269-277.

(88) Gratzel, M. *Inorg. Chem.* **2005**, *44*, 6841-6851.

(89) Koumura, N.; Wang, Z. S.; Mori, S.; Miyashita, M.; Suzuki, E.; Hara, K. *J. Am. Chem. Soc.* **2006**, *128*, 14256-14257.

(90) Coakley, K. M.; McGehee, M. D. *Chem. Mater.* **2004**, *16*, 4533-4542.

(91) Kim, Y.-G.; Walker, J.; Samuleson, L. A.; Kumer, J. *Nano Lett.* **2003**, *3*, 523-525.

(92) Yanagida, S.; Senadeera, G. K. R.; Nakamura, K.; Kitamura, T.; Wada, Y. *J. Photochem. Photobio., A* **2004**, *166*, 75-80.

(93) Mwaura, J. K.; Zhao, X.; Jiang, H.; Schanze, K. S.; Reynolds, J. R. *Chem. Mater.* **2006**, *18*, 6109-6111.

(94) Mio, M. J.; Prince, R. B.; Moore, J. S.; Kuebel, C.; Martin, D. C. *J. Am. Chem. Soc.* **2000**, *122*, 6134-6135.

(95) Arnt, L.; Tew, G. N. *J. Am. Chem. Soc.* **2002**, *124*, 7664-7665.

(96) Tan, C. Y.; Pinto, M. R.; Kose, M. E.; Ghiviriga, I.; Schanze, K. S. *Adv. Mater.* **2004**, *16*, 1208-1211.

(97) Arnt, L.; Tew, G. N. *Langmuir* **2003**, *19*, 2404-2408.

(98) Arnt, L.; Tew, G. N. *Macromolecules* **2004**, *37*, 1283-1288.

(99) Breitenkamp, R. B.; Arnt, L.; Tew, G. N. *Polym. Adv. Technol.* **2005**, *16*, 189-194.

(100) Kim, T.; Arnt, L.; Atkins, E.; Tew, G. N. *Chem.- Eur. J.* **2006**, *12*, 2423-2427.

(101) Prince, R. B.; Brunsveld, L.; Meijer, E. W.; Moore, J. S. *Angew. Chem., Int. Ed.* **2000**, *39*, 228-230.

(102) Gin, M. S.; Yokozawa, T.; Prince, R. B.; Moore, J. S. *J. Am. Chem. Soc.* **1999**, *121*, 2643-2644.

(103) Prince, R. B.; Barnes, S. A.; Moore, J. S. *J. Am. Chem. Soc.* **2000**, *122*, 2758-2762.

(104) Endres, A.; Maas, G. *Tetrahedron* **2002**, *58*, 3999-4005.

(105) Moore, J. S.; Stupp, S. I. *Macromolecules* **1990**, *23*, 65-70.

(106) Takahashi, S.; Kuroyama, Y.; Sonogashira, K.; Hagihara, N. *Synthesis-Stuttgart* **1980**, 627-630.

(107) Berova, N.; Nakanishi, K.; Woody, R. *Circular Dichroism: Principles and Applications*; 2nd ed.; Wiley-VCH: New York, 2000.

(108) Zahn, S.; Swager, T. M. *Angew. Chem., Int. Ed.* **2002**, *41*, 4225-4230.

(109) Erkkila, K. E.; Odom, D. T.; Barton, J. K. *Chem. Rev.* **1999**, *99*, 2777-2795.

(110) Cuniberti, C.; Guenza, M. *Biophys. Chem.* **1990**, *38*, 11-22.

(111) Powers, J. C.; Peticola.Wl *J. Phys. Chem.* **1967**, *71*, 3191-3195.

(112) Kumar, C. V.; Asuncion, E. H. *J. Am. Chem. Soc.* **1993**, *115*, 8547-8553.

(113) Becker, H. C.; Norden, B. *J. Am. Chem. Soc.* **2000**, *122*, 8344-8349.

(114) Brun, A. M.; Harriman, A. *J. Am. Chem. Soc.* **1991**, *113*, 8153-8159.

(115) Jenkins, Y.; Friedman, A. E.; Turro, N. J.; Barton, J. K. *Biochemistry* **1992**, *31*, 10809-10816.

(116) Holmlin, R. E.; Yao, J. A.; Barton, J. K. *Inorg. Chem.* **1999**, *38*, 174-189.

(117) Pyle, A. M.; Chiang, M. Y.; Barton, J. K. *Inorg. Chem.* **1990**, *29*, 4487-4495.

(118) Kirschbaum, T.; Briehn, C. A.; Bauerle, P. *J. Chem. Soc., Perkin Trans. 1* **2000**, *8*, 1211-1216.

(119) Friedman, A. E.; Chambron, J. C.; Sauvage, J. P.; Turro, N. J.; Barton, J. K. *J. Am. Chem. Soc.* **1990**, *112*, 4960-4962.

(120) Dervan, P. B.; Burli, R. W. *Curr. Opin. Chem. Biol.* **1999**, *3*, 688-693.

(121) Pelton, J. G.; Wemmer, D. E. *Proc. Natl. Acad. Sci. U. S. A.* **1989**, *86*, 5723-5727.

(122) Seifert, J. L.; Connor, R. E.; Kushon, S. A.; Wang, M.; Armitage, B. A. *J. Am. Chem. Soc.* **1999**, *121*, 2987-2995.

(123) Wang, M. M.; Silva, G. L.; Armitage, B. A. *J. Am. Chem. Soc.* **2000**, *122*, 9977-9986.

(124) Garoff, R. A.; Litzinger, E. A.; Connor, R. E.; Fishman, I.; Armitage, B. A. *Langmuir* **2002**, *18*, 6330-6337.

(125) Hannah, K. C.; Armitage, B. A. *Acc. Chem. Res.* **2004**, *37*, 845-853.

(126) Tan, C. Y.; Alas, E.; Muller, J. G.; Pinto, M. R.; Kleiman, V. D.; Schanze, K. S. *J. Am. Chem. Soc.* **2004**, *126*, 13685-13694.

(127) Sullivan, B. P.; Salmon, D. J.; Meyer, T. J. *Inorg. Chem.* **1978**, *17*, 3334-3341.

(128) Amouyal, E.; Homsi, A.; Chambron, J. C.; Sauvage, J. P. *J. Chem. Soc., Dalton Trans.* **1990**, 1841-1845.

(129) Schanze, K. S.; Zhao, X. Y. In *Handbook of Conducting Polymers*; Skotheim, T. A., Reynolds, J. R., Eds.; CRC Press: Boca Raton, 2007; Vol. 3, p 1-29.

(130) Greene, T. W.; Wuts, P. G. M. *Protective groups in Organic Synthesis*; 3rd ed.; Wiley: New York, 1999.

(131) Ewbank, P. C.; Loewe, R. S.; Zhai, L.; Reddinger, J.; Sauve, G.; McCullough, R. D. *Tetrahedron* **2004**, *60*, 11269-11275.

(132) Rininsland, F.; Xia, W. S.; Wittenburg, S.; Shi, X. B.; Stankewicz, C.; Achyuthan, K.; McBranch, D.; Whitten, D. *Proc. Natl. Acad. Sci. U. S. A.* **2004**, *101*, 15295-15300.

(133) Odian, G. G. *Principles of Polymerization*; 4th ed.; John Wiley & Sons, Inc.: Hoboken, N.J., 2004.

(134) Haskins-Glusac, K.; Pinto, M. R.; Tan, C. Y.; Schanze, K. S. *J. Am. Chem. Soc.* **2004**, *126*, 14964-14971.

(135) Zhao, X. Y.; Pinto, M. R.; Hardison, L. M.; Mwaura, J.; Muller, J.; Jiang, H.; Witker, D.; Kleiman, V. D.; Reynolds, J. R.; Schanze, K. S. *Macromolecules* **2006**, *39*, 6355-6366.

(136) Mohan, J. *Organic spectroscopy: Principles and Applications*; 1st ed.; CRC Press: New York, 2000.

(137) Evans, D. A. In *http://daecr1.harvard.edu/pdf/evans_pKa_table.pdf*.

(138) McQuade, D. T.; Hegedus, A. H.; Swager, T. M. *J. Am. Chem. Soc.* **2000**, *122*, 12389-12390.

(139) Levitsky, I. A.; Kim, J.; Swager, T. M. *Macromolecules* **2001**, *34*, 2315-2319.

(140) Kim, J.; Swager, T. M. *Nature* **2001**, *411*, 1030-1034.

(141) Kim, J.; Levitsky, I. A.; McQuade, D. T.; Swager, T. M. *J. Am. Chem. Soc.* **2002**, *124*, 7710-7718.

(142) Kim, I. B.; Dunkhorst, A.; Gilbert, J.; Bunz, U. H. F. *Macromolecules* **2005**, *38*, 4560-4562.

(143) Kim, I. B.; Bunz, U. H. F. *J. Am. Chem. Soc.* **2006**, *128*, 2818-2819.

(144) Kim, I. B.; Phillips, R.; Bunz, U. H. F. *Macromolecules* **2007**, *40*, 814-817.

(145) Fan, L. J.; Jones, W. E. *J. Am. Chem. Soc.* **2006**, *128*, 6784-6785.

(146) Fan, C. H.; Wang, S.; Hong, J. W.; Bazan, G. C.; Plaxco, K. W.; Heeger, A. J. *Proc. Natl. Acad. Sci. U. S. A.* **2003**, *100*, 6297-6301.

(147) Nelson, D. L.; Cox, M. M. *Lehninger Principle of Biochemistry*; 3rd ed.; Worth Publishers: New York, NY, 2000.

(148) Lee, D. H.; Kim, S. Y.; Hong, J. I. *Angew. Chem., Int. Ed.* **2004**, *43*, 4777-4780.

(149) Vance, D. H.; Czarnik, A. W. *J. Am. Chem. Soc.* **1994**, *116*, 9397-9398.

(150) Lee, H. N.; Swamy, K. M. K.; Kim, S. K.; Kwon, J. Y.; Kim, Y.; Kim, S. J.; Yoon, Y. J.; Yoon, J. *Org. Lett.* **2007**, *9*, 243-246.

(151) Lee, H. N.; Xu, Z.; Kim, S. K.; Swamy, K. M. K.; Kim, Y.; Kim, S. J.; Yoon, J. *J. Am. Chem. Soc.* **2007**, *129*, 3828-3829.

(152) Jang, Y. J.; Jun, E. J.; Lee, Y. J.; Kim, Y. S.; Kim, J. S.; Yoon, J. *J. Org. Chem.* **2005**, *70*, 9603-9606.

(153) Fabbrizzi, L.; Marcotte, N.; Stomeo, F.; Taglietti, A. *Angew. Chem., Int. Ed.* **2002**, *41*, 3811-3814.

(154) Hanshaw, R. G.; Hilkert, S. M.; Hua, J.; Smith, B. D. *Tetrahedron Lett.* **2004**, *45*, 8721-8724.

(155) McDonough, M. J.; Reynolds, A. J.; Lee, W. Y. G.; Jolliffe, K. A. *Chem. Commun.* **2006**, 2971-2973.

(156) Ambade, A. V.; Sandanaraj, B. S.; Klaikherd, A.; Thayumanavan, S. *Polym. Int.* **2007**, *56*, 474-481.

(157) Aldakov, D.; Palacios, M. A.; Anzenbacher, P. *Chem. Mater.* **2005**, *17*, 5238-5241.

(158) Valcarcel, M. *Principles of Analytical Chemistry: A textbook*; Springer-Verlag: New York, 2000.

(159) Lee, D. H.; Im, J. H.; Son, S. U.; Chung, Y. K.; Hong, J. I. *J. Am. Chem. Soc.* **2003**, *125*, 7752-7753.

(160) Martin, R. E.; Diederich, F. *Angew. Chem., Int. Ed.* **1999**, *38*, 1350-1377.

(161) Moore, J. S. *Acc. Chem. Res.* **1997**, *30*, 402-413.

(162) Roncali, J. *Acc. Chem. Res.* **2000**, *33*, 147-156.

(163) Khan, M. S.; Al-Mandhary, M. R. A.; Al-Suti, M. K.; Ahrens, B.; Mahon, M. F.; Male, L.; Raithby, P. R.; Boothby, C. E.; Kohler, A. *Dalton Trans.* **2003**, 74-84.

(164) Meier, H.; Ickenroth, D.; Stalmach, U.; Koynov, K.; Bahtiar, A.; Bubeck, C. *Eur. J. Org. Chem.* **2001**, 4431-4443.

(165) Jorgensen, M.; Krebs, F. C. *J. Org. Chem.* **2005**, *70*, 6004-6017.

(166) Koynov, K.; Bahtiar, A.; Ahn, T.; Cordeiro, R. M.; Horhold, H. H.; Bubeck, C. *Macromolecules* **2006**, *39*, 8692-8698.

(167) Goh, C.; Kline, R. J.; McGehee, M. D.; Kadnikova, E. N.; Frechet, J. M. J. *Appl. Phys. Lett.* **2005**, *86*, 122110-122113.

(168) Cabarcos, E. L.; Carter, S. A. *Macromolecules* **2005**, *38*, 10537-10541.

(169) Sperling, L. H. *Introduction to Physical Polymer Science*; John Wiley & Sons, Inc.: New York, 2001.

(170) Erdelyi, M.; Gogoll, A. *J. Org. Chem.* **2001**, *66*, 4165-4169.

(171) Pearson, D. L.; Schumm, J. S.; Tour, J. M. *Macromolecules* **1994**, *27*, 2348-2350.

(172) Jiang, H.; Zhao, X.; Schanze, K. S. *Langmuir* **2006**, *22*, 5541-5543.

(173) Jones, G.; Jackson, W. R.; Choi, C.; Bergmark, W. R. *J. Phys. Chem.* **1985**, *89*, 294-300.

(174) Nguyen, T. Q.; Wu, J. J.; Doan, V.; Schwartz, B. J.; Tolbert, S. H. *Science* **2000**, *288*, 652-656.

(175) Barltrop, J. A.; Jackson, A. C. *J. Chem. Soc., Perkin Trans. 2* **1984**, 367-371.

(176) Feng, D. J.; Li, X. Q.; Wang, X. Z.; Jiang, X. K.; Li, Z. T. *Tetrahedron* **2004**, *60*, 6137-6144.

(177) Roncali, J. *Chem. Rev.* **1997**, *97*, 173-205.

(178) van Mullekom, H. A. M.; Vekemans, J. A. J. M.; Havinga, E. E.; Meijer, E. W. *Mat. Sci. Eng. R.* **2001**, *32*, 1-40.

(179) Mitschke, U.; Bauerle, P. *J. Mater. Chem.* **2000**, *10*, 1471-1507.

(180) Wright, A. T.; Anslyn, E. V. *Chem. Soc. Rev.* **2006**, *35*, 14-28.

(181) Winder, C.; Sariciftci, N. S. *J. Mater. Chem.* **2004**, *14*, 1077-1086.

(182) Nilsson, K. P. R.; Rydberg, J.; Baltzer, L.; Inganas, O. *Proc. Natl. Acad. Sci. U. S. A.* **2003**, *100*, 10170-10174.

(183) Marsitzky, D.; Vestberg, R.; Blainey, P.; Tang, B. T.; Hawker, C. J.; Carter, K. R. *J. Am. Chem. Soc.* **2001**, *123*, 6965-6972.

(184) Setayesh, S.; Grimsdale, A. C.; Weil, T.; Enkelmann, V.; Mullen, K.; Meghdadi, F.; List, E. J. W.; Leising, G. *J. Am. Chem. Soc.* **2001**, *123*, 946-953.

(185) Chou, C. H.; Shu, C. F. *Macromolecules* **2002**, *35*, 9673-9677.

(186) Jiang, D. L.; Choi, C. K.; Honda, K.; Li, W. S.; Yuzawa, T.; Aida, T. *J. Am. Chem. Soc.* **2004**, *126*, 12084-12089.

(187) Zhu, B.; Han, Y.; Sun, M. H.; Bo, Z. S. *Macromolecules* **2007**, *40*, 4494-4500.

(188) Dominguez, X.; Lopez, I. C.; Franco, R. *J. Org. Chem.* **1961**, *26*, 1625-&.

(189) Miteva, T.; Palmer, L.; Kloppenburg, L.; Neher, D.; Bunz, U. H. F. *Macromolecules* **2000**, *33*, 652-654.

(190) Hou, J.; Yang, C.; Qiao, J.; Li, Y. *Synth. Met.* **2005**, *150*, 297.

(191) Yamamoto, T.; Fang, Q.; Morikita, T. *Macromolecules* **2003**, *36*, 4262-4267.

(192) Yasuda, T.; Imase, T.; Nakamura, Y.; Yamamoto, T. *Macromolecules* **2005**, *38*, 4687-4697.

(193) Harriman, A. *J. Chem. Soc., Chem. Commun.* **1977**, 777-778.

(194) Thornton, N. B. Ph. D. Dissertation, University of Florida, 1995.

(195) Wang, F. K.; Bazan, G. C. *J. Am. Chem. Soc.* **2006**, *128*, 15786-15792.

(196) Fan, C. H.; Plaxco, K. W.; Heeger, A. J. *Trends In Biotechnology* **2005**, *23*, 186-192.

(197) Mwaura, J. K.; Pinto, M. R.; Witker, D.; Ananthakrishnan, N.; Schanze, K. S.; Reynolds, J. R. *Langmuir* **2005**, *21*, 10119-10126.

(198) Mwaura, J. K.; Zhao, X. Y.; Jiang, H.; Schanze, K. S.; Reynolds, J. R. *Chem. Mater.* **2006**, *18*, 6109-6111.

(199) Argazzi, R.; Bignozzi, C. A.; Heimer, T. A.; Castellano, F. N.; Meyer, G. J. *Inorg. Chem.* **1994**, *33*, 5741-5749.

(200) Newkome, G. R.; Behera, R. K.; Moorefield, C. N.; Baker, G. R. *J. Org. Chem.* **1991**, *56*, 7162-7167.

(201) Joester, D.; Losson, M.; Pugin, R.; Heinzelmann, H.; Walter, E.; Merkle, H. P.; Diederich, F. *Angew. Chem., Int. Ed.* **2003**, *42*, 1486-1490.

BIOGRAPHICAL SKETCH

Xiaoyong Zhao was born in Shannxi province, China. He spent his delightful childhood in the countryside and then moved with his parents in 1985 to a small town named Fugu, which lies at the west side of the Yellow River. There, he went to the primary school and high school. In 1996, he left his home town and went to Changchun, a city locating in the far Northeast of China to attend the college. After getting his bachelor's degree in 2000 from Jilin University, he was admitted to the Institute of Chemistry, Chinese Academy of Sciences in Beijing as a graduate student. In the first year of his graduate study, he decided to come to the United States of America to pursue his Ph. D. In August 2003, one month after he obtained his master's degree; he came to the University of Florida and started his training here at Gainesville. In the past four years, he did research in the area of water-soluble conjugated polymers under the supervision of Dr. Kirk S. Schanze. He and his wife Huimeng, who is also pursuing Ph. D. in the same department, were married in 2004 and had their first daughter, Duoduo, in the winter of 2005. After his Ph. D., Xiaoyong will spend two years doing postdoctoral research in the group of Dr. Jean M. J. Fréchet at the University of California, Berkeley.